Diss. ETH Nr.: 21733

Thermal Behaviour and Compensation of Rotary Axes in 5-Axis Machine Tools

A thesis submitted to attain the degree of

DOCTOR OF SCIENCES of ETH ZURICH
(Dr. sc. ETH)

presented by

MICHAEL GEBHARDT
M.Sc., University of Bayreuth
born on April 22nd, 1982
citizen of Germany

accepted on the recommendation of
Prof. Dr. Konrad Wegener, examinor
Prof. Dr. Atsushi Matsubara, co-examinor
Dr. sc. techn. Wolfgang Knapp, co-examinor

2014

To my family.

Acknowledgment

This thesis as well as my time at the *Institute of Machine Tools and Manufacturing (IWF)* would not have been the same without the generous support of a lot of people, who helped me invaluably throughout my dissertation at ETH Zurich.

First of all I would like to thank my supervisor Prof. Konrad Wegener giving me the opportunity to do a doctorate at his renowned Institute, giving me the possibility to intensify my knowledge of engineering, manufacturing and production. I would like to thank him for all his generous support, his patience, his trust and all the inspiring discussions.

I would like to thank my co-supervisor Prof. Dr. Atsushi Matsubara, head of the Machining, Measurement, and Control Laboratory of Kyoto University, for his interest in my Ph.D.-thesis, his reviews, his support and his helpful suggestions.

Very special thanks go to my co-supervisor Dr. Wolfgang Knapp for my professional education in the field of manufacturing and metrology. I thank him for all the support and trust in all phases of my employment and Ph.D. work. His patient explanations allowed me to build up the knowledge in the field of metrology and manufacturing I needed to finish this work.

Special thanks go to the head of my working-group Dr. Sascha Weikert for all his support during my employment and all his technical help, technical education, patient explanations and cheerful discussions.

I am grateful for the intriguing works of my students, who allowed me to supervise them for their Bachelor Theses, Semester Projects, and Master Theses: Philip von Cube, Thomas Anliker, Jerome Käser, Flurin Heini, Stefano Capparelli, Moritz Wiessner, Pascal Zurbrügg, Daniel Vincent, Simon Müller, Alex Schneeberger, Benjamin Massow, Tobias Widmer, Nils Furrer and Philip Blaser. Through their invaluable contributions, a profound base for my work and other fields was built. They represent the best mechanical engineers.

Special gratitude I owe to my friend a and office colleague Mr. Jens Boos, laboratory supervisor. He always helped me sacrificially whenever I asked him and needed his helping hand. Furthermore, he was always a great listener whenever I had non-technical problems.

Special thanks go to Dr. Markus Ess for all his support during my time at the Institute, for his advice in performing research and for a wonderful friendship.

Special thanks go to Dr. Karl Deibel for supporting me technically and morally throughout

Contents

List of Symbols

Symbol	Unit	Description
$\underline{v}$	–	Vector
$\underline{\underline{M}}$	–	Matrix
A	°	Coordinate of A-axis
A_s	m²	Surface
A_c	m²	Contact surface
B	°	Coordinate of B-axis
b	–	Bed / machine bed
C	°	Coordinate of C-axis
c_p	$\dfrac{\text{J}}{\text{kg K}}$	Heat capacity
d	m	Diameter
d_p	m	Distance from a point of a point cloud to the best fit plane
e_x	–	Normal vector in X-direction
e_y	–	Normal vector in Y-direction
e_z	–	Normal vector in Z-direction
F	N	Force
f_{mes}	Hz	Measurement frequency
Gr	–	Grasshof number
g	$\dfrac{\text{m}}{\text{s}^2}$	Gravitation constant
h_{tab}	mm	Hight of table
f	Hz	Frequency
l	m	Length
l_{eff}	m	Effective length
m	kg	Mass
Nu	–	Nusselt number
n	$\frac{1}{\min}$	Rotational speed
n_{MP}	–	Number of measurement points
P	W	Power
$\dot{Q}$	W	Heat flux

Symbol	Unit	Description
$[R]$	–	Rotational matrix for continuing R-Test
Ra	–	Rayleigh number
Re	–	Reynolds number
r	m	Radius
T	K	Temperature
T_{env}	K	Environmental temperature
T_{grow}	mm	Table growth
t	s	Time
u	–	Input parameter for phenomenological model
p	–	Measurement position of discrete R-Test
t	s	Time
t_{avg}	s	Effective measurement time, measurement values are averaged
t_g	min	Time gap between two R-test measurements
U	J	Internal energy
v	$\frac{mm}{min}$	feed speed
v_{rot}	$\frac{\circ}{min}$	Rotational feed speed
V	–	Vertical machine tool
W	J	Work
w	–	Workpiece
X	m	Coordinate of X-axis
Y	m	Coordinate of Y-axis
Z	m	Coordinate of Z-axis

Greek Symbol	Unit	Description
α	$^\circ$	angular measurement range for continual R-Test measurements
α_e	$\dfrac{\mu\text{m}}{\text{m} \cdot \text{K}}$	Expansion coefficient
α_{fc}	$\text{W}/(\text{m}^2\text{K})$	Heat transfer coefficient for forced convection
α_{cv}	$\dfrac{\text{W}}{\text{m}^2} \cdot \text{K}$	Heat transfer coefficient for free convection
ϵ	$-$	Emission
η	$-$	Index of bodies of physical model
λ	$\dfrac{\text{W}}{\text{m} \cdot \text{K}}$	Thermal conductivity
ν	m^2/s	Kinematic viscosity
Θ	K	Temperature
ρ	$\dfrac{\text{kg}}{\text{m}^3}$	Density
τ	$-$	Transmission
ξ	$\dfrac{\mu\text{m}}{\text{m}}$	Conversion factor from rad to $\dfrac{\mu\text{m}}{\text{m}}$

Subscript	Description
act	Actual
avg	Average
b	Machine bed
b_1	B-Body
c	Cooling
c_1	C-Body 2
c_2	C-Body 1
cv	Convection
cor	Corrected
E	Environment
hc	Heat conduction
I	Input
i	Number of measurement cycle
k	Number of R-Test discrete measurement position
max	Maximum
nom	Nominal
off	Offset
raw	Raw
rm	Rotated measurement points
rot	Rotational
t	Table
tot	Total

List of Abbreviations

Abbreviation	Description
CAD	Computer Aided Design
CAM	Computer Aided Manufacturing
CFRP	Carbon fibre reinforced plastic
CL	Cooling lubricant
CMS	Code Modification Software
CNC	Computerized numerical control
DE	Differential Equation
DIS	Draft International Standard
ETVE	Environmental temperature variation error
FL	Fuzzy logic
FDM	Finite difference method
FDEM	Finite difference element method
FEM	Finite element method
FO	Functional oriantation
FOCAS2	Fanuc Open CNC API Sepcification Version 2
FP	Functional point
IP	International protection
ISO	International Standard Organisation
LM	Linear motor
MCS	Machine tool coordinate system
MOR	Model order reduction
MRF	Magnetorheological fluids
NC	Numerical control
NN	Neuronal networks
NTC	Negative temperature coefficient thermistor
ODE	Ordinary Differential Equation
PC	Personal computer
PCM	Phase change materials
PTC	Positive temperature coefficient thermistor
RM	Regression model
SEA	Spindle Error Analyser
SMA	Shape memory alloys
SVM	Support Vector machine Model
TCP	Tool Centre Point
WPCS	Work piece coordinate system

Abstract

Thermal deviations of machine tools represent one of the most significant influences to the geometric accuracy of manufactured workpieces. In the past years, research focused on thermally caused deviations of 3-axis machine tools, induced by the environment, the main spindle and the linear axes. At the same time, 5-axis machine tools became increasingly popular and are even used for precision manufacturing. But up to now, scientific investigations regarding the rotary axes of these machine tools focused on the geometrically location and component errors. Thermal influences have not been investigated in detail.

This thesis deals with the characterization of the thermal behaviour of 5-axis machine tools. The focus is on the thermal errors induced by the rotary and swivelling axes.

In order to achieve a fundamental understanding regarding the thermally induced errors of rotary and swivelling axes, temperature measurements are carried out. Heat sources and heat flux in the machine tools structure cause a temporal and spatial variable temperature distribution. This is visualized and quantified systematically during different operating states on two machine tools with a different kinematic setup. The temperature effects lead to thermo-elastic deviations, which are responsible for displacements between tool and workpiece. In order to identify these displacements, measurement procedures based on the *R-Test* measurement device are presented. In addition to displacements, which are evaluated, when geometric measurements of rotary axes are carried out, the presented methods cover also errors which only occur due to thermal influences, such as deviations from the zero angle or displacements of functional surfaces like the machine tool table.

In order to classify the impact of the thermally induced errors of rotary and swivelling axes into the total thermal error of 5-axis machine tools, other significant contributors like the influence of the environment, the main spindle and the linear axes are analysed with methods according to the state of the art. Comparison of the magnitude of these impacts with the influence of the rotary / swivelling axes shows that the measured effects are within the same range.

For the reduction of thermally caused displacements between tool and workpiece, three fundamentally different approaches are available: thermal influences can be prevented, for example by conditioning the environmental air or reducing friction in the machine tool. Thermal influences can be compensated physically, for example by heating or by cooling certain machine tool components. And thermal influences can be compensated by correcting axis movements via the numerical control of the machine tool. For an effective compensation, the errors must be known accurately. This can be realized either with measurements carried out on the machine tool, by prediction models which are able to compute occurring displacements based on auxiliary input parameters, or by a suitable

combination of both procedures.

In this thesis, two model approaches are presented to predict the thermal errors induced by and of the rotary axes based on internal signals of the numerical control. Due to the flexibility of the prediction model, also the program code of the planned process on the machine tool can be used for the prediction of the deviations.

The efficiency of the compensation strategies is verified by measurements on 5-axis machine tools. The range and the arithmetic mean of the thermal error induced by the rotary axes of the machine tools is reduced by up to 85%.

Kurzfassung

Thermisch bedingte Abweichungen sind für bis zu 75% der geometrischen Fehler an einem bearbeiteten Bauteil verantwortlich. Während sich die Forschung in den letzten Jahren verstärkt mit Abweichungen an 3-achsigen Werkzeugmaschinen verursacht durch den thermischen Einfluss der Umgebung, der Hauptspindel und der Linearachsen von Werkzeugmaschinen bschäftigt hat, werden 5-achsige Fräsmaschinen immer beliebter und zunehmend auch zur Bearbeitung präziser Bauteile eingesetzt. Die auf diesen Maschinen vorhandenen Dreh- und Schwenkachsen werden vor allem geometrisch bzgl. ihrer Lage- und Komponentenabweichungen untersucht und optimiert. Der thermische Einfluss dieser Achsen ist bis heute nur unzureichend erforscht.

Die folgende Arbeit beschäftigt sich mit der Charakterisierung des thermischen Verhaltens 5-achsiger Werkzeugmaschinen. Der Fokus liegt auf den thermisch bedingten Abweichungen verursacht durch die Dreh- und Schwenkachsen.

Ein grundlegendes Verständnis für die durch Dreh-/ Schwenkachsen verursachten Verlagerungen im Maschinenkoordinatensystem wird durch eine systematische, experimentelle Untersuchung des Temperaturfelds an zwei 5-Achs Werkzeugmaschinen mit unterschiedlicher Achskonfiguration bei maschinentypischen Belastungszyklen durch die Rotationsachsen erarbeitet. Mit der systematischen Methode werden die Wärmeentwicklung und die Wärmeflüsse in der Struktur visualisiert und quantifiziert. Die hierdurch hervorgerufenen zeitlichen und örtlichen Änderungen des Temperaturfeldes in der Maschine verursachen thermo-elastische Verlagerungen, welche für die Abweichungen zwischen Werkzeug und Werkstück verantwortlich sind. Zur Erfassung dieser Abweichungen werden Messverfahren basierend auf dem Messsystem *R-Test* vorgestellt. Zusätzlich zu den Abweichungen, die bei geometrischen Messungen von Rotationsachsen bestimmt werden, erfassen die vorgestellten Methoden Abweichungen, die nur thermisch induziert auftreten, wie z.B. Nullwinkelfehler oder Abweichungen von funktionalen Flächen wie z.B. Werkstückspannflächen.

Um die thermischen Einflüsse der Rotationsachsen klassifizieren zu können, werden andere thermische Einflüsse auf den untersuchten Maschinen, wie z.B. Umgebungseinflüsse, der Einfluss der Hauptspindel oder der Linearachsen, nach dem aktuellen Stand der Technik charakterisiert. Der Vergleich mit dem Einfluss der Dreh- und Schwenkachsen zeigt, dass die festzustellenden Abweichungen in der selben Grössenordnung liegen.

Zur Reduktion thermisch bedingter Abweichungen zwischen Werkzeug und Werkstück stehen drei grundsätzlich verschiedene Ansätze zur Verfügung: Die Vermeidung thermischer Einflüsse, z.B. durch eine Raumklimatisierung oder durch die Reduktion von inneren Wärmequellen wie z.B. Reibung. Die physikalische Kompensation thermischer Einflüsse, z.B. durch das Temperieren bestimmter Komponenten. Und die steuerungs-

seitige Kompensation thermischer Einflüsse z.B. durch korrigierende Achsbewegungen. Für eine wirkungsvolle, steuerungsseitige Kompensation müssen die zu korrigierenden Verlagerungen bekannt sein: sie können entweder über Messungen auf der Maschine zur Verfügung gestellt oder über entsprechende Modelle berechnet werden.

In dieser Arbeit werden zwei Modellansätze vorgestellt, die die thermisch induzierten Abweichungen von Dreh -/ Schwenkachsen auf Basis steuerungsinterner Signale berechnen. Die Flexibilität der Methoden ermöglicht es zusätzlich an Stelle der maschineninternen Signale, den Programmcode für die geplante Bearbeitung als Eingangsparameter zu verwenden.

Die Qualität der Kompensationsmodelle wird durch Messungen auf 5-Achs Bearbeitungszentren verifiziert. Die durch die berechneten Korrekturwerte erzielte Reduktion der thermischen Maschinenabweichungen verursacht von den Dreh-/ Schwenkachsen, liegt bei bis zu 85% der Spanne und des arithmetischen Mittelwertes der ohne Kompensation gemessenen Abweichungen.

1 Introduction

Thermal influences are one of the main error sources influencing the accuracy of machine tools: according to [1], up to 75% of the overall geometrical errors observed at a manufactured workpiece are caused by thermo-elastic deformations. Therefore, precision machine tool design always implies avoidance strategies to minimize thermally induced distortions. This can be realized by minimizing the energy input into machine tools, by isolating heat sources or sinks from the machine tool structure, by an active temperature control of certain components or by a design, which minimizes thermo-elastic deformations. Further active compensation strategies are developed to reduce the thermally induced errors either based on internal signals or by the use of measurements, like temperatures of significant machine tool parts.

Reducing thermal deviations by the design of the machine tool, or by an implemented error model becomes even more important, since manufacturing industry is changing with regard to the responsibility for the thermal deviations: for a long time, the machine tool users took care of reducing thermal deviations by defined environmental conditions or specific warm-up cycles. According to [2], in the meantime the responsibility of thermal error management is passed on to the machine tool manufacturers due to the market pressure in the manufacturing industry.

As written in [3], advances in mechatronics always lead to higher precision of machine tools. Therefor, the manner of consideration of thermal influences changed: manufacturing industry expects a continuous increase of accuracy, repeatability and stability. A significant part of this can only be reached by reducing thermal errors.

In addition to the call for a higher accuracy, the demand for productivity of machine tools increases. These growing requirements lead to a rise of spindle speeds, feed rates and axis acceleration [4, 5]. Friction can be found in all drives. The increase of the total operating performance leads to an increased heat flux into the machine tool structure. According to [6], all these effects, combined with the need for higher accuracy, have led to a rising effort regarding the minimization of thermo-elastic deformations or its compensation.

5-axis machine tools represent a significant evolution in the history of machine tool designs: the extension of three linear axes with two rotary axes enables the machining of complex surfaces without re-clamping of the workpiece. Regarding milling machine tools, many complex freeform surfaces are only machinable by a kinematic setup consisting of three linear and two rotary axes. Thereby, a significant reduction of the machining time can be reached with an increased machining accuracy at the same time, even though the enhancement of two additional axes means additional location and component errors [7].

The combination and synchronisation of five axes for high precision machining is a very

complex issue: up to now, as written in [8], the optimization of the geometric accuracy and the dynamic behaviour was prioritized. Machine tool manufacturers had to gain experience with designing rotary / swivelling units with a high geometric accuracy, a high stiffness and sufficient acceleration and velocity. Measurement devices, setups and procedures had to be investigated to calibrate five-axis machine tools geometrically [9]. Up to now, thermally induced errors of rotary axes are not considered sufficiently.

In this work, the thermal behaviour of rotary axes of five-axis machine tools is investigated. The analysis of the heat flux and the temperature distribution of the machine tool structure depending on different operating states of the rotary axes enables a deeper understanding of the thermal behaviour. Displacement measurements show, that the thermally induced deviations of rotary axes are within the same range compared to influences caused by the environment, the spindle or the linear axes. This underlines the need for a more detailed analysis of the thermal behaviour of rotary axes.

Two different approaches to compute and compensate on-line thermally induced errors of rotary axes based on internal control signals are introduced. With these models, correction strategies for the reduction of thermal errors are successfully realized on two different machine tools. Up to 85 % of the thermal deviations are compensated. Thereby, an important step towards increasing the accuracy of five-axis machine tools is done.

2 State of the Art

Summarizing the discussions in [6, 10–12], the occurrence and value of thermo-elastic deformations as well as their reduction and / or compensation, are influenced by several factors, like the kinematic of the machine tool itself, the built-in drives, the used materials, the arrangement and type of measuring devices and the compensation strategies. Mayr et al. summarizes in [1] the current state of research, especially regarding the measurement of temperatures and thermal errors, its computation and its compensation.

The following chapter describes the occurrence of thermo-elastic deformations of machine tools and the state of the art regarding measurement, computation, and compensation with a focus on rotary axes of five-axis machine tools.

2.1 Thermal Influences on Machine Tools

In 1990, Bryan [13] analyses the main contributors to the overall thermally induced error and categorises them as follows:

- heat generated from the (cutting) process,

- heat generated by the machine (drives,...),

- heat exchange due to tempering devices (cooling and heating),

- heat exchange with the environment,

- the effect of people,

- thermal memory from any previous environment.

Bryan explains, that any deviation from the reference temperature of 20°C (as defined in [14]), or temporal and spatial temperature variations caused by one of the six contributors are the source of the resulting thermal deviation. The origination of this total thermal error, due to temperature differences of the workpiece, the measurement systems and the machine frame as well as different thermal expansion coefficients of these three elements is illustrated in the thermal effects diagram (Figure 2.1)

2.1.1 External Heat Sources

A variation of the environmental temperature or local temperature gradients both in vertical and horizontal direction cause thermo-elastic deformations of a machine tool and prevent that a steady-state can be reached. Weck [15], specifies the factors influencing the magnitude of this temperature as:

Thermal effects diagram

Room en-vironment	Coolants	People	Machine	Cutting process

	Cutting fluid
	Lube oil
	Hydraulic oil
	Frame
	  stabilizing
			Electronics
			Mechanical friction
			Hydraulic friction
			Motors &Transducers
			Electrical
			Frame stabilization
			  heaters	

Heat flow

Conduction   **Convection**   **Radiation**

Thermal memory from previous environment

Temp. gradients or static effect

Temp. variation or dynamic effect

Uniform temp. other than 20°C

Non-uniform temperature

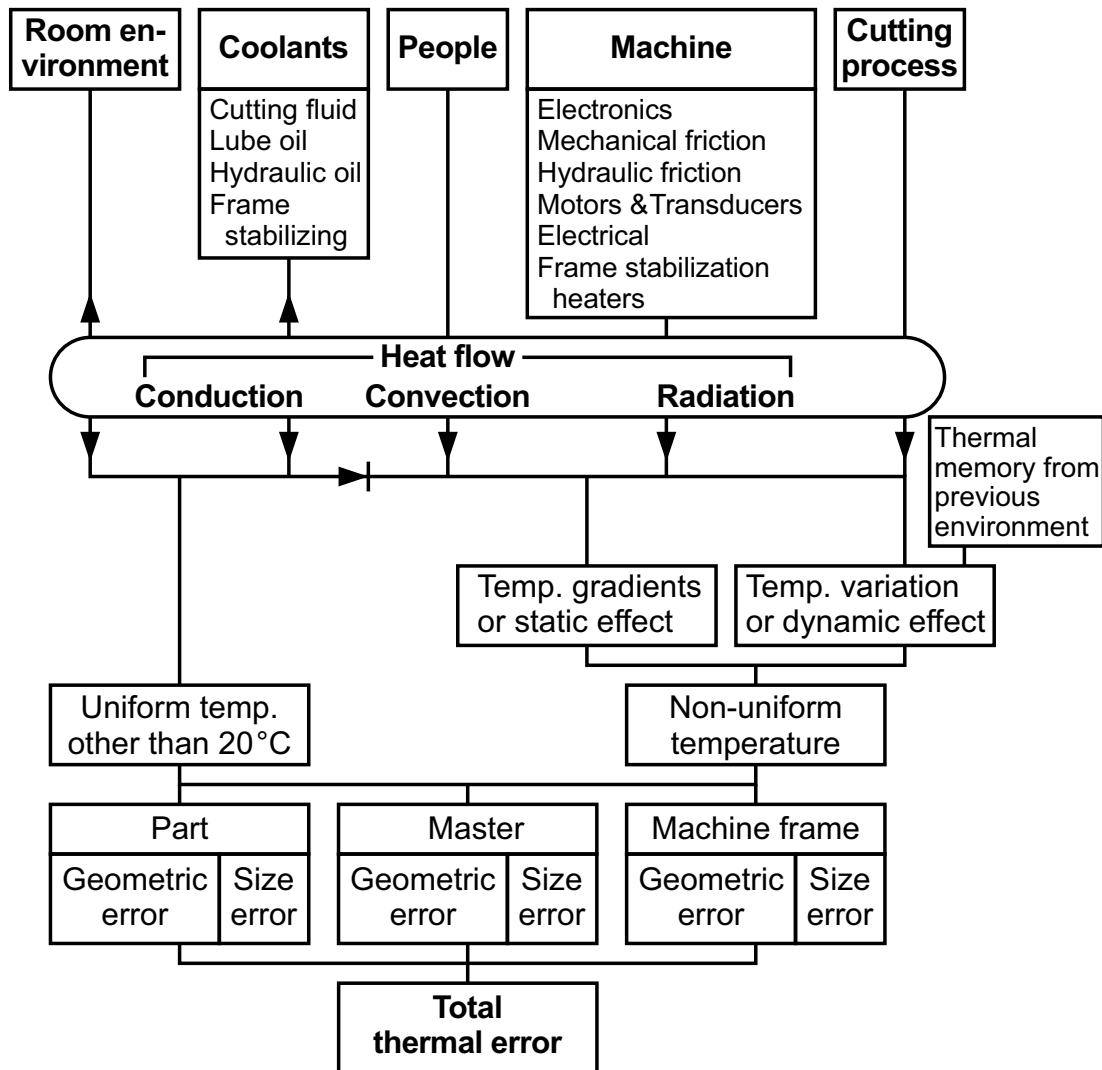| Part		Master		Machine frame	
Geometric error	Size error	Geometric error	Size error	Geometric error	Size error

Total thermal error

Figure 2.1: Thermal effects diagram [13]: The diagram illustrates the concept that every measuring and machining operation unavoidably consists of a three-element system made up of the part, the machine frame, and the master (or scale). The six sources of thermal influence are identified as (1) heat generated from the cutting process, (2) heat generated by the machine, (3) heating or cooling influence provided by the various cooling systems, (4) heating or cooling influence provided by the room, (5) the effect of people, and (6) thermal memory from any previous environment.
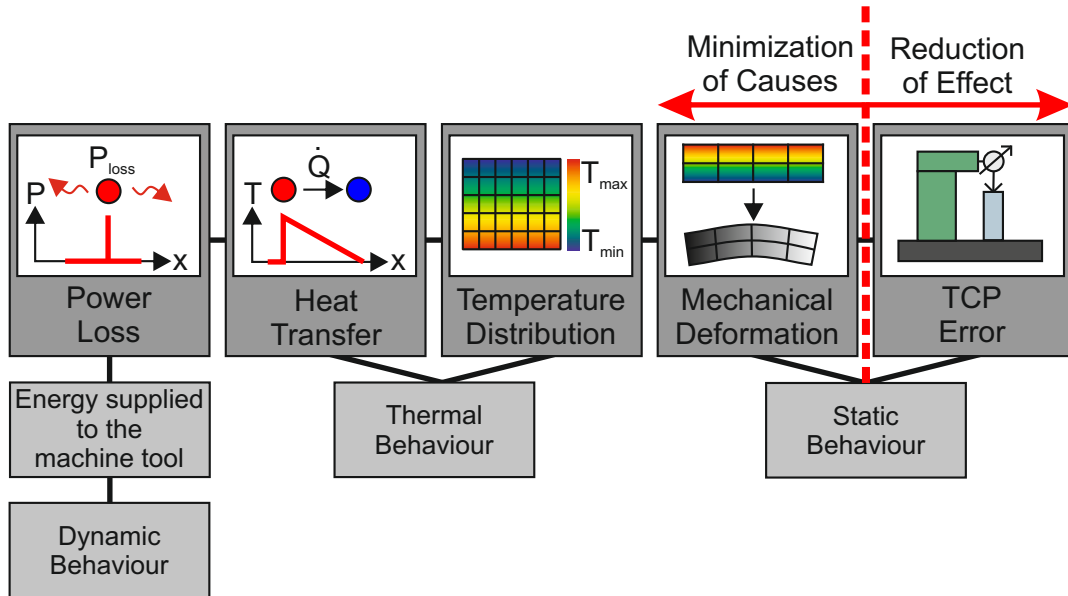
Figure 2.2: Thermal flow diagram for internal sources [16].

- the geography location,

- the season and

- the thermal characteristic of the machine shop.

In addition to the environmental situation of the machine tool, the previous environment of the workpiece, e.g. temperature in the stock, is important and has to be considered. The time needed for acclimatization must always be considered.

2.1.2 Internal Heat Sources

The root cause for thermally induced TCP displacements caused by internal heat sources are power-losses generated by energy supplied to the machine tool [17, 18]. As written in [19], these local power-losses, for example arise in the drives and bearings of the machine tool, cause a heat transfer in the machine tool structure resulting in an inhomogeneous temperature field. This temperature distribution results in an elastic deformation, which is depending on the static behaviour and more precicesly the stiffness - finally responsible for the resulting TCP displacements (Figure 2.2) [16, 20].

2.1.3 Standards

Three relevant standards are dealing with the determination of thermal effects. The most general standard is ISO 230-3:2010 [21], which deals with thermally induced position and orientation errors (summarized as "location errors" in the following text) caused by environmental temperature variation, rotating spindles or moving linear axes. The same measurements are presented in ISO 10791-10:2007 [22], dealing with machining centres
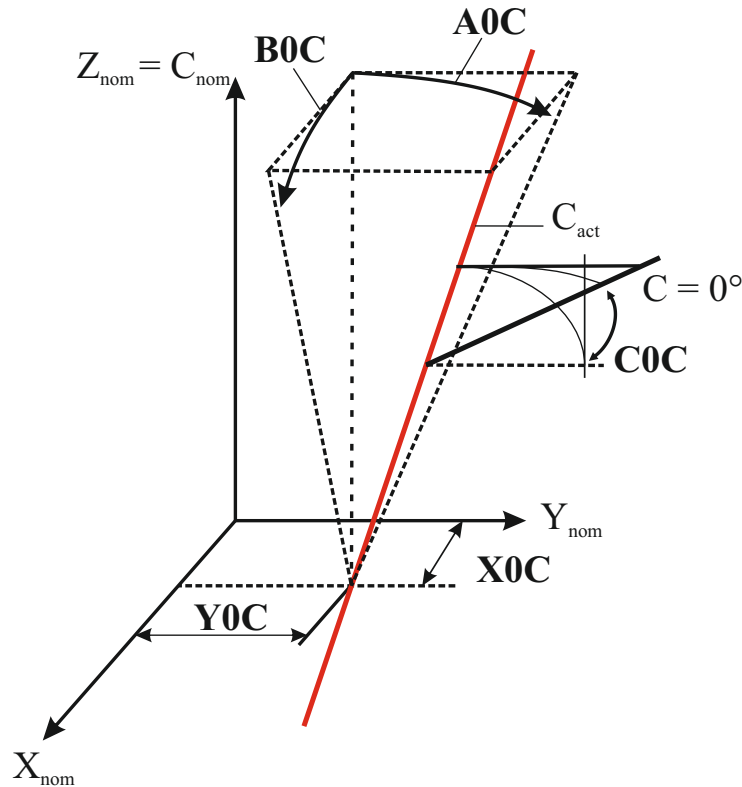
Figure 2.3: Position and orientation errors of a rotary axis according to ISO 230-1:2012(E) [24].

and ISO 13041-8:2004 [23], dealing with turning machines and turning centres (The measurement setups and strategies used in this work are explained in detail in chapter 4.1.2).

Location errors of rotary axes, illustrated in Figure 2.3, are defined in ISO 230-1:2012(E) [24]. In ISO 230-7:2007 [25], specifications and tests regarding the evaluation of the geometric accuracy of rotary axes are defined. The thermal behaviour of rotary axes is not included in any international standard yet and can only partly be derived from what has been specified in ISO 230-3 for linear axes, spindles and the environmental temperature influence.

2.2 Metrology

2.2.1 Temperature Measurements

The measurement of temperatures is important for a fundamental understanding of the thermal behaviour of machine tools. According to Weck and Brecher [26], temperature measurements can be distinguished in two basic principles: contacting and non-contacting measurements.

Non-contacting Temperature Measurement

For non-contact temperature measurements with infrared cameras or pyrometers, the surface temperature of the device under test is determined by intensity measurements of
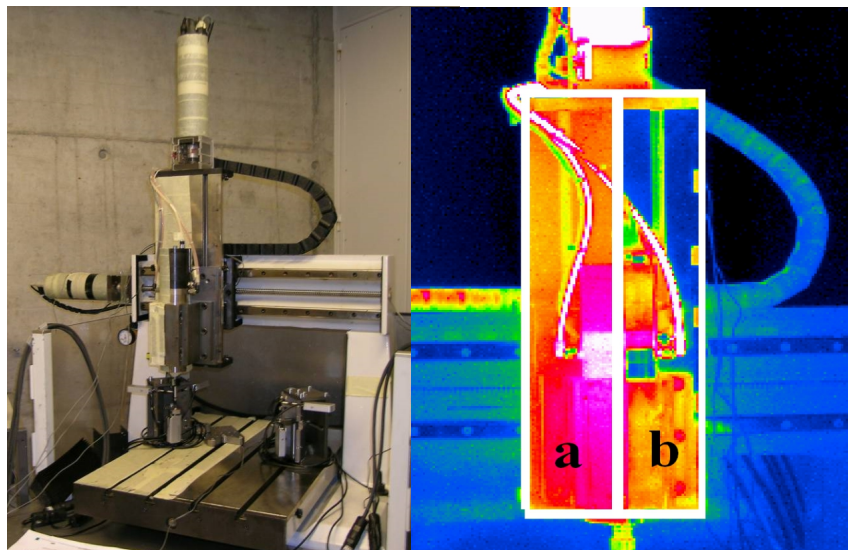
Figure 2.4: Left: three axis milling machine; right: infrared temperature measurement of the Z-axis with (a) surfaces prepared with adhesive tape and (b) unprepared metallic surfaces of spindle housing [2].

its infrared radiation. Every body with a temperature of more than 0 K emits electromagnetic waves whereupon the spectrum of emitted waves moves to shorter wavelengths with rising temperature. The intensity of the infrared radiation can be measured with an infrared camera or a pyrometer. With knowledge concerning the emission characteristics, associated temperatures can be computed.

Non-contact temperature measurements show a high dependency on the emission characteristics and the reflectivity of the analysed surface. The relationship between emission ϵ, reflection ρ and transmission τ is given by

$$\epsilon + \rho + \tau = 1 \tag{2.1}$$

whereby according to [2], the transmission can be neglected for metals.

Regarding the reflectivity, Figure 2.4 shows the influence of different surfaces: a left half of a vertical axis is pasted up with adhesive tape, which leads to an emissivity coefficient near to one. The right half is the original metallic surface that reflects the radiation of cooler surroundings.
Another example for this high dependency on the surface quality of the analysed structure can be seen in Figure 2.5. The evaluated temperature of a Rugotest differs strongly with changing roughness between Ra 0.4 μm to 50 μm at room temperature of 20.5°C.

The principles of non-contact measurement based on infrared radiation are mainly applicable for bodies with a low thermal capacity or conductivity (compared to contacting sensors with respect to the required measurement frequency), high temperatures (up to 2000°C), rotating components or locations difficult to access. Examples due to limited access are given by [27, 28]: the temperature profile of a linear axis drive is measured in order to identify position-dependent thermal deviations. This is done along the axis for
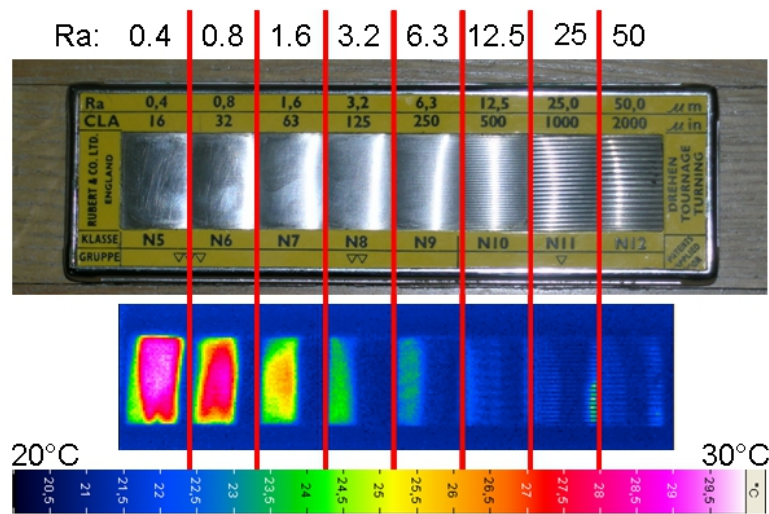
Figure 2.5: Reflection of heat on a Rugotest reference part for turning with Ra 0.4 μm to 50 μm at room temperature of 20.5°C [1].

semi-closed loop drive systems and along the length gauge for layouts with closed loop drive systems.

Contacting Temperature Measurement

Due to a reduced technical effort, contact temperature sensors are common measurement devices for the characterization of temperatures of accessible structures. Additionally, the emission characteristic of the analysed structure does not need to be known. For this purpose, according to [26] different sensor types are used:

- Resistance thermometers
  - Metal resistance thermometers (e.g. Pt100, Pt1000) are robust and have a high linear characteristic. Accuracies (< 0.3°C) can be reached with a reference resistance and a bridge circuit to minimize thermal influences from the input wire.
  - Negative / positive temperature coefficient thermistors (NTC thermistor, PTC thermistor) have a high sensibility and a short response time. Because of their high non-linearity, they are frequently used as limit indicators.

- Thermocouple sensors which are very robust, compact, economically priced and can be calibrated by two reference measurements at the beginning and the end of the expected temperature range. A disadvantage is the low signal level: as an example, a typical thermocouple iron-constantan shows a thermoelectric voltage of 53 μV/K . Therefore, an extensive signal amplification is necessary.

- Quartz thermometers have high accuracy ($\pm$ 0.1°). Disadvantages are the price and the big dimensions compared to metal resistance thermometers.
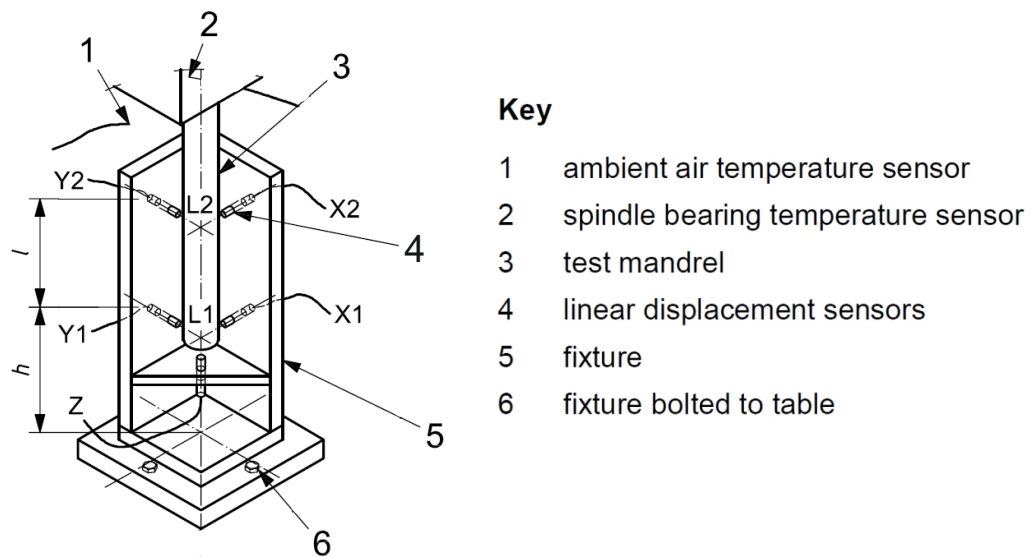
Figure 2.6: Measurement set-up up provided by ISO 230-3:2007 for recording thermally induced errors by the environment, spindles running and moving linear axes [21]. Rotary axes are not covered by ISO 230-3:2007.

2.2.2 Measurement of Thermo-Elastic Deformations of Five-Axis Machine Tools

In ISO/TC 39/SC 2 N 2062: 2013 [29], a *"cutting tool centre point or point associated with a component on the machine tool where cutting tool would contact the part for the purposes of material removal"* is defined as functional point (FP). An example for a functional point is the TCP. A *"relative orientation between the tool side and the workpiece side"* is defined as functional orientation (FO), such as the squareness errors of a rotary C-axis to the X- and Y-axis (Figure 2.3). The effective measurement of changes regarding the position of the FP and the FO are fundamental for a deep understanding of the thermal behaviour of the machine tool. It enables the reduction of significant errors by design improvements or numerical compensation approaches.

Looking at geometric errors of five-axis machine tools, a lot of research was carried out concerning the measurement and calibration as described in [30–34]. Regarding thermally induced errors, ISO 230-3:2007 [21] provides a measurement setup that allows the qualification of errors induced by the environment, the spindle or linear axes (Figure 2.6).

With five linear displacement sensors (representing the workpiece) measuring against a precision test mandrel (in Figure 2.6 representing the tool), the change of position and orientation between tool side and workpiece side can be measured in three translational and two rotational directions. It is emphasised that all tests provided by ISO 230-3:2007 [21] are tests under no-load or finishing cutting conditions. In [35], the characteristics of thermal error models in real cutting conditions are studied and compared to free air-cutting conditions. Brecher et al. [36] uses a stressing unit to simulate cutting conditions for a milling machine (Figure 2.7). In [37], the heat flux induced by the cutting process is
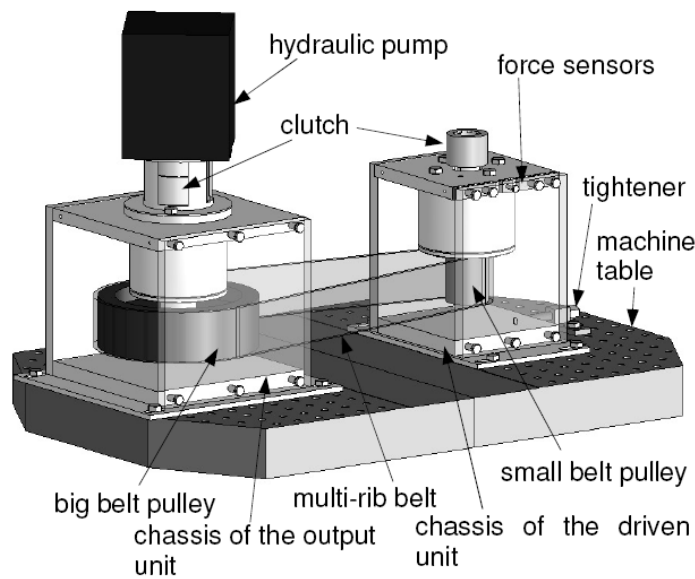
9

Figure 2.7: Stressing unit to measure the thermal distortion under load condition (forces are simulated with a hydraulic pump) [36].

analysed in detail.

Another possibility to determine thermo-mechanical displacements are 1D length measurement devices like a double ball bar, a laser ball bar and laser interferometers [38–45]. For the contactless measurement of thermal errors, thermography and short-distance photogrammetry can be used as introduced in [28, 46]. Figure 2.8 [47] shows a method to calculate the thermally induced positioning errors of a ball screw feed drive based on thermographic measurements. Digital imaging processing and photogrammetry with defined reference points on the structure of the feed drive and the surrounding machine components are used to transform the 3D-object into a 2D-image. Thereby, the defined structure points in the thermographic picture can be identified. With the help of the temperature information contained in the thermographic images, the respective thermally induced errors can then be calculated depending on the respective axial position by means of a temperature deformation model.

Measuring thermally induced errors of rotary axis is a novel field of research. In recent years, the focus in research was on the geometric and dynamic analysis of rotary axes. In 1990, Knapp and Wirtz [49] present a 2D probe where the rotary axes of a machine tool is tested in combination with other axes in order to check the individual geometric error of the rotary axis and the performance of the numerical control. In 2004, Weikert and Knapp [50] present a new device for the measurement of relative TCP deviations between a sphere and a probing system called ”R-Test”. In [8], Weikert describes how to use the measurement device to calibrate geometric errors capable for parametrisation like backlash, positioning error, squareness, parallelism, etc. In [9], a procedure for a model-based calibration of five-axis machining centres is presented. Dynamic measurements with the R-Test are presented in [38], where a dynamic backlash error of a rotary axis is analysed by clockwise and counter-clockwise measurements. A non-contact R-Test device with laser
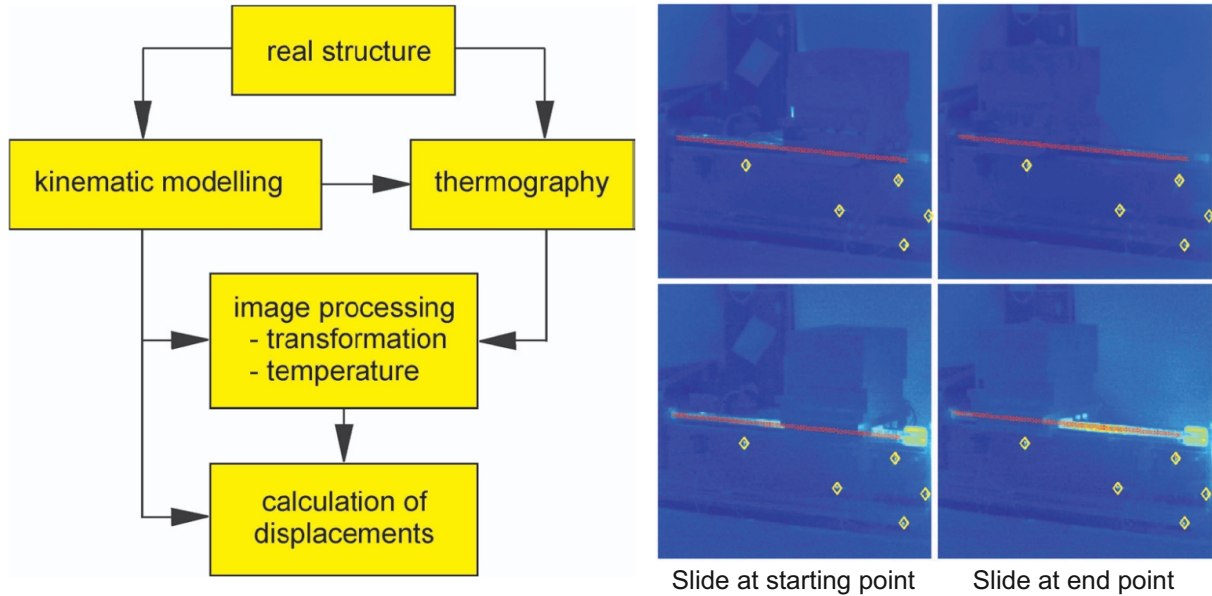
Figure 2.8: Left: Scheme of calculation model based on a combined thermographic and short-distance photogrammetric analysis. Right: Thermografic images of a ball screw before (top) and after (below) 4000 cycles with an axis travel of 100 mm and a load of 600 kg. Red crosses: temperature measurement points. Yellow rhombuses: identified markings [48].

displacement sensors is presented in [48]. Initial, thermal testings of rotary axes with the R-Test are carried out by Ess [51] and Ibaraki [52]. Further measurement devices to quantify thermally induced errors are laser tracker or LaserTracer. The LaserTracer uses the principle of multilateration to identify the relative position of the TCP to the machine tool table [31]. In [53], the procedure to identify thermal deviations in the whole processing area with a Laser Tracer is introduced.

2.3 Computation of Thermo-Mechanical Errors of Machine Tools

There are a lot of different approaches to model the thermo-elastic behaviour of machine tools in order to compensate occurring errors. Generally, these approaches can be divied into the two different classes

- phenomenological models and

- physical models.

Phenomenological models use empirically proven correlations between input parameters (e.g. temperatures) and an output value (e.g. TCP displacement). Experiments are carried out at different loads and the results over time are approximated by a regression model (RM). Also methods using neuronal networks (NN) or fuzzy logic (FL) for compensation belong to this group of procedures. Examples are given in [54–61].
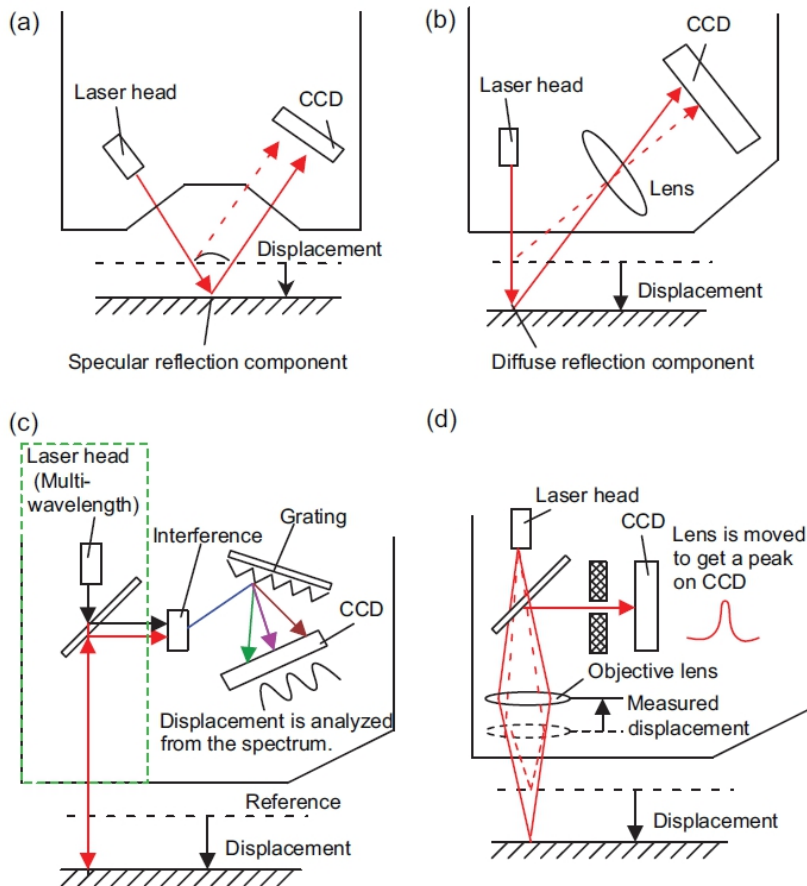
Figure 2.9: For the contactless R-Test, four different laser measurement sensors have been analysed. The picture shows the schematic measuring principle of these four sensors: (a) specular reflection type (LK-G10), (b) diffuse reflection type, (c) spectral interference type and (d) confocal type [48].
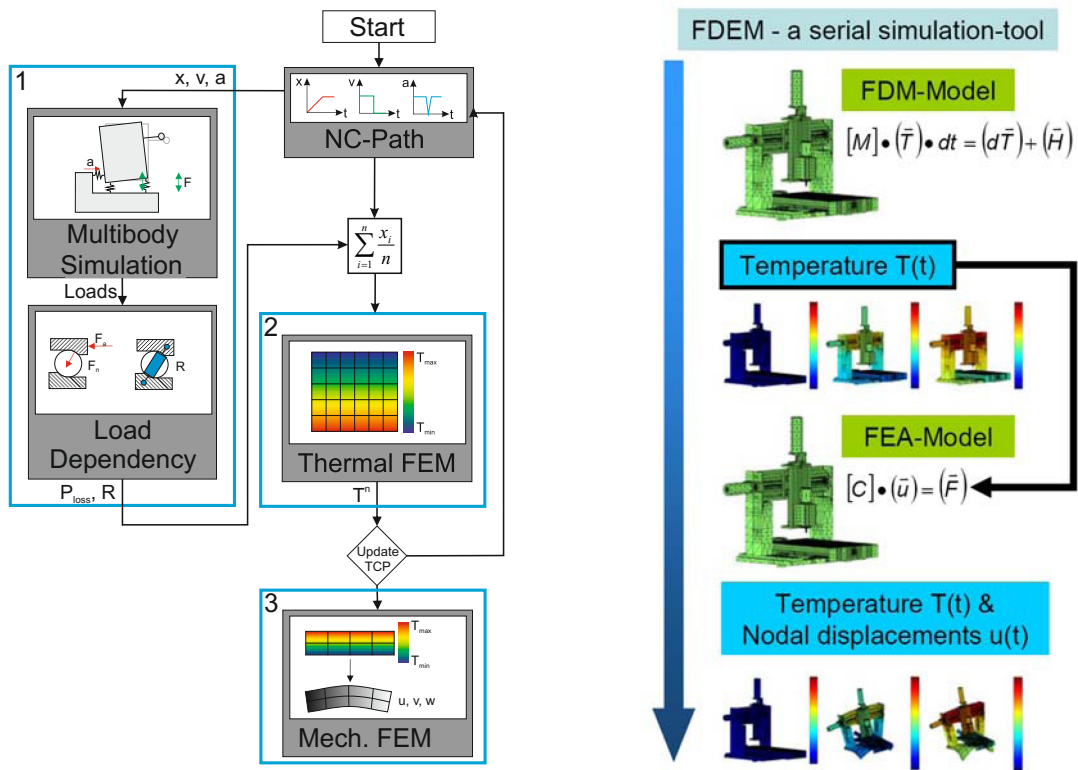
Figure 2.10: Schematic of thermal FEM according to [16] (left) and FDEM according to [2] (right).

Physical models distinguish the calculation of thermally induced errors into the calculation of the temperature distribution using thermal load data, and the calculation of the distortions in order to determine TCP - deviations. This approach,based on the consideration of the underlying physical effects, enable a n extrapolation so that any thermal load can be considered. At the same time, the separation into a calculation of the temperature field and a calculation of the distortions enables real-time applications. Examples are introduced by [2, 16].

Large subsets of physical models are Finite Element Method (FEM) models (Figure 2.10, left) and Finite Difference Method (FDM) models. Examples for FEM models can be found in [16, 62–64], examples for FDM models can be found in [65, 66].

An effective combination of both approaches is the Finite Differences Element Method (FDEM) [2, 67–69]. Especially in the design phase, FEM is a powerful tool to compute different internal and external influences on several machine tool parts. Analysing a broad spectrum of thermal loads and boundary conditions, the computation with complex FEM models can be very time-consuming due to the large number of degrees of freedom. In [2, 16, 70], ways to reduce this computation effort are presented with different model-order-reduction (MOR) methods.

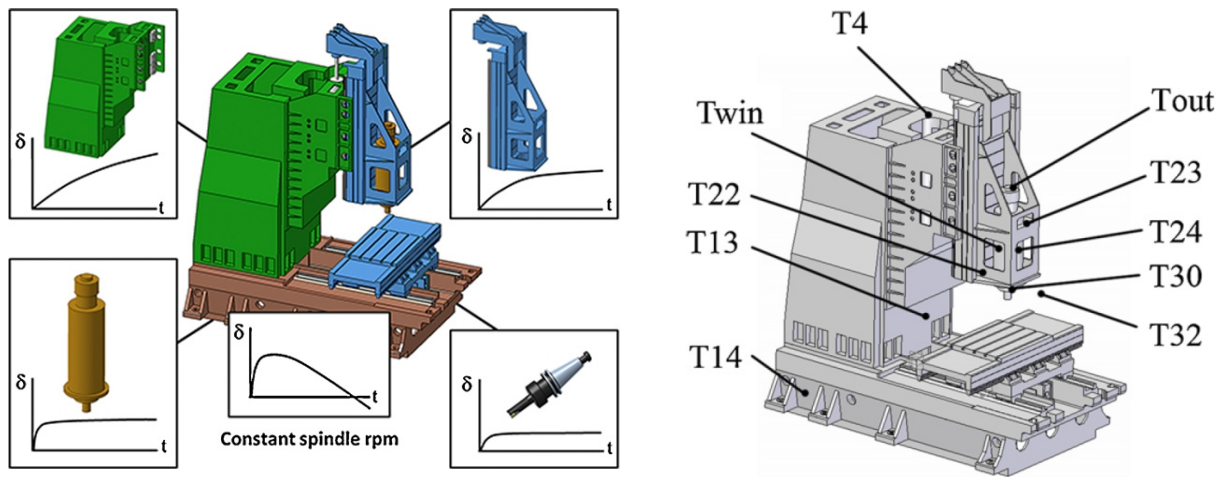In the following sections, 2.3.1 to 2.3.5, different modelling aproaches are introduced.

Figure 2.11: Decomposition of modelled structure and placement of chosen temperature sensors according to [81] where δ is the thermally induced deformation, t is the time and T stands for temperature sensor.

2.3.1 Modelling of Thermal Errors of Machine Tool Structures

Heat generated by internal sources forced by electric losses like in drives, or by friction for example in bearings causes an inhomogeneous, time dependent temperature field resulting in distortions of the machine tool structure [58]. In addition to internal heat sources, the heat exchange with the environment represents a significant source of the overall thermal behaviour of a machine tool, which is modelled in [71]. To measure environmental influence on machine tools, a temperature chamber that is able to control the time-dependent air and foundation temperatures, is introduced in [72]. The bed of machine tools is often assumed as one homogeneous body. In reality, there are a lot of contact interfaces influencing the heat transfer so that a more complex system needs to be described. This is analysed in [73]. In [62], Jungnickel describes the heat transfer in joints.

2.3.2 Modelling of Thermal Errors of Spindles and Rotary Axes

High energy losses in spindles lead to large thermal deviations which make spindles be one of the most significant contributors to the total thermal error. Because of this, the thermal behaviour of spindles has always been in the centre of research activities [74–76], and a lot of different models to predict the load dependent thermal errors have been developed. Especially high speed spindles are in the focus of current research activities [77–79]. According to [80], they show a more complicated dynamic, non-stationary and speed-dependent thermal characteristics than conventional spindles which is constituted by the higher centrifugal forces and thermal expansion occurring on the bearings and motor rotor which change the thermal characteristics of the built-in motor, bearings and assembly joints.

Analytical approaches to model the thermal behaviour of precison spindles are presented in [82, 83]. A so called *decomposition method* is presented by Vyroubal [81] and shown in Figure 2.11. A special developed measuring frame enables to measure the deformation of machine column, headstock, spindle and tool simultaneously. Afterwards, the com-
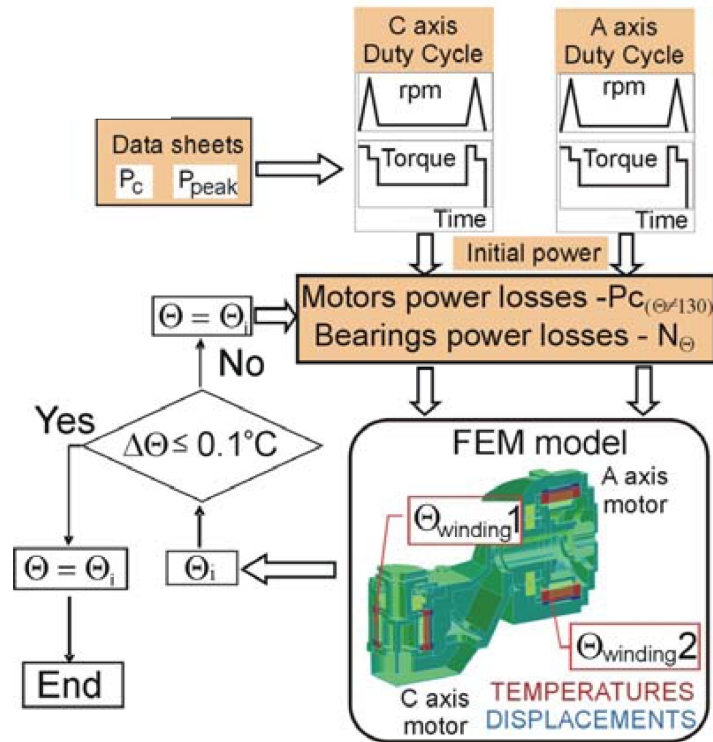
Figure 2.12: Algorithm for calculating power losses in torque motors according to [85] (Θ = temperature, P = power).

pensation is calculated as a sum of multinomial regression equations using temperature measurement.

Veldhuis et al. [84] present a neural network model to compensate errors of a five-axis machine tool based on thermocouple measurement data and axis positions. With the model, thermal errors caused by rotating the spindle and by moving the Z-axis of the machine tool are considered. Blazejewski [85] presents mathematical models representing power losses in tilting rotary table units with direct drive systems (Figure 2.12). The computation of the temperature distribution during heating up and the determination of resulting deviations are realized by FEM calculations. In [86], a FEM model of a swivelling axis is presented. The model uses the real axis movement to compute the temperature distribution in the structure for deriving design measures from the resulting deformation analysis.

2.3.3 Modelling of Thermal Errors of Linear Axes

Heat generated by ball screw drives and linear direct drives induces thermal errors in linear axis [87, 88].

The occurrence of these errors is either based on the temperature induced change of the length of the linear scale, or a thermal shift of the

An error source regarding drives with linear motors can be found in a temperature induced change of the length of the linear scale or a thermal shift of the encoder relative

to the machine tool bed. This effect strongly depends on the coefficient of expansion and the fixing point of the encoder which is described in [65]. Kim et al. [89] investigated a machine tool equipped with linear motors operating at high speed. By measurements and FEM calculations, he identified heat loss in the linear motor (LM), frictional heat from the LM block, and the cooling system for the linear motor as the dominating heat sources and sinks. With the model of the heat sources and measured temperatures the heat flux into the structure as well as the corresponding thermal errors of the NC-axes can be computed.

An experiment based model to predict thermally induced errors of a three-axis machine tool is introduced in [58, 90]. It is found that the increasing temperature of the ball screw nut during operation has the strongest impact on the thermal error of the NC axes. Based on the Bayersian network, tests have been classified. The mapping of temperature data with positioning errors has been carried out with a regression tool called "Support Vector machine Model (SVM).

Mayr et al. [91, 92] present a thermal equivalent circuit model of a ball screw. Measurements have shown that a major heat source on the analysed machine tool are the ball screws. The heat flows from the ball screw into the nut. A temperature rise of the nut due to this heat flux is prevented by the cooling of the nut. Thereby, the thermally induced error can be reduced, which is shown by simulations (Fig. 2.13).

In [68, 93], a FDEM model approach of a machine tool drivetrain is presented, which includes all losses and frictional forces for every machine element as input data. It is shown that the model is able to predict temperatures, losses and power consumption of the CNC axis for a given NC path.

2.3.4 Integrated Models of Thermal Errors

In [94], Brecher et al. describe that the interaction between several internal and external heat sources and sinks makes the calculation of the total thermal error very complex. They postulate that a superposition of the thermal errors of single assemblies like linear axes or the spindle to the overall thermal error is not possible. Integrated models described in [95] (Fig. 2.14) show this fact.

Heisel [96] designed a FEM model which considers the cutting process and the machine tool structure. The model computes the cutting forces, chip shape, chip size, temperature distribution, and thermal deformation of machine tool and workpiece, whereby no rotational axes are included in the model.

2.4 Reduction of Thermally Induced errors

In Fig. 2.2, the two basic strategies for thermo-elastic optimization of machine tools are shown: either the causes of the TCP-error can be minimized, or the TCP-error itself can be reduced by compensation. As written in [97], the correction can be based on internal signals of the NC regarding the compensation of occurring errors. An other method is described in [98], where auxiliary quantities like temperature sensors are used as reference input for the compensation. Both possibilities are considered in detail in this chapter.

Figure 2.13: According to [92], Figure a) shows a thermal equivalent circuit diagram of a ball screw system with R: thermal resistance, TA: ambient temperature, T: rolling element temperature b) computation results of TCP-displacements during three load cycles: a pendular movement with $3\,\mathrm{m/min}$, a pendular movement of $5\,\mathrm{m/min}$ and a cool-down phase. Simulation is carried out for three different cases: without nut-cooling and with two different cases of water-cooled ball-screw nuts to avoid a heat flux into the structure and therefor to prevent thermal errors: a moderate cooling cycle ("nut cooling 1") and a cooling cycle for heavily loaded ball screws ("nut cooling 2").
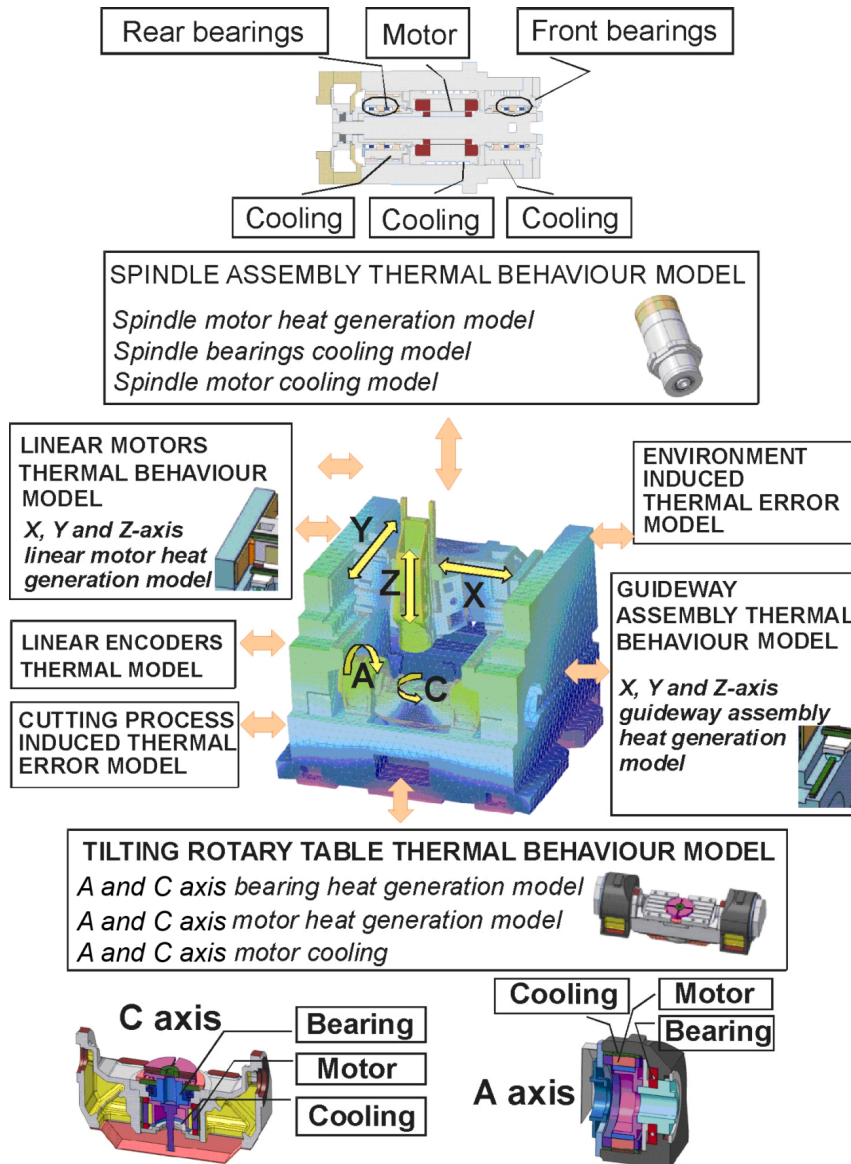
Figure 2.14: Integrated model of thermal behaviour of a five-axis machine tool [95].
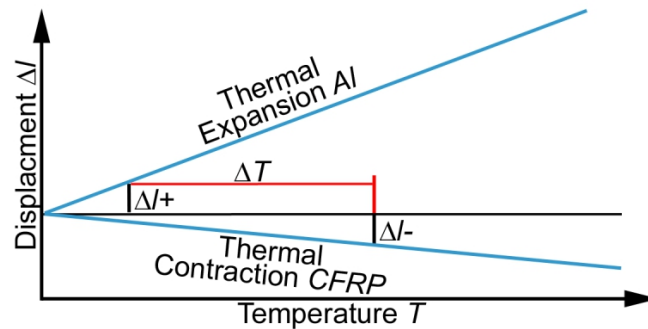
Figure 2.15: Alternative materials for compensation of thermal displacements, principle of contrarily expansion; Al = Aluminium (expansion with rising temperature), CFRP = Carbon fibre reinforced plastic (in this case: contraction with rising temperature) [101].

2.4.1 Minimization of Physical Causes

The mimimization of physical causes for thermally induced errros can basically be subdivided into the avoidance (e.g. design changes as described in [99]) and the reduction (e.g. active tempering as described in [100]) of physical causes.

An important issue regarding the design stage is to realise a thermo-optimized design. Topology and material optimization helps to reduce the impact of temperature changes on structural distortions. An example for the use of alternative materials to reduce thermal displacements is given in [101, 102]. Carbon fibre reinforced plastic (CFRP), can show a negative linear expansion coefficient depending on the orientation of the carbon fibres. It is used to compensate thermal displacements caused by materials like steel or aluminium, which have positive linear expansion coefficients (Figure 2.15).

Another example for the application of alternative materials to reduce thermal distortions is the use of polymer concrete for machine tool beds. As written in [103], a reduction 30% of thermal displacements is reached by casting in steel fixings for the linear guideways in the polymer concrete to improve heat conduction.

The influence of different coatings for machine tools is discussed in [104]. It is shown, that any coating influences the heat transfer, depending on the thickness of the coating, the coefficient of heat conductivity and the emission characteristics from the machine tool structure, to the environment significantly. In [105], the use of smart materials to reduce thermal errors is discussed. They enable to control the heat flux in the machine tool and homogenise the temporal distributed temperature field in the machine tool structure. Examples for implementations are

- additional heat capacities realized by phase-change materials (PCM) (e.g. paraffin);

- controllable heat conduction by shape memory alloys (SMA);

- controllable heat conduction by magneto-rheological fluids (MRF).

Regarding the avoidance and reduction of thermal loads, the most important design modification is to install dominating heat sources and sinks, such as motors, coolers and transmissions, more separated from the machine tool structure. Significant heat sources like drives, the nut of a ball screw drive or for example spindle bearings should be insulated from the structure. Then, by cooling, heat should be dissipated from these components before it flows into the rest of the structure.

The active tempering of the whole machine tool or single components can be realized by sprinkling, flow-through or a coolant reservoir. In [106], axial and angular deviations of a turning machine are reduced by heating.

Weber et al. [107] discuss the problem of the high energy consumption by active fluid power systems to temper tools and certain machine tool components. Using an optimised supply of coolant increases the efficiency of cooling the spindle unit and the tool.

With a knowledge base of the thermal behaviour of certain machine tool assemblies, derived from measurements or simulations, optimising design modifications are possible. Examples for a thermo-optimized design of precise machine tools are given by [108].

2.4.2 Compensation of Thermal Effects

In general, thermal deviations can be compensated by two different approaches [99, 109]: direct and indirect compensation. A direct compensation determines thermal caused TCP - errors by a measurement system. Indirect compensation identify the deviations by an auxiliary quantity like temperatures or an axis movement, This value is used as an input parameter for a model to compute the thermal error in order to be able to correct it [53]. Grossmann [110] distinguishes the indirect compensation into 3 phases:

- Phase 1: data acquisition;

- Phase 2: model update;

- Phase 3: axis correction.

During data acquisition, the auxiliary quantity is recorded with a time resolution depending on the time constants of the machine tool and the requirements regarding the data preparation. The model update can be carried out on a separate PC. For using the model parallel to the process, computation has to be faster than operation in real time. Nevertheless, the update cycle of the calculated distortions can be slow due to the slow change of thermal deviations. The axis correction with respect to the computed deviations is implemented in the NC, whereby the time resolution of the correction model depends on the axis feed rate.

Many models have been developed in order to compensate the thermal error by readjustment of the machine tools coordinate system [109, 111–116].

In [117, 118], CFRP structures are used for an active compensation of main spindle housings angular deviations as shown in Fig. 2.16. Thermal sensors, controllers and CFRP actuators enable a controlled heating of the CFRP laminate by heating filaments and Peltier elements. In [82], piezoelectric elements are used to compensate bending in a welded steel machine bed.
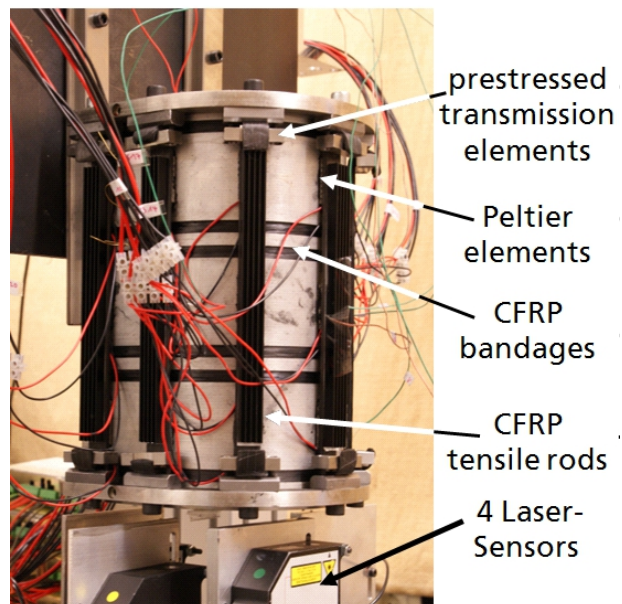
Figure 2.16: Active Compensation of a main spindle housing [117, 118].

3 Research Gap and Aim of the Work

In the past decades, a lot of research has been carried out with the goal to reduce thermal errors of machined parts. The majority of all effort was focused on the influence of the environment and the spindle, as the two main factors for thermally caused deviations of machine tools. Also the linear axes were analysed, and physical as well as phenomenological models to predict the behaviour of the described contributors respectively to generate compensation values regarding the described influences were developed.

Regarding rotary axes of 5-axis machine tools, the geometric and kinematic accuracy was in the focus of research for a long time. With an increasing geometric and kinematic accuracy of this type of machine tools, the thermal behaviour of rotary axes becomes more important: measurements show a magnitude of displacements induced by the rotary axes in the same range as errors induced by spindles, linear axes and the environment. This underlines the important of considerating this type of axis and of defining precise measurement procedures and efficient simulation models.

The aim of this work is to understand, model and compensate the thermal errors of rotary axes of five-axis machine tools. Figure 3.1 illustrates the planned procedure.
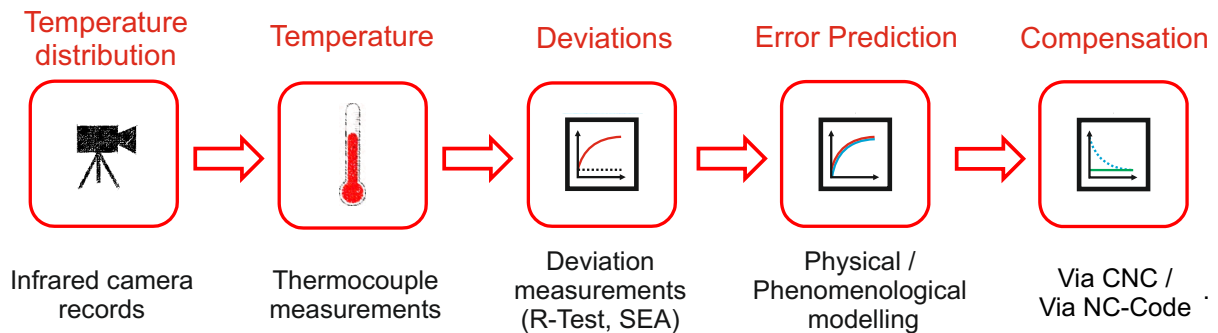

Figure 3.1: Sequence of analysing and compensating the thermal errors of rotary axes.

In a first step, a detailed analysis of the heat flux and the temperature distribution in the machine tool structure depending on the operating state and the load of the analysed axis is carried out. Therefore, comprehensive, systematic measurements of the temperature field in the machine tool structure are performed.

In a second step, thermally induced deviations are measured. Therefore, a usable measurement setup and strategy has to be designed. These measurements create knowledge on the sensitivity of the machine tools to the heat input by the rotary axes.

With the knowledge of the thermal behaviour, a model with a physical and a model with a phenomenological approach are developed. These models base on internal control

signals, to avoid the need for additional sensors or a monitoring system in the machine tool.

With the developed models, thermally induced errors of the rotary axes are minimised by a CNC- or a NC-Code - compensation for an arbitrarily chosen test cycle.

Summarized, the research gap can be described by

- Missing standards concerning the identification of thermally induced errors of rotary axes,

- Missing research results regarding the measurement and the behaviour of thermally induced errors of rotary axes, especially compared to other contributors to the total thermal error like spindles or linear axes,

- Missing compensation models for thermally induced errors of rotary axes.

Within scope of this thesis are

- Measurement and classification of all relevant contributors to the total thermal error of two different machine tools;

- Introduction of measurement devices and procedures for the measurement of thermally induced errors of rotary and swivelling axes;

- Physical and phenomenological modelling of thermal behaviour of rotary and swivelling axes;

- Compensation of relevant thermal errors induced by rotary and swivelling axes.

Out of scope of this thesis are

- Errors of rotary and sviveling axes induced by temperature fields of machine tool due to other energy sources than environment and moving rotary axes;

- Detailed analysis of thermally induced component errors of rotary and swivelling axes;

- Detailed analysis of influence of cooling lubricant and the heat dissipated in the cutting process;

- Consideration of process forces.

4 Thermal Characterisation of 5-Axis Machine Tools

Parts of this chapter are publishedThe main object of this thesis is the characterisation of the thermal behaviour of five-axis machine tools including the simulation and compensation of identified location errors with focus on rotary axes. In order to assess the contribution of the rotary axes to the total thermal error of a machine tool, all other relevant contributors like the environment, the spindle and the linear axes have been analysed. In the following chapter, measurement devices and methods as well as measurement results are presented.

The chapter is complemented by Appendix A which describes the measurement uncertainty of the R-Test device.

The measurements have been carried out on two different five-axis machine tools. Their kinematic setting is shown in Figure 4.1 and described in Table 4.1 according to ISO / DIS 10791-1:2013 [119]. Due to the different kinematic setup of the rotary- / swivelling table unit, in the following thesis, these machine tools are named **Machine tool B/C** and **Machine tool A/C**.

Some part of the following content has been published by the author in [120–127].

4.1 Devices and Methods for Identification of Temperatures and Thermally Induced Deviations

For the thermal characterisation of machine tools, measurements of thermally caused deviations as well as measurements of significant temperatures such as temperature of the environment, drives or parts of the structure of the machine tool are necessary. The following chapter describes measurement devices, methods and procedures, which are used in this thesis.

Table 4.1: Kinematic setup of both analysed five-axis machine tools according to ISO / DIS 10791-1:2013 [119].

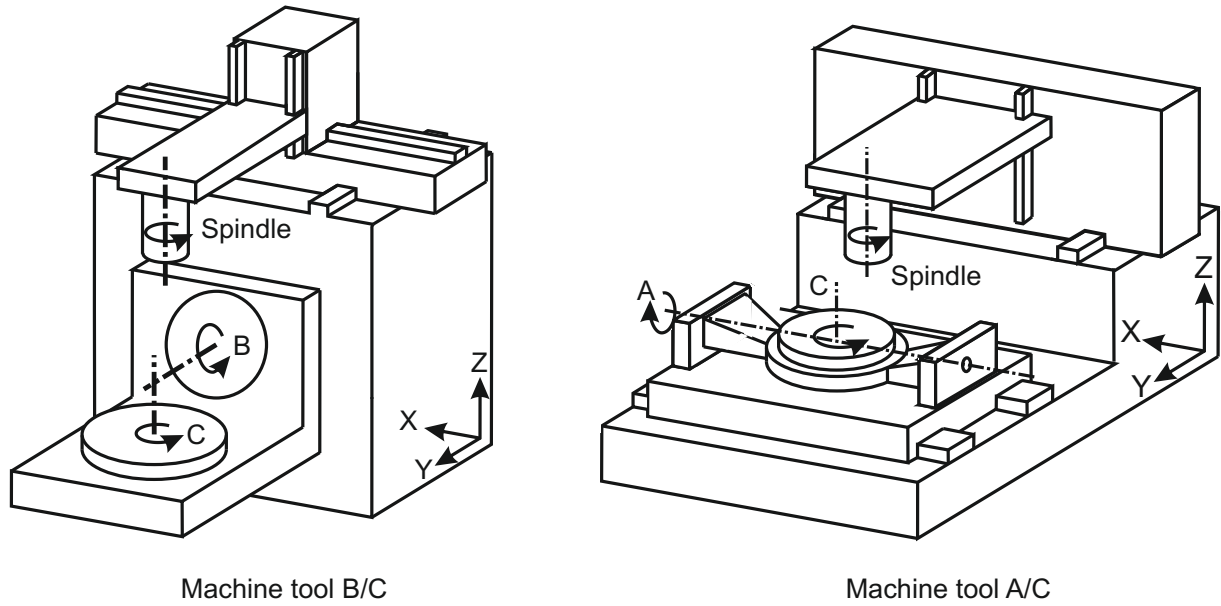|	
Machine tool "B/C"	*V [w C2' B' b[Y1 Y2] X [Z1 Z2] (C1) t]*
Machine tool "A/C"	*V [w C2' A' X' b Y X Z (C1) t]*

Figure 4.1: Schematic draft of both analysed machine tools.

4.1.1 Measurement of Temperatures

In order to get a qualitative overview of the temperature distribution and the heat flux in the structure of the analysed machine tools, measurements with an infrared camera (Table 4.2, *System* 1) are carried out. Due to the high reflectivity of machined metal surfaces for infrared radiation, thin crepe tape with a high emissivity is used to prepare these surfaces in order to decrease reflectivity according to [16]. For more accurate temperature measurements of single points or the environment, three different measurement systems are used depending on the measurement task (Table 4.2, *Systems* $2-4$). The resistance thermometer Hygrosens TLOG USB20 is used for long time measurements on drives, structural parts and the environment. The 16 channel thermocouple sensor system NI 9214 (National Instruments) is used for measurements of selected machine tool parts like machine tables, where a small inertia of the sensor and a good thermal conductivity between surface and sensor is important. Finally, the single channel thermocouple sensor NI USB-TC01 (National Instruments) is used for environmental temperature measurements during compensation experiments.

During the measurements of thermally induced errors under several load cycles, the temperature of all significant machine tool components are recorded. Examples for measurement points are drives, parts of the axis structures, bearings, cooling units and the environment. Sensors on the machine tool structure are attached with a special thermal ceramic paste to ensure heat conduction between sensor and surface. Reliable temperature measurements of rotating machine parts like a machine tool table are difficult to carry out: temperature loggers are a wireless solution, but most systems show an insufficient resolution, storage capacity for long-time measurements and accuracy. Additionally, there is no possibility for an on-line evaluation, when using these systems.

A second challenge is the fixation, which has to resist high rotary speeds and also even cooling lubricant. For this, a temperature measurement device based on the 16 channel

Table 4.2: Properties of the measurement systems used for temperature measurements.

|	System 1	System 2	System 3	System 4
Type	Infrared camera	Resistance thermometer	Thermocouple sensor	Thermocouple sensor
Model	Jenaoptik VarioTHERM head II	Hygrosens TLOG-USB20	National Instruments NI 9214	National Instruments NI USB-TC01
Meas. range	$-25°C$ – $1200°C$	$-55°C$ – $125°C$	Depending on type of thermoelement	Depending on type of thermoelement
Accuracy	$\pm 2.0K$, $\pm 2.0\%$ of operating range	$\pm 0.5°C$	$\pm 0.3°C$ + accuracy of thermocouple	$\pm 0.75\%$ of measured value
Channels	256x256 pixel	20	16	1
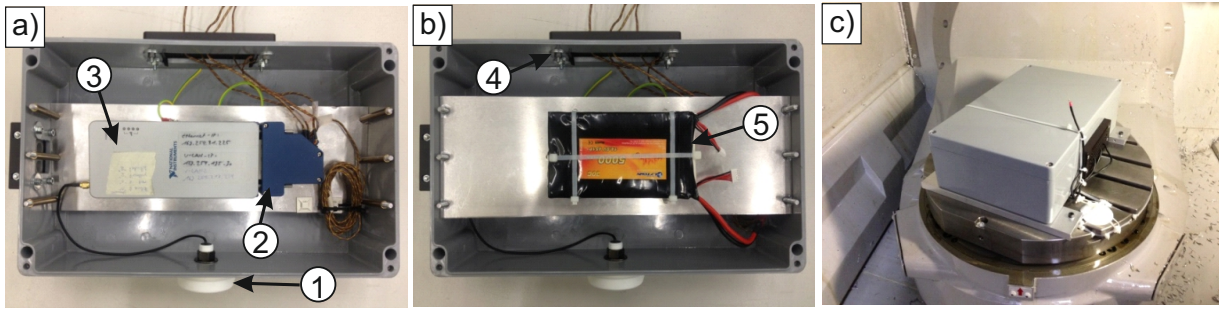
Figure 4.2: Temperature measurement system with wireless data transmission for measurements on rotating machine tool tables: 1 = external Wireless Fidelity (WiFi) antenna, 2 = measuring board, 3 = Wi-Fi module (Figure (a)), 4 = IP65 [128] channel for sensors, 5 = battery pack (Figure (b)); Measurement system during operation (Figure (c)).

National Instruments NI-9214 measuring board was designed (Figure 4.2, System 3 in Table 4.2). The system is powered by a battery pack. Measurement data are transmitted on-line via Wi-Fi. The housing provides protection class *IP65* [128]. The whole device was tested for rotational speeds up to 600 min^{-1} for a measurement duration of 24 h.

4.1.2 Measurement of Displacements

Temperature changes of the environment as well as internal heat sources and sinks cause transient and spatial temperature changes of the machine tool structure that lead to location and component errors of the machine tool axes. These displacements are measured with two different setups: the ISO 230-3 [21] and the R-Test setup. Their use depends on the application. The following section describes the measurement devices, procedures and the corresponding errors that were measured.
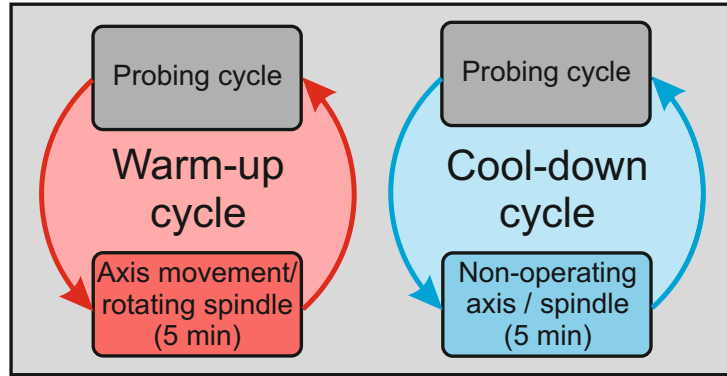
Figure 4.3: Standard test cycle for thermal measurements: four hours warm-up period, four hours cool-down period. Location error measurements are carried out with a time gap of five minutes between the end of one measurement cycle and the start of the next measurement cycle. Test cycles deviating from the standard test cycle are described separately.

Table 4.3: Type and main characteristics of HEIDENHAIN probes for the measurement with ISO 230-3 setup.

Model code	MT 1281	MT 1287
Measurement	ETVE	Spindle, Linear axes
Actuation	test object	pneumatically
Measuring range	12 mm	12 mm
Accuracy of sensor	$\pm 0.2 \mu m$	$\pm 0.2 \mu m$

Measurements according to ISO 230-3

As described in section 2.1.3, ISO 230-3 provides a setup for measurement of translational and rotational deviations caused by the environment, the main spindle or linear axes (Figure 2.6). All measurements according to ISO 230-3 are carried out with linear displacement sensors of HEIDENHAIN according to Table 4.3 unless otherwise specified. Measurements regarding the influence of linear axes and the main spindle consist of a warm-up and a cool-down cycle (Figure 4.3). During warm-up, probing cycles are carried out with a time gap of five minutes between the end of one cycle and the start of the next cycle. During warm-up, heat is brought into the system for five minutes by a certain load cycle. This is realized by different spindle speeds respectively certain axis feed rates. This procedure is repeated for at least four hours or till a steady state is reached. All measurements are carried out under no load conditions and except measurements described in section 4.2.3 without cooling lubricant.
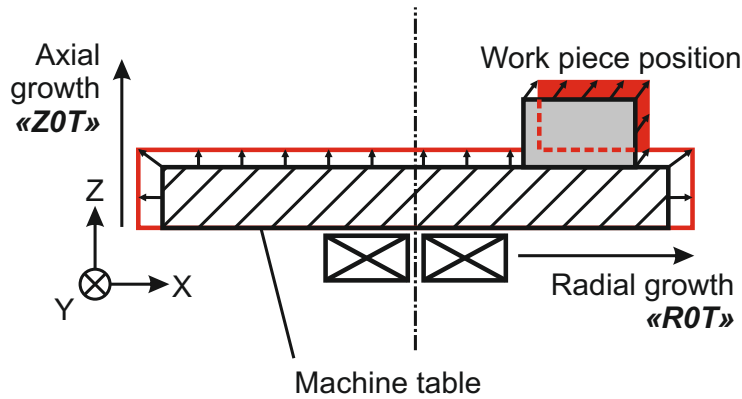
Figure 4.4: Functional surfaces like a machine tool table show additional location and size errors compared to the errors described in ISO 230-1: example shows axial growth ($Z0T$) and change of radius ($R0T$) of the machine tool table [122].
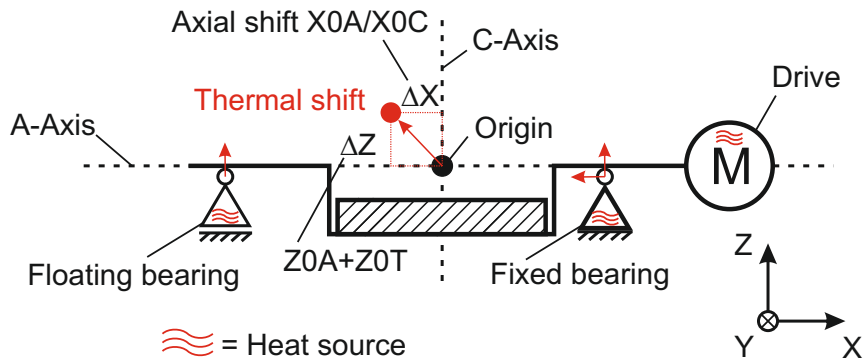

Figure 4.5: An example for an additional error of a horizontal, swivelling table is the axial shift. The shift in Z-direction is already covered by ISO 230-7.

Measuring the location errors of a rotary axis

In ISO 230-1 [24], five location errors of a rotary axis are defined according to Figure 2.3. In addition to these errors, when thermal location errors are to be considered, a machine tool shows additional displacements caused by its rotary axes depending on the kinematic setup of the machine tool. Figure 4.4 shows the axial and radial growth of a machine tool table (C-axis) due to temperature changes in the axis / table structure. The reference for both deviations is the functional surface "*table*". The radius error is named $R0T$, the axial growth is described as $Z0T$. Both parameters show a significant, temperature depending behaviour but are not included in any standard yet. A similar example is given by Figure 4.5, which shows a horizontal, swivelling axis (A-axis of **Machine tool A/C**). The axis has a fixed bearing at the side of the drive, and a floating bearing at the opposite side. Depending on the load cycle, heat is brought into the structure by the axis drive, and the two bearings. This heat flux leads, among other effects, to an axial shift of any functional surface in X-direction which is not defined in ISO 230-1. One possibility to tag this location error would be $X0T$, where T is again the functional surface "*table*" mounted on the A-Axis. If there is a C-axis mounted on the A-Axis like it is described in Figure 4.5, it is $X0C$.

A very suitable device to measure these errors is the R-Test setup [50] (section 2.2.2)

which is used for the determination of thermally induced location errors of rotary axes in this thesis. For the thermal characterisation of vertical and horizontal axes, the R-Test set-up is used in two different applications: *"R-Test discrete"* and *"continuous R-Test"*.

Before using the R-Test, a transformation measurement has to be carried out to transform probe signals to movements in the machine tool coordinate system. In this thesis, the transformation procedure always is carried out by doing a relative movement of $\pm$ 2 mm between tool and workpiece in each axis direction X, Y, and Z. Every final position (-2 or 2 mm) is reached from the same direction to avoid an influence by any reversal errors of the axis. Based on this movement, a transformation matrix is calculated which is used to transform the probe signals during the subsequent measurements into a relative movement between spindle and workpiece in the machine coordinate system.

For the example of a measurement with four sensors, (4.1) shows the relation between the matrix $\underline{\underline{D}}$ containing the nominal displacements, the transformation matrix $\underline{\underline{T}}$ and the matrix with the values measured during the transformation procedure $\underline{\underline{M}}$:

$$\underline{\underline{M}} \cdot \underline{\underline{T}} = \underline{\underline{D}} \tag{4.1}$$

With the nominal displacements d_{ij} for $i = 6$ plateaus of $|d| = 2$ mm and $j = 3$ axis directions X, Y and Z, and the measurement results m_{ik} representing the mean value of the sensor k at the plateau number i, the equation used for calibration with $i = 4$ sensors and $j = 6$ plateaus can be described by

$$\begin{bmatrix} m_{11} & m_{12} & m_{13} & m_{14} \\ m_{21} & m_{22} & m_{23} & m_{24} \\ m_{31} & m_{32} & m_{33} & m_{34} \\ m_{41} & m_{42} & m_{43} & m_{44} \\ m_{51} & m_{52} & m_{53} & m_{54} \\ m_{61} & m_{62} & m_{63} & m_{64} \end{bmatrix} \cdot \begin{bmatrix} t_{11} & t_{12} & t_{13} \\ t_{21} & t_{22} & t_{23} \\ t_{31} & t_{32} & t_{33} \end{bmatrix} = \begin{bmatrix} -2 & 0 & 0 \\ 2 & 0 & 0 \\ 0 & -2 & 0 \\ 0 & 2 & 0 \\ 0 & 0 & -2 \\ 0 & 0 & 2 \end{bmatrix} \tag{4.2}$$

Equation (4.2) is solved via least squares by

$$\underline{\underline{T}} = (\underline{\underline{M}}^T \underline{\underline{M}})^{-1} \underline{\underline{M}}^T \underline{\underline{D}} \tag{4.3}$$

In addition to the calibration procedure, the location of the measurement system in relation to the analyzed axis of the machine tool has to be known. This can be read-out of the CNC.

Vertical axes: R-Test discrete
Significant parts of this chapter have been presented in [129].

An example for the use of the discrete R-Test on a vertical C-axis (table of a five-axis machine tool) is given in Figure 4.6. Three probes are mounted in a probe holder tripod like geometry to have 3 independent coordinates. The tripod is then fixed in the spindle. The spindles rotational position is locked during measurements to avoid influences due to rotational movements of the sphere. A precision sphere is eccentrically mounted with
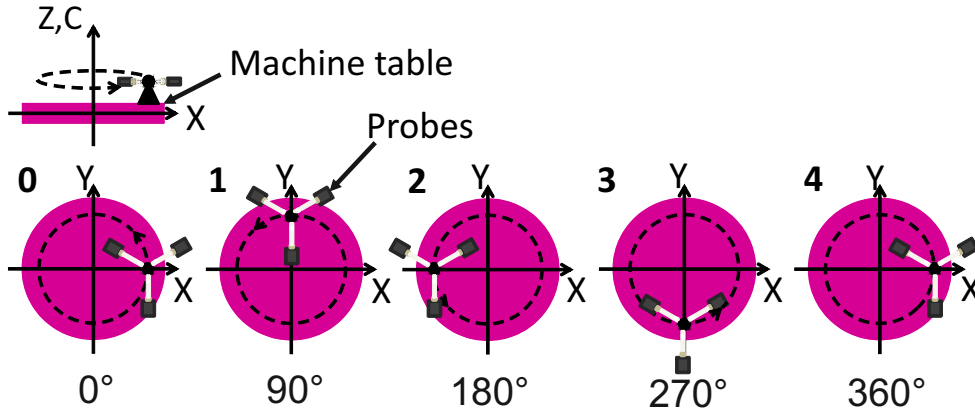
Figure 4.6: "R-Test discrete": 5 measurements are carried out at $90°$, $180°$, $270°$ and $360°$. The TCP movement is realized by a rotation of the analysed axis of rotation (e.g. C) in combination with a movement of the linear axes (e.g. X, Y) [120].

radius r to the vertical table axis on the machine tool table. This sphere is firstly positioned at the nominal position $p_{nom_1} = 0°$. The probes mounted in the spindle and the precision sphere are brought in contact at the actual position $p_{act_1} = 0°$ which is set to zero as a reference. Afterwards, the analysed axis is rotated by $90°$, the three probes in the spindle are positioned at the sphere (position p_{nom_2}) and the actual position of the sphere p_{act_2} is measured. This procedure is carried out for $k = 5$ nominal positions

$$p_{nom_k} = \begin{pmatrix} x_{nom_k} \\ y_{nom_k} \\ z_{nom_k} \end{pmatrix} \tag{4.4}$$

where x_{nom_k}, y_{nom_k} and z_{nom_k} are the coordinates of the nominal center of the sphere.

In order to avoid start / stop effects, no measurement is carried out directly after starting or stopping the axis. By averaging the recorded values over the effective measurement time $\Delta t_{avg} = 1$ s, vibration effects are eliminated. On the machine tool under test, at every nominal position $\{p_{nom_k}\}$ data are recorded with a sampling rate of 100 Hz for three seconds. The effective measurement time $\Delta t_{avg} = 1$ s, because the first and the last second is deleted in order to omit dynamic effects. x_{act_k}, y_{act_k} and z_{act_k} are the actual coordinates of the sphere centre known by the transformation procedure and the axes positions read-out of the CNC. They are described by

$$p_{act_k} = \begin{pmatrix} x_{act_k} \\ y_{act_k} \\ z_{act_k} \end{pmatrix} \tag{4.5}$$

To analyse the thermal behaviour of an axis over a certain period, the measurement procedure is carried out i times with a time gap Δt_g between the end of one measurement and the start of the next measurement. In this work, a time gap $\Delta t_g = 5$ min is chosen for all measurements unless otherwise specified. This delivers a matrix of measurement values
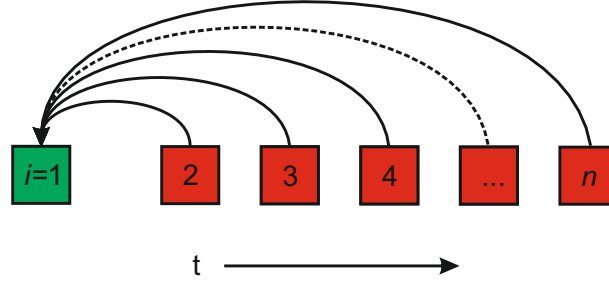
Figure 4.7: All R-Test measurements are related to the first R-Test which is set as zero reference point.

where the second index identifies the time step number

$$
\underline{\underline{P}}_{act_{i,k}} =
\begin{bmatrix}
\underline{p}_{act_{1,1}} & \underline{p}_{act_{2,1}} & \cdots & \underline{p}_{act_{i,1}} \\
\underline{p}_{act_{1,2}} & \underline{p}_{act_{2,2}} & \cdots & \underline{p}_{act_{i,2}} \\
\vdots & \vdots & \ddots & \vdots \\
\underline{p}_{act_{1,5}} & \underline{p}_{act_{2,5}} & \cdots & \underline{p}_{act_{i,5}}
\end{bmatrix}
\tag{4.6}
$$

The redundant measurement of the point $p_{nom_1} = p_{nom_5}$, gives an information about the repeatability of the measurement. For evaluation of the thermal errors it is not needed. The matrix reduces, with the measuring data necessary for evaluation of all thermal errors for a single measurement cycle i to

$$
\underline{\underline{P}}_{act_{i,k}} =
\begin{bmatrix}
\underline{p}_{act_{1,1}} & \underline{p}_{act_{2,1}} & \cdots & \underline{p}_{act_{i,1}} \\
\underline{p}_{act_{1,2}} & \underline{p}_{act_{2,2}} & \cdots & \underline{p}_{act_{i,2}} \\
\underline{p}_{act_{1,3}} & \underline{p}_{act_{2,3}} & \cdots & \underline{p}_{act_{i,3}} \\
\underline{p}_{act_{1,4}} & \underline{p}_{act_{2,4}} & \cdots & \underline{p}_{act_{i,4}}
\end{bmatrix}
\tag{4.7}
$$

In order to consider only the thermal effects, the geometric errors of the analysed axis are mathematically eliminated by subtracting a first measurement ($i = 1$), which is set as zero reference point for the following measurements ($i = 2...k$) (Figure 4.7).

For the example shown in Figure 4.6, the following relations for the axis errors can be derived according to Figure 4.8: the 3 translational deviations of the ith measurement $X0C_i$, $Y0C_i$ and $Z0T_i$ can be obtained for i measurements by

$$
X0C_i = \frac{1}{4}\sum_{k=1}^{4}\underline{p}_{act_{i,k}}\underline{e}_x - \frac{1}{4}\sum_{k=1}^{4}\underline{p}_{act_{1,k}}\underline{e}_x
\tag{4.8}
$$

$$
Y0C_i = \frac{1}{4}\sum_{k=1}^{4}\underline{p}_{act_{i,k}}\underline{e}_y - \frac{1}{4}\sum_{k=1}^{4}\underline{p}_{act_{1,k}}\underline{e}_y
\tag{4.9}
$$

$$
Z0T_i = \frac{1}{4}\sum_{k=1}^{4}\underline{p}_{act_{i,k}}\underline{e}_z - \frac{1}{4}\sum_{k=1}^{4}\underline{p}_{act_{1,k}}\underline{e}_z
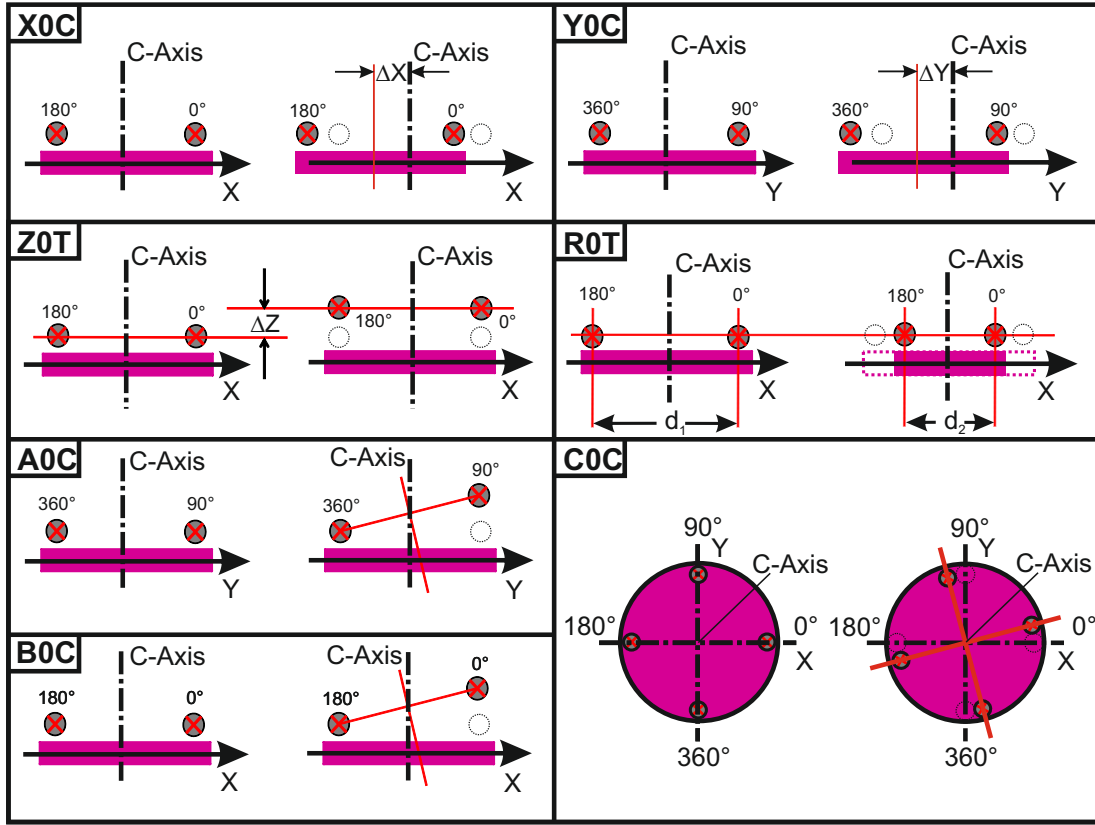\tag{4.10}
$$

Figure 4.8: R-Test discrete: Evaluation schemes for the errors of a vertical C-axis table.

Depending on the offset $\frac{d}{2}$ of the sphere centre relative to the rotary axis, the two squareness errors $A0C$ and $B0C$ can be obtained via

$$A0C_i = \frac{1}{d}(\underline{p}_{act_{i,1}}\underline{e}_z - \underline{p}_{act_{i,3}}\underline{e}_z) - \frac{1}{d}(\underline{p}_{act_{1,1}}\underline{e}_z - \underline{p}_{act_{1,3}}\underline{e}_z) \tag{4.11}$$

$$B0C_i = \frac{1}{d}(\underline{p}_{act_{i,2}}\underline{e}_z - \underline{p}_{act_{i,4}}\underline{e}_z) - \frac{1}{d}(\underline{p}_{act_{1,2}}\underline{e}_z - \underline{p}_{act_{1,4}}\underline{e}_z) \tag{4.12}$$

The deviation of the zero angle $C0C$ for measurement i is

$$
\begin{aligned}
C0C_i = {} & \frac{1}{2d}(\underline{p}_{act_{i,3}}\underline{e}_x + \underline{p}_{act_{i,4}}\underline{e}_y - \underline{p}_{act_{i,1}}\underline{e}_x - \underline{p}_{act_{i,2}}\underline{e}_y) \\
& - \frac{1}{2d}(\underline{p}_{act_{1,3}}\underline{e}_x + \underline{p}_{act_{1,4}}\underline{e}_y - \underline{p}_{act_{1,1}}\underline{e}_x - \underline{p}_{act_{1,2}}\underline{e}_y)
\end{aligned}
\tag{4.13}
$$

The radius error of the machine tool table at the measurement position (distance $\frac{d}{2}$ to the axis) is calculated according to

$$
\begin{aligned}
R0T_i = {} & \frac{1}{4}(\underline{p}_{act_{i,1}}\underline{e}_y + \underline{p}_{act_{i,2}}\underline{e}_x - \underline{p}_{act_{i,3}}\underline{e}_y - \underline{p}_{act_{i,4}}\underline{e}_x) \\
& - \frac{1}{4}(\underline{p}_{act_{1,1}}\underline{e}_y + \underline{p}_{act_{1,2}}\underline{e}_x - \underline{p}_{act_{1,3}}\underline{e}_y - \underline{p}_{act_{1,4}}\underline{e}_x)
\end{aligned}
\tag{4.14}
$$

It is necessary to measure in four positions during a 360°-movement, in order to be able to evaluate all errors. The mounting side of the precision sphere (spindle or table side)
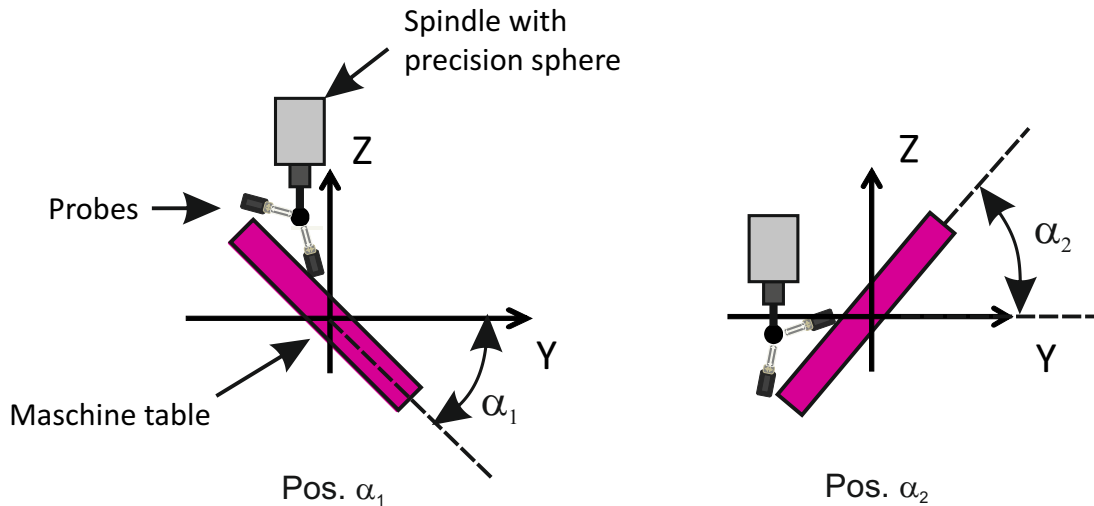
Figure 4.9: Continuous R-Test for an interpolation of $Y-$, $Z-$ and $A-$axis. Machine table is swivelling from Pos α_1 to Pos. α_2, while the spindle with the precision sphere follows the TCP by a Y- and Z-axis movement.

does not matter and can be chosen in a way that the execution of the measurement is more practical. The position of the starting point can be chosen arbitrarily, as long as it is considered that the radius r is large enough.

The advantage of the *R-Test discrete* - sequence compared to a continuing movement is a shorter measuring time during which the machine is subjected to cool down. The disadvantage is, that an angular range of 360° is necessary to compute all thermally induced errors of a rotary axes. With the continuous R-Test, much more measurement points for evaluation are recorded. Therefore, a smaller angular range can be used.

Horizontal axes: continous R-Test
Significant parts of this chapter have been presented in [130].

For the R-Test discrete, a total measurement range of 360° is necessary. When the kinematic axis structure of the analysed machine tool inhibits to measure the horizontal axis with the *R-Test discrete* because of a restricted swivelling angle $< 360°$, the *continuous R-Test* is chosen to determine the thermal errors. The basic measurement procedure is shown in Figure 4.9 for a B-axis. The measuring frame of the R-Test is mounted on the table. The precision sphere is clamped in the spindle. The spindles rotational position is locked during measurements to avoid influences due to rotational movements of the sphere.

Sphere and probes in the tripod like measuring frame are brought in contact at the starting angle α_1, which is one end position of the total swivelling range. After three seconds of standstill, the swivelling axis is tilted to the second position α_2. During all measurements in this thesis, an angular feed speed v_{rot} of 600°/min is chosen in order to avoid dynamic effects but keep the duration of the probing cycle short. After keeping the axis at the angle α_2 for three seconds, the backlash of the axes is cancelled by moving it incrementally 0.1° over the position of α_2. Afterwards it is moved back to the point $\alpha = \alpha_2$. After that, the axis is kept once more in standstill for three seconds. Finally, the axis is swivelled back to α_1 with an angular feed rate $v_{rot} = 600°/\text{min}$. During the entire
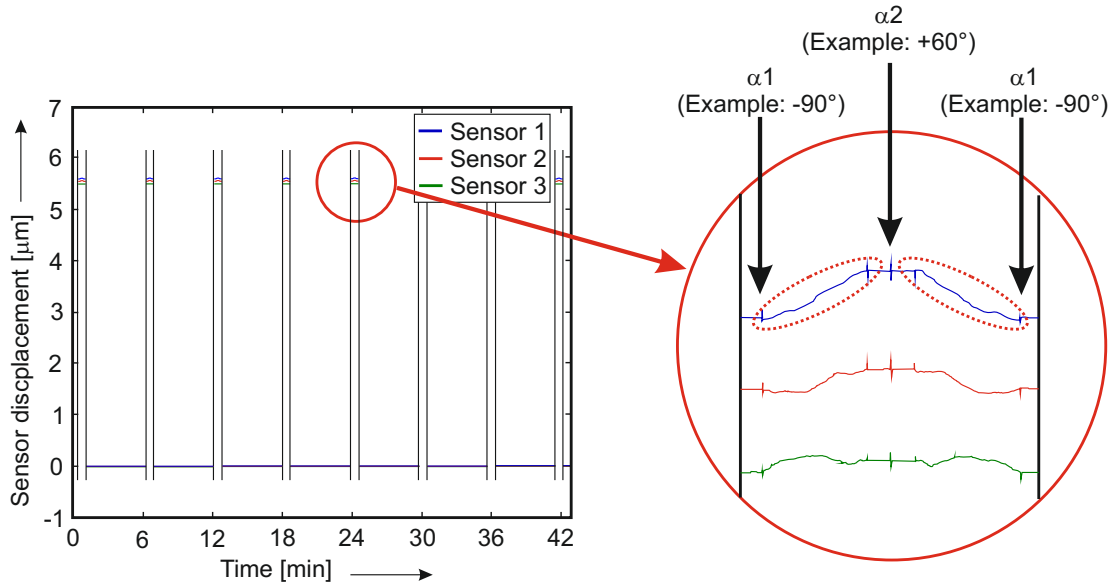
Figure 4.10: Evaluation of continuous R-Test when moving a horizontal axis. Left: eight R-Tests with a time gap of five minutes between the end of one measurement and the start of the next measurement. Right: Three probe signal during interpolation movement from $\alpha_1 = -90°$ to $\alpha_2 = +60°$ and back.

measurement, the precision sphere and the mounted probes are moved simultaneously. To avoid backlash, axes are always approaching the measurement position from the same direction.

The measurement frequency f_{mes}, the offset of the precision sphere to the axis r and the rotation speed v_{rot} define the number of available measurement points n_{MP} for calculating the axis location and orientation errors according to

$$n_{MP} = \frac{\alpha_{tot}}{v_{rot}} \cdot f_{mes} \tag{4.15}$$

Figure 4.10 shows the raw data of eight continuous R-Tests with a measurement duration of 42 minutes with a five minutes gap between the end of every R-Test and the start of the next R-Test. By a suitable triggering procedure, the axis positions of the R-Tests, where the interpolation procedure of a rotary A-axis, a linear Y- and a linear Z-axes was recorded with three sensors, can be extracted and processed afterwards with the calibration data of the system. The single R-Test records can be illustrated in the machine tool coordinate system (MCS, Figure 4.11)

The evaluation of the continuous R-Test measurement is explained by means of the measurement setup of the A-axis in Figure 4.9. For every measurement cycle i, q measurement points $\underline{r}_{act_{p,i}}$ with the coordinates

$$\underline{r}_{act_{p,i}} = \begin{pmatrix} x_{act_p} \\ y_{act_p} \\ z_{act_p} \end{pmatrix}_i, \qquad p \in 1...q \tag{4.16}$$

are recorded. In Fig. 4.11, all measurement points for one complete continuous R-Test sequence with a total measurement angle of 150° are shown. The black curve illustrates
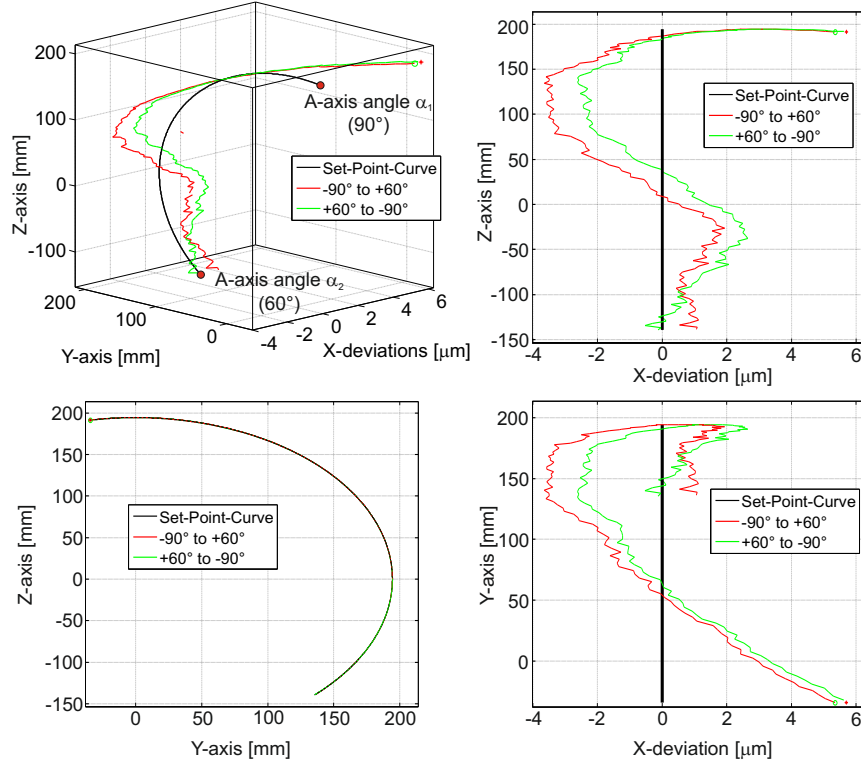
Figure 4.11: 3D - plot of one R-Test sequence according to the example of Figure 4.9.

the nominal circle section, the red curve represents the first section from $\alpha_1 = -90°$ to $\alpha_2 = 60°$ and the green curve represents the second movement from $\alpha_2 = 60°$ to $\alpha_1 = -90°$. In the following section, the R-Test evaluation is explained for one measurement sequence i. Based on the Hesse normal form of the planar equation

$$n_1 \cdot x + n_2 \cdot y + n_3 \cdot z - 1 = 0 \tag{4.17}$$

with the distance d_p from every measuring point r_{act_p} of the point cloud to a given plane can be calculated according to

$$d_p = n_1 \cdot x + n_2 \cdot y + n_3 \cdot z - 1 \tag{4.18}$$

The parameters n_1, n_2 and n_3 have to be chosen in a way that the square sum of the distances d_p for all q points to the fit plane to be searched is minimized according to

$$S_i = \sum_{p=1}^{q} d_{p,i}^2 \tag{4.19}$$

Zero setting of the partial derivatives

$$\frac{\partial S_i}{\partial n_1} = 0, \frac{\partial S_i}{\partial n_2} = 0, \frac{\partial S_i}{\partial n_3} = 0 \tag{4.20}$$

delivers an explicit result for n_1, n_2 and n_3 which is equivalent to the components of the normal vector of the fit plane. The angles between this normal vector and the normal vector of the initial uninclined plane ($x = 0$) can be calculated via

$$B_i = \beta_i = atan(\frac{n_2}{n_3}) \tag{4.21}$$

and

$$C_i = \gamma_i = atan(\frac{n_1}{n_3}) \tag{4.22}$$

β and γ are representing the orientation errors around $B-$ and $C - direction$ of the analysed rotary axes (A). These two angles enable the determination of the rotation matrix $\underline{\underline{R_i}}$ according to

$$\underline{\underline{R_i}} = \begin{bmatrix} cos(-\gamma_i) & 0 & sin(-\gamma_i) \\ sin(-\gamma_i)sin(-\gamma_i) & cos(-\beta_i) & -cos(-\gamma_i)sin(-\beta_i) \\ cos(-\beta_i)sin(-\gamma_i) & sin(-\beta_i) & cos(-\beta_i)cos(-\gamma_i) \end{bmatrix} \tag{4.23}$$

With $\underline{\underline{R_i}}$, the cloud of measuring points can be rotated in the best fit plane for every measurement i which delivers new measuring points

$$\underline{r}_{p,r_i} = \begin{pmatrix} y_{p_r} \\ z_{p_r} \\ x_{p_r} \end{pmatrix}_i = \underline{\underline{R_i}} \begin{pmatrix} y_{act_p} \\ z_{act_p} \\ x_{act_p} \end{pmatrix}_i \tag{4.24}$$

where the index r indicates that the measurement points have been rotated.

Based on these measurement points, the center of a best fit circle can be calculated based on the algorithm of Bucher [131] with

$$\begin{bmatrix} y_{r1} & z_{r1} & 1 \\ \vdots & \vdots & \vdots \\ y_{rn} & z_{rn} & 1 \end{bmatrix}_i = - \left(\begin{pmatrix} y_{r1}^2 \\ \vdots \\ y_{rn}^2 \end{pmatrix} + \begin{pmatrix} z_{r1}^2 \\ \vdots \\ z_{rn}^2 \end{pmatrix} \right) \cdot \underline{s}_i \tag{4.25}$$

By solving (4.25) with the Gaussian elimination method, the vector

$$\underline{s} = \begin{pmatrix} s_1 \\ s_2 \\ s_3 \end{pmatrix} \tag{4.26}$$

can be computed. It delivers the parameters s_1 and s_2 which can be used to calculate the centre coordinates in the machine tools coordinate system of the best fit circle y_{rm} and z_{rm} according to

$$y_{rm_i} = -\frac{1}{2} \cdot s_{1_i} \qquad with \ i = 1...q \tag{4.27}$$

$$z_{rm_i} = -\frac{1}{2} \cdot s_{2_i} \qquad with \ i = 1...q \tag{4.28}$$

With the parameter s_3, the radius of the index circle can be calculated, which is not necessary for the evaluation of the thermal shift.

This procedure delivers for every measurement i a new circle centrer in the machine coordinate system. Its change represents the thermally caused shift of the A-axis in Y- and Z-direction. As described in Figure 4.7, the first measurement $i = 1$ is subtracted from all other measurements in order to eliminate the geometric errors ((4.29) to (4.33)).
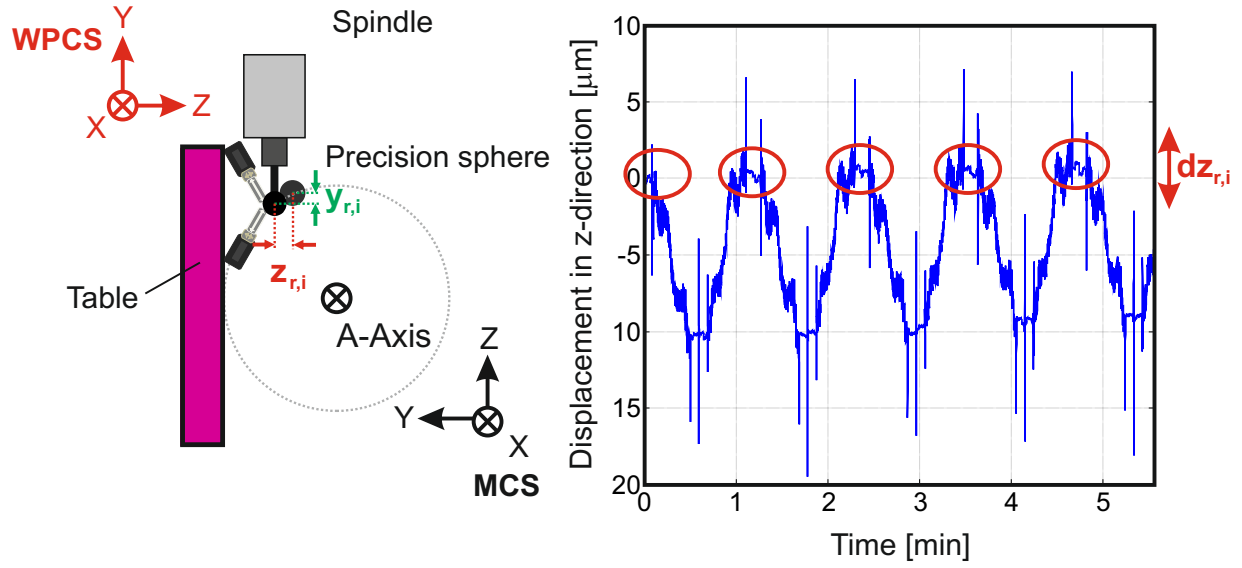
Figure 4.12: Determination of the TCP-shift in Z-direction (MCS) is necessary for the calculation of $A0A$.

With the circle centre parameters y_{rm} and z_{rm} and the orientation angles β and γ, the four location errors $Y0A$, $Z0A$, $B0A$ and $C0A$ can be evaluated according to

$$Y0A_i = y_{rm_i} - y_{rm_{i=1}} \tag{4.29}$$

$$Z0A_i = z_{rm_i} - z_{rm_{i=1}} \tag{4.30}$$

$$B0A_i = (\beta_i - \beta_{i=1}) \cdot \xi \tag{4.31}$$

$$C0A_i = (\gamma_i - \gamma_{i=1}) \cdot \xi \tag{4.32}$$

where

$$\xi = 4.848 \cdot (\frac{360}{2 \cdot \pi} \cdot 3600) \tag{4.33}$$

is a factor to convert the rotational deviations $B0A$ and $C0A$ from radian measure to the unit $\frac{\mu m}{m}$.

When the continuous R-Test is carried-out in order to identify the geometric errors of rotary axes, the angular positioning error $A0A$ is not considered because there is no reference point for its deviation. This is different regarding the thermally caused change of $A0A$. The first of several consecutively carried out R-Test measurements can be used as a reference measurement which enables the computation of the angular positioning error with the subsequent measurements. On the left side of Fig. 4.12, the swivelling axis unit with the R-Test nest (red coloured coordinate system = work piece coordinate system, WPCS) and the precision sphere can be seen at an axis position of 90° (black coloured coordinate system = machine tool coordinate system, MCS). The precision sphere shifts due to the thermal influence in Y- and Z-direction of the R-Test coordinate system. In order to determine this thermal shift, the plateaus of the measurement data during standstill at the beginning of each measurement cycle i (red circles in right side of Fig. 4.12) are
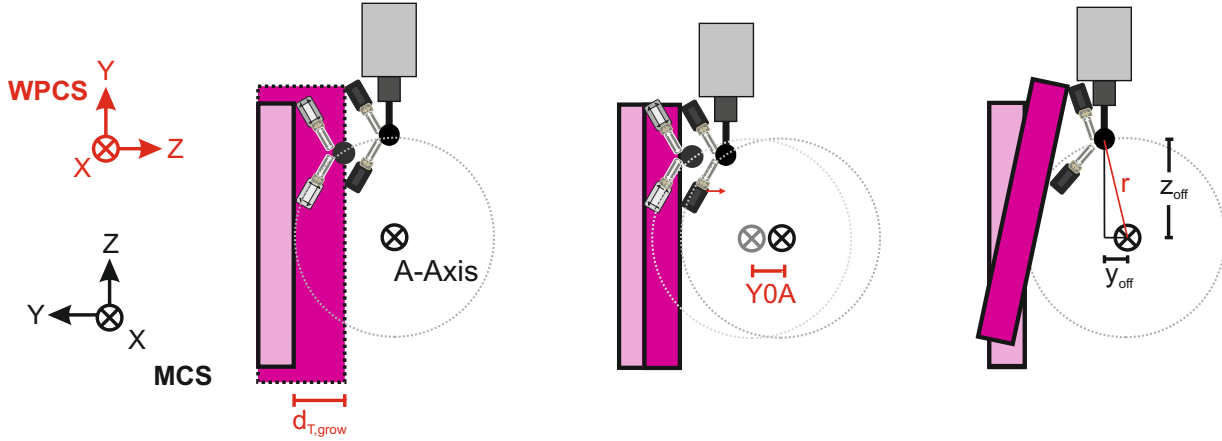
Figure 4.13: Contributors to the displacement of the precision sphere. WPCS: Work piece coordinate system, MCS: Machine tool coordinate system. z_{off} and y_{off} can be read out of the CNC.

detected. Dynamic effects at the beginning and the end of each plateau are omitted. In this thesis, each plateau has a length of 3s. The first and the third second are cut-off. The measurement values recorded during the middle second are averaged. The two occurring offsets are defined as $z_{r,i}$ and $y_{r,i}$ (WPCS). The displacement $dz_{r,i}$ relative to the first R-Test measurement is calculated according to :

$$dz_{r,i} = z_{r,i} - z_{r,1} \tag{4.34}$$

The resulting relative displacement of the sphere in Z-direction (WPCS) $dz_{r,i}$ can be used to calculate the thermal shift of the axis during all i R-Test sequences. It is influenced by the angular positioning error $A0A_i$, by the thermally caused table growth $d_{T_{grow,i}}$ and the location error $Y0A_i$ according to

$$dz_{r,i} = d_{T_{grow,i}} + Y0A_i + A0A_i \cdot r \tag{4.35}$$

where r is the distance of the axis to the precision sphere. With the offset of the axis in Z- and Y-direction z_{off} and y_{off}, which can be read-out of the CNC, r is calculated via

$$r = \sqrt{z_{off}^2 + y_{off}^2} \tag{4.36}$$

$Y0A_i$, the displacement of the swivelling unit in Y-direction, is given by (4.29). The positive or negative growth of the machine tool table $d_{T_{grow,i}}$ due to a certain load cycle of the swivelling axis, caused by the temperature change within the structure of the turning table, may have different sources: heat flux from the drives and bearings into the machine tool axis, the internal cooling of the rotary axes or the process, for example with cooling lubricant or hot chips. This is discussed in more detail in section 4.2.2. This term can not be determined with the R-Test measurement. The table growth can be determined isolated by a separate measurement. With the knowledge about the geometry, expansion coefficient and temperature change of the table, an other possibility is to calculate the deviation according to

$$d_{T_{grow,i}} = \alpha_e \cdot \Delta T_{tab} \cdot h_{tab} \tag{4.37}$$

where α_e is the thermal expansion coefficient, ΔT_{tab} is the temperature change and h_{tab} is the height of the table which represents the effective length (Offset from the swivelling axis to the table surface).

In this thesis, temperature measurements show, that ΔT of both machine tools during a horizontal axis movement cycle is small enough to neglect this term.

Finally, the axial location error of the horizontal axis ($X0T$ in example of Figure 4.9) has to be determined. As the deviation is directly measured by the R-Test setup, the evaluation does not require any transformation of the measurement data. By considering the X-coordinate x_{act_p} of each measurement point $p \in 1...q$, the average X-position of the axis can be identified via

$$x_i = \frac{1}{q} \sum_{p=1}^{q} \underline{r}_{p,i} \underline{e}_x \tag{4.38}$$

per R-Test sequence i.

Given the average X-position of every R-Test measurement according to (4.38), the translational location error $X0T$ for the ith R-Test is defined as

$$X0T_i = (\frac{1}{q} \sum_{p=1}^{q} \underline{r}_{p,i} \underline{e}_x - \frac{1}{q} \sum_{p=1}^{q} \underline{r}_{p,i=1} \underline{e}_x) \tag{4.39}$$

Thereby, all occurring thermally induced errors are evaluated.

In [132], Lotze describes, that in addition to the number of points, their distribution is very important in order to compute the correct centre of a circular arc. Therefore, the angular range α_{tot}

$$\alpha_{tot} = \alpha_i - \alpha_0 \tag{4.40}$$

should be chosen as large as possible to increase the quality of the measurement. The limitation is usually the kinematic setup of the analysed machine tool. In order to analyse this influence, the fitting calculation of the index circle to evaluate the location errors $Y0A$, $Z0A$, $B0A$ and $C0A$ (Example 4.9) is carried out for the three different angular ranges

- $\alpha_{tot_1} = 45°$

- $\alpha_{tot_2} = 90°$

- $\alpha_{tot_3} = 150°$

according to Figure 4.14. The simulation was carried out for 1000 R-Tests. A position accuracy of ± 3 μm per axis direction is assumed (uniform distributed), including the machine tool accuracy and the accuracy of the measurement device. Figure 4.15 shows clouds of circle centres as a result of the Monte Carlo - simulation of 1000 R-Tests with a feed rate $v_{rot} = 600°/min$, an assumed measurement frequency $f = 100$ Hz and a distance of the precision sphere to the analysed axis of $r = 190$ mm. Based on this data, the uncertainty of estimation of the circle centre in Y- and Z-direction is shown. As expected, the scattering of the circle centre is larger for smaller measurement angles.
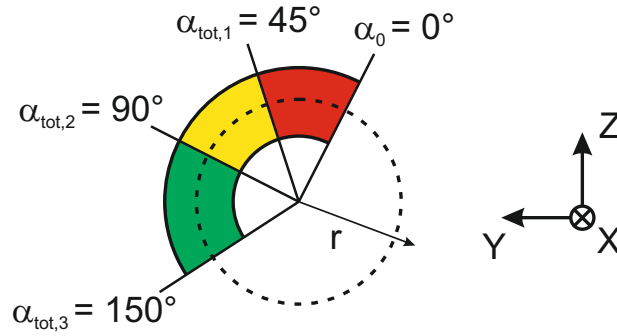
Figure 4.14: Three different angular ranges α used for the evaluation of their effects on the resulting parameter uncertainty

The translational errors $Z0A$ and $Y0A$ can be reduced from 21 μm ($Z0A$) respectively 45 μm ($Y0A$) at a measuring range of 45° to 3 μm ($Z0A$) respectively 2 μm ($Y0A$) with a measurement range of 150°.

According to the Guide to the Expression of Uncertainty in Measurement (GUM [133]), the standard uncertainty u_i for a rectangular distribution with a range of $2a$ can be calculated via

$$u_i = \frac{a}{\sqrt{3}} \tag{4.41}$$

Therefore, the uncertainties of estimating the errors $Z0A$ (U_{Z0A}) and $Y0A$ (U_{Y0A}) can be calculated to

$$U_{Z0A} \, (k = 2) = 2 \cdot \frac{1.5 \ \mu\text{m}}{\sqrt{3}} = 1.7 \mu\text{m} \tag{4.42}$$

and

$$U_{Y0A} \, (k = 2) = 2 \cdot \frac{1 \ \mu\text{m}}{\sqrt{3}} = 1.2 \mu\text{m} \tag{4.43}$$

for the case of a volumetric accuracy of ± 3 μm including the machine tool and the measurement device, a measurement range of 150° and a coverage factor $k = 2$.

Depending on different measurement positions on the circumference (Figure 4.14), the form and alignment of the ellipsoidal point cloud varies.

In reality, the cloud of measurement points is 3-dimensional because of the additional position accuracy of the system in X-direction. But on the one hand, the position of the circle centre in X-direction has no influence on the estimation of $Y0A$ and $Z0A$, and on the other hand, it doesn't depend on the measurement angle. It only varies with the assumed resulting range of the X-measurement values which is ± 3 μm. Regarding the estimation of the rotational location error $B0A$ (Figure 4.16), the position accuracy in X-direction has a significant influence. The theoretical determined uncertainty amounts up to 115 μm/m with measuring over an angular range of 45°. For a measured angular range of 150°, the margin decreases to about 4 μm/m. For this case, the uncertainty U_{B0C} can be calculated by

$$U_{B0A} \, (k = 2) = 2 \cdot \frac{2 \ \mu\text{m/m}}{\sqrt{3}} = 2.3 \ \mu\text{m/m} \tag{4.44}$$
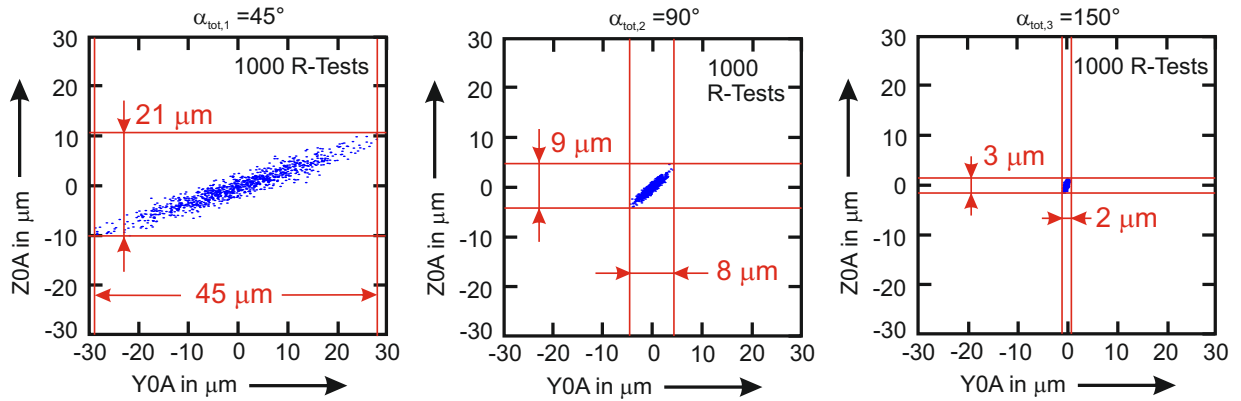
Figure 4.15: Influence of measurement angle α_{tot} to the uncertainty of the computed axis centre for a horizontal A-axis (supposed position uncertainty of values is $\pm\,3\;\mu m$ in every axis direction).
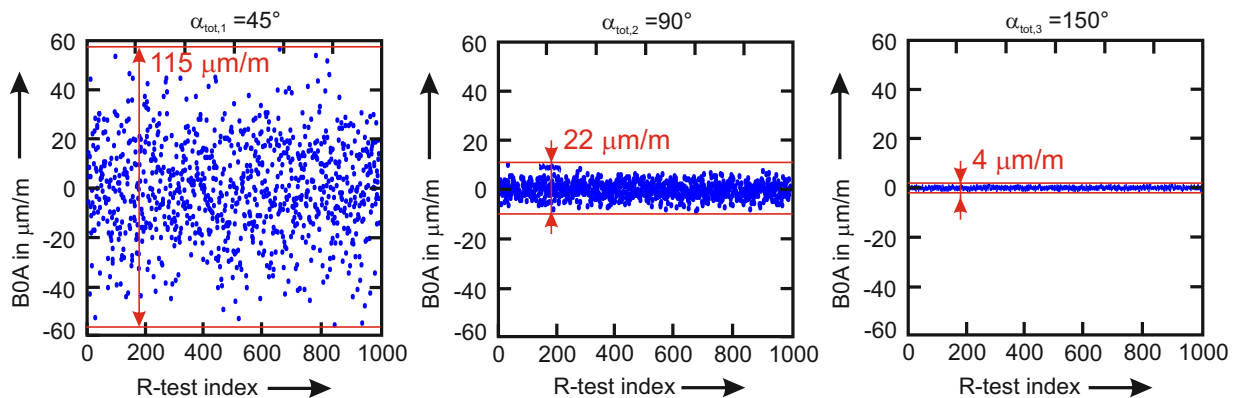

Figure 4.16: Influence of measurement angle α_{tot} on the uncertainty of the calculated axis inclination for a horizontal A-axis (supposed position uncertainty of values is $\pm 3\;\mu$m in every axis direction). R-Test index specifies the number of the simulated R-Tests.
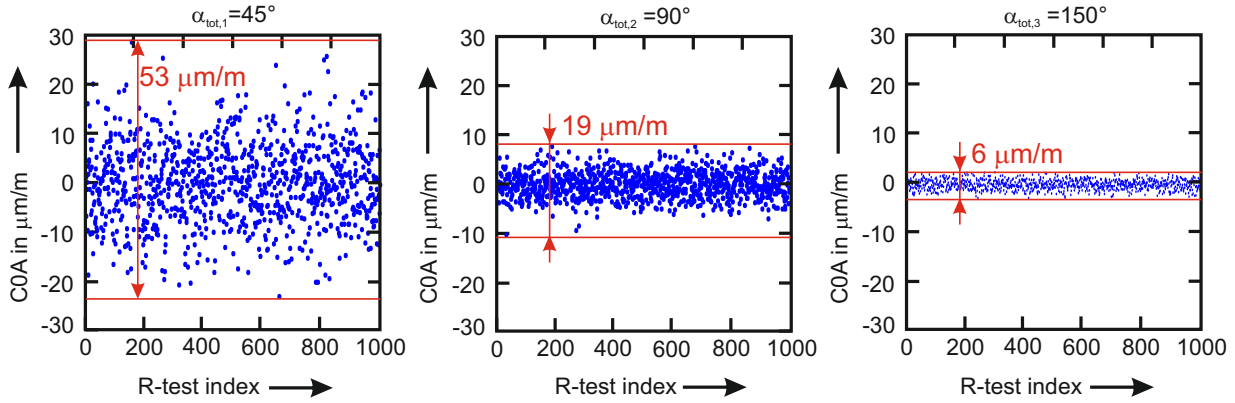
Figure 4.17: Influence of angular measurement range α_{tot} to the uncertainty of the calculated axis inclination for a horizontal axis (supposed position uncertainty of values is ± 3 μm in every axis direction) R-Test index specifies the number of the simulated R-Tests.

according to the previously made assumptions.

A similar dependency on the measurement angle can be seen regarding the squareness error $C0A$. With enlarging the measurement angle from 45° to 150°, its margin decreases from 53 μm/m to 6 μm/m (Figure 4.17), which leads to an uncertainty of

$$U_{C0A}\ (k=2) = 2 \cdot \frac{3\ \mu\text{m/m}}{\sqrt{3}} = 3.5\ \mu\text{m/m} \tag{4.45}$$

according to the previously made assumptions.

In order to validate these theoretical simulations concerning the uncertainty of the measurement procedure, appropriate measurements have been performed. Figure 4.18 and Figure 4.19 show the evaluated values for the errors $Y0A/Z0A$ and $C0A/B0A$ during 25 R-Tests for three different angular measurement ranges α ($\alpha_1 = 45°$, $\alpha_2 = 90°$ and $\alpha_3 = 150°$). The nominal value, being zero for each R-Test, is illustrated by the dashed red line. A best fit line was computed for every measurement angle (dotted line in the same colour as the corresponding measurement). This best fit line represents the shift of the location errors due to thermal effect during the 25 R-Tests. In order to characterise the differences between the single measurements, two parameters of the measurement series are determined: the straightness and the parallelism to the zero level. While the variation in the straightness is proportional to the scatter due to the size of the measurement angle, the magnitude of parallelism is caused by environmental temperature change during the 25 R-Tests or by a different heat input due to different thermal loads. In both cases, it is independent of the angular evaluation range and can therefore be neglected. It can be seen, that the scatter of the evaluated location errors rises with decreasing measurement angle. With a measurement angle of 150°, as it is used in this work, the scattering of the calculated parameters is below 10% of the systematic shift due to thermal influences of this machine tool under test.
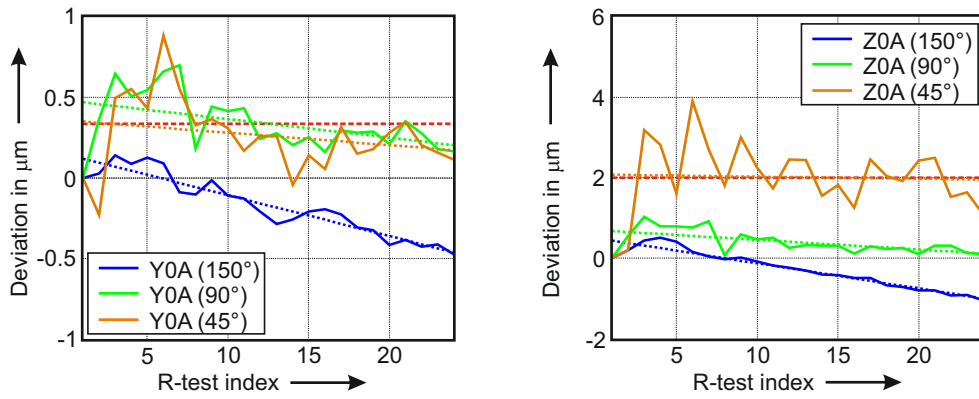
Figure 4.18: 25 R-Test measurements carried out over three different angular evaluation ranges. The uncertainty of the computed location errors can be estimated with the range around the best fit line of the values.

Figure 4.19: 25 R-Test measurements carried out over three different angular evaluation ranges. The uncertainty of the computed location errors can be estimated with the range around the best fit line of the values.
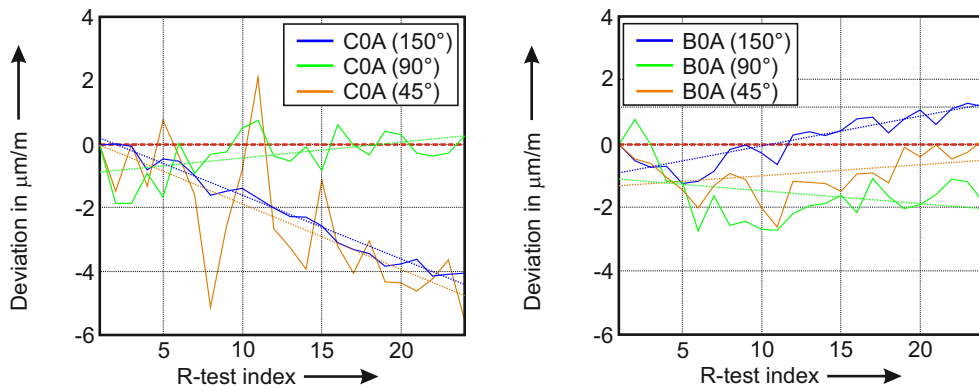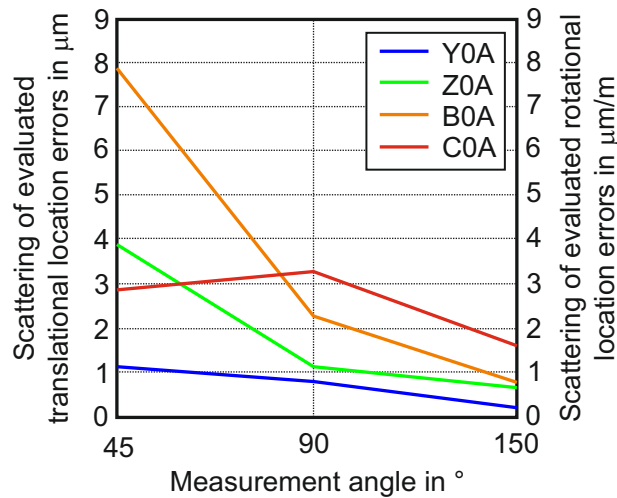

Figure 4.20: Variation of the ranges of the location errors $Y0A$, $Z0A$, $B0A$ and $C0A$ during 25 R-Tests with three different measurement angles.

4.2 Measurement of Different Contributors to the Total Thermal Deviation

In order to define relevant areas of investigation, all influences have been investigated including location errors due to environmental temperature changes, main spindle rotation and linear axes movement. Based on these measurements, rotary and swivel axes have been found to be of major importance.

4.2.1 Measurements According to ISO 230-3

Influence of Environment

Environmental temperature influences as described in section 2.1 are determined with the test setup described in ISO 230-3:2007 [21]. During the test, the machine tool status is *"NC on"*, which means that all axes are position controlled, but no movement is carried out on the machine tool. Assuming that vertical or slant axes do not warm up, this enables that the thermal influence of the environment can be quantified in an isolated manner.

   To give an example, the following section describes the results of an ETVE-test of **Machine tool B/C** over six days. In Figure 4.21, translational deviations in X-, Y- and Z-direction are plotted in the upper diagram. The lower diagram shows the corresponding environmental air temperature, which is recorded by two sensors at the height of the spindle nose as suggested in ISO 230-3 (the evaluated value is the mean value of the two sensors). The overall test duration is six days. The diurnal temperature variation is approximately $3°$C, on day three it is $5°$C. The change of the temperature induced deviations and the temperature variation exhibit the same periodicity. Also amplitudes are corresponding. Maximum deviations can be found in Y-direction with 5 μm per day (9 μm on day 3). In addition to the diurnal temperature variation, an increase of the mean temperature over the whole test duration of about $2°$C can be observed. The test started with a completely cold machine tool in order to display the warm-up behaviour. This explains the shifts at the beginning of Figure 4.21. After approximately two hours, the deviations start their periodic behaviour depending on the environmental temperature variation. The different magnitudes of these deviations in X-, Y- and Z-direction indicate the different temperature sensitivities of the machine tool. This is shown in detail in Figure 4.22, where deviations are plotted as functions of the environmental temperature. A best fit line shows a very small sensitivity in X-direction (-0.3 μm/K) due to the thermo-symmetric design of the machine tool. Also in Z-direction, the sensitivity is quite small with with 0.2 μm/K. The Y-axis shows the largest temperature sensitivity of -1.8 μm/K - explained by the asymmetrical design of the machine tool regarding this direction.

Figure 4.23 shows the rotatory deviations measured with the ETVE-test. The range of the deviation is 60 μm/m for A-direction and 25 μm/m for B-direction. Again, the course of the error fits with the change of the environmental air temperature (Figure 4.24). An overview of all measured deviations and the corresponding sensitivities during a maximum temperature change of 5.5 K is given by Table 4.4.
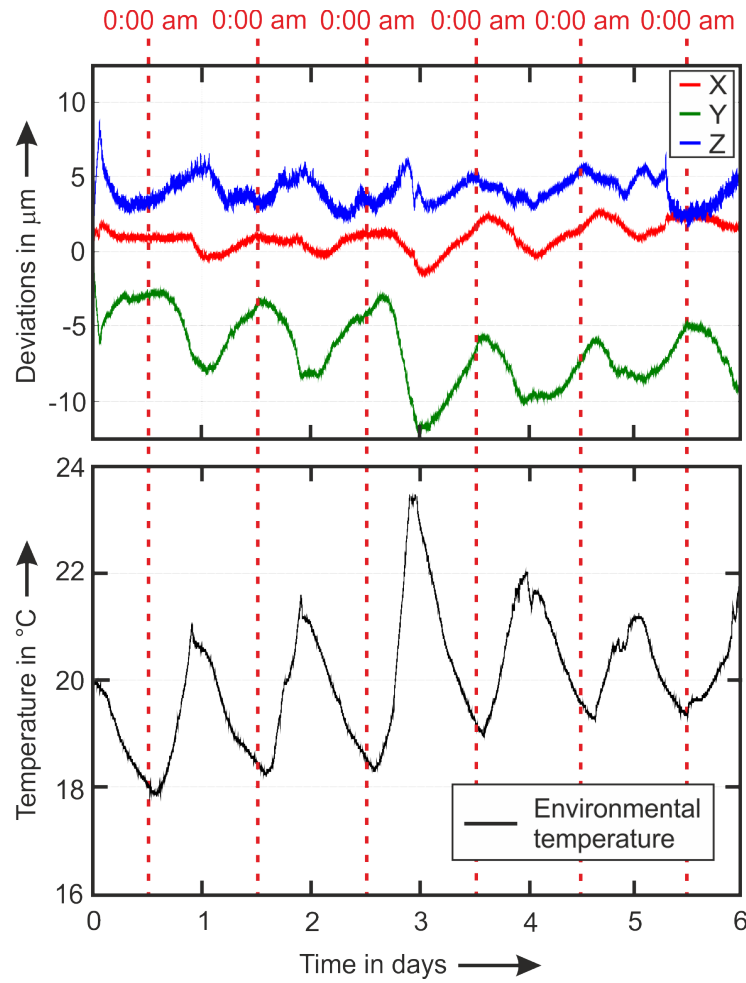
Figure 4.21: ETVE - test carried out on **Machine tool B/C** over six days. Upper diagram: translational deviations, lower diagram: environmental temperature [122].
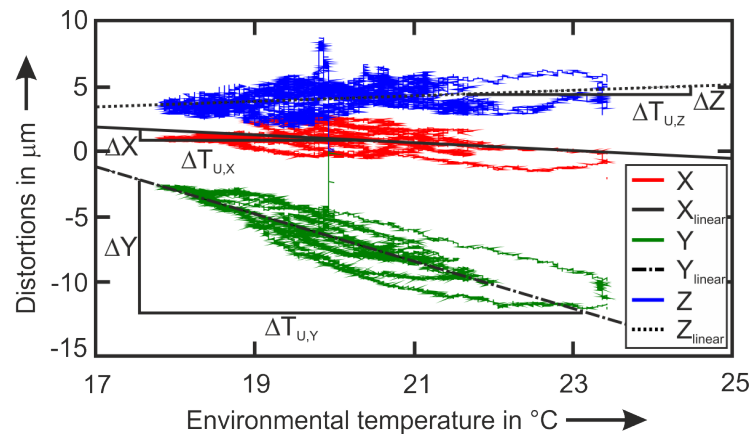

Figure 4.22: Machine tool B/C: Relationship between environmental air temperature and translational deviations of ETVE - test [122].

Table 4.4: Range of deviations and sensitivities of ETVE-test of Machine tool B/C during an environmental temperature change of 5.5 K [122].

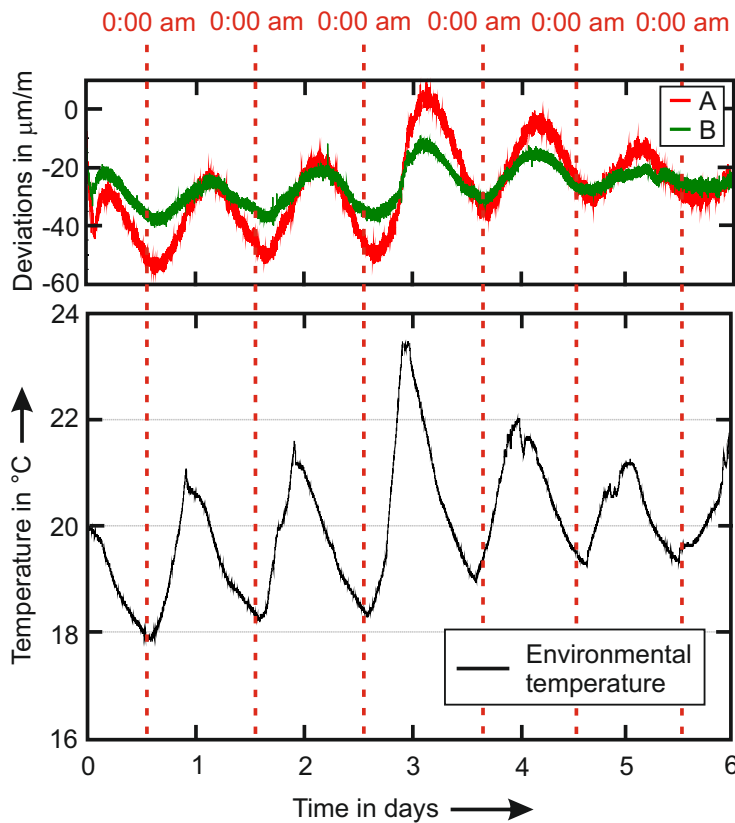|	Range	Gradient
	$[\mu m]$	$[\mu m/K]$
X	6	-0.3
Y	12	-1.8
Z	8	0.2
	$[\mu m/m]$	$[(\mu m/m)/K]$
A	60	9.0
B	25	4.0

Figure 4.23: ETVE - test carried out on **Machine tool B/C** over six days. Upper diagram: rotational deviations A and B, lower diagram: environmental temperature.
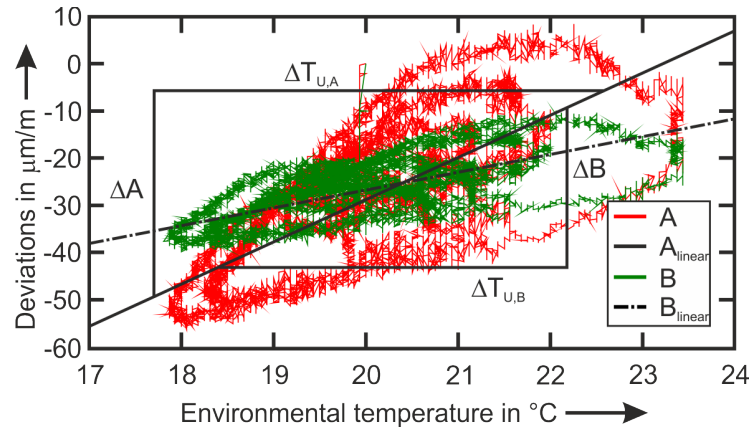
Figure 4.24: Machine tool B/C: Relationship between environmental air temperature and rotational deviations of ETVE - test.

Influence of Spindles

Because of the high power requirements, any main spindle is a machine part with a potential for large thermal influence on deviations - but as explained in section 2.4, a lot of strategies are in use to reduce thermal input by spindle drives or to compensate the resulting errors.

Measurements in this thesis are carried out according to ISO 230-3 over six to eight hours net time (four hours warm-up at a predefined rotational speed, four hours cool-down). During both phases, a probing cycle is carried out every five minutes by pneumatic probes, so that the measuring cycle can be limited to approximately ten seconds. To avoid dynamic influences due to the probing procedure, the first and the last two seconds are omitted. The remaining values are averaged. Due to the temperature influence during the measurement cycle, the sequence of the test cycle (five minutes movement / ten seconds measurement) has to be considered, when measurements are compared to other spindle measurements. All compensation options of the analysed machine tools are turned on during the tests.

Figure 4.25 shows the translational and rotational deviations (upper diagram) and corresponding temperatures (lower diagram) of a six hours spindle test (four hours warm-up, two hours cool down) of **Machine tool B/C**. Translational deviations are within 14 μm, rotational deviations within 12 μm/m. In X-direction, no significant deviations can be seen. The deviations in Y-direction correspond quite nicely with the environmental temperature profile: after a little bit more than 2 hours, the environmental temperature rises which leads to a shift of the TCP in negative Y-direction according to the results presented in Figure 4.21 / Table 4.4. In Z-direction, a significant displacement is measured: after starting the spindle, the TCP shifts roughly 4 μm in negative Z-direction. After stopping the load cycle, the displacement increases from -6 to $+8$ μm which can be explained by the cooling of the spindle. The internal cooling system is cooling down the spindle even after the spindle rotation has stopped. Simultaneously, the machine bed temperature rises corresponding to the environmental air temperature (Figure 4.25, below), which explains the Z-offset at the end of the measurement.

The upper diagram of Figure 4.26 shows the translational and rotational TCP-

Figure 4.25: Translational and rotational deviations during a spindle test on **Machine tool B/C** ($n_{spindle} = 3000 \ min^{-1}$). Every five minutes, the rotation is stopped to carry out a measurement with a duration of ten seconds. During cool-down, the measurement is carried out continuously. During warm-up, the abscissa shows the net warm-up time with the measurement duration cut-out.
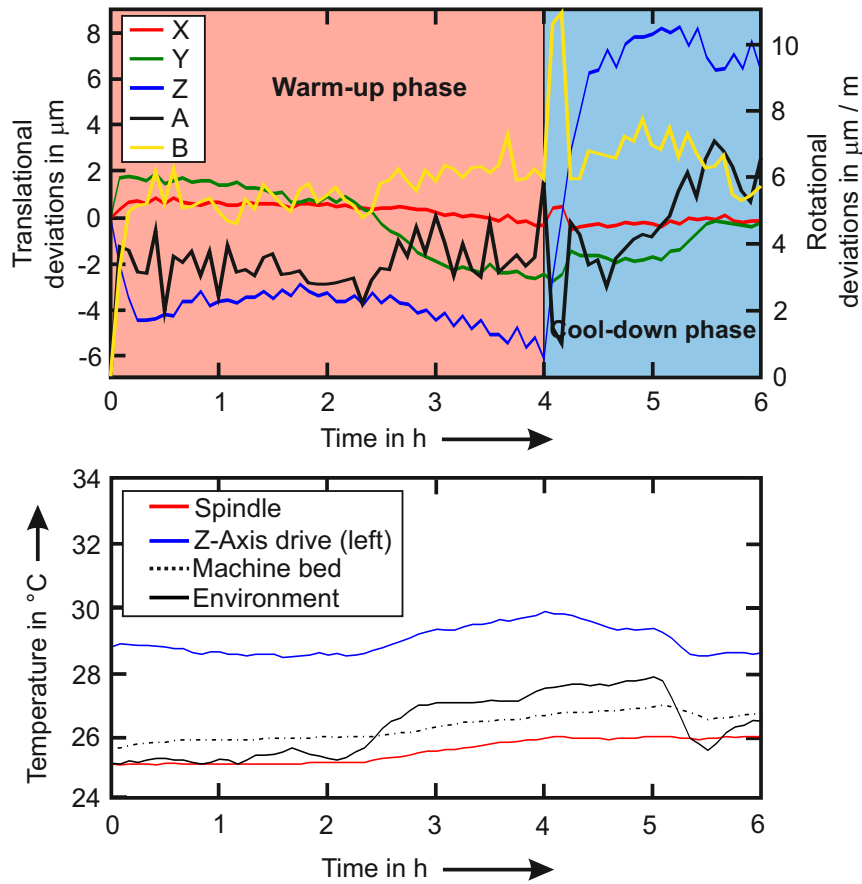
Figure 4.26: Translational and rotational deviations during a spindle test on **Machine tool A/C** ($n_{spindle}$ = 6000 min^{-1}). Every five minutes, the rotation is stopped to carry out a measurement with a duration of ten seconds. During cool-down, the measurement is carried out continuously. During warm-up, the abscissa shows the net war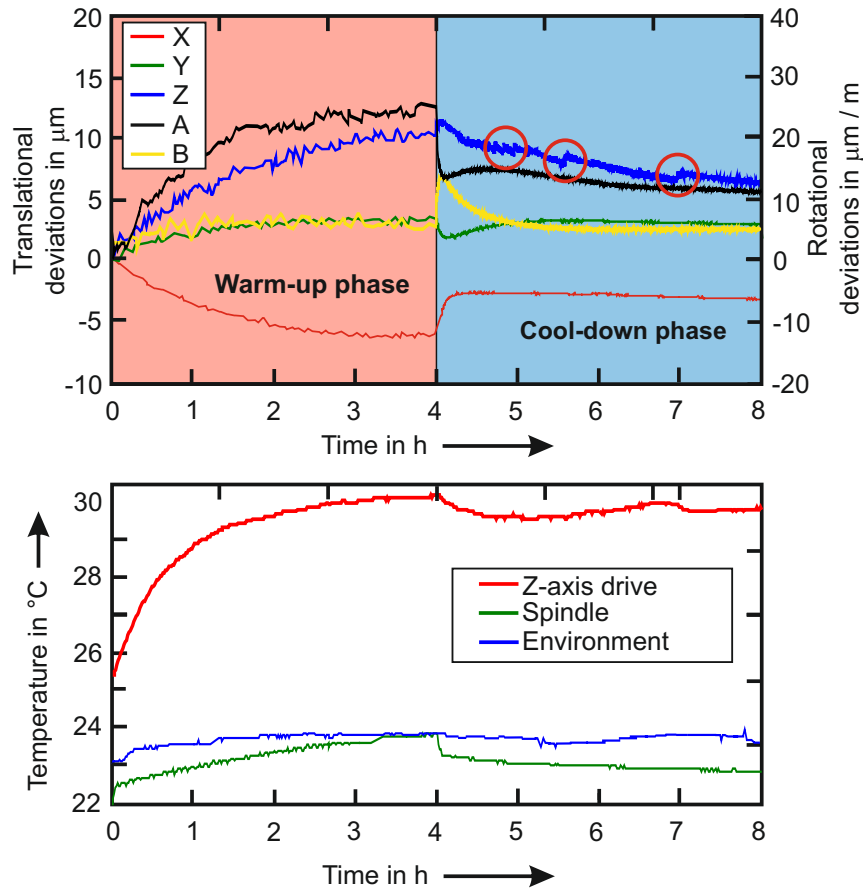m-up time with the measurement duration cut-out. Red marks show the compensating intervention of the NC. They can only be seen during cool down, because the measurement interval of five minutes during warm-up acts as a filter.

displacements due to a spindle rotation of **Machine tool A/C** during a test cycle with a warm-up phase of four hours rotational speed of 6000 min^{-1} and four hours cool down phase. During warm-up, a measurement point is recorded every five minutes. During cool-down, the measurement is carried out continuously. The lower diagram shows temperatures of the Z-axis drive, the spindle and the environment. During warm-up, significant TCP-displacements in translational direction are measured with 10 μm in Z-direction and 7 μm in X-direction. The Y-direction shows only a slight thermo-dependent shift with a magnitude of 3 μm. Rotational deviations are roughly 25 μm in A-direction. After stopping the spindle, all deviations systematically decrease. Peaks after stopping the spindle have two basic reasons: the internal cooling unit changes the operational mode, and the environmental conditions change due to the changed convection. Regarding the cool-down curve of the Z-direction, the compensation interventions of the CNC (Eddy Current sensor measuring the gap between rotor and stator of the spindle) can bee seen (red markers).

Influences of Linear Axes

For the characterisation of the thermal influences of linear axes, the ISO 230-3 measurement setup is used again. The used load cycle consists of a warm-up phase of four hours (net warm-up time) and a consecutive cool-down phase of four hours. The heat input during warm-up is realised by a pendular movement of the axis with a defined feed speed. Every five minutes, a measurement with a duration of ten seconds has been carried out. To avoid dynamic influences due to the probing procedure, the first and the last two seconds are omitted. The remaining values are averaged. During the cool-down phase, the measurement has been executed continuously. In this section, the influence of the Z-axes of both analysed machine tools are presented exemplary.

Figure 4.27 shows the evaluated deviations and corresponding, significant temperatures recorded during the pendular movement of the Z-axis of **Machine tool B/C** with a feed speed of 500 mm/min. The environmental temperature shows a change of 3.5°C. When comparing the course of the Y-axis deviation and the environmental air temperature change, it can be assumed that the cause for the TCP-error in Y-direction is the environmental temperature change, not the underlying load of the pendular movement of the Z-axis. This influence of the environment can nicely be seen in the time interval of seven hours: the buckle of the environmental air temperature, which is due to an opened outside door next to the machine tool, directly leads to a change of the deviation in Y-direction. When comparing the magnitude of the deviation with the environmental temperature change, the results of the ETVE - test (Table 4.4) show a TCP displacement of -1.8 μm per K temperature change. This fits well to the results of Figure 4.27. In X-direction, no load-depended TCP-displacement can be seen. The shift of 6 μm is due to the general warm-up of the machine tool and environmental influences. This underlines the benefit of the thermo-symmetric design of the machine tool in this direction. In Z-direction, the TCP-displacements correspond with the underlying load cycle: during the warm-up phase, the Z-axis displacement rises to -5 μm. When entering the cool down phase, the displacement decreases before it rises again at the end of the cool-down phase. This rise occurs simultaneous with a peak of the environmental temperature. Even since the sensitivity does not fit with the results of the ETVE-test, a case by case correlation can be established: a heavy and fast outside temperature decrease leads to a fast and strong decrease of the temperatures in the machine shop, especially the non-protected Z-axis drives on top of the machine tool. This can be seen regarding the Z-axis temperature in Figure 4.27. Therefore, it is assumed that this influence by the environmental temperature is responsible for the change of the deviation in Z-direction in the last two hours of the measurement.

The rotary deviations A and B show no load depending, systematic thermally caused behaviour. Both are quite small with a range of 7 μm/m (A) and -12 μm/m (B). The shift around B can be explained by an environmental temperature gradient in X-direction of the machine tool. Because of the location of the machine tool near an outside wall in the workshop, a temperature gradient occurs when the outside air temperature strongly differs from the air temperature in the machine shop. A distance between the two X-axes of 1 m, an effective height of 1 m, an assumed change in the environmental temperature of 1 K between the left and the right side of the machine tool and a thermal expansion coefficient
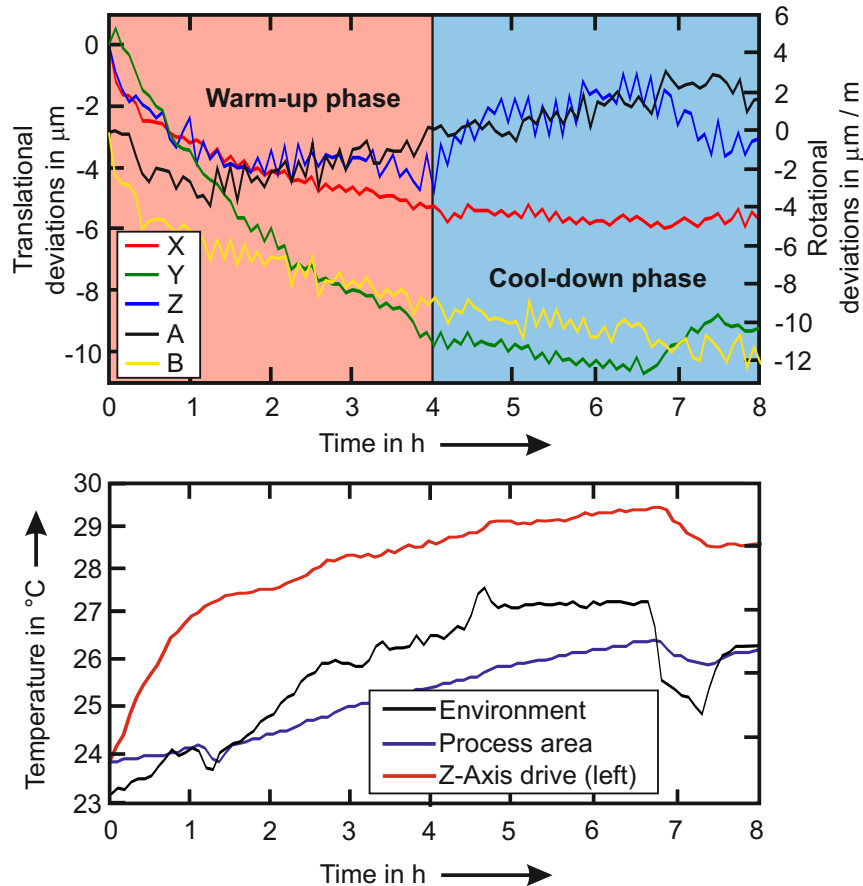
Figure 4.27: Machine tool B/C - Z-Axis pendular movement with a feed rate of 500 mm/min during four hours followed by a cooling phase of four hours with the internal cooling system and the environmental temperature change as underlying thermal load. Upper diagram: deviations, lower diagram: temperature of drive and environmental temperatures. The jagged course of the Z-deviation is due to the repeatability of the unidirectional positioning of the Z-axis of this machine tool, which is measured with 2 μm. The heavy temperature change around seven hours is due to an opened outside door next to the machine tool.

α of 12 μm m^{-1} K^{-1}, lead to a deviation of 12 μm/m which is a reliable estimation.

Figure 4.28 shows significant temperatures (lower diagram) and the deviations caused by a pendular movement at 500 mm/min of the Z-axis (upper diagram) of **Machine tool A/C**. In Y-direction, due to the thermo-symmetric design of the machine tool, no significant systematic thermal behaviour is identifiable. In X- and Z-direction, maximum deviations of approximately 8 μm respectively 5 μm are measured. These errors are caused by the heat brought in by the Z-axis drive during the movement which leads to a deformation of the Z-axis structure and therefore to a displacement at the TCP. The values of the Z-deviation show a different shape during the warm-up and the cool-down phase. This behaviour is caused by an Eddy-Current sensor, which is part of a compensation strategy of the machine tool in Z-direction. The sensor measures the gap between the rotor and the stator of the spindle. It needs a minimum rotational speed to work reliable. With no rotation of the spindle, the feedback control of the sensor
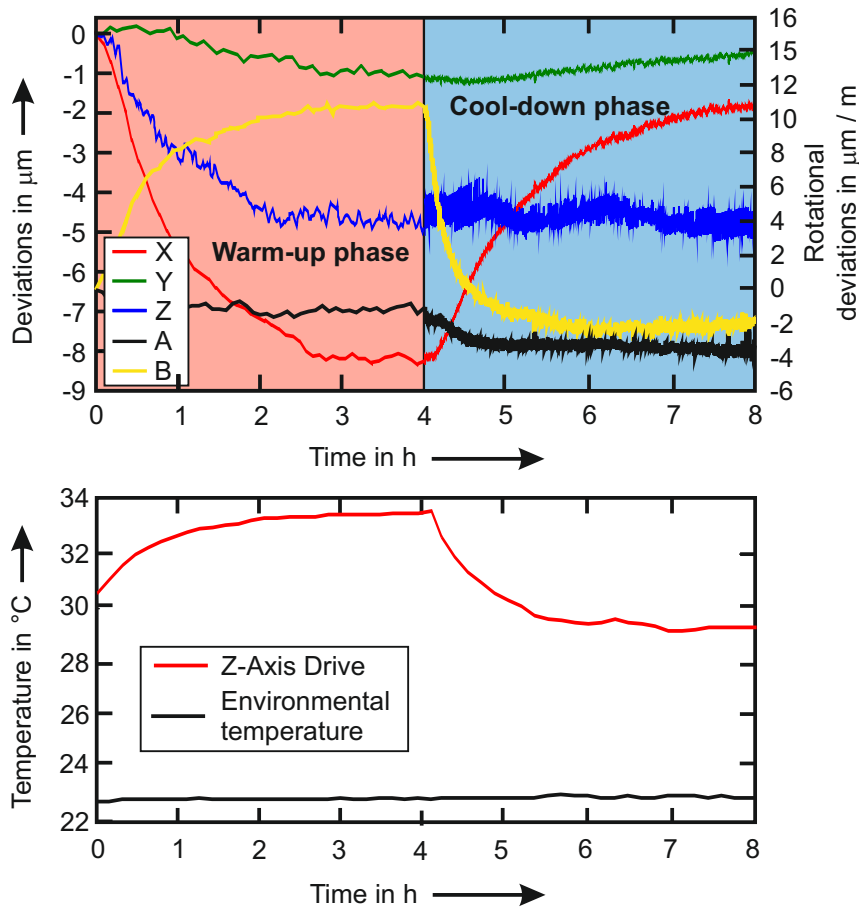
Figure 4.28: Machine tool A/C: *Z*-Axis pendular movement with a feed rate of $500~\mathrm{mm/min}$ during four hours followed by a cooling phase of four hours with the internal cooling system and the environmental temperature change as thermal load. Upper diagram: deviations, lower diagram: temperature of drive and environmental temperatures.

fluctuates by $\pm~0.5~\mu$m. This is basically the same during the warm-up phase where deviations are not measured continuously: only every five minutes one measurement is carried out, which leads to a smoothing of the curve.

The largest deviations can be obtained in *X*- and *B*- direction. The warm-up due to the axis movement leads to a displacement of the spindle in these two directions. After stopping the warm-up movement, both deviations decrease approximately to the zero level again.

The environmental temperature plot shows the very nice steady conditions in the workshop. The temperature of the *Z*-axis drive is significantly higher as the environmental air temperature even at the start of the measurement, which is due to the fact that the weight compensation of the *Z*-axis is realised by this drive, which means it is permanently operating.

4.2.2 Influences of Rotary Axes

As described in chapter 2.2.2, up to now, only few research regarding the thermal behaviour of rotary axes was done. First measurements of the thermally induced error of rotary axes are presented in [16, 51, 52, 120, 121].

In a first step, the heat development in the structure around the rotary axes is investigated by an infrared camera. These measurements are verified with thermocouple measurements. After that, thermo-mechanical deviations are measured with the R-Test. Because of the different operating states and the different measurement setups required, this chapter is divided into horizontal and vertical axes.

Horizontal Axes

Horizontal axes show two different significant operating states: the pendular movement between two positions and the standstill at a certain angle without clamping the axis mechanically. Figure 4.29 shows the A-axis of machine tool **Machine tool A/C**, which is realized with a cradle-design. The axis stands still at 45° under position control for 2.5 h, after that the A-axis is held at 90° for again 2.5 h, after that it is cooled down at 0° for 4 h. Then, the same cycle is repeated for −90°, −45° and again 0°. Thereby the heat development in the structure can be seen from both sides of the swivelling axis: in Figures A and B of 4.29 it can be seen that the bottom of the swivelling structure is not influenced by the heat produced during the load cycle. Images D and E show the top side of the axis during the load cycle: it can be seen that the structure around the drive of the axis is heated up, but the cooling unit manages to cool the drive enough, so that the heat is not flowing into the table structure. After 4 h at 0 the structure is cooled-down completely again.

Figure 4.30 shows temperature measurements with four thermocouple sensors (Table 4.2, System 2), which are carried out to verify the infrared camera measurements. Therefore, the underlying load cycle is exactly the same. The measurement positions of the temperature sensors are shown in the left pictures. The machine tool table and the bottom of the swivelling bridge are not influenced by the thermal load induced by the A-axis drive. Maximum temperatures at the positions 45° and 90° after 2.5 h are approximately 25°C and 27.5°C. This corresponds with the infrared camera records within 1°C.

Both measurements show the correlation of the heat input in the structure with the swivelling angle of the axis, which leads to the conclusion that the power input of the axis drive strongly correlates with the angular position. Figure 4.31(1) shows the electric power of the A-axis drive during a movement from 0° to 90° in 5° steps, rising from 0 W to 3.5 kW. The axis is held in standstill for 30 seconds every 5° and the drive power is read out of the NC. It can be seen, that the supplied electrical power changes, when approaching a position from different directions. The measured electrical power can deviate up to nearly 1 kW. The same effect can be observed in the right image of Figure 4.31 (2). The axis is in position-control at −90° and −45° for 150 s each. The approaching direction is changed every 30 s.

Figure 4.32 shows the heat development in the structure around the A-axis drive for
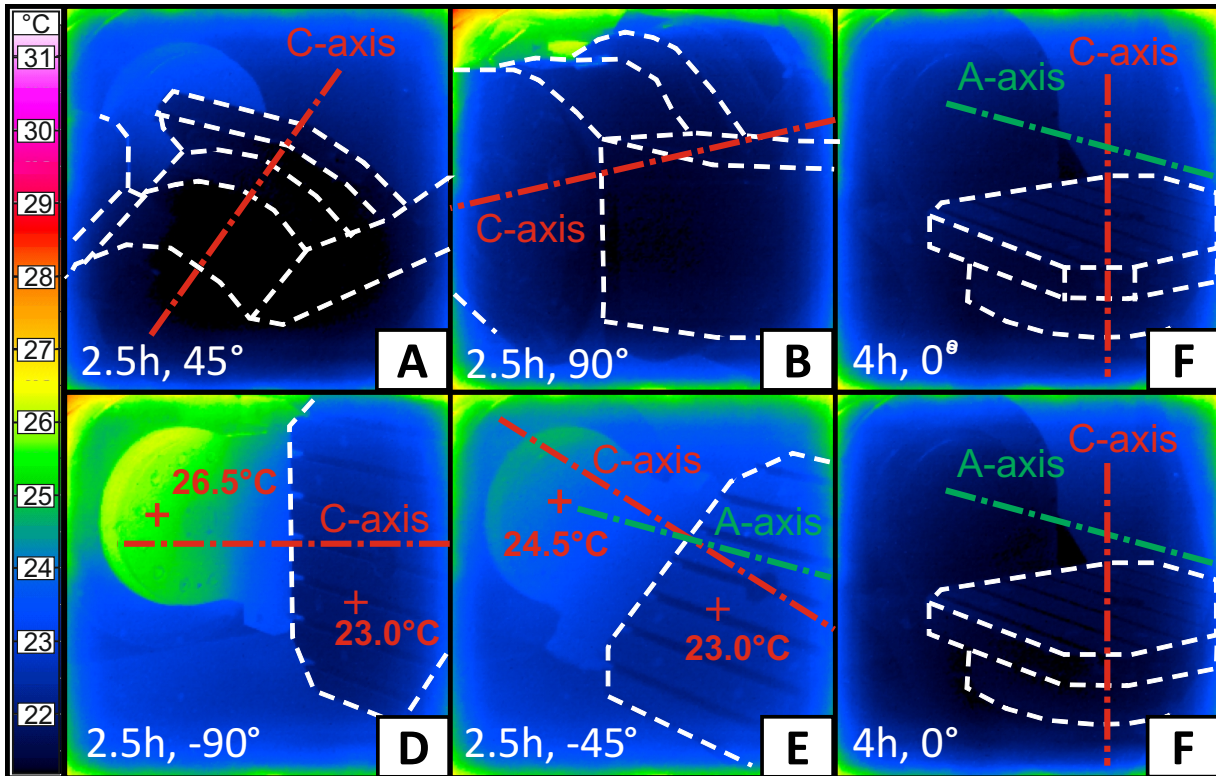
Figure 4.29: Machine tool A/C - IR-camera measurement of temperature distribution in the machine tool structure: Thermal load input by horizontal swivelling axis. A: $2.5\,\mathrm{h}$ standstill at $45°$ tilting angle (view from the bottom / side of the swivelling unit), B: $2.5\,\mathrm{h}$ / $90°$ (view from the bottom of the swivelling unit), C: Cool-down $4\,\mathrm{h}$ / $0°$, D: $2.5\,\mathrm{h}$ / $-90°$, E: $2.5\,\mathrm{h}$ / $-45°$, F: $4\,\mathrm{h}$ / $0°$.
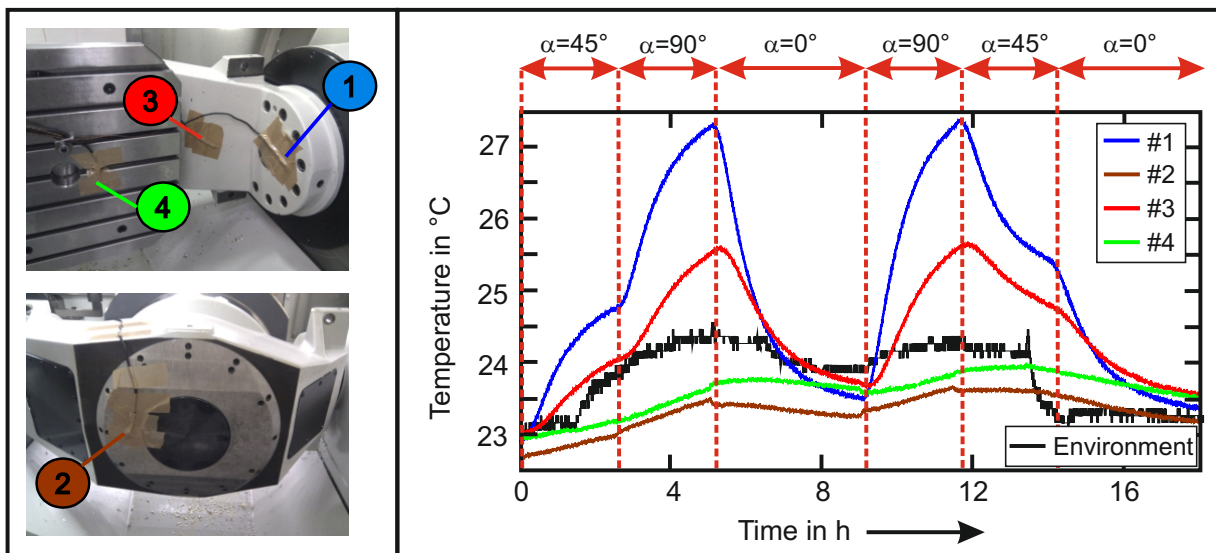

Figure 4.30: Machine tool A/C - Measurement of surface-temperatures of a swivelling axis with thermo-elements during different conditions: standstill at a tilting angle of $45°$ / $90°$ / $0°$ / $-90°$ / $-45°$ /$0°$. Nr. $1-4$ mark the four sensor positions according to the measurement in the right diagram (corresponding colours).
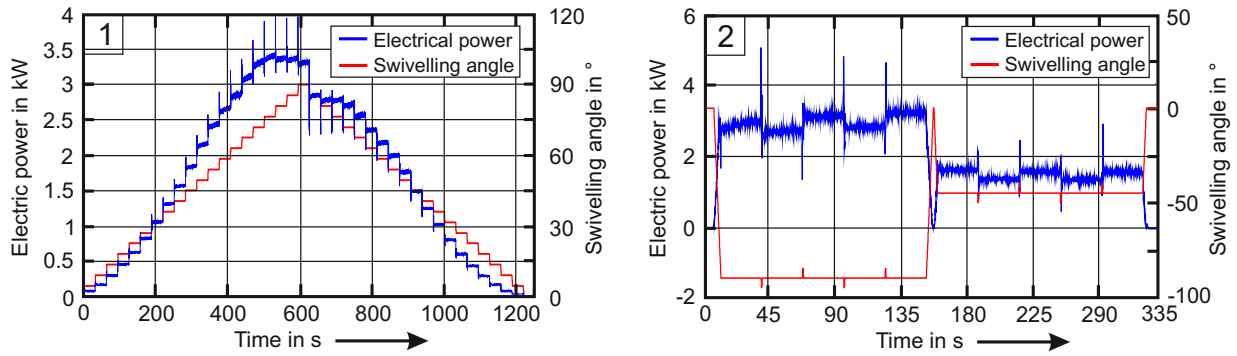
Figure 4.31: Machine tool A/C - (1): Drive power for the swivelling axis during a movement from $0°$ tilting angle to $90°$ and back in steps of $5°$. Input power in dependency on the swivelling angle of a horizontal axis. (2): direction-dependency of drive power.

a 5 h pendular movement between $-90°$ and $90°$ (A), a 4 h cool-down phase (B) and a 5 h pendular movement between $-45°$ and $45°$ (C). Again, it can be seen that the structure around the drive is heated-up, but no significant flow of heat into the table is noticeable from these images. With a swivelling angle of $\pm90°$ the heat input is obviously higher than for $\pm45°$, depending on the higher amount of power input and friction in the bearings of the axis. Additionally it can be seen, that 4 h cool-down time is enough for a complete cooling of the structure. Figure 4.33 shows a measurement of the same cycle with thermocouples. The measuring points have been chosen after evaluating the infrared camera measurements and are shown on the left two images of Figure 4.33. Again it can be seen that the temperatures on the top and on the bottom of the machine tool table are not strongly influenced by the heat input of the horizontal axis drive but they are at the same level as the environmental temperature. The maximal temperatures at the measuring point 1 are $32°C$ for a swivelling angle of $\pm90°$ and $29.5°C$ for $\pm45°$. Measurement point 2 shows temperatures of $28.5°C$ ($\pm90°$) and $27.5°C$ ($\pm45°$). The table surface temperature (Sensor 4) is quite constant between $23.5°C$ and $24.5°C$ These temperatures match with the infrared camera measurements shown in Figure 4.32 within $1°C$. The difference between sensor 1, 2 and 3 confirms, what is shown by the thermal images: the cooling system manages to prevent a heat flux from the A-axis drive to the machine tool table.

Figure 4.34 shows the machine tool table temperature measurement of **Machine tool B/C**. This machine tool has one cooling circuit for both rotary axes. The cooler control is triggered by the difference between the reflux temperature of the cooling system for the rotary / swivel axis unit and the environmental temperature. When the B-axis is positioned, the produced heat leads to a rise of the reflux temperature. This causes the activation of the cooling unit and therefore a reduction of the inlet temperature. Because there is no thermal load input of the C-axis, the table temperature decreases from $17°$ to $16°$. After 4 h, the B-axis is swivelled back to $0°$, the cooling control stops cooling the rotary / swivelling axis unit and the table temperature rises again till it reaches the process area temperature.

Figure 4.36 shows significant deviations (left) and the corresponding drive power, cooling power and environmental temperature (right) of the A-axis of **Machine tool A/C**. The
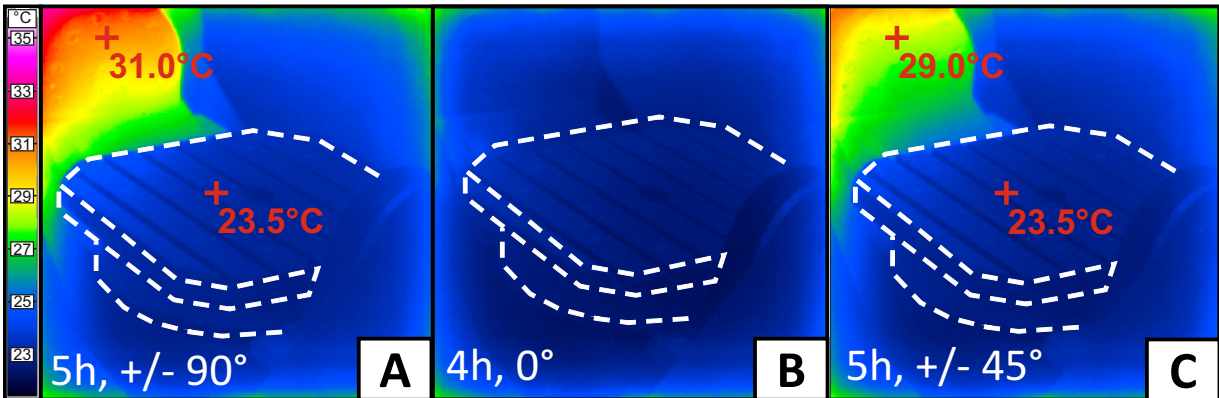
Figure 4.32: Machine tool A/C - Heat generation in structure around axis drive - underlying thermal load caused by a pendular movement inbetween A: $\pm 90°$ and C: $\pm 45°$. In B: cool-down at $0°$ for four hours [126].

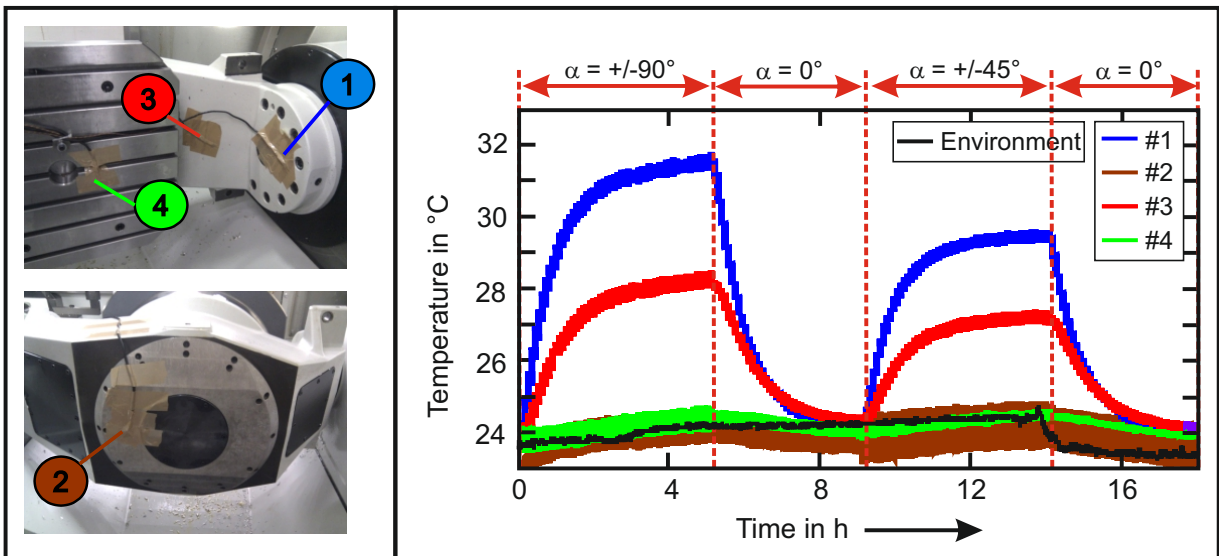**Figure 4.33: Machine tool A/C** - Temperature rise of structure during a pendular movement between $\pm 90°$ and $\pm 45°$. Nr. $1-4$ mark the four sensor positions according to the measurement in the right diagram (corresponding colours).
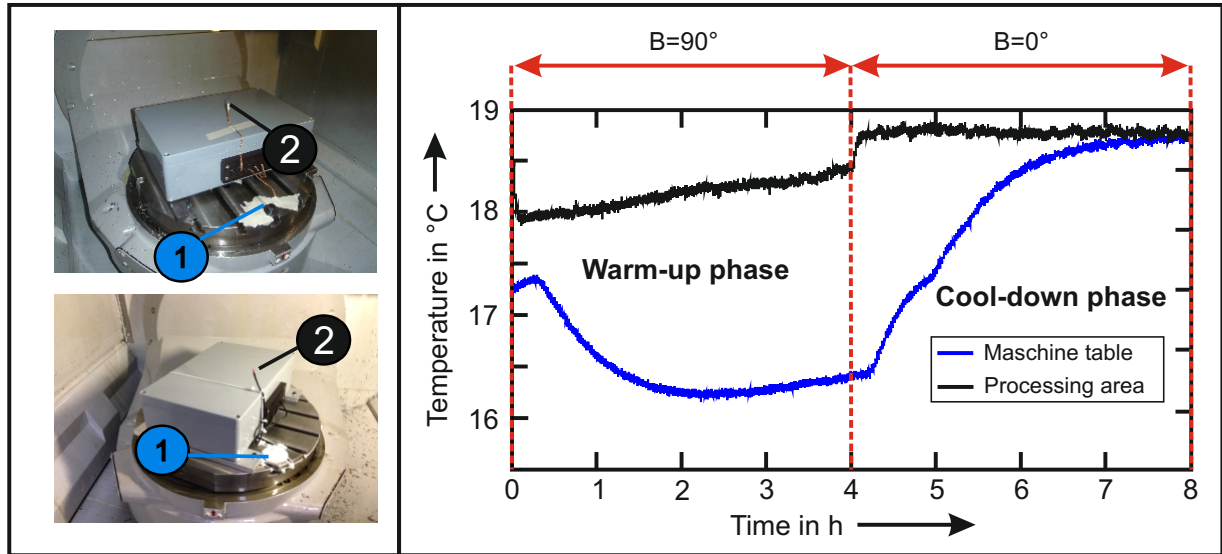
Figure 4.34: Machine tool B/C - Table Temperature while B-axis holds at $B = 90°$ - Tilted position of B leads to a cooling of the rotary swivelling tabel unit (one cooling circuit for both axis) which leads to a decrease of the machine tool table temperature. Nr. 1 and 2 mark the two sensor positions according to the measurement in the right diagram (corresponding colours).

underlying load cycle is a pendular movement between $\pm90°$ for 16 h. Maximum deviations are $X0T$ with 18 μm, $Z0T$ with 7 μm and $A0A$ with 50 μm/m. All other location errors are not considered, because they show no thermal dependency due to the thermo-symmetric design of the machine tool. As already seen, when executing the measurements according to ISO 230-3, the environmental air temperature has a large influence on the deviations. Characteristic changes of the environmental temperature cause corresponding changes in errors (red marks in Figure 4.36). Regarding the absolute change of the environmental temperature, which is within 1°C, it becomes clear that not this temperature variation causes the environmental temperature change error, but the change of the forced convection by the nearby outlet of an air conditioner in the shop floor. Figure 4.35 shows the environmental temperature and the temperature of the Z-axis drive during 3.5 days. The machine tool status is "NC on", no movement is carried out but the Z-axis drive works against the gravity. Therefore, the temperature of the drive is higher than the environmental temperature. During the weeks-end (marked in Figure 4.35), the air condition operates in a different setting than during the week. Therefore, only small changes of the temperatures are visible during week-end. On Monday when the air-condition system changes its operational mode, a diurnal temperature profile with a change within 1°C becomes visible. This change leads to a change of the temperature of the Z-axis drive of roughly 4°C a day. This temperature difference can be explained by the change of convection due to the changed air flow leaving the outlet of the air-condition system.

The averaged power demand of the A-axis during this load cycle is approximately 1.75 kW. This heat can basically be removed by the cooling system (cooling power = red line). This confirms the results of the temperature measurements: the heat around the axis drive is not flowing into the adjacent structure.
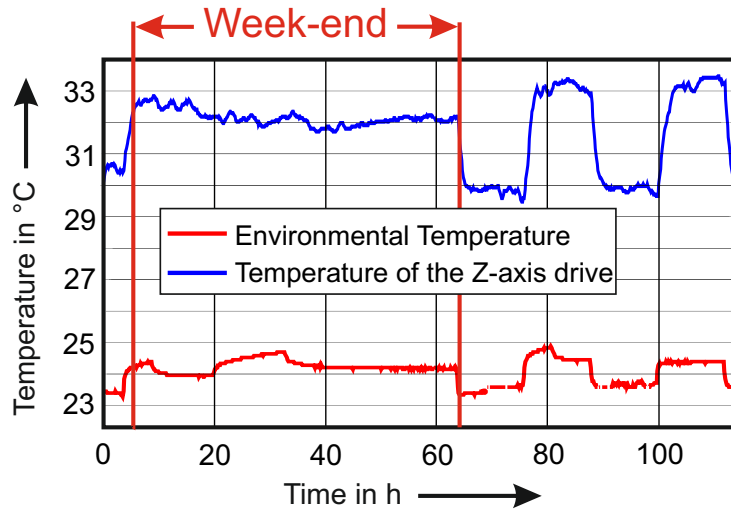
Figure 4.35: Machine tool A/C - Environmental temperature variation and Z-axis drive temperature variation during an ETVE-Test over 115 hours. The week-end mode of the air-condition system starts on Friday, 8 p.m. and stops on Monday, 8 a.m. (total of 60 hours)
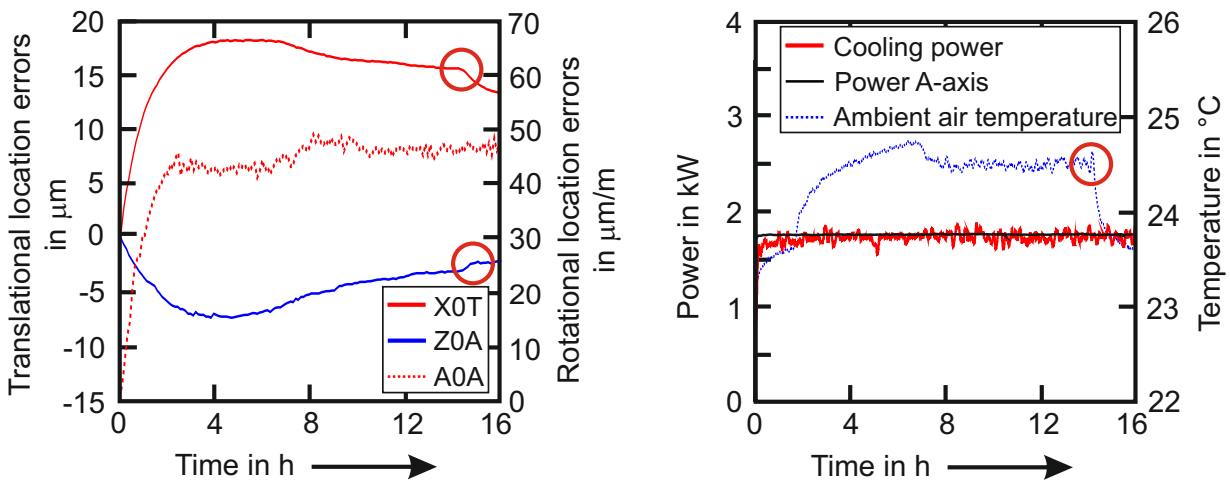
Figure 4.36: Machine tool A/C - Underlying movement: Pendular movement of a horizontal rotary axis in-between $\pm 90°$ for 16 hours. Left: significant location errors $X0T$, $Z0A$, $A0A$. Right: Drive Power, Cooling power and environmental temperature variation. Red marks label the influence of a change in the environmental conditions (temperature, convection) on the thermally induced errors [126].

Figure 4.37: Machine tool A/C - Underlying movement: Swivelling the horizontal rotary axis to $90°$ where the axis remains under control for 16 hours. Left: significant location errors $X0T$, $Z0A$, $A0A$. Right: Drive Power, Cooling power and environmental temperature variation. Red marks label the influence of a change in the environmental conditions (temperature, convection) on the thermally induced errors.
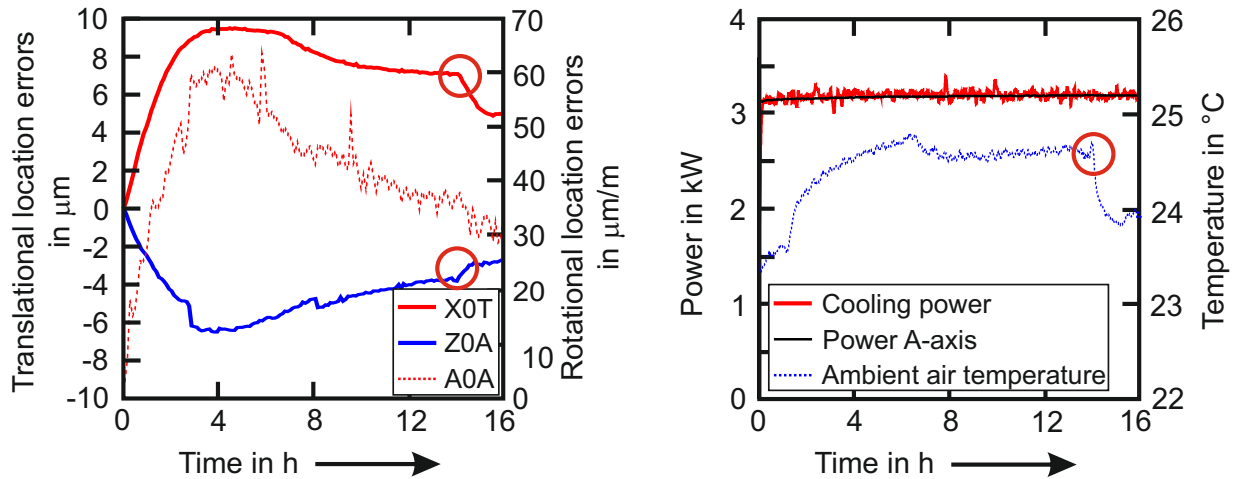
Figure 4.37 again shows the location error $X0T$, $Z0T$ and $A0C$ (left) and the corresponding drive power, cooling power and environmental temperature (right) of the A-axis of **Machine tool A/C**. During this measurement, the underlying load cycle is the position control of the axis at an angle of $-90°$ for 16 h. The deviations are $X0T = 9.5$ μm, $Z0A = 6.5$ μm and $A0A = 65$ μm/m. While the environmental temperature is very similar to the measurements of the pendular movement presented in Figure 4.36, the average drive power is larger (approximately 3.2 kW). In spite of this higher demand for power, the measured deviations in translational direction are much smaller than during the pendular movement. This can be explained by the missing friction in the bearings of the axis.

Vertical Axes

All analysis of vertical, rotary axes in this section are carried out without workpieces and under no load and no cutting conditions. Varying thermal load has been simulated by a varying rotational speed over the whole speed range of the axis. Again, in a first step, the heat flux in the analysed machine tools due to a rotation of the vertical axis is measured with an infrared camera and with thermocouple sensors. After that, errors of the axes were determined by the R-Test.

Figure 4.38 shows IR-images of the C-axis machine table of **Machine tool A/C**. The table is rotated at an A-axis position of $90°$ with a feed rate of $v_{rot_{max}} = 21600°/\text{min}$ (Figure 4.38 A). After that, the table cools down for 4 h (Figure 4.38 B). Then, the table is rotated with $0.5 \ v_{rot_{max}} = 10.800°/\text{min}$ at a A-axis position of $0°$ for 5 h (Figure 4.38 C). Afterwards it is rotated again with $v_{rot_{max}} = 21600°/\text{min}$ (Figure 4.38 D) before it finally cools-down for 4 h (Figure 4.38 E). By using two different A-axis angles, the heat flux on the top and on the bottom of the swivelling unit structure could be visualized. It can be seen that the heat flux induced by the C-axis drive only leads to a heat-up of the
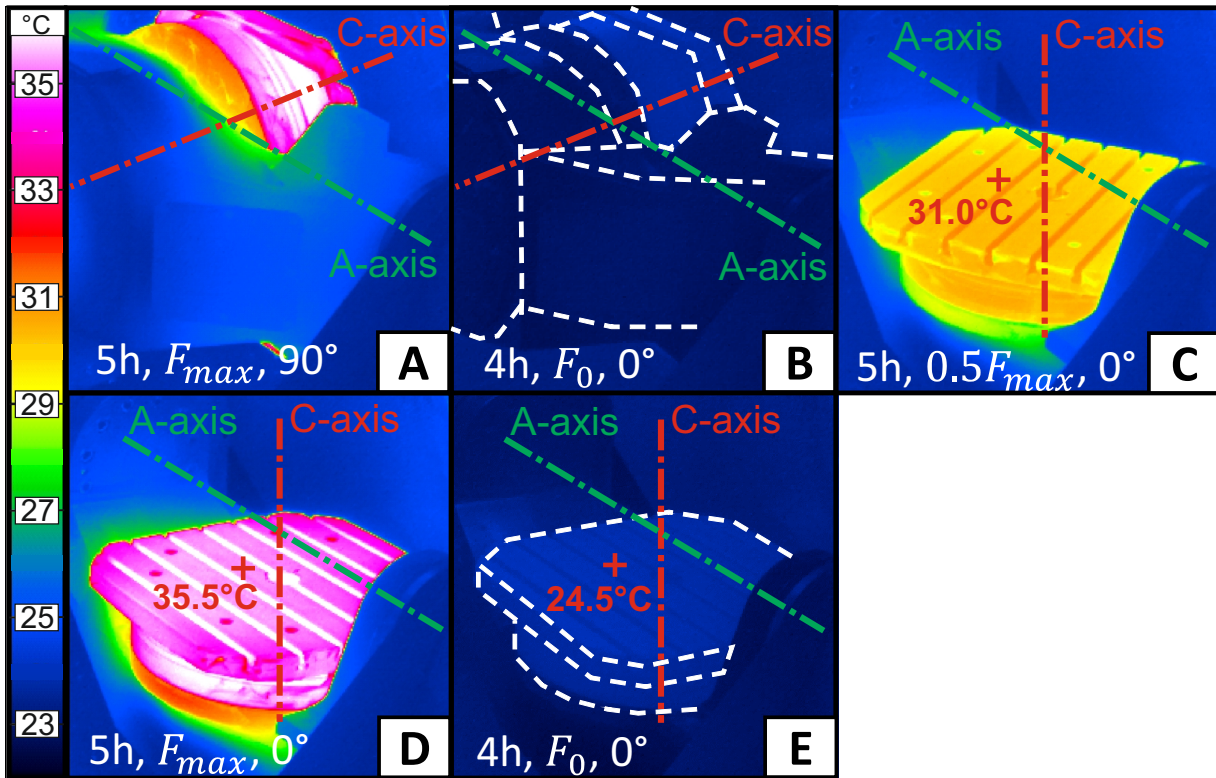
Figure 4.38: Machine tool A/C - Rotating a machine tool table with $60 \ \text{min}^{-1}$ for five hours in Figures A/D and with $30 \ \text{min}^{-1}$ for five hours in Figure C. Cool down for four hours in Figures B/E. View Figures A/B at a tilting angle of the swivelling axis of $90°$, Figures C/D/E at a tilting angle of $0°$ [126].

table structure. Because of the cooling of the unit, the rest of the structure shows only a very slight warm-up of approximately 1°C (Figure 4.38 A/C/D), which can be assigned to the warm-up of the air in the working space. In (Figure 4.38 B) and (Figure 4.38 E), it can be seen that a 4 h cool down phase is enough to reach initial conditions again. The difference of the rotational speed (Figure 4.38 A/D: $v_{rot_{max}}$, C: 0.5 $v_{rot_{max}}$) results in a significant temperature difference between these two conditions of approximately 5°C. In total, the magnitude of the temperature rise is about 12°C regarding $v_{rot_{max}}$ and 7°C regarding $0.5 v_{rot_{max}}$.

Figure 4.39 shows the verification of the infrared camera records by thermocouple sensor measurements. Basically, the measurement confirms the temperature values from Figure 4.38 except the peak temperatures, which are approximately 2°C higher. This can be explained by the additional load applied by the temperature measurement system which is mounted on the machine tool table.

In Figure 4.40, the temperature change of the machine tool table (C-axis) of **Machine tool B/C** during a load cycle of 4 h rotation with $600 \ \text{min}^{-1}$ and 4 h cool down can be seen with a temperature rise during warm-up phase with approximately 5°C. The measurements show two interesting effects: After stopping the C-axis, the table temperature shows a small peak. This is due to the stall which leads to a significant reduction of the convective flow of heat. This effect in combination with an ongoing heat flux from the drive to the machine tool table leads to the temperature peak. The other interesting effect can be seen between
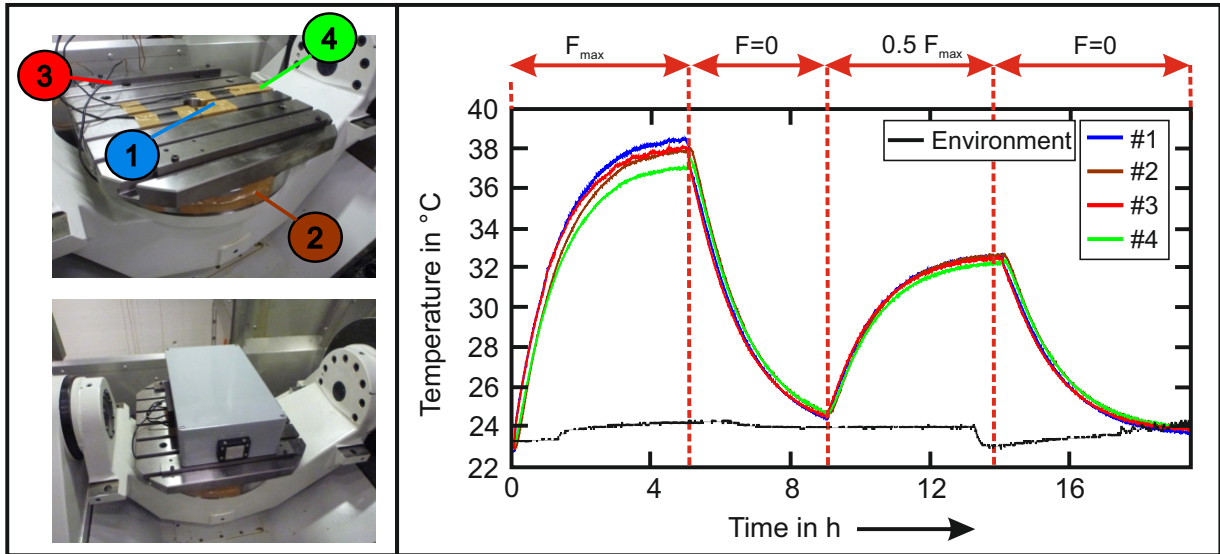
Figure 4.39: Machine tool A/C - Rotating a machine tool table with $v_{max} = 60 \ \text{min}^{-1}$ for five hours followed by a cool-down of four hours. After that, rotating the table with $0.5v_{max} = 30\text{min}^{-1}$ for five hours, followed again by a cool-down of four hours. Nr. $1-4$ mark the four sensor positions according to the measurement in the right diagram (corresponding colours).

six and seven hours: the cooling curve shows a break which is due to the automatic stop of the internal cooling system.

After measuring the temperature distribution under different thermal loads, the resulting TCP-displacements are measured with the R-Test system. Figure 4.41 shows all measured errors of the C-axis table of **Machine tool B/C**: $X0C$, $Y0C$, $R0T$, $Z0T$, $A0C$, $B0C$ and $C0C$. All measurements are carried out with four hours warm-up time and four hours cool down time at six different rotational speeds from 200 min^{-1} to 1200 min^{-1}. A measurement is carried out every five minutes with a measurement duration of approximately 50 seconds. In all diagrams showing the thermally induced errors, the measurement time is cut-out. The location errors $X0C$, $B0C$ and $C0C$ show no systematic dependency on the underlying thermal load. $Z0T$ is the largest contribution to the measured deviation: at 1200 min^{-1}, the deviation increases up to 28 μm. This error has two sources: a shift of the C-axis bearing in Z-direction caused by the thermal expansion of the structure around the C-axis drive in combination with a expansion of the machine tool table with its rotating shaft. When the heat, produced by the drive and in the bearings, and the heat release by the cooling-system, heat transfer in the surrounding structure and forced convection equilibrate, the deviation reaches a steady-state. Another large TCP-error occurs in $Y0C$-direction with roughly 26 μm. In this direction, no steady state value is reached: due to the heat induced by the C-axis drive, the whole rotary / swivelling axis unit expands. Because of the cantilever structure and one sided bearing support of the unit, this expansion results in a negative $Y0C$-displacement. After two hours, due to the homogenization of the temperature field in the machine tool structure, the TCP-displacement decreases. This effect can be seen very systematically at all six rotation speeds. The same effect can be seen regarding $R0T$ and $A0C$. These errors show small deviations up to 12 μm/m. All significant errors do not reach the zero level again after the cool-down. This can be
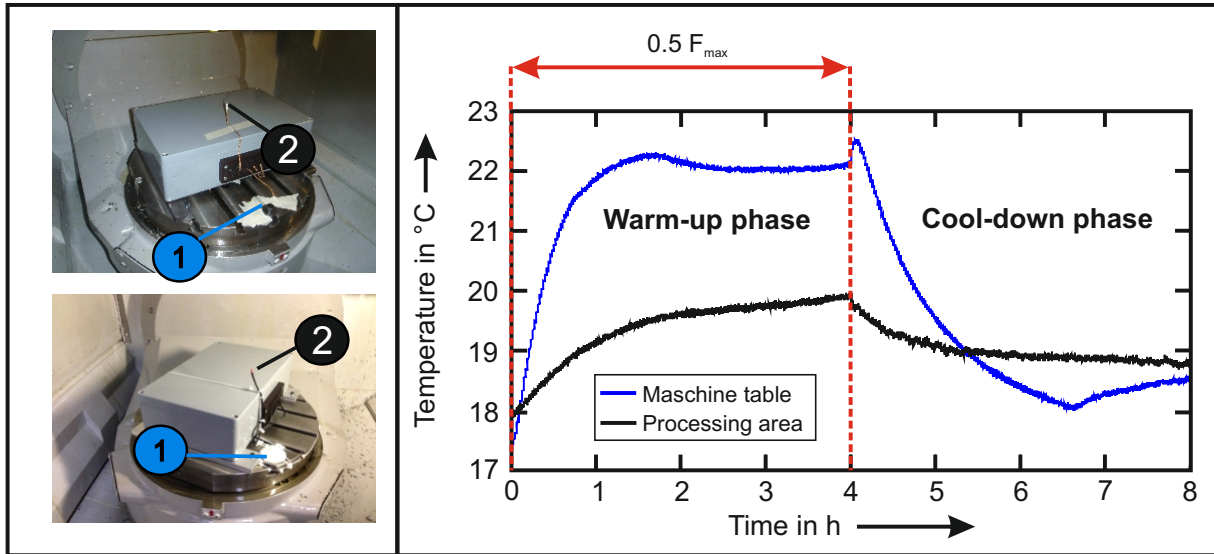
Figure 4.40: Table temperature of **Machine tool B/C** during a four hour warm-up phase (Rotation with 600 min^{-1}) and a cool down phase of additional four hours. Nr. 1 and 2 mark the two sensor positions according to the measurement in the right diagram (corresponding colours).

explained by the internal cooling unit: The control of this system is cooling the flow till the return flow temperature corresponds with the environmental temperature. All measurements are started approximately in the forenoon and stopped in the late evening, which means that the environmental temperatures at the end of the measurements were clearly lower (Figure 4.21). This results in a zero-crossing of the location errors and a non-zero final value.

4.2.3 Influence of Cooling Lubricant (CL)

Significant parts of this chapter have been presented in [134].

All previously presented measurements are carried out without using cooling lubricant (CL). Because CL is expected to have a significant influence on the thermal behaviour of machine tools, additional measurements are carried out on **Machine tool B/C** with CL in order to get an idea of this influence. During the measurements, the lubricant was applied by three noozles (Illustration (2) in Figure 4.42) spraying extensive over the whole table surface. During the rotation of the table, the lubricant dispersed so that it has been distributed in the whole processing area.

In a first step, thermography measurements are carried out in order to get a qualitative overview of the heat flux in the machine tool structure and the general temperature distribution under the use of cooling lubricant. In a second step, temperatures are recorded with thermocouple temperature sensors (Fig. 4.42, left). Finally, the occurring location errors are measured with the discrete R-Test measurement system (Fig. 4.42, right). Therefore, all sensors, cables and plugs had to be protected against the quite aggressive CL (Fig.
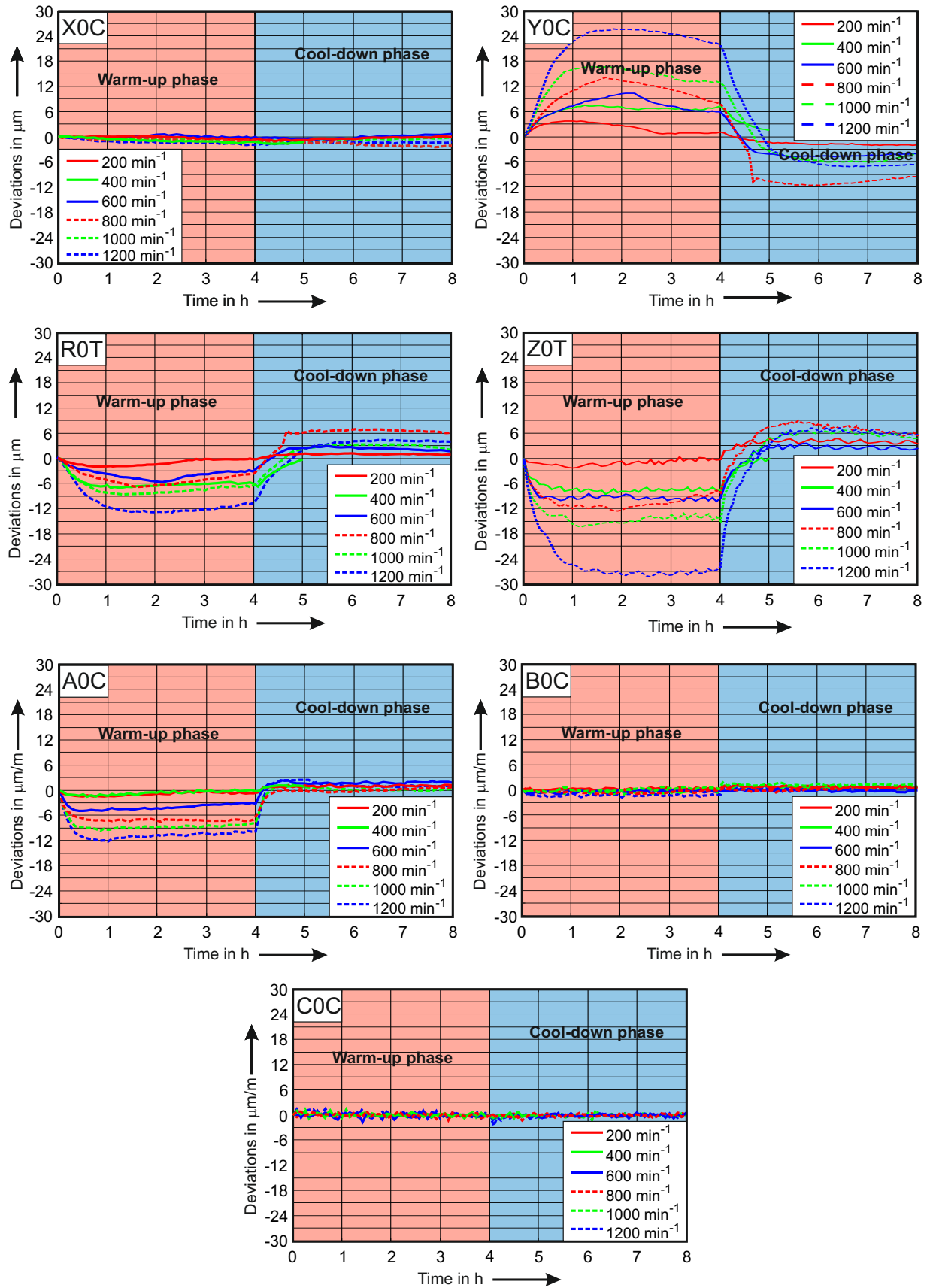
Figure 4.41: Machine tool B/C - Location Errors $X0C$, $Y0C$, $R0T$, $Z0T$, $A0C$, $B0C$ and $C0C$ of a table rotating with a vertical C-axis. Measurements were carried out at six different speeds from 200 up to 1200 min^{-1}.
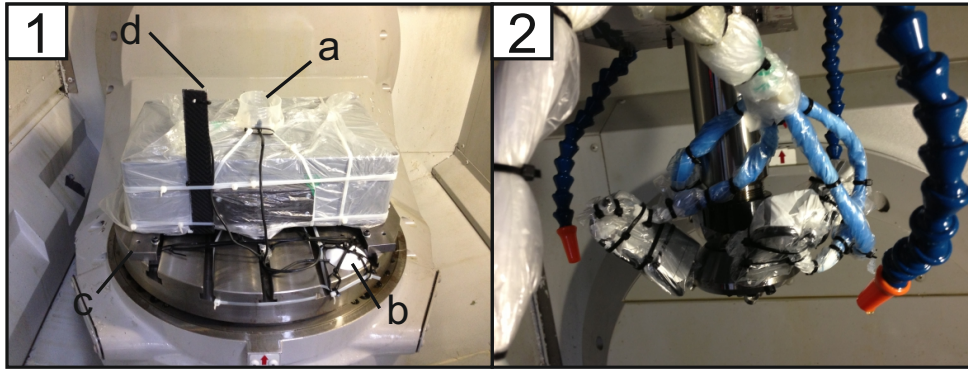
Figure 4.42: Machine tool B/C - Protected measurement systems for the characterisation of the thermal behaviour under CL: (1) wireless temperature measurement system with a) cup for the measurement of CL lubricant temperature, b) fixture for the table edge temperature sensor, c) fixture for the mounting of the temperature measurement system, d) sensor for the measurement of the air temperature in the process area; (2) R-Test system and wires protected with plastic sheets.

Table 4.5: Summary of measurements carried out on **Machine tool B/C** at different load levels with different axes to characterize the influence of CL ($+$: yes $-$: no).

Axes	Load level	Cooling lubricant	Thermography	Thermocouple	R-Test
C	1 (300 min^{-1})	$\pm$	$-$	$+$	$+$
C	2 (600 min^{-1})	$\pm$	$-$	$+$	$+$
C	3 (1200 min^{-1})	$\pm$	$+$	$-$	$+$
B	4 (90°)	$\pm$	$-$	$+$	$-$
C, B	5 Stepwise variation	$\pm$	$-$	$-$	$+$

4.42, right). All measurements have been carried out at different load levels with and without cooling lubricant according to Table 4.5, to be able to compare both conditions directly.

Figure 4.43 shows infrared records during an operation over 240 min at 600 min^{-1} without (upper figures) and with (lower figures) CL. Measurements with CL show two significant differences:

- a higher temperature increase;

- the whole B-axis corpus is affected by spraying CL.

In order to investigate this behaviour more detailed, temperature measurements are carried out as described above. In addition to the environmental, table and process area temperature, the temperature of the CL is measured. Figure 4.44 shows the temperature development with (Figure 4.44 (2),(4)) and without (Figure 4.44 (1),(3)) CL during a load cycle where the table of **Machine tool B/C** is rotated with 300 min^{-1} (Figure 4.44
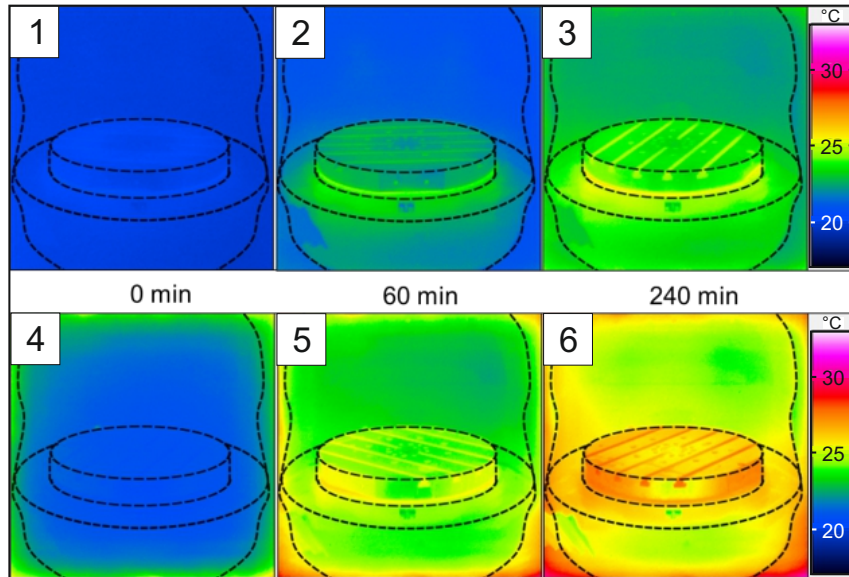
Figure 4.43: Machine tool B/C - Infrared camera measurements showing the influence of CL on rotary axes, rotational speed: 600 min^{-1}. Total measurement time: 240 min. Top: without CL / bottom: with CL [125].

(1),(2)) and 600 min^{-1} (Figure 4.44 (3),(4)) over 15 h, because after 4 h measuring time as chosen standard cycle the thermal drift shows no steady-state behaviour. Due to the increased warm-up time, also the cool-down time was enlarged. After ten hours, steady-state is reached. Regarding measurements without CL, the table temperature measured at the edge of the table is higher than in the middle. Both, the direct drive and the bearings inner ring, cause that the main heat source is located outside the C-axis centre. With stopping the rotational operation after 15 h, all temperature sensors show a slight increase because of the stall, which leads to a significant reduction of the transport of heat by convection combined with a continuing heat flux from the drives and bearings. Generally, the measured temperatures of the machine tool show a quite stable behaviour after approximately two hours warm-up phase. Maximum temperatures are determined with 22.5°C (300 min^{-1}) and 25.0°C (600 min^{-1}) at the edge of the table.

Regarding the temperature distribution with CL, a completely different behaviour is measured: temperatures are significantly higher, maximum values are measured with 31.0°C. This applies to both operation speeds: 300 and 600 min^{-1}. At the same time, measurements with CL show a much higher delay to reach the steady state level. An explanation of this effect can be found in the design of the process cooling system: the tank for the lubricant has no cooling system - a defined amount of lubricant per minute is pumped in a circuit. This leads to an increase of the lubricant temperature due to the heat input by the pump and by friction. Finally, the fluid is released to the overflow surfaces in the process area of the machine tool which explained the large temperature increase.

This phenomena shows, how important the design and the operation procedure of the process cooling system is regarding the heat flux in the machine tool structure. It can be expected, that systems with a cooling unit for the lubrication, or with a central tank for
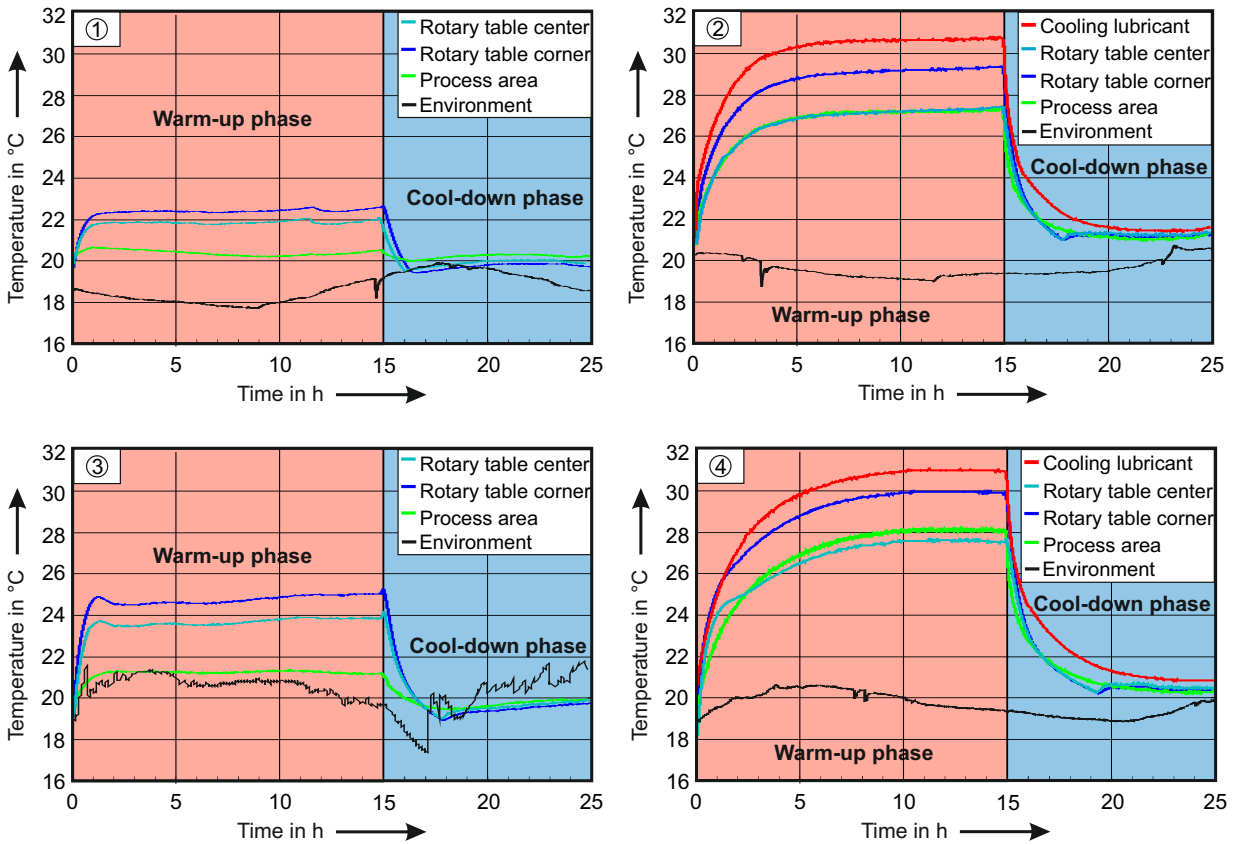
Figure 4.44: Machine tool B/C - Temperature measurements during a C-axis operation of 15 h warm-up and 10 hours cool-down phase: 1) 300 min^{-1}, without CL 2) 300 min^{-1}, with CL, 3) 600 min^{-1}, without CL, 4) 600 min^{-1}, with CL [125].

several machine tools influencing each other, show a significantly different behaviour.

Figure 4.45 shows the location errors corresponding to the load cycle 300 min^{-1} with (Figure 4.45(2),(4)) and without (Figure 4.45(1),(3)) CL. The upper Figures represent the translational deviations, the lower figures represent the rotational deviations. Like described in section 4.2.2, **Machine tool B/C** shows no temperature depending behaviour regarding the location errors $X0C$, $B0C$ and $C0C$. All other errors show a larger magnitude with CL than without, explained by the higher temperatures. With stopping the warm-up cycle after 15 hours, the location errors decrease immediately. After further approximately two hours, the internal cooling unit stops, so that an additional characteristic peak can bee seen in the measured errors. The most significant changes can be seen regarding $Y0C$ with an increase of the magnitude from 10 to 25 μm and $A0C$ from 5 to 20 μm/m.

The same effect can be seen regarding the measurement with a rotation speed of 600 min^{-1} (Figure 4.46). While the errors during the measurement without CL is clearly larger due to the larger thermal input by the drives and by friction, the behaviour with CL is quite similar to the measurement with 300 min^{-1}. This shows that the temperature of the cooling lubricant is dominating the influence of the internal heat sources, such as drives and bearings.

Figure 4.45: Machine tool B/C - Errors measured with R-Test during a C-axis operation of 15 h warm-up and 10 h cool-down phase: 1) Translational deviations, 300 min^{-1}, without CL 2) Translational deviations, 300 min^{-1} with CL, 3) Rotational deviations, 300 min^{-1}, without CL, 4) Rotational deviations, 300 min^{-1}, with CL [125].
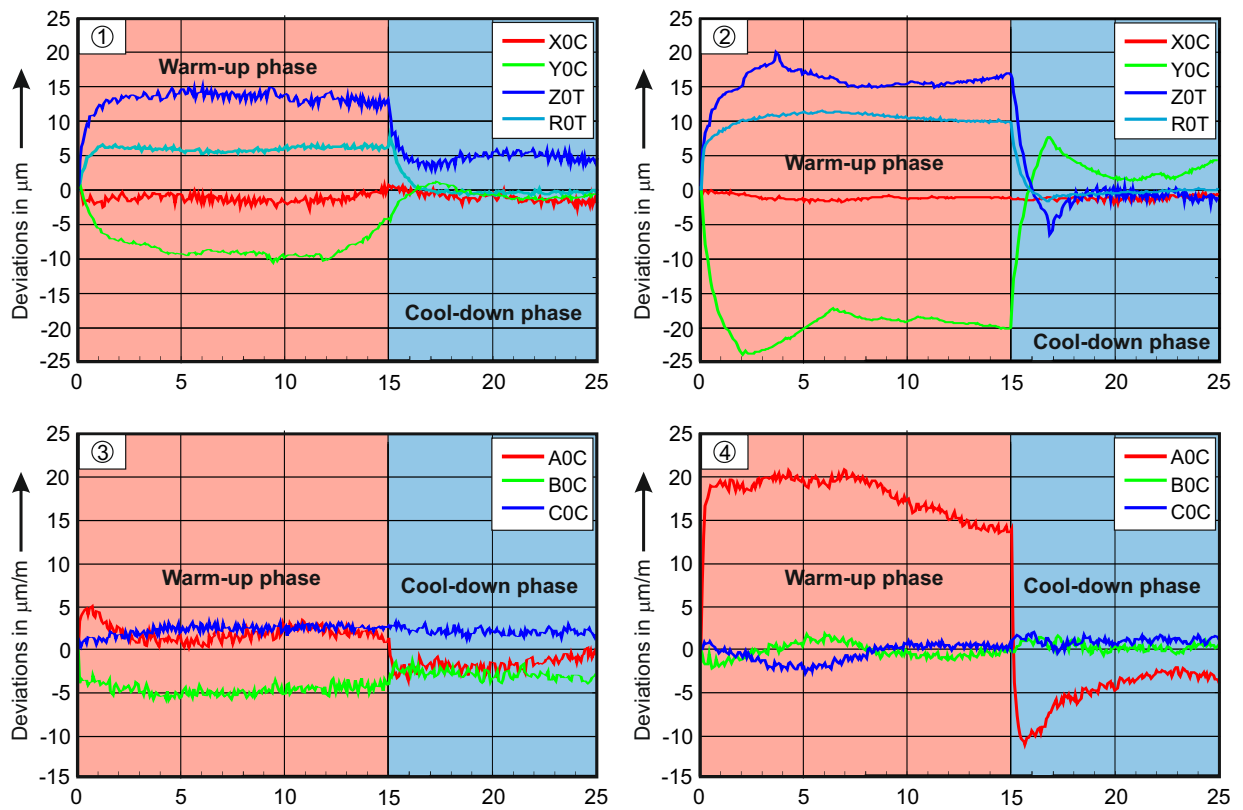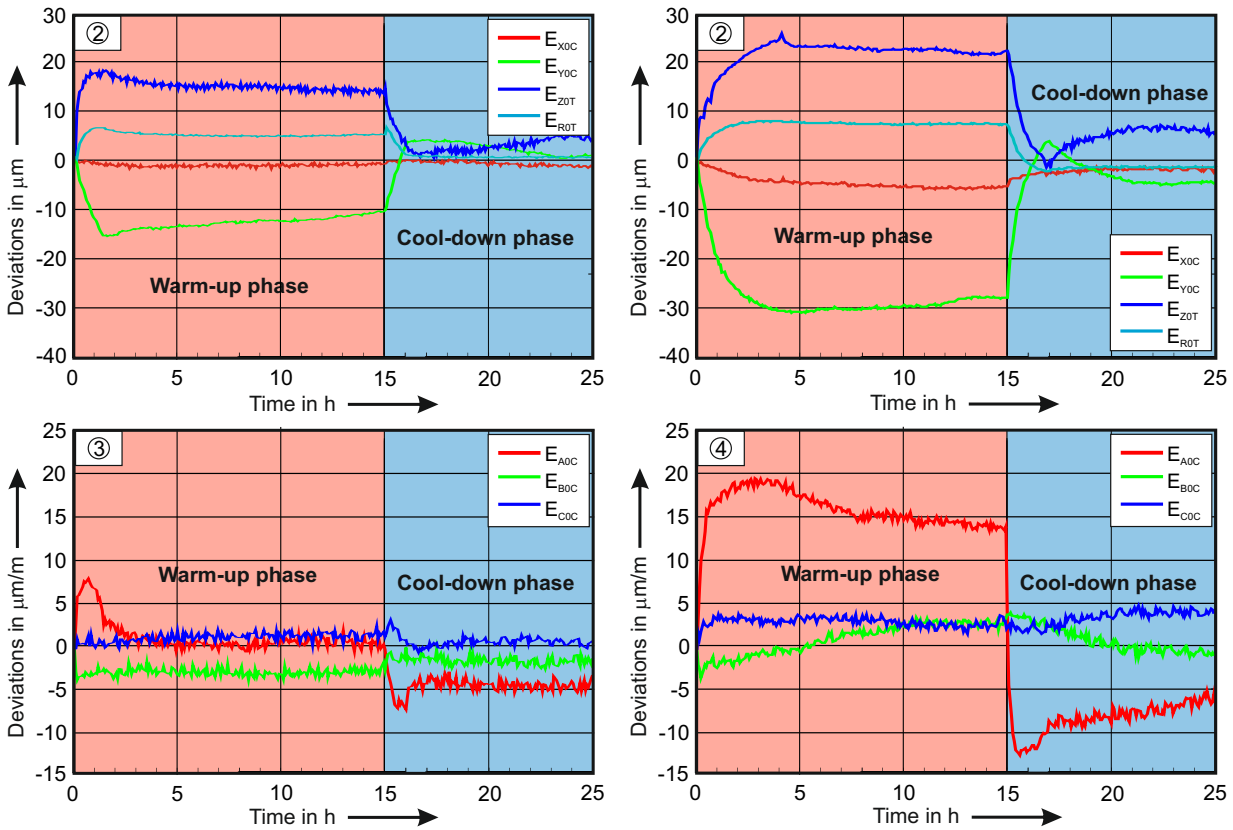
Figure 4.46: Machine tool B/C - Errors measured with R-Test during a C-axis operation of 15 h warm-up and 10 hours cool-down phase: 1) Translational deviations, 600 min^{-1}, without CL, 2) Translational deviations, 600 min^{-1}, with CL, 3) Rotational deviations, 600 min^{-1}, without CL, 4) Rotational deviations, 600 min^{-1}, with CL [125].

Summarizing the measurements with cooling lubricant, it is very important to consider the enormous influence. It is quite difficult to compare machine tools, because of the different cooling units and cooling strategies, but investigations showed that the behaviour of the machine tools strongly corresponds with the temperature of the cooling lubricant. Therefore, compensation strategies could be base on an online temperature measurement of the cooling lubricant.

4.3 Comparison of Contributors to the Total Thermal Error

In this section, the thermal behaviour of two five-axis machine tools was investigated in detail at selected feed rates and spindle speeds summarised in Appendix C. Feed rates and spindle speeds were chosen as they are used for typical finishing applications. The maximum errors measured according to ISO 230-3 are summarised in Table 4.6 and Table 4.7. In addition, the errors of the rotary C-axes of **Machine tool B/C** and **Machine tool A/C** are supplemented.

When comparing the listed deviations, it can be seen that the magnitude of the location

Table 4.6: Summary of different shares to the total thermal error of **Machine tool B/C**. Duration of ETVE: 7 d, Range of environmental temperature change during ETVE tets: 5.5°C, Rotational speed for spindle test: 3000 $1/min$, Feed speed for linear axis tests: 500 mm/min, Rotational speed for C-axis test: 400 1/min.

	ETVE	Spindle	X-Axis	Y-Axis	Z-Axis	C-Axis
	$[\mu m]$	$[\mu m]$	$[\mu m]$	$[\mu m]$	$[\mu m]$	$[\mu m]$
X	6	2	2	4	6	2
Y	12	5	4	10	10	15
Z	8	14	7	5	5	14
	$[\mu m/m]$	$[\mu m/m]$	$[\mu m/m]$	$[\mu m/m]$	$[\mu m/m]$	$[\mu m/m]$
A	60	8	12	8	7	8
B	25	12	5	6	12	2

Table 4.7: Summary of different shares to the total thermal error of **Machine tool A/C**. Duration of ETVE: 4.7 d, Range of environmental temperature change during ETVE tets: 2°C, Rotational speed for spindle test: 6000 $1/min$, Feed speed for linear axis tests: 500 mm/min, Rotational speed for C-axis test: 30 1/min.

	ETVE	Spindle	X-Axis	Y-Axis	Z-Axis	C-Axis
	$[\mu m]$	$[\mu m]$	$[\mu m]$	$[\mu m]$	$[\mu m]$	$[\mu m]$
X	5	7	2	4	6	11
Y	8	3	2	1	5	2
Z	14	10	8	1	5	17
	$[\mu m/m]$	$[\mu m/m]$	$[\mu m/m]$	$[\mu m/m]$	$[\mu m/m]$	$[\mu m/m]$
A	18	25	4	4	4	6
B	15	14	12	12	15	2

errors of rotary axes (caused by a movement of the rotary axes) is at least of the size of other contributors like the environment, the spindle and the linear axes evaluated according to ISO 230-3. Of course, this is due to the fact that for influences considered in ISO 230-3, compensation and correction effort is already carried out either regarding the design of machine tools or NC-based correction techniques. These measurements show, that this effort also has to be done for the rotary axes, which become more and more important - also regarding precision manufacturing - with the increasing demand for five-axis machine tools.

In this work, only location errors of the rotary axes or functional surfaces and the dimension deviation $R0T$ are considered. Regarding geometric measurements, also component errors of rotary axes are quite important. To estimate the magnitude of the thermal component errors, measurements with contactless capacitive sensors according to ISO 230-3 are carried out. With a precision test mandrel on the machine tool table and five probes mounted in the spindle, component errors are measured continuously during four hours. One measurement is carried out with a rotational speed of 300 min^{-1} (Figure 4.47, (1), (3) and (5)), one measurement was carried out with 600 min^{-1} (Figure 4.47, (2), (4) and (6)). After starting the tests, a very slight increase of the radial errors E_{XC} and E_{YC} as well as the axial error E_{ZC} can be seen. After one hour, the distortions reach steady state level. A similar behaviour can be seen regarding the measurement with 600 min^{-1}, where the magnitude is higher because of the larger, thermal load. At 3.5 h, a buckle can be seen which is supposable due to the internal cooling system. Regarding the wobbling errors E_{AC} and E_{BC} in (Figure 4.47, (3) and (4)), the signal is interfered but not increasing or decreasing during the measurement. Environmental temperatures during the measurements are quite stable (Figure 4.47, (5) and (6)). Measurement show a magnitude, which is approximately ten times smaller than the magnitude of location errors. This entitles the neglect of the component errors in this work and the concentration on thermally induced location errors.
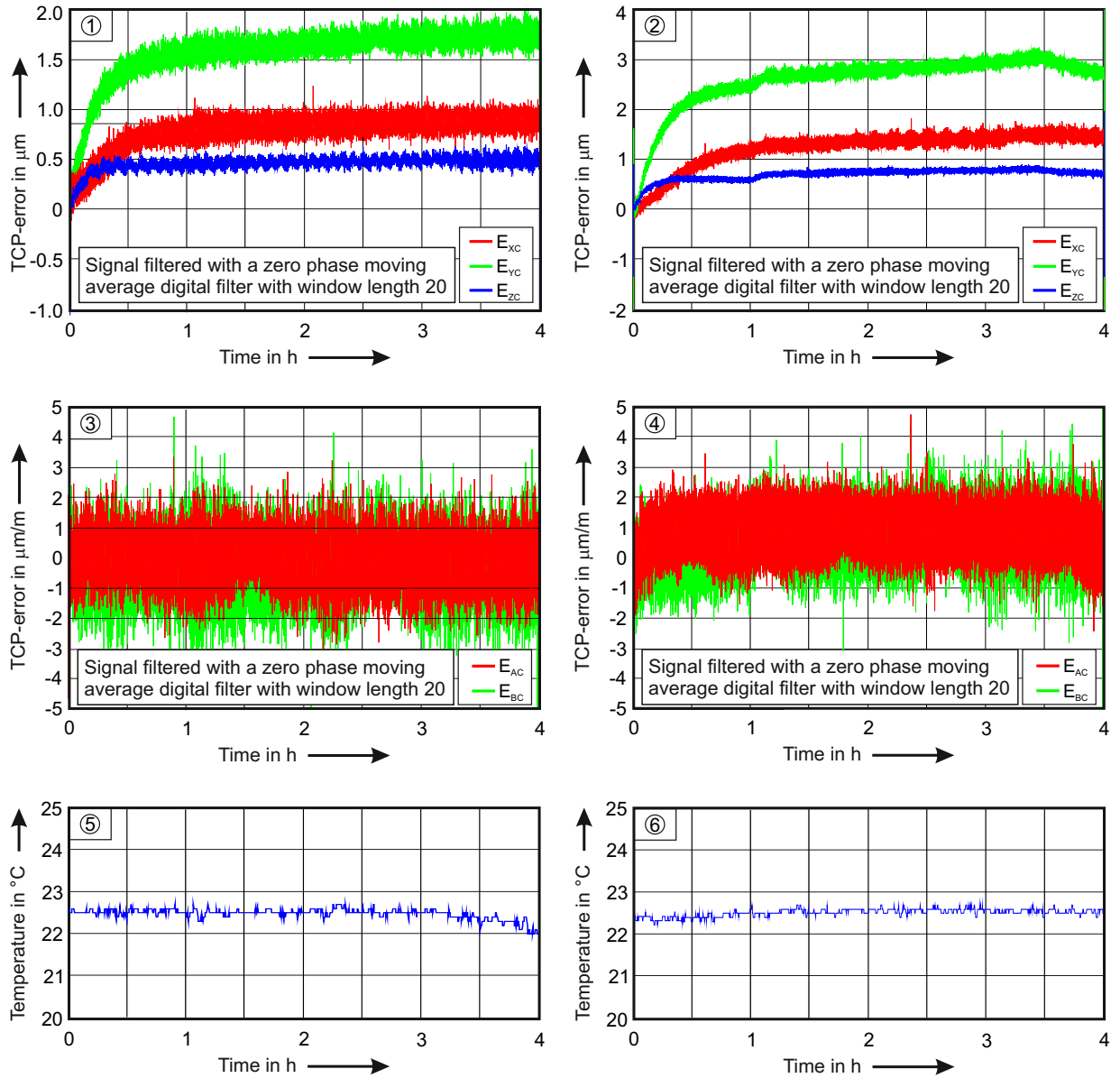
Figure 4.47: Translational component errors E_{XC}, E_{YC} and E_{ZC} (Figures 1/2), rotational component errors E_{AC} and E_{BC} (Figures 3/4) and corresponding environmental temperature (Figures 5/6) during a four hours rotational movement of the C-axis of **Machine tool B/C** with $300 \min^{-1}$ (Figures 1/3/5) and $600 \min^{-1}$ (Figures 2/4/6)

5 Modelling of Thermo-Elastic Deformations of Rotary Axes

In this work, two different approaches for simulation models are presented: a physical approach in section 5.1 and a phenomenological approach in section 5.2. The aim of both models is to predict thermally induced errors of rotary axes of five axes machine tools in dependency of a varying thermal load. In section 5.3, both models are compared.

Some part of the following content has been published by the author in [121–124, 126, 127, 135].

5.1 Physical Simulation Model

Significant parts of this chapter have been presented in [136] and [137].

The physical model approach presented in this thesis consists of three components: the evaluation of thermal loads, the computation of the temperature distribution and the computation of the TCP-displacements. In step 1, the change of the temperature distribution is computed depending on the underlying load. In step 2, the computation of relating TCP-displacements and changes of the functional orientation between tool and workpiece is carried out based on the temperature computations of step 1.

The approach in this thesis aims for the simplification of the significant structure of the machine tool (rotary / swivelling unit) by introducing several bodies, assumed to be homogeneous. With the power input to the drives, the cooling power provided by the internal cooling unit, the heat transfer between the bodies and between the environment, temperatures of the single bodies are computed. With the knowledge of the expansion coefficients, the effective lengths of the bodies and the offsets between the single bearings, thermally induced deviations can be predicted. The advantage of the simplified machine tool structure is, that it can effectively be adapted for other machine tools, especially for other machine tools within a series. The structure is represented by an analogous model consisting of n different bodies, supposed to be ideal homogeneous. The number of bodies n has to be minimized in order to simplify the structure, but has to be as large as necessary to compute all significant displacements. The significant displacements are known from measurements, which were carried out previously (section 4.2).

In Figure 5.1, the analogous model of the rotary / swivelling axis unit of **Machine tool B/C** can be seen. The body *Bed* represents the bed of the machine tool. Its large thermal mass is important in order to consider the inert behaviour of the machine tool. The *C*-axis unit of the machine tool is divided into three different bodies *Table*, *C-Body 1* and *C-Body 2*. The analysis of the design drawings of **Machine tool B/C** shows,
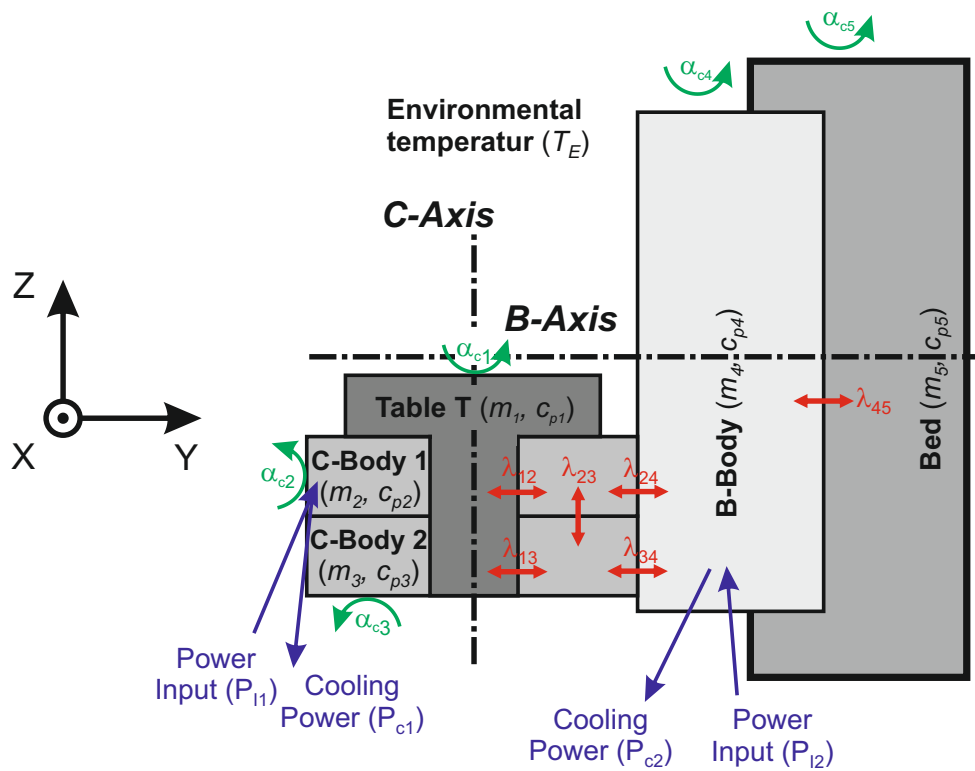
Figure 5.1: Schematic of discretized bodies for calculation of the thermally induced errors $X0C$, $Y0C$, $Z0T$, $A0C$ and $R0T$ for **Machine tool B/C** with m is the mass, c_p is the specific heat capacity, α_{ci} is the coefficient for convective heat transfer, λ_{ij} is the coefficient for heat transfer by conduction, P_I stands for input power, P_C means cooling power and T_E is the environmental temperature. All parameters are described in Table 5.1.

Table 5.1: Used bodies and their acronym

Body	Acronym
Table	t
C-Body 1	c_1
C-Body 2	c_2
B-Body	b_1
Machine bed	b

that the direct drive of the C-axis and the cooling channels are located directly under the machine tool table. This implies, that the main power input happens in the upper part of the C-Body. Therefore, the C-Body was separated into the two vertical bodies *C-Body 1* and *C-Body 2*. This allows to model the squareness error $A0C$ which occurs because of the heterogeneous power input and the resulting heterogeneous and transient temperature field in the C-Body, which leads to a kind of a bimetallic effect. The machine tool table is modelled as a separate body, because it is required for the calculation of the radial growth of the machine tool table ($R0T$). The boundary to the adjacent body *C-Body 1* represents the physical system transition between stationary and moved components. The fixed bearing of the table is separated in the middle. The drive is divided into the stator (belonging to *C-Body 1*) and rotor (belonging to the body *Table*). By this, the system boundary is defined in a way, that the power input P_{I1} to the C-axis drive is split and given to the two bodies *Table* and *C-Body 1* in equal shares. This assumption is adjusted by the calibration of the model (section 5.1.3). The B-axis unit is represented by *B-Body*. With this discretization of the machine tool structure, the four significant location errors $Y0C$, $Z0T$, $R0T$ and $A0C$ can be considered and represented. Table 5.1 allocates symbols to the single bodies which are used in the following thesis.

The disadvantage of assuming the bodies to be homogeneous, is that parameters such as the thermal conductivity or the heat capacity can not be estimated by literature values. The body *C-Body 1* for example, consists of different materials and structural elements like the drive, parts of the cooling system, bearings or simply cavities.
In addition to that, many other parameters can only be estimated roughly: Without a detailed CAD model, masses, surfaces and material specific data are only assumed or estimated. Therefore, a calibration of the model is necessary: measurements of thermal errors between tool side and workpiece side due to a certain thermal load are used to compare the real machine tool behaviour with the model. Then, the model is changed by a numerically carried out parameter adjustments in order to harmonize computational results with reality (section 5.1.3). All input- and model parameters necessary for the calculation of the thermally induced errors are listed in Table 5.2.

Table 5.2: Model constants and input parameters. Index n defines bodies according to Table 5.1.

Parameter	Symbol	Unit
Input Parameters		
Power from drives	P_I	[W]
Cooling power	P_c	[W]
Axes position	$(A\hat{x}is)$	[mm]
Model constants		
Mass of body i	m_i	[kg]
Surface of body i	A_{S_i}	[m^2]
Contact surface between bodies i &j	$A_{c_{ij}}$	[m^2]
Effective length between bodies i & j	$l_{eff_{ij}}$	[m^2]
Thermal conductivity between bodies i & j	λ_{ij}	[W m^{-1} K^{-1}]
Specific heat capacity of body i	c_{pi}	[J kg^{-1} K^{-1}]
Convection coefficient of body i	α_{ci}	[W m^{-2} K^{-1}]

5.1.1 Computation of the Temperature Distribution

This section describes the computation of the load-dependent temperatures of the single bodies.

The first law of thermodynamics describes that the change of internal energy ΔU of a closed system is equal to the sum of the change of heat ΔQ and the change of work ΔW [138]. Thus, the internal energy U can only be changed by an energy transport over the system boundaries. Based on this physical law, the thermally induced errors of the swivelling / rotary axis unit shall be computed via the temperature change in these bodies and the associated thermal expansion. The internal energy U of every body η is influenced by $\dot{Q}$, which is in this case more detailed and separated in the heat exchange with the adjacent bodies respectively the environment and $\dot{P}$, the power which is supplied or discharged, for example by the drives or a cooling system according to

$$\dot{U} = \sum \dot{Q} + \sum \dot{P} \tag{5.1}$$

According to [138], the change of the internal energy of a body can be expressed by its mass m, its specific heat capacity c_p and the time-dependent temperature-change $\dfrac{\partial T}{\partial t}$, which leads to a differential equation

$$m \cdot c_p \frac{\partial T}{\partial t} = \sum \dot{Q} + \sum \dot{P} \tag{5.2}$$

for every body of the introduced multi-body simulation model. Consequentially, a system of differential equations results, which can be solved numerically according to [139] by

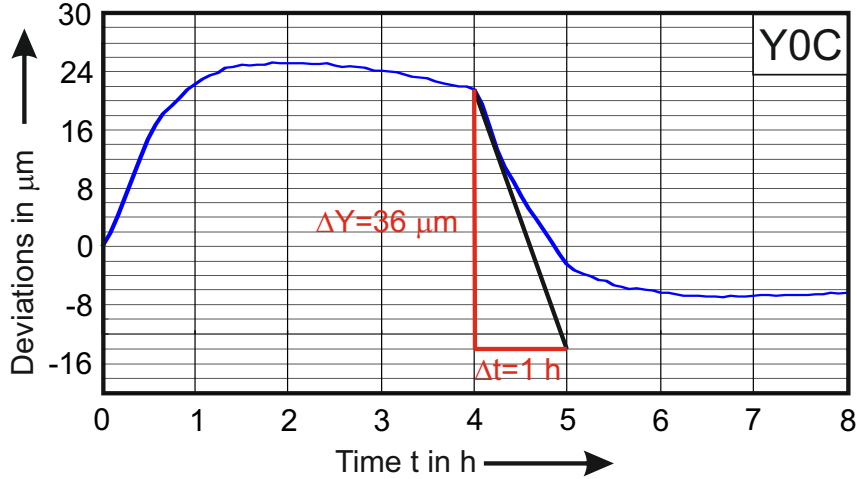$$\frac{\partial T}{\partial t} = \lim_{\Delta t \to 0} \frac{T_{t+1} - T_t}{\Delta t} \tag{5.3}$$

Figure 5.2: Maximum gradient measured on **Machine tool B/C**: Location error $Y0C$ shows $\frac{36\ \mu m}{h}$ during cool down after rotating four hours with $1200min^{-1}$.

Solving the equation for T_{t+1} leads to

$$T_{t+1} = T_t + \frac{(\sum \dot{Q} + \sum \dot{P}) \cdot \Delta t}{m \cdot c_p} \tag{5.4}$$

Now, the temperature of every body can be calculated via numerical integration. According to (5.3), the step size should approach zero, which is not feasible in practice. For the computation of thermally induced deviations, which show an inert behaviour, small increments deliver satisfying accuracy. In this work, a step size of

$$\Delta t = 0.5s \tag{5.5}$$

is chosen. Regarding the measured, thermally induced deviations, the maximum gradient is detected with $36\frac{\mu m}{h}$ ($Y0C$ during cooling down after four hours turning with $1200\ min^{-1}$, Figure 5.2). This equals 5 nm per time step of 0.5 s - therefore, the chosen time step is small enough but the computation is still performable easily on the used PC.

The total heat flux $\dot{Q}_{tot_n}$ in and out of every body n, which is considered for the calculation is

$$\dot{Q}_{tot_n} = \sum \dot{Q}_{hc_n} + \dot{Q}_{cv_n} \tag{5.6}$$

with $\dot{Q}_{hc_n}$ is the heat conduction and $\dot{Q}_{cv_n}$ is the heat transfer by convection. All heat flux into a body is positive, heat flux out of a body is negative. According to [16], for temperatures smaller than $100°C$ the magnitude of thermal radiation is negligible, so it is not taken into account.

In the following sections, the single contributors to the total heat flux are described in detail.

Heat conduction $\dot{Q}_{hc}$

The largest share of the total thermal flow $\dot{Q}_{tot}$ between two adjacent bodies i and j is in general heat conduction $\dot{Q}_{hc_{ij}}$ due to the materials, the geometry and the temperatures,

which prevail in a machine tool. It is calculated according to

$$\dot{Q}_{hc_{ij}} = \lambda \cdot \frac{A}{d}(T_j - T_i) \tag{5.7}$$

with the heat conduction coefficient λ, the cross-section A, the distance of both body centres d and the temperatures T_i of body i and T_j of body j.

Heat transfer by convection $\dot{Q}_{cv}$

The heat transfer by convection of a body i can be described with

$$\dot{Q}_{cv_i} = \alpha_{cv_i} \cdot A \cdot (T_i - T_o) \tag{5.8}$$

with α_{cv_i} is the convection coefficient of body i and T_o is the environmental air temperature. In this thesis, the environmental temperature is assumed to be the same for all bodies. It is measured with a temperature sensor (System 4 in Table 4.2) in front of the machine tool. The temperature values are read-in with a frequency of 1 Hz and used for the online - computation of the heat transfer by convection.

α_{cv} strongly depends on the speed difference of the observed surface compared to the passing air flow Δv_a (free convection or forced convection). In the analysed case of rotary swivelling axis units, the heat conduction by convection varies significantly depending on the rotary speed of the machine tool table. For the physical model, two cases are defined:

- $\Delta v_a = 0$ (free convection)

- $\Delta v_a \neq 0$ (forced convection)

Regarding the case of standstill (free convection), the convection coefficient of a body i depends on the surface conditions, the orientation and the temperature [140]. It is calculated via

$$\alpha_{cv_i} \, (\Delta v_a = 0) = \frac{Nu \cdot \lambda_o}{l} \tag{5.9}$$

with Nu is the dimensionless Nusselt number, λ_o is the thermal conductivity of the environmental air (assumed with $0.0268 \frac{W}{m^2 \cdot K}$, [140]) and l is the length of the overflowed surface.

Table 5.3 shows the values for parameters of the significant surfaces used for the calculations. They are determined according to engineering drawings and measurements. The calculation of the Nusselt number strongly depends on the orientation of the surface which is regarded, and the direction of the heat release. Figure 5.3 shows the different surface types and the corresponding equations for the calculation of the Nusselt number, used in this thesis according to [140].

In case of no motion, convection is quite insignificant for the analysed machine tool under the conditions prevailing. Therefore, a simplified average convection coefficient is computed for the free convection so that an overall surface temperature of 30°C, and a characteristic length of 1 m is assumed according to temperature measurements respectively the geometry of the machine tool. Simulation results show that varying both

Table 5.3: Geometric relevant parameters for calculating the heat transfer by convection for **Machine tool B/C**.

Body / part	Relevant surface	Type (Figure 5.3)
name	m^2	
Table t	0.2	A
Table t	0.1	C
$C - Body\ 1\ (c_1)$	0.2	A
$C - Body\ 1\ (c_1)$	0.1	C
$C - Body\ 2\ (c_2)$	0.4	B
$C - Body\ 2\ (c_2)$	0.1	C
$B - Body\ \ (b_1)$	0.6	A
$B - Body\ \ (b_1)$	0.1	B
$B - Body\ \ (b_1)$	0.1	C
Machine bed (b)	5.0	A
Machine bed (b)	18.0	C
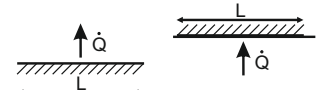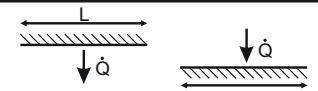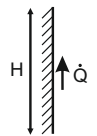
Type	Geometry	Constraints	Nusselt number
A	Horizontal plate, heat emission on the top side or heat input on the bottom side	$10^4 \leq Ra \leq 10^7$	$Nu = 0.54\ Ra^{0.25}$
		$10^7 \leq Ra \leq 10^{11}$	$Nu = 0.15\ Ra^{0.33}$
B	Horizontal plate, heat emission on the bottom side or heat input on the top side	$10^5 \leq Ra \leq 10^{10}$	$Nu = 0.27\ Ra^{0.25}$
C	Vertical plate	$10^{-1} \leq Ra \leq 10^{12}$	$Nu = \left\{ 0.825 + \dfrac{0.387\ Ra^{1/6}}{[1 + (0.492\ /\ Pr)^{9/16}]^{8/27}} \right\}$

Figure 5.3: Calculation of Nusselt number for different types of surfaces [140]

parameters by $\pm 50\%$ leads to a difference in the temperature computation of less than 1%. This shows that the assumption which is made is not critical.

After calculating the Nusselt Number according to equations $A - C$ in Figure 5.3, the Rayleigh number Ra has to be determined by

$$Ra = Gr \cdot Pr \tag{5.10}$$

with the Prandtl number Pr assumed as 0.7 [140] and the Grashof number Gr calculated according to

$$Gr = \frac{g \cdot l^3 (T - T_o)}{\nu_o^2 \cdot T_o} \tag{5.11}$$

In (5.11), g is the acceleration due to gravitation ($9.81\frac{m}{s^2}$), l again is the length of the overflowed surface l, T is the mean body temperature, T_o is the environmental air temperature T_o provided by a temperature sensor and the kinematic viscosity of the air ν_o^2 is $16.1 \cdot 10^{-6}\frac{m^2}{s}$ according to [140].

In case of motion, the convection coefficient rises significantly. In [141] and [142], the convection coefficient of a rotating disk (diameter $d = 450$ mm) is investigated by experiments for up to 4400 min^{-1}. For reasons of simplification, the machine table can be assumed to be a rotating disk, especially under no cutting conditions, when no additional workpiece is mounted which would change the convection significantly. The Reynolds number for rotating disks is calculated with the radius r, the angular speed ω and the kinematic viscosity ν_o according to

$$Re = \frac{\omega \cdot r^2}{\nu_o} \tag{5.12}$$

For low rotary speeds with $Re < 260'000$, the flow is laminar, and the Nusselt number is

$$Nu = 0.355 \cdot \sqrt{Re} \tag{5.13}$$

according to [143]. Figure 5.4 shows the Nusselt number as a function of the Reynolds number for rotary disks. For Reynolds numbers between 260'000 and 320'000, the Nusselt number is described by

$$Nu = 8.01 \cdot 10^{-14} \cdot Re^{2.8} \tag{5.14}$$

For disks with high rotary speeds and Reynold numbers over 320'000, flow is turbulent. In this case, the Nusselt number is calculated with

$$Nu = 0.0163 \cdot Re^{0.8} \tag{5.15}$$

After evaluating the Nusselt number in respect to the rotational speed, the convection coefficient of forced convection can be estimated according to

$$\alpha_{fc}(\Delta v_a \neq 0) = \frac{Nu \cdot \lambda}{l} \tag{5.16}$$

Due to the geometry of the process area of the analysed structure, the surfaces of the bodies C-Body 1, C-Body 2 and B-Body of 5.1 are influenced by the air flow in the process area caused by the rotating table. Therefore, the convection coefficients α_{C1}, α_{C2}
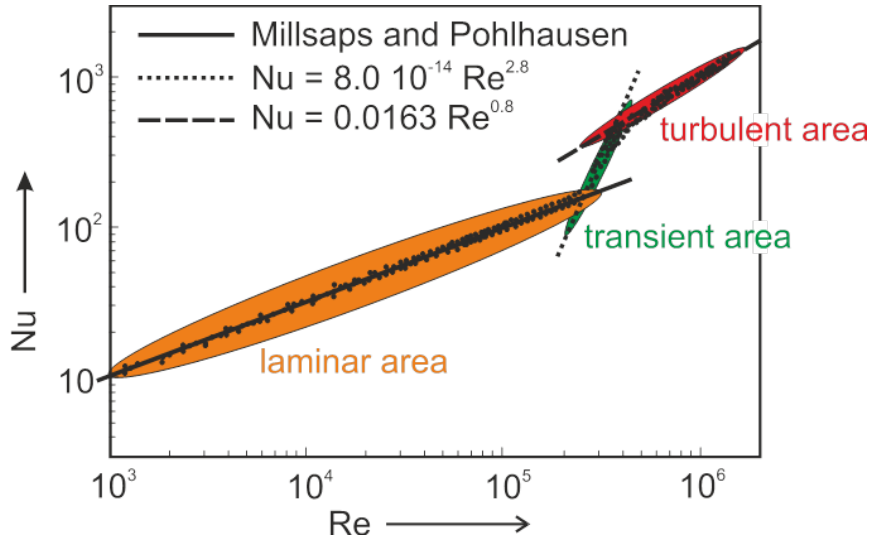
Figure 5.4: Nusselt number as a function of the Reynolds number for a rotating disks according to [141]

and α_B are described as functions of the convection coefficient of the table during motion α_t. According to [140] and [16], the functional relationship is assumed to

$$\alpha_{fc_{C1}} = 0.3 \cdot \alpha_{fc_t} \tag{5.17}$$

$$\alpha_{fc_{C2}} = 0.1 \cdot \alpha_{fc_t} \tag{5.18}$$

$$\alpha_{fc_B} = 0.1 \cdot \alpha_{fc_t} \tag{5.19}$$

Cooling power $\dot{P}_c$

The internal cooling unit of **Machine tool B/C** has a large influence on the thermal behaviour of the machine tool: depending on the setting of the cooling unit, the inlet temperature of the cooling fluid $T_{c_{in}}$ (flow from cooling unit to machine tool) can be controlled either by the difference of the outlet temperature $T_{c_{out}}$ (flow from machine tool to cooling unit) to the machine bed temperature T_b or by the difference of the outlet temperature to the environmental temperature T_o. In this thesis, a setting of the cooling unit was used where the machine bed temperature is used to control the inlet temperature. The resulting cooling power of the cooling unit during an certain load cycle for a body i can be calculated according to

$$\dot{P}_{c_i} = \dot{V}_c \cdot c_{p,c} \cdot \rho_c (T_{c_{out}} - T_{c_{in}}) \tag{5.20}$$

where $\dot{V}_c$ is the volume flow, $c_{p,c}$ is the specific heat capacity of the cooling fluid, ρ_c is the density of the cooling fluid, $T_{c_{out}}$ is the outlet temperature of the cooling fluid and $T_{c_{in}}$ is the inlet temperature of the cooling fluid.

The specific heat capacity $c_{p,c}$ of the cooling fluid is specified with 1940 $\frac{J}{kg \cdot K}$ by the manufacturer. The volume flow and the density of the cooling fluid measured with $\dot{V}_c = 1.3 \frac{m^3}{s}$ and $\rho_c = 815 \frac{kg}{m^3}$ with a measurement system *Promass 831* of *Endress und Hausser*.
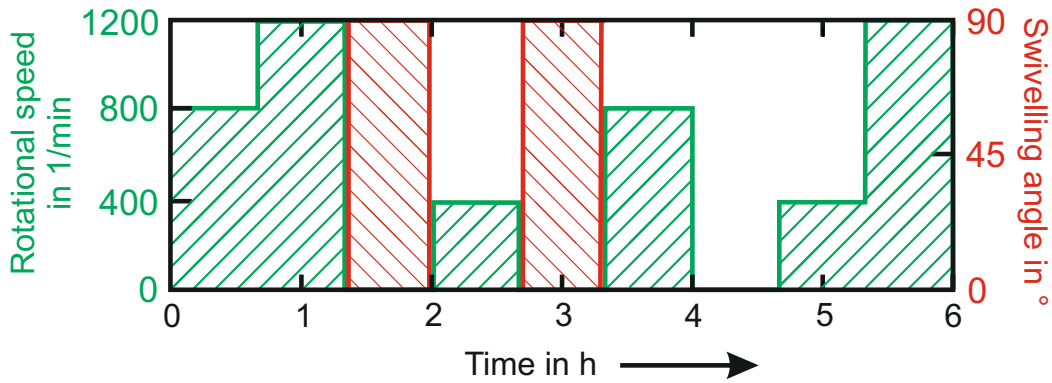
Figure 5.5: Arbitrary chosen load cycle used to evaluate the physical error prediction model. Green areas represent axis movements of the rotational C-axis, red areas represent movements of the swivelling B-axis.

In order to implement the cooling power into the model, the temperatures of the cooling inlet and outlet are measured during the operation of the machine tool. Then, the temperature values are used to calculate the cooling power in real-time and used in the temperature computation model.

In this thesis, an arbitrarily chosen test-cycle was used to verify the functionality of the physical model on **Machine tool B/C**. The test cycle is shown in Figure 5.5. The green parts represent a continuous movement of the C-axis, the red parts a standstill of the A-axis under postion control at a defined angle (90° in Figure 5.5). Every five minutes, a R-Test measurement cycle is carried out.

The power consumption of the axis drives for the axis movements illustrated in Figure 5.5 is shown in Figure 5.6. The single peaks represent the axis acceleration after the R-Tests. It represents the basic input parameter for the calculation of the temperatures and errors.

In Figure 5.7, the temperatures of the outlet and the inlet of the cooling of the machine tool are plotted together with the environmental temperature during the arbitrarily chosen load cycle of Figure 5.5. It can be seen, that the outlet temperatures of the $C-$ and $B-$ axis rise with an increasing load of each axis. At the same time, the inlet temperature is brought down actively by the cooler in the cooling unit. But also cross-influences can be seen: when the inlet temperature is reduced after one hour because of the heat produced by the drives in the C-axis unit, B-axis outlet temperature decreases proportionally with the cooled down inlet temperature because no heat is produced in the B-body.

5.1.2 Computation of the TCP-displacements

Based on the calculated temperature changes in the discretized bodies representing the rotary / swivelling axis unit of the machine tool presented in section 5.1.1, location errors of the C- and B-axis are computed. With the model presented in this work, all significant location errors of the analysed machine tool can be simulated. The distances which
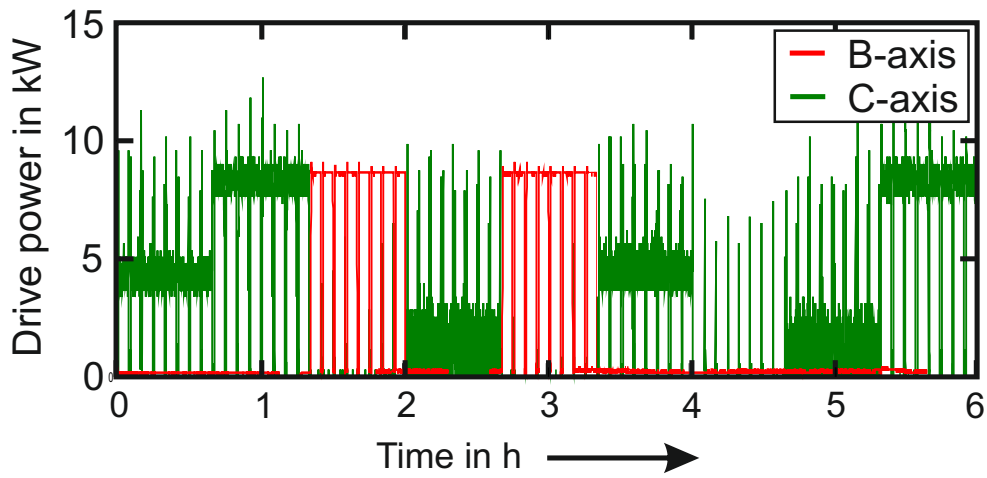
Figure 5.6: Input power of B- and C-Axis drives read out of the NC of **Machine Tool B/C**. The corresponding nominal movements are shown in Figure 5.5. Peaks are due to acceleration phases after R-Test measurements.
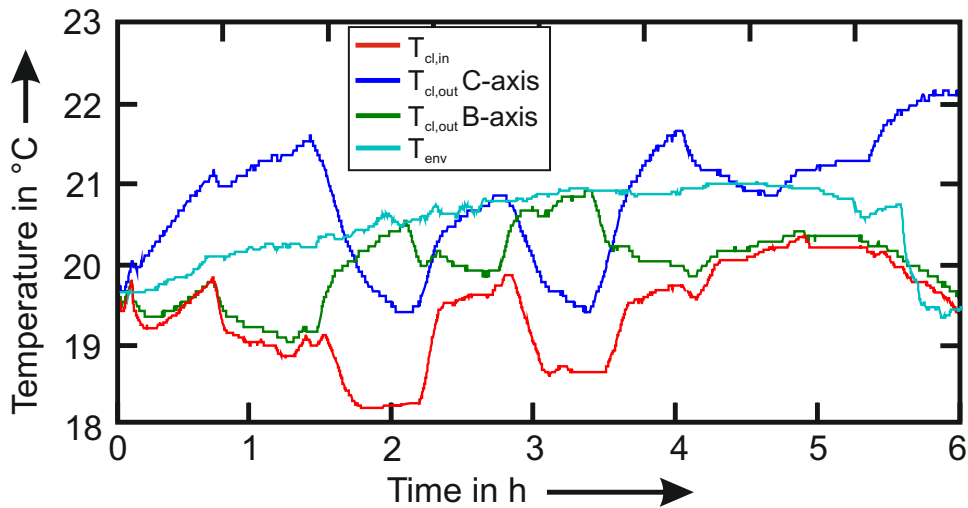

Figure 5.7: Measured temperatures of the inlet ($T_{c,in}$) and the outlet ($T_{c,out}$) and the environmental temperature (T_{env}) during a load cycle with axes movements of the rotational axis C and the swivelling axis B as shown in Figure 5.5.

Table 5.4: Effective lengths used for the calculation of location errors as defined in Figure 5.8.

Parameter	Length in m
d_1	0.300
d_2	0.240
d_3	0.082
d_4	0.153
d_5	0.063
d_6	0.121
r_T	0.160
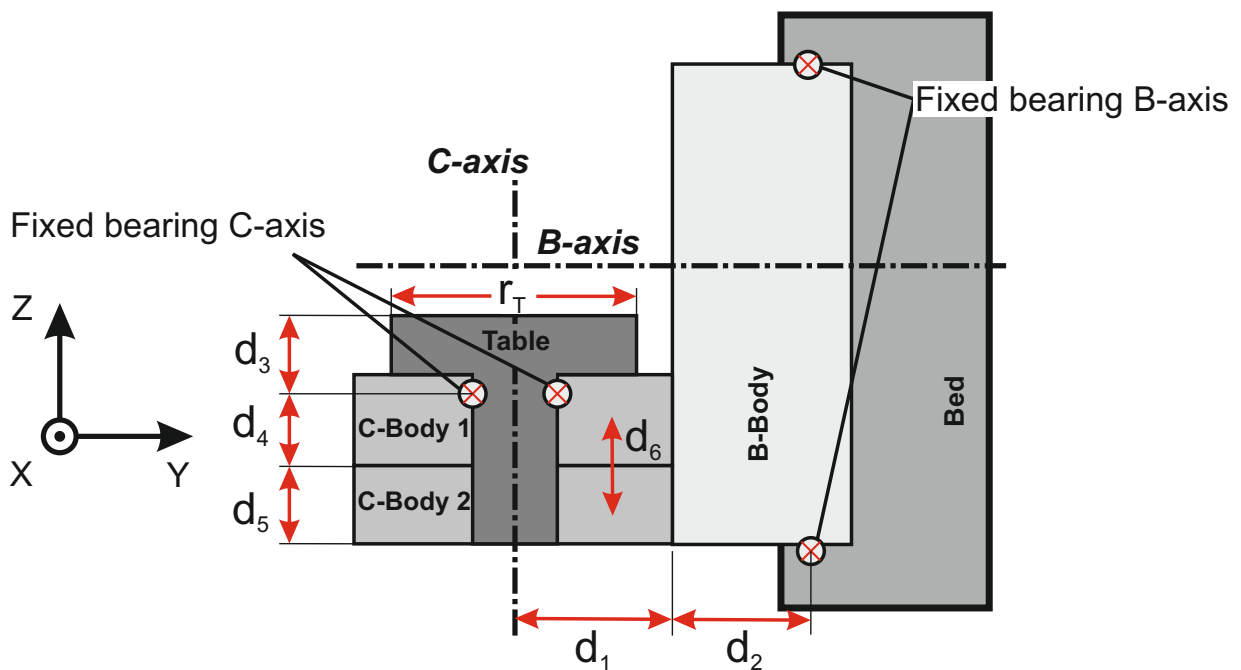
Figure 5.8: Geometric model for the computation of thermal errors

are relevant for thermal expansions are estimated by measurements and according to a simplified CAD - model of the rotary / swivelling axis unit. They are listed in Table 5.4 and visualized in Figure 5.8.

All heat expansion coefficients in this work are assumed with $12.4 \frac{\mu m}{m \cdot K}$ for cast iron EN-JS 1030 [140]. Like described above, this assumption leads to an error regarding the calculation of the thermal displacements. This is taken into account by the calibration procedure explained in section 5.1.3.

Figure 5.9 illustrates the relationship between the modelled bodies and the four thermally induced errors $Y0C$, $Z0T$, $R0T$ and $A0C$ which are calculated by the model. All calculations are carried out for a height of 25 mm over the table surface, where the R-Test measurements of the C-axis are carried out.
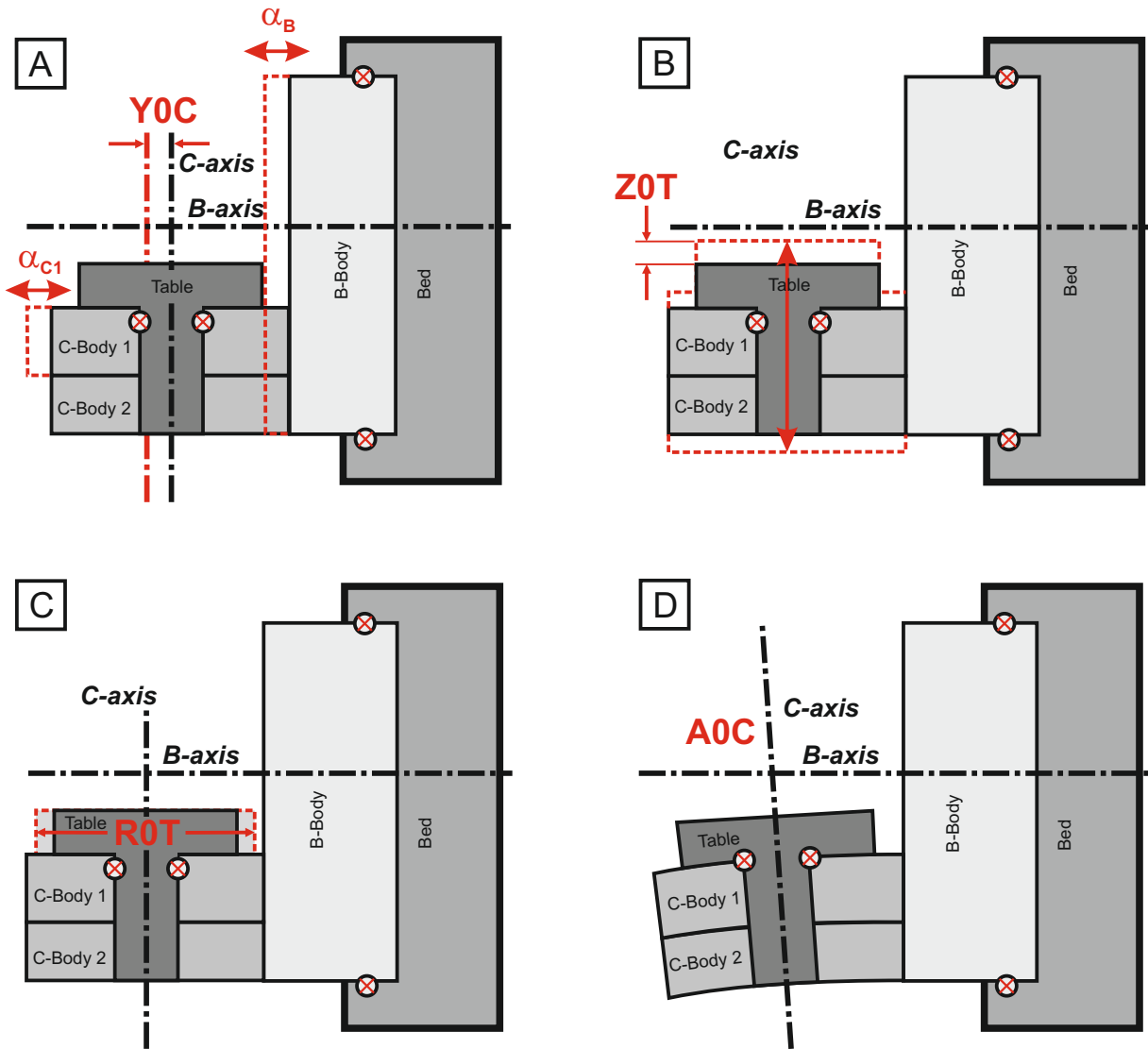
Figure 5.9: Schematic illustration of thermally induced errors based on expansion of defined bodies. All errors are computed for TCP 25mm over the table surface.
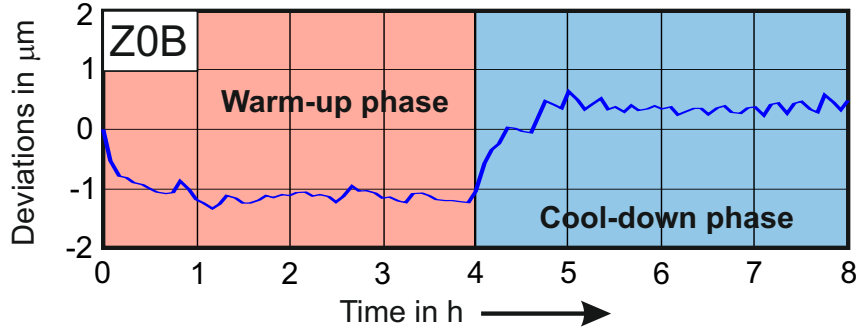
Figure 5.10: Location error $Z0B$ during four hours warm up (pendular movement of B-axis with $v_{max} = 18.000° \ min^{-1}$) and four hours cool down. Every five minutes, a R-Test was carried out.

The deviation $Y0C$ is caused by the thermal expansion of the C-Body 1 and the B-Body according to

$$Y0C = \Delta T_{c1} \cdot \alpha_e \cdot d_1 + \Delta T_{b1} \cdot \alpha_e \cdot d_2 \tag{5.21}$$

with ΔT_{C1} and ΔT_B represent the body temperature changes from the starting temperature to the current temperature. The effective length of the C-Body 1 is d_1, the horizontal distance of C-Body 1 to the boundary surface to the B-Body. For the B-body, d_2 is the horizontal distance from the boundary surface to the fixed bearing of the B-axis.

With a varying squareness error $A0C$, $Y0C$ changes depending on the Z-coordinate. In this thesis, $Y0C$ is measured 25 mm over the table surface. With the assumption, that the basis of expansion is in the middle of $d_4 + d_5$ (Figure 5.8, Table 5.4), $Y0C$ is calculated for a distance of 190mm below the table surface. The maximum occurring $A0C$-deviation is measured with 12 μm/m. At the same time, $Y0C$ is measured with 27 μm. Regarding the effective distance of 215 mm between the calculated and the measured Z-position of $Y0C$, this leads to a maximum deviation of $< 10\%$. Therefore, the influence of the Z-position to the $Y0C$-deviation is neglected for this calculation.

The first contributor to the location error $Z0T$ is the axial expansion of the Body *Table*. The effective length d_3 represents the distance between the upper surface of the Body *Table* and the bearing of the C-Axis. Two other contributors are the dilations of the two bodies c_1 and c_2, which are only considered up to the fixed bearing and one half each, because they expand homogeneously in positive and negative Z-direction.

$$Z0T = \Delta T_{Table} \cdot \alpha_e \cdot d_3 + \frac{1}{2} \cdot (\Delta T_{C1} \cdot \alpha_e \cdot d_4 + \Delta T_{C2} \cdot \alpha_e \cdot d_5) \tag{5.22}$$

Figure 5.10 shows a measurement of the location error $Z0B$ during four hours warm up and four hours cool down of the B-axis drive. The load cycle is a pendular movement between $-90°$ and $+90°$ with $v_{max} = 18.000° \ min^{-1}$). It can be seen, that the resulting location error is small, namely within $\pm 1\mu$m. Therefore, the influence of the B-Body to the Z-axis is neglected and the radial expansion of the B-Body is not considered in (5.22).

The radial table growth $R0T$ at the distance r related to the rotary axis is calculated via

$$R0T = \Delta T_{Table} \cdot \alpha_e \cdot r \tag{5.23}$$

As described in Figure 5.1, the C-unit is divided into two single bodies for modelling the location error $A0C$. Because of the direct drive, a rise of the power input leads to an inhomogeneous temperature distribution: C-Body 1 is warmer than C-Body 2 during power input to the C-axis drive. This leads to a mechanical deformation according to the bimetallic effect and results in the thermally induced squareness error $A0C$. After a certain time, the temperature field becomes more homogeneous, and $A0C$ is decreasing again. This effect is also shown in Figure 4.41. For small angles, the bending angle is the difference of the thermal expansion of the bodies over the distance to the centre of the bodies d_6. The effective length of both bodies represents the distance from the B-body surface to the C-axis, i.e. d_1. Therefore, the error $A0C$ can be calculated according to

$$A0C = \frac{1}{d_6}(\Delta T_1 \cdot \alpha_e \cdot d_1 - \Delta T_2 \cdot \alpha_e \cdot d_1) \tag{5.24}$$

With (5.21) to (5.24), all significant errors can be estimated.

5.1.3 Calibration of the Model

As described above, the computation of temperature changes and resulting thermal errors is based on several assumptions and simplifications. This can be accepted, because the idea in this thesis is that the effective parameters of the model are calibrated by measurements.

The calibration procedure, which is illustrated in Figure 5.11, is executed manually in this thesis. Based on the measurements presented in section 4.2.2, the plausibility of the assumed model parameters is proven and the parameters are corrected. In a second step, the raw location errors computed by the model ERR_{raw} are adjusted by two parameters k_1 and k_2 according to

$$ERR_{cor}(t) = k_1 \cdot ERR_{raw}(t) \cdot (1 - e^{\frac{t}{k_2}}) \tag{5.25}$$

Thereby, the linear parameter k_1 covers the static behaviour. The exponential parameter k_2 represents the time constant of the system and is used to adjust the dynamic behaviour. The estimation of both parameters is based on a least squares fitting of model outputs and measurements at different load levels according to Figure 4.41.

Giving an example of the differences between the unmodified and the modified model results, Figure 5.12 shows the drive power of the C-axis during a measurement, where the axis rotated four hours with 600 min^{-1} before cooling down another four hours. The single peaks in Figure 5.12 are caused by the acceleration of the axis after R-Tests. Similar but smaller peaks occur also during cool down, when the axis is moving between the single measurement positions of the R-Test discrete.

Figure 5.13 shows the calculated temperatures during this load cycle. It can be seen that the environmental temperature is assumed as constant. During real compensation, the model receives the actual environmental temperature of a temperature sensor. The body with the largest temperature rise is the *table*, followed by the C-axis body. The
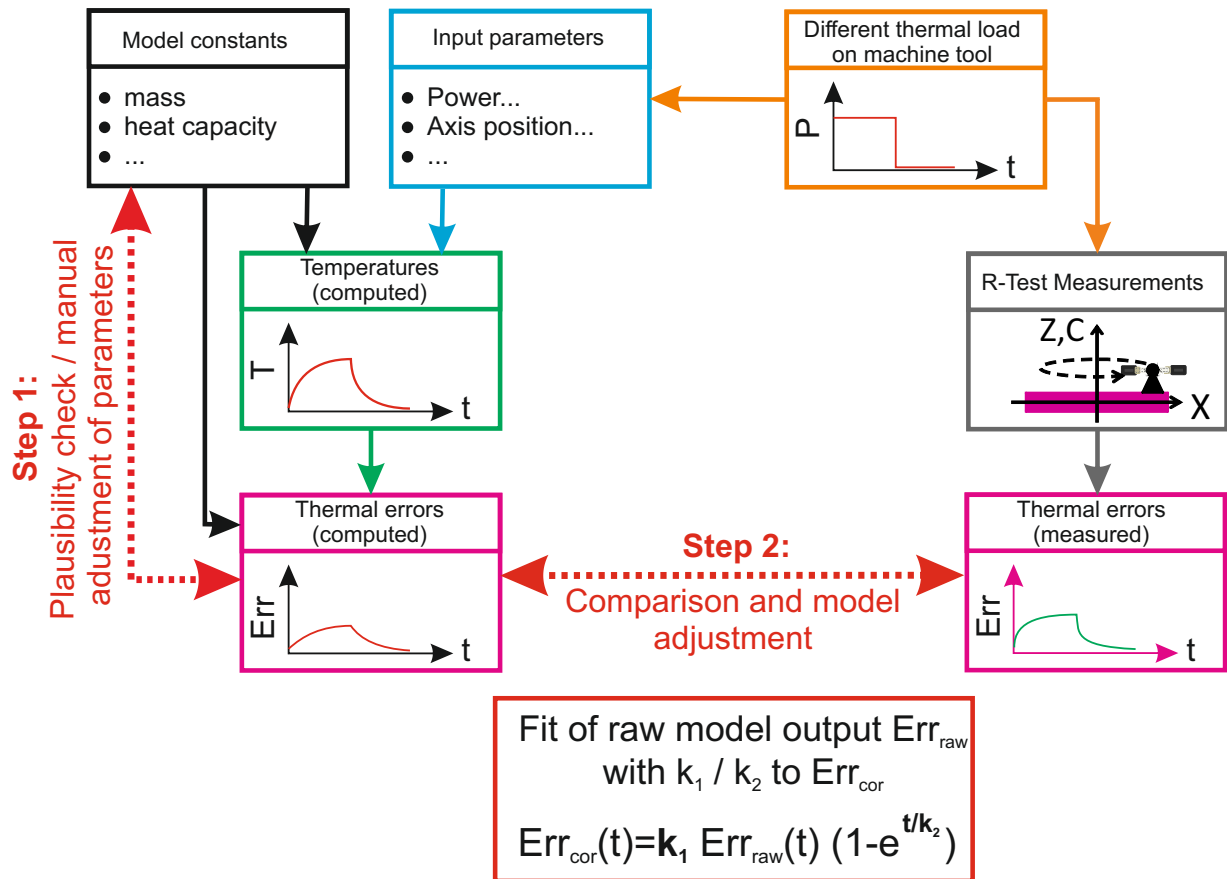
Figure 5.11: Calibration of the physical model for an arbitrary chosen load cycle of the C-axis of **Machine tool B/C**
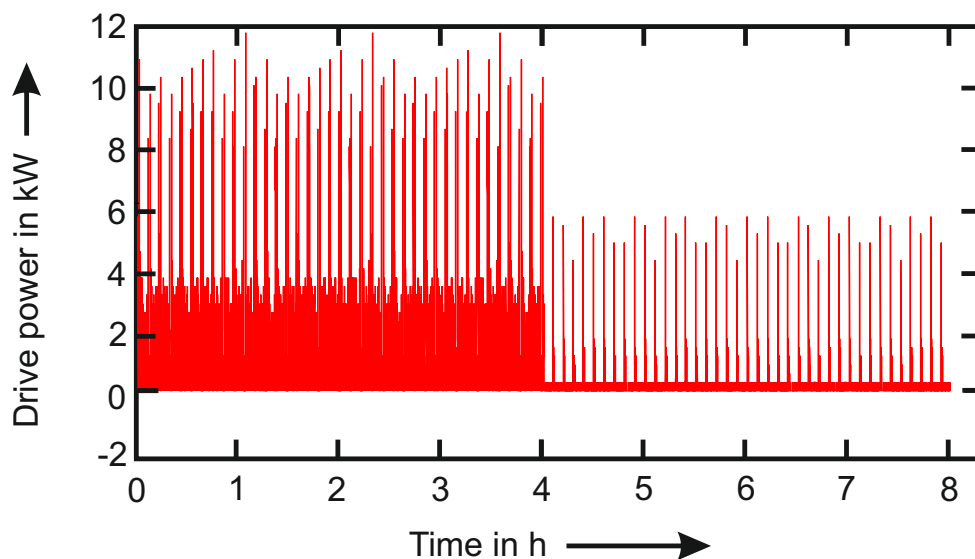

Figure 5.12: Four hours warm-up, four hours cool down. Movement of C-axis during warm-up with $600 \ \mathrm{min}^{-1}$. Peaks are due to axis acceleration after R-Test measurements. Between two measurements, the C-axis is moved for 5 minutes. With the duration of the measurement itself, nine R-Tests are carried out per hour.
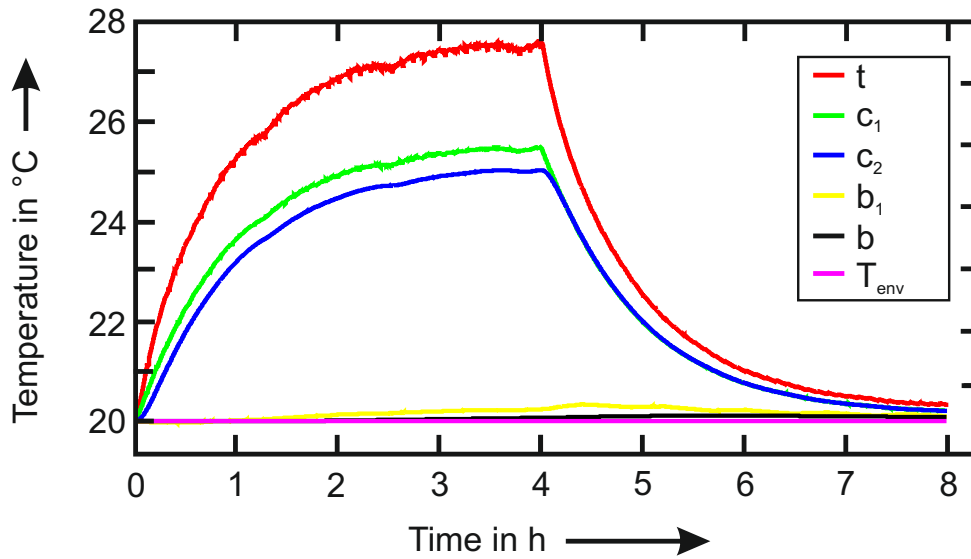
Figure 5.13: Computed temperatures of the *Table* (t), *C-Body 1* (c_1), *C-Body 2* (c_2), *B-Body* (b_1) and the Machine bed (b) corresponding to the power input of Figure 5.12. For this illustration, a constant environmental temperature of $20°\mathrm{C}$ is assumed. .

B-body and the machine tool bed (b) show no significant temperature rise. Regarding the machine tool bed, this is due to the large mass. Regarding the B-Body, the low temperature rise can be explained by the cooling unit which is triggered by the C-axis and therefore it is also cooling the B-Body although no heat is released by the B-axis drive.

Figures 5.14 compares the raw, non-modified errors computed by the model based on the power input shown in Figure 5.12 with the output of the calibrated model.

In order to validate the calibration parameters, an arbitrarily chosen test cycle, different from the measurements used for parameter identification, is used (Figure 5.6). The test-cycle is carried out on **Machine tool B/C** and thermally induced errors are measured. Figure 5.15 shows the computed (dashed lines) and the measured (solid lines) deviations. It can be seen that the qualitative course of the deviations and the magnitudes during the different sequences of the cycle can be reproduced by the model. In section 6.1, this is discussed in more detail.

5.2 Phenomenological Model

The model presented in this section is a pure mathematical approach to predict thermally induced errors in dependency of certain input parameters such as a feed speed of an axis, or the power demand of an axis drive. The model enables the identification of all necessary parameters to describe the thermal behaviour of a machine tool axis caused by internal heat sources based on one measurement procedure of approximately 40 hours of duration. A measurement time as short as possible is useful, because a machine tool is not available for other tests or operations during commissioning when thermal measurements are carried out. The presented parameter identification and compensation model runs fully-
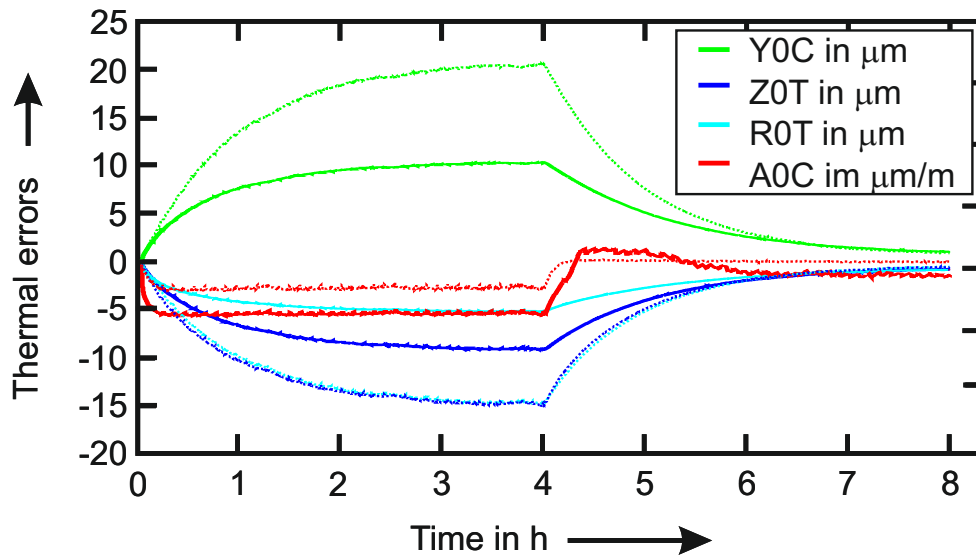
Figure 5.14: Computation of thermally induced errors caused by a power input according to Figure 5.12. Dotted lines represent the raw model output, solid lines represent the adjusted model output.
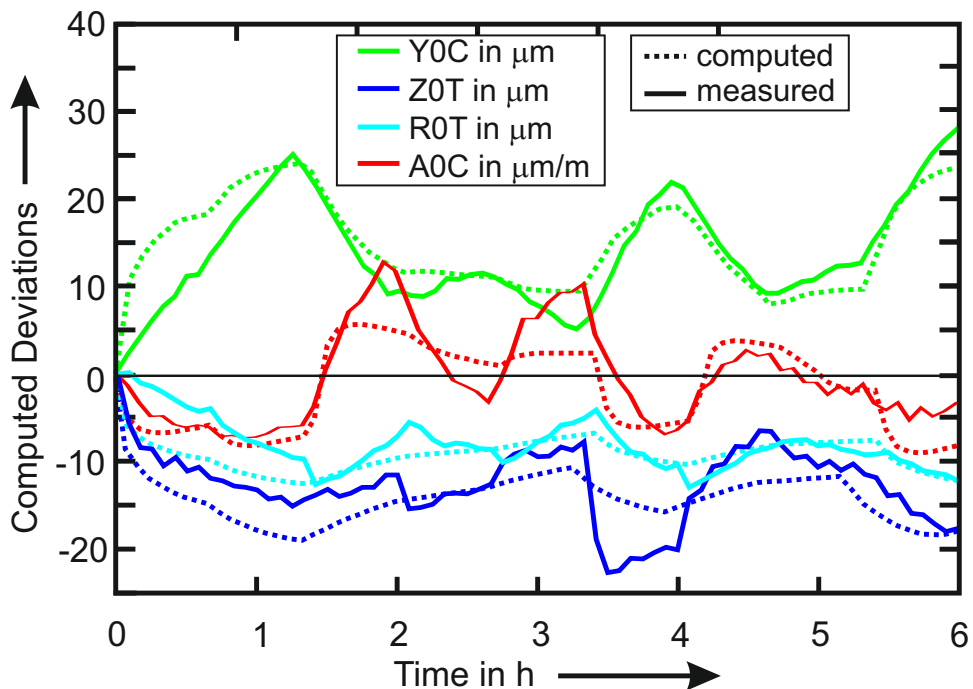

Figure 5.15: Computed (dashed lines) and measured (solid lines) deviations due to the load cycle shown in Figure 5.5. Computed deviations are the output of the calibrated model.
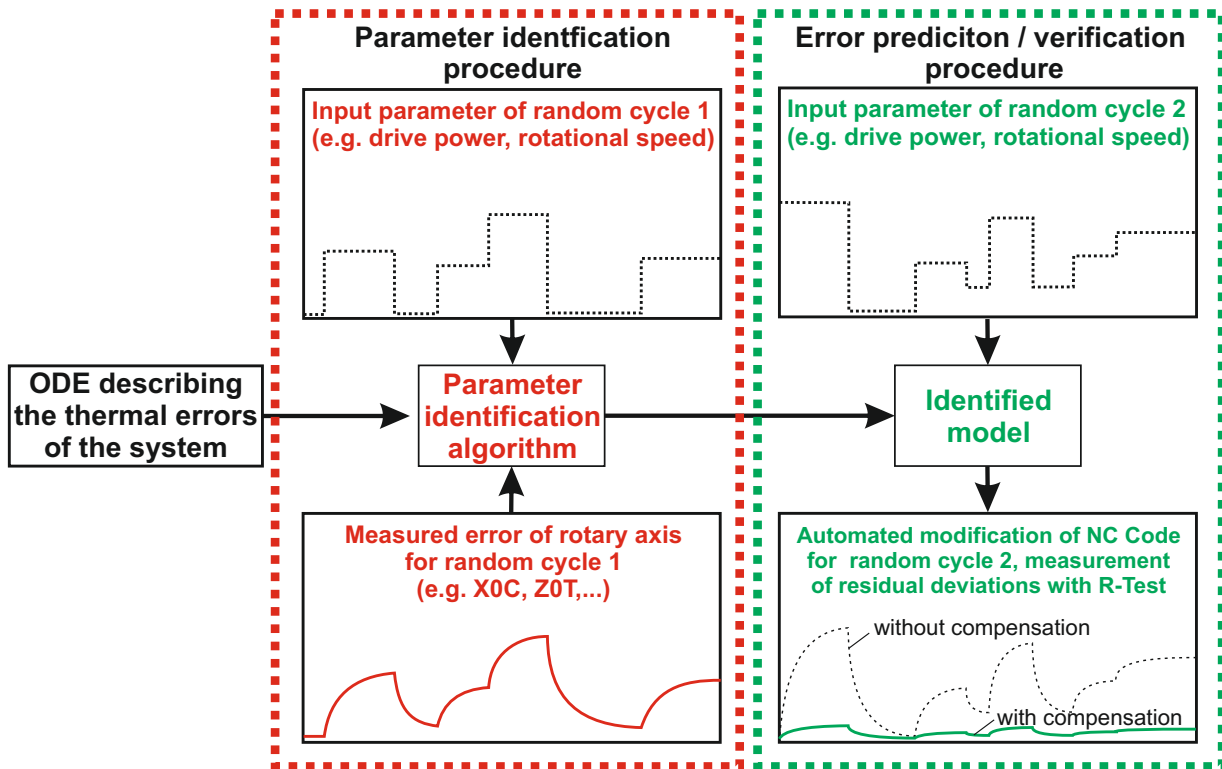
Figure 5.16: Procedure of phenomenological modelling: an arbitrarily chosen load cycle is used to identify parameters necessary to describe the thermal behaviour of an axis with an ordinary differential equation (ODE). The parameters set are verified using a second, also arbitrarily chosen but different load cycle.

automated. Because of the flexible design, any additional fundamental input parameters such as axes positions, temperatures, but also discrete values like for example the condition of a machine shop door (e.g. closed / opened), can be integrated in the model. This is shown by the example of a swivelling axis. The procedure of parameter identification and error prediction is illustrated in Figure 5.16.

5.2.1 Model for Rotary Axes

The thermal error of a machine tool is caused by a system of heat transfer and thermal expansion. The idea of the phenomenological model approach is to use an ordinary differential equation (ODE) describing the change of thermally induced deviations due to a arbitrarily varying load level with fitting parameters identified by measurements. This fitting parameters can be used afterwards to compute the error course due to a different load level.

Equation (5.26) is used as ODE to describe the system change of a thermally induced error y(t) of a rotary axes due to the input parameter $u_1(t)$ and the constant parameters p_1, p_2 and p_3. This differential equation is chosen because thermal deviations can be represented by first order lag elements. For each thermal error which shall be predicted by
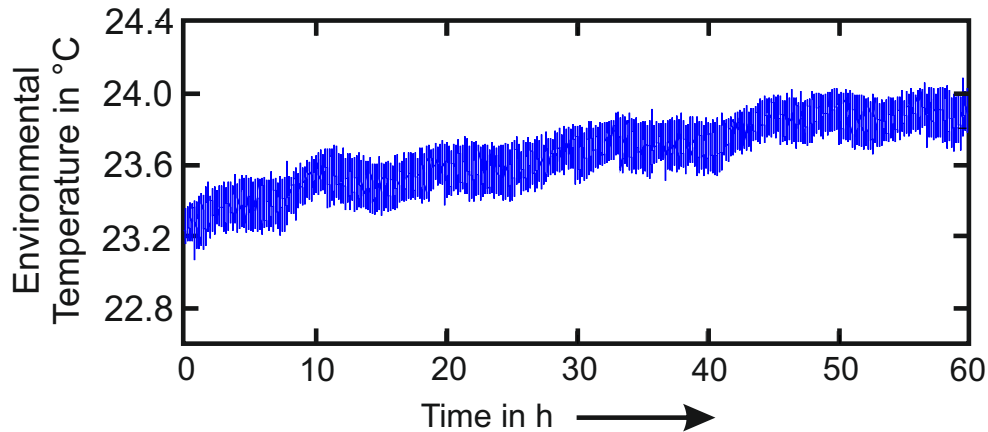
Figure 5.17: Slight rise of environmental temperature (within $1°C$) in machine shop of **Machine tool A/C** during a 60 hours arbitrary chosen test-cycle for parameter identification.

the phenomenological model, one equation has to be solved according to

$$\frac{dy}{dt} = p_1 \cdot y + p_2 \cdot [u_1 + p_3] \tag{5.26}$$

Here $u_1(t)$ is either the axis speed, or the power consumption of the axis drive, read-out of the machine tool control. For using the axis speed, a software is designed that allows the analysis of NC-Code (in this thesis: Heidenhain NC-Code) in order to extract the single axis movements. Based on these axis movements, the thermally induced errors can be predicted. This allows using the model as a post-processing compensation software e.g. implemented in a Computer Aided Manufacturing (CAM) software. When using the drive power, the model can be implemented directly on the machine tool control. Thereby, the model can be used in two different ways. Regarding the rotary, vertical axis of the analysed machine tool, the axis movement was extracted fully-automated out of the NC Code and used as input parameter $u_1(t)$ for error prediction.

The first part of (5.26), $p_1 \cdot y$, introduces the systems initial condition, $p_2 \cdot u_1$ represents the source term (which represents the drive power in this example), and with $p_2 \cdot p_3$, a linear shift in the environmental temperature change during the measurement time can be considered. This is necessary, because all measurements for parameter identification are carried out during week-end because the environmental conditions are much more stable then (Figure 4.35). A disadvantage is, that due to a reduced performance of the air condition system during week-end, the temperature in the machine shop rises slightly over the total measurement time due to the heat release of the machine tool cooling unit. Figure 5.17 shows this slight temperature increase: during a measurement of 60 hours (Friday 8 p.m. - Monday 8.a.m. which represents the time where the air condition is in week-end mode, Figure 4.35), the environmental temperature rises within approximately $1°C$. Therefore the influence covered by the term $p_2 \cdot p_3$ is quite small in the analysis carried out in this thesis.

All constant parameters p_i are derived from measurements, found using a simplex algorithm. To get a data set for this identification procedure, arbitrarily generated axis
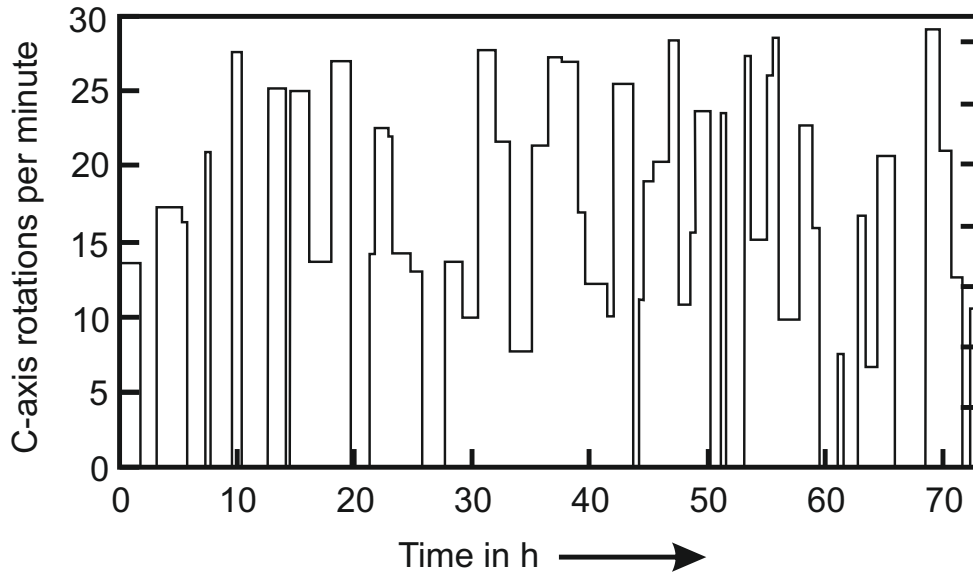
Figure 5.18: "Test cycle 1" Automatically and arbitrarily generated C-axis movement with a duration of approximately 73 hours.

movements are generated by a software developed in C++. Regarding rotary axes, the software strings intervals with a variable length (in this thesis: five minutes). For each interval (number of intervals has to be defined by user), a random generator sets a rotational speed for all rotational axes between two set limits. After each interval, it is randomly chosen, whether the next interval continues with individual axis speed, or speed is changed. The settings for these random generators can be adjusted. Figure 5.18 shows an arbitrarily generated NC Code ("Test cycle 1"). The limits for the rotational speed of the C-axis are set to zero and $\frac{v_{max}}{2} = 30$ min^{-1}. Figure 5.19 shows a different, arbitrarily generated C-axis movement ("Test cycle 2"). In this case, it defined, that after a certain rotational speed $\neq 0$, the next rotational speed is set to zero. This was done in order to simulated the periodically occurring complete switching-off of axis drive during parameter verification. A mixed verification measurement with the combination of both settings is presented in section 6.2.

The automatically carried-out NC-Code generation has two significant advantages: it is a convenient method to generate very long NC-Codes, which can hardly be programmed manually; secondly, when the software is once proofed systematically, every NC-Code can be run on the machine tool without an additional check.

Based on R-Test measurements carried out with arbitrarily generated NC-Code as described above, the parameter identification software, which is implemented in Matlab, is fitting a user defined differential equation (5.26) in this thesis in case of a vertical rotational axis) until a set convergence criteria is reached. If no convergence is reached, the fitting procedure is aborted. In this thesis, the convergence criteria is reached, when the change of the Euclidean norm of the parameter vector $\underline{p}$ is smaller than $1 \cdot 10^{-6}$.

Figure 5.20 and Figure 5.21 show the location errors $X0T$ and $Z0T$ during the load cycle
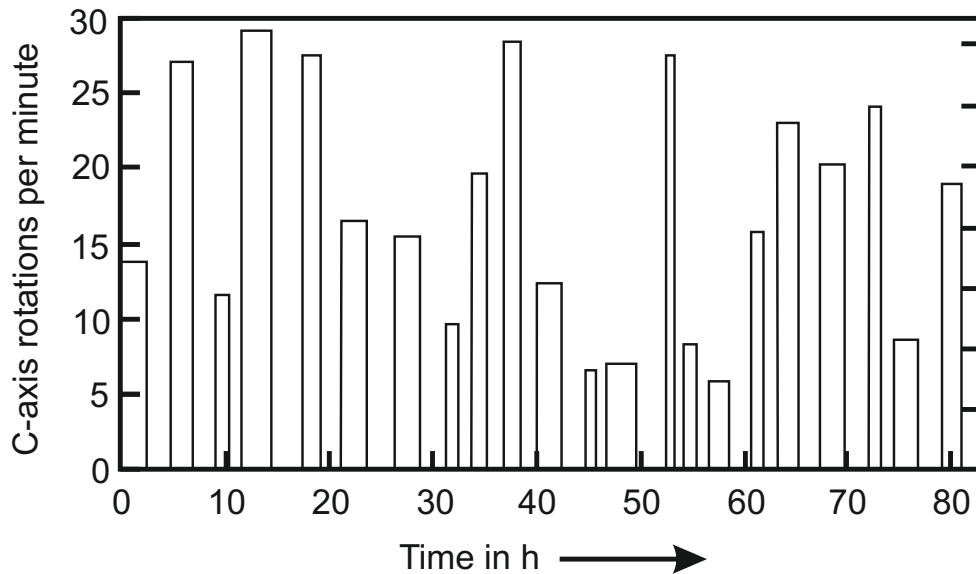
Figure 5.19: "Test cycle 2" Automatically and arbitrarily generated C-axis movement with a duration of approximately 83 hours.

illustrated in Figure 5.18 on **Machine tool A/C**. The blue curve is the measurement of the errors. The red line is the fit, after identification of appropriate parameters $p1...p3$.

With the developed ODE, the thermally induced errors of the machine tool caused by the rotary axis are computed using the Euler method.

Figure 5.22 shows the measurement of $Z0T$ (blue line) during an other arbitrarily chosen load cycle "Test cycle 2", illustrated in Figure 5.19. The red line shows the computed deviations, but in this case, the fit is carried out based on the parameters $p1...p3$ found with measurement of Figure 5.21. It can be seen, that no significant long-time deviations between the measured and the computed curve occur even after approximately 83 hours.

The measurement duration is chosen arbitrarily. In order to reduce this duration, the measurement time, which is necessary for an appropriate identification of the parameters has to be estimated. Therefore, arbitrarily chosen sections of a certain length but different location regarding the measurement time are cut-out of the measurement data. An example is given by Figure 5.23, where four sections of the same length (11 hours) are chosen to be cut out of the measurement presented in Figure 5.22. This procedure is done 100 times. Then, for the 100 sections (of the same length) but different location, the fitting parameters $p_1...p_3$ are calculated and the least square residual of every calculation is recorded. After that, the measurement length is raised. Again, 100 sections of the same, raised length are chosen to compute the fitting parameters $p_1...p_3$ and the least square residual of the fitting procedure is computed for each of the sections. This is done as long as no more significant change is detectable. Then, the calculated least square residuals are summarized in a boxplot.

Figure 5.24 gives an example of a boxplot for the least square residuals of parameter estimation of the Z0T deviations illustrated in 5.22. Nine different section durations are
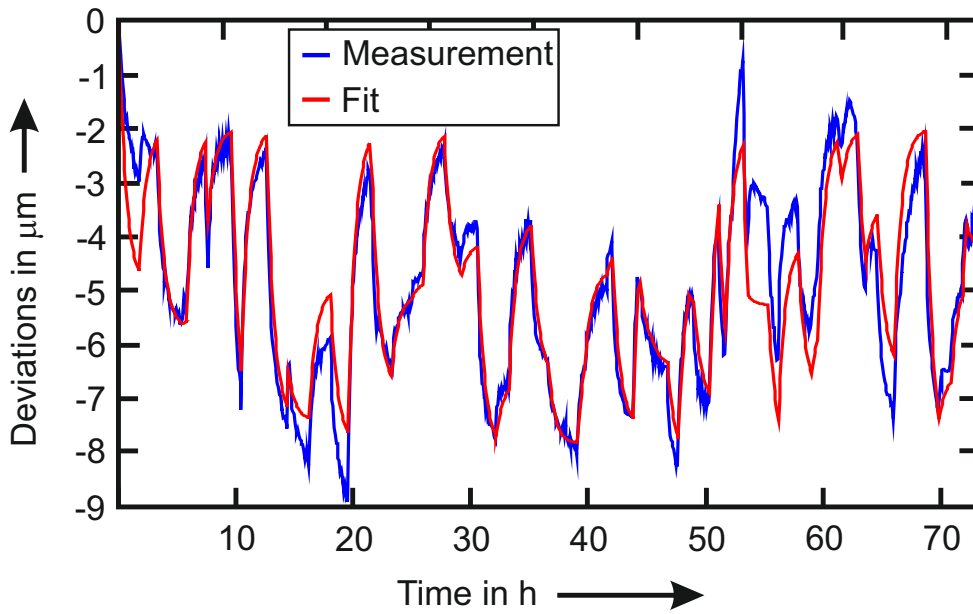
Figure 5.20: Location error $X0C$: Measurements and fitted curve for parameter identification during "Test cycle 1" (Figure 5.18).
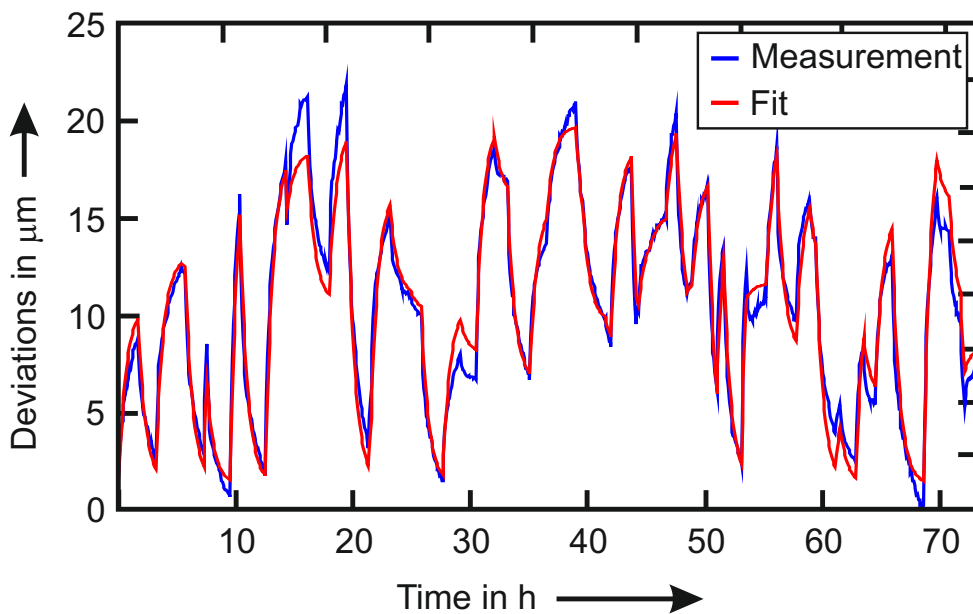
Figure 5.21: Location error $Z0T$: Measurements and fitted curve for parameter identification during "Test cycle 1" (Figure 5.18) [126].
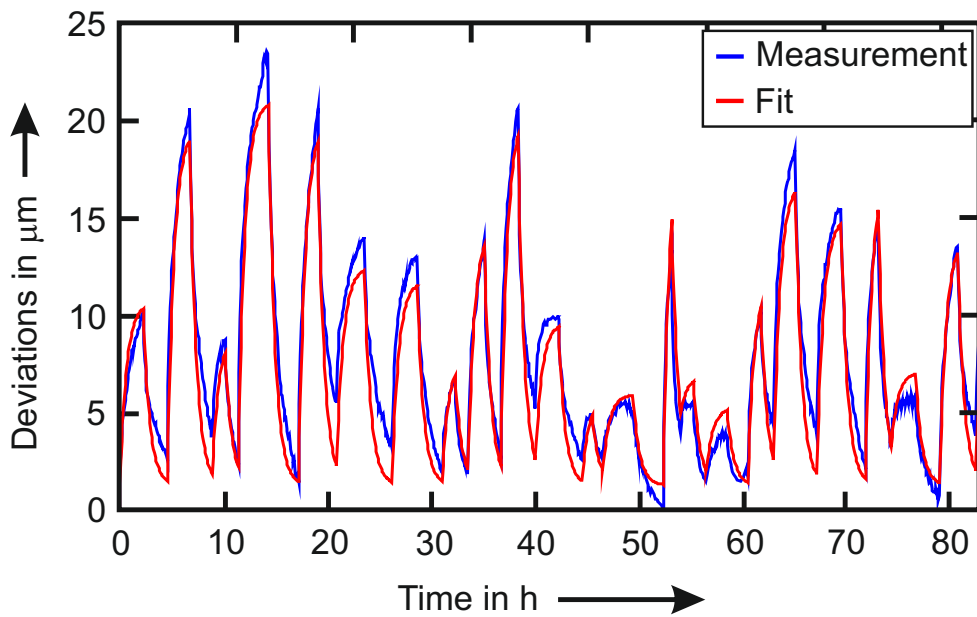
Figure 5.22: Computation of $Z0T$-deviations based on "Test cycle 2" (Figure 5.19). Parameters for computation are identified in "Test cycle 1" (Figure 5.18) [126].
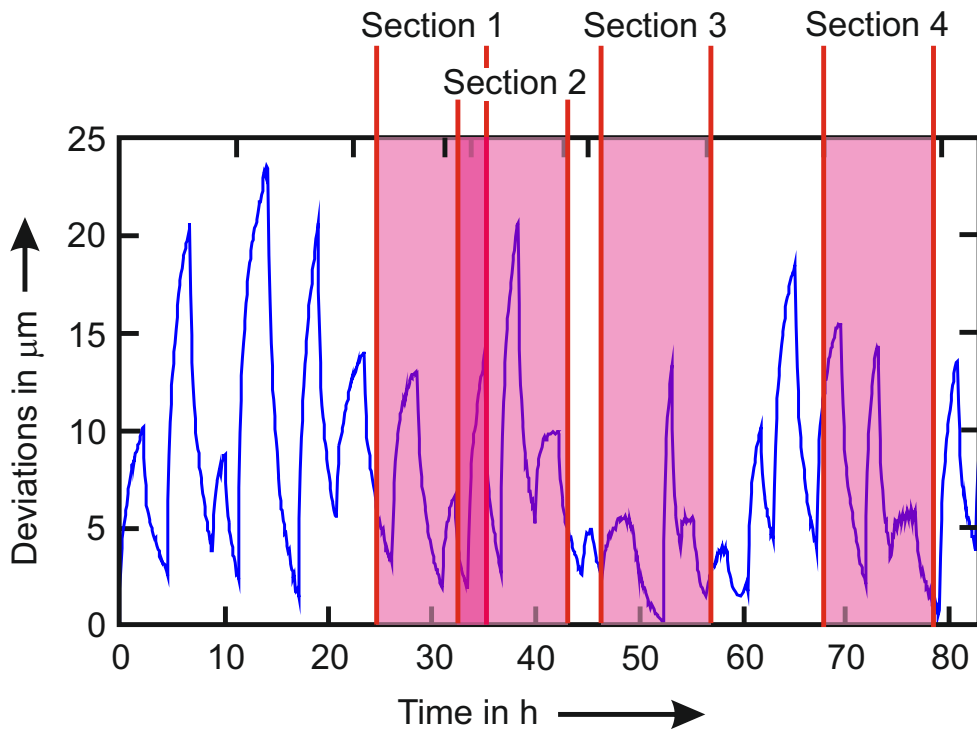
Figure 5.23: Example for four different sections of 11 h length cut out of the measurement data for $Z0T$ presented in Figure 5.22. For the boxplot illustrated in Figure 5.24, 100 different sections for the arbitrarily chosen measurement durations 5 h, 11 h, 17 h, 23 h, 29 h, 35 h, 41 h, 47 h and 53 h were chosen.
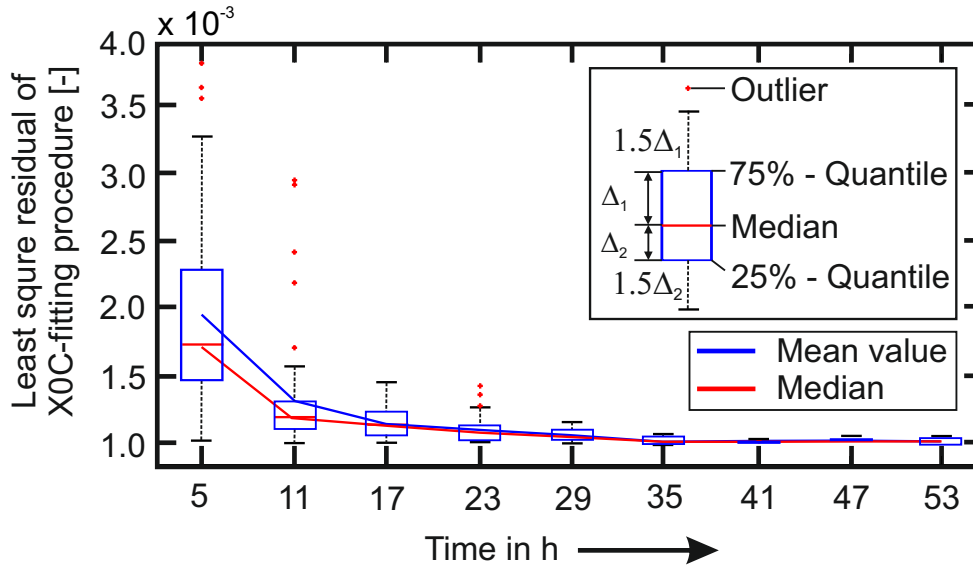
Figure 5.24: Least square residual of X0C-fitting procedure for nine time intervals of different lengths (100 calculations per duration). The red line in the boxplot represents the median of the data set. The blue box covers the 25% and the 75% quantile. The black lines (antennas) span 1.5 times the length between the 25% respectively 75% quantile and the median. Red crosses are outlier which are not covered by the two antennas [126].

analysed. The red line in the boxplot represents the median of the data set. The blue box covers the 25% and the 75% quantile, so that 50% of all measurement values are inside this area while 25% are above and 25% are below this box. The black lines (antennas) span 1.5 times the length between the 25% and the median (Δ_2) respectively the 75% quantile and the median (Δ_1). Red crosses are outliers, which are not covered by the two antennas.

Figure 5.24 show, that the scattering decreases with rising measurement time. Up to approximately 30 hours, the decrease is significant. After that, the scattering of the residuum keeps at the same level which means that a measurement duration of 30 hours shall be chosen as a sufficient long measurement time for this machine tool with the environmental conditions that existed when the measurement was done. Therefore, the procedure to generate the boxplots which is explained above is implemented as an option in the compensation software. It can be carried out fully-automatically after every parameter identification procedure, so that significant changes can directly be observed.

5.2.2 Model for Swivelling Axes

Equation (5.26) describes the system of an axis with one relevant input parameter such as the rotational speed or the drive power. If the speed is zero, also the power consumption measurement and therefore u_1 becomes zero. In this case, the thermal behaviour of the machine tool depends on the initial state and the ambient temperature. But there are also axes on machine tools that have several functional states. An example are horizontal, swivelling axes. The electric drive of such an axis consumes power even if the axis is not moving but under position control at an angular position, where gravity affects the axis.
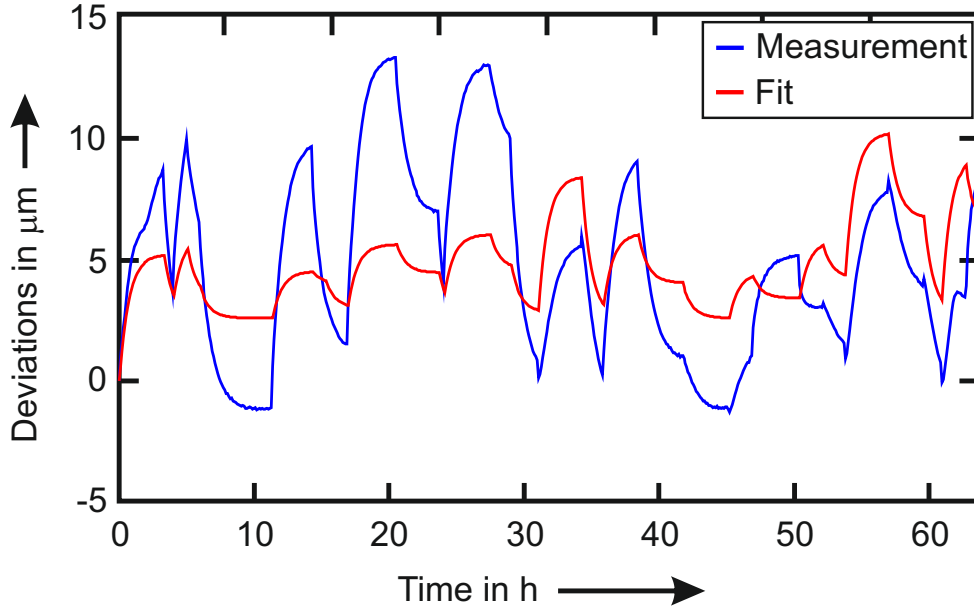
Figure 5.25: A-Axis movement: measurement and fitting of $X0T$ for parameter identification based on (5.26). Because of the more complex relationship between the power inlet, the functional state and the resulting location errors, the fitting procedure is not very effective [126].

In this case, the thermally induced errors can differ if the axis is moving or if it stands still, even if the power consumption is equal, e.g. due to heat development by friction, heat input at different locations or a changed convection behaviour. The horizontal, swivelling axis of **Machine tool A/C** shows such a behaviour: like described in section 4.2.2, the resulting location errors are not only depending on the power consumption of the drive, but also on the functional state (swivelling vs. standstill under position control at different angles).

Figure 5.25 shows the measurement and the fit of the thermally induced error $X0A$ according to (5.26). It can be seen, that the fit is poor, because one input parameter is not enough to describe the relationship between the underlying power consumption and the resulting TCP error. Therefore, the functional state of the axis has to be considered in the model, which is realised by a switcher implemented in the axis ODE. For the swivelling axis, (5.26) is extended to:

$$\frac{dy}{dt} = (u_2) \cdot (p_1 \cdot y + p_2 \cdot [u_1 + p_3]) + (1 - u_2) \cdot (p_4 \cdot y + p_5 \cdot [u_1 + p_6]) \quad (5.27)$$

where $p_1...p_3$ are the constant parameters for moving the axis, $p_4...p_6$ are the constant parameters for standstill of the axis, u_1 is the power consumption of the axis read-out from the machine tool control and u_2 is the switcher derived from the axis position. For a moving axis, u_2 is one. For an axis standing still, u_2 becomes zero.

In general, the eccentric position of table load should be taken into account in a similar manner regarding (5.26). The simplification made is sufficient in this case, because firstly, computations in this thesis are made under the assumption of no load and no cutting conditions. Secondly, in the analysed case, the large structural weight of the swivelling unit on the A-axis drive (which is the reason for implementing the switch in (5.27)) has
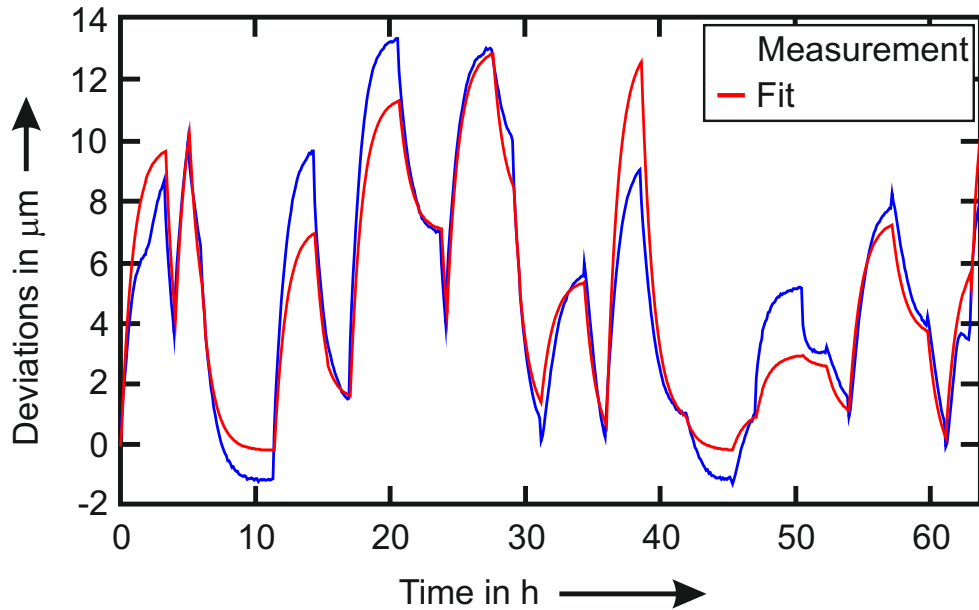
Figure 5.26: Location error $X0T$ caused by power input to a horizontal, swivelling axis. Parameter identification during an arbitrarily generated test cycle over 75 hours [126].

a significantly larger influence compared to an eccentric load caused by an average sized workpiece. Also the offset from the centre of mass to the axis is larger regarding the A-axis compared to the C-axis. Therefore, the simplification made in, (5.26) is reasonable.

Figure 5.26 shows the fit of $X0T$ (same load cycle as in Figure 5.25) based on (5.27).

Analogue to the boxplot analysis of the vertical axis, the influence of the measurement time regarding the parameter identification of the swivelling axis is analysed in order to minimise it. Figure 5.27 shows a boxplot based on the measurement presented in Figure 5.26. According to the example of vertical axis (Figure 5.23), sections of different length and location are cut-out the complete measurement record and used for parameter identification (100 different section per chosen length). Then, the least square residual of the parameter fitting procedure is plotted in the boxplot (Figure 5.27). It can be seen that it takes 40 hours, till the scattering of the least square residuals is no more decreasing significantly.

5.3 Comparison of Both Model Approaches

In the previous sections, two different approaches to model the thermal behaviour of rotary-/swivelling axes are introduced.

The simplified, physical approach calculates temperature changes for a minimized number of bodies representing the significant axis structure based on estimated model parameters and based on only the significant temperature influences taken from measurements. Based on these temperatures and depending on the geometry, deviations of a rotary -/ swivelling axis unit are computed. Because of the assumptions made during

Figure 5.27: Least square residual of X0C-fitting procedure for nine time intervals of different lengths (100 calculations per duration). The red line in the boxplot represents the median of the data set. The blue box covers the 25% and the $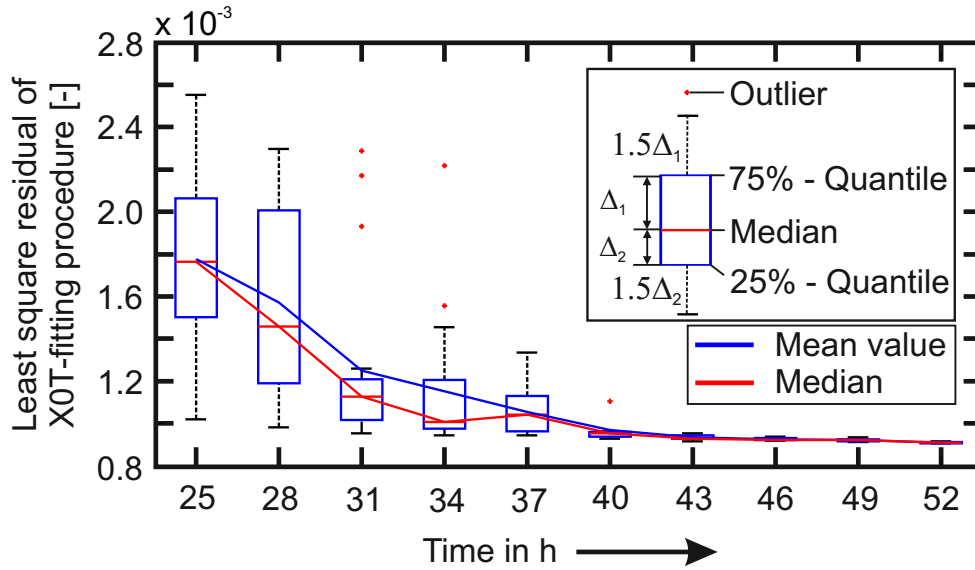75\%$ quantile. The black lines (antennas) span 1.5 times the length between the 25% and the median (Δ_2) respectively the 75% quantile and the median (Δ_1). Red crosses are outlier which are not covered by the two antennas.

parameter identification, an adjustment of the model is necessary, which is done by calibration measurements.

The phenomenological model uses pure mathematical methods. It fits parameters of an ordinary differential equation based on deviation measurements due to a defined input signal such as the drive power or the feed speed of an axis. With the estimated fitting parameters, the prediction of the thermal behaviour of the analysed axes becomes possible. This procedure is highly automated in this thesis. An approach to use more input signals for more complex predictions is carried out successfully. This is done for horizontal, swivelling axis by using the axis position in addition to the drive power, in order to consider differences regarding the power consumption, when the axis is swivelling or is just in standstill at angles different from $0°$.

While the building of the physical model can not be automated but needs engineering know-how because of the individual simplification process of the relevant structure into single bodies, a further improvement would be an automated parameter identification process. This is already realized regarding the phenomenolial approach. By disregarding the underlying physics and specific parameters of the machine tool structure, but using a measurement procedure to identify parameters for the mathematically prediction of the machine tools thermal behaviour, the user needs no detailed information of the machine tool like CAD models or drawings.

By considering the underlying physics, an extrapolation of the model to unknown conditions seems possible. This is critical regarding a pure mathematical approach, when

based on limited informations, deviations shall be predicted for unknown conditions. Therefore, the measurements should be as extensive as possible, but at the same time measurement durations should be minimized regarding the machine tool availability. This conflict is solvable for rotary / swivelling axes, which is shown in this thesis.

Nevertheless, simplifications are made concerning the modelling: thermal errors are only considered axis by axis, and the total thermal error is evaluated according to the principle of superposition which leads here to success because the cooling of the rotary-/ swivelling axis structure decomposes the problem. Additionally, position influences of one of the rotational axes on the respective other one due to convection or load have been neglected. When trying to extrapolate the approach to other axes of the machine tool, investigations regarding mutual influences of the single axes and regarding the optimisation of the measurement procedure for parameter identification have to be carried out. In generally, the problem complexity of both models increases significantly when a complete 5-axis machine tool is considered.

6 Thermal Compensation of Rotary Axes of 5-Axis-Machine-Tools

In the last preceding chapter, model approaches for the prediction of thermally induced errors of rotary / swivelling axes of five-axis machine tools were presented. Now, these models are used to compensate occurring errors on a machine tool. During compensation, R-Tests are carried out with a time gap of five minutes between the ending and the start of each measurement in order to verify the compensation results.

Some part of the following content has been published by the author in [121–123, 126, 127, 135].

6.1 Compensation Based on Physical Model

Significant parts of this chapter have been presented in [136] and [137].

The compensation procedure based on the physical model on **Machine tool B/C** is shown in Figure 6.1. During the characterization of the machine tool, only the errors $Y0C$, $Z0T$, $R0T$ and $A0C$ have been identified as significant. Therefore, only these deviations are considered by the compensation procedure. The computation of errors is carried out on a PC, which is connected via Ethernet with the CNC of the machine tool. The communication between PC and CNC is realized via FOCAS2 (*Fanuc Open CNC API Sepcification Version 2*), which is a transmission protocol provided by the CNC manufacturer FANUC. It allows the access to the CNC by a PC. Thereby, all parameters allocated by the CNC can be processed on the PC in real time and coordinate offsets can be returned from the PC to the CNC [144] per each axis. This feature is used for the compensation: the software generated in this thesis reads the drive power of the rotary- and swivelling axis as well as the current axis positions $\hat{X}$, $\hat{Y}$ and $\hat{B}$. These are necessary for the compensation of position dependent errors. In addition to the drive power and the axis positions, the cooling power and the environmental temperature, both provided by temperature sensors (section 5.1.1), are read-in by the compensation software. Then, correction parameters are computed based on the prediction of thermal errors (as described in section 5.1.2) under consideration of the kinematic structure of the machine tool, and returned to the CNC as offset parameters. The calculation of the offset parameters is done according to (6.1) to (6.9).

The compensation in Y-direction is independent from any axis position but is simply the negative value of $Y0C$ and can be described by

$$C_{Y,Y0C} = -Y0C \tag{6.1}$$
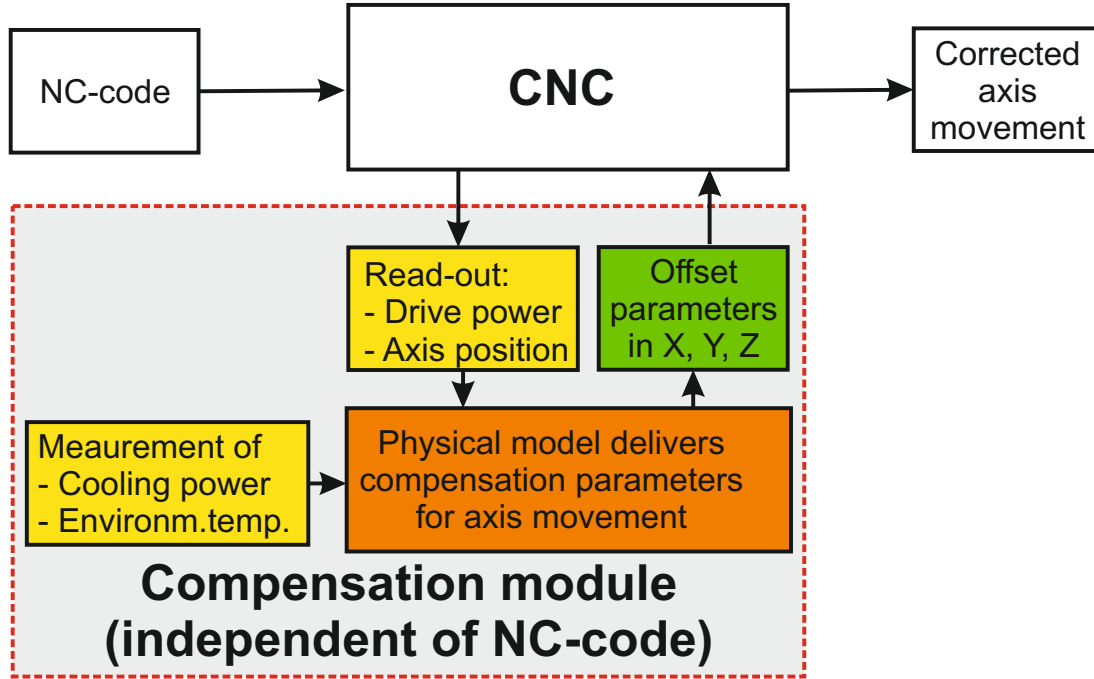
Figure 6.1: Procedure of compensation based on physical model: Input parameters for the model are measured and read-out from the NC on-line and other measurement devices. Then, compensation parameters are computed and sent back to the NC with a time step of 0.5 s.

The change of Z-position of table $Z0T$ shows, depending on the B-axis position $\hat{B}$, a component in Z- and in X-direction according to

$$C_{X,Z0T} = -Z0T \cdot sin \ \hat{B} \tag{6.2}$$

$$C_{Z,Z0T} = -Z0T \cdot cos \ \hat{B} \tag{6.3}$$

The radius error of the C-axis table, $R0T$, depends on the distance of the TCP to the C-axis. Therefore, the axis positions $\hat{X}$ and $\hat{Y}$ have to be considered according to

$$C_{X,R0T} = -\hat{X} \cdot \frac{R0T}{r} \cdot cos \ \hat{B} \tag{6.4}$$

$$C_{Y,R0T} = -\hat{Y} \cdot \frac{R0T}{r} \tag{6.5}$$

Additionally, the error depends on the angular position of the B-axis, which is considered by

$$C_{Z,R0T} = -\hat{X} \cdot \frac{R0T}{r} \cdot sin \ \hat{B} \tag{6.6}$$

Regarding the squareness error $A0C$, only the linear component can be compensated on the analysed machine tool. For a full compensation of the angle, an A-axis would be necessary on the machine tool, which is not the case. The error $A0C$ shows a component in Y-direction, independent of the Z-position of the TCP which is considered by

$$C_{Y,A0C} = -\hat{Z} \cdot A0C \tag{6.7}$$

Figure 6.2: Origin of machine tool coordinate system during compensation. Axis positions $\hat{X}$, $\hat{Y}$ and $\hat{Z}$ read out of the NC are zero in the origin. $\hat{B}$ is zero when the table surface is parallel to the X-direction.

In addition, with a varying Y-position of the TCP, the error shows depending on the angular position of the B-axis $\hat{B}$ two components in X-direction with

$$C_{X,A0C} = -\hat{Y} \cdot A0C \cdot sin\ \hat{B} \tag{6.8}$$

and in Z-direction with

$$C_{Z,A0C} = -\hat{Y} \cdot A0C \cdot cos\ \hat{B} \tag{6.9}$$
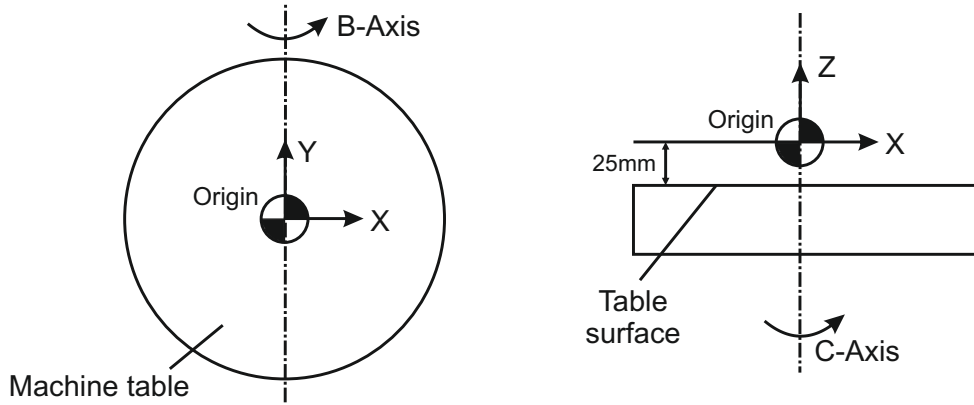
Based on the introduced compensation parameters for the single error components, the overall compensation values C_X, C_Y and C_Z for X-, Y- and Z-direction are calculated according to

$$C_X = C_{X,Z0T} + C_{X,R0T} + C_{X,A0C} \tag{6.10}$$

$$C_Y = C_{Y,Y0C} + C_{Y,R0T} + C_{Y,A0C} \tag{6.11}$$

$$C_Z = C_{Z,Z0T} + C_{Z,R0T} + C_{Z,A0C} \tag{6.12}$$

They are used as offset parameters in order to adjust the origin of the machine tools coordinate system (Figure 6.2). The B- and C-axis of the machine tool are not used for compensation, because the significant errors measured on the machine tool don't need these axis to be compensated. These axes can be implemented into the compensation procedure when e.g. a squareness error $B0C$, or an error of the zero angle of the C axis $C0C$ would have to be considered.

In this thesis, these compensation parameters are sent to the CNC during the compensation cycle every $0.5\ s$ based on the data read-out at the beginning of the time step. This is fast enough for the used verification cycle. During real application, the time step should probably be reduced, depending on the underlying axes movement. A reduction of the time step is no problem due to the simplified model which allows faster calculation cycles.

Figures 6.3 to 6.6 show the measured errors $Y0C$, $Z0T$, $R0T$ and $A0C$ on **Machine tool B/C** during the arbitrarily chosen load cycle of Figure 5.5. The straight line / finely hatched areas represent the thermal errors without compensation, dotted lines / roughly
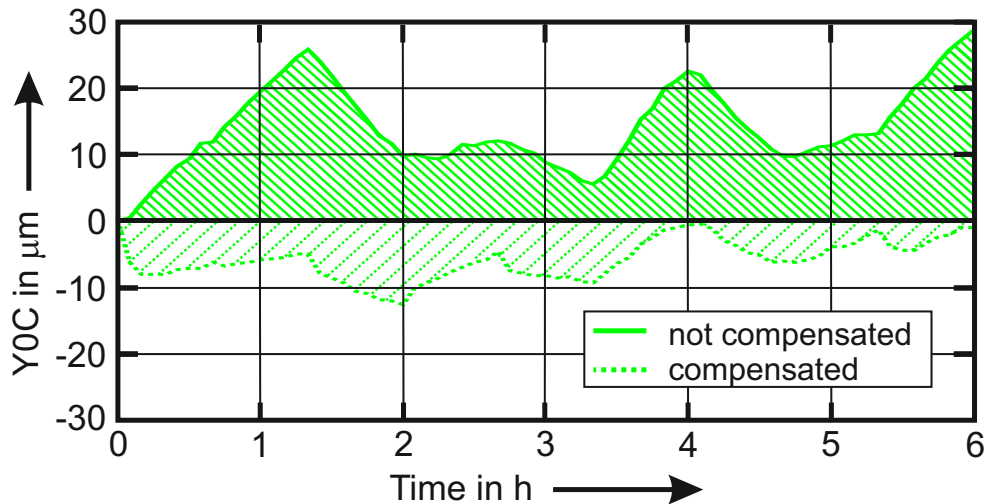
Figure 6.3: Location error $Y0C$ (Y-position of C): Comparison without and with active compensation according to the load cycle presented in Figure 5.5. Both error courses are measured on the machine tool. Therefore, R-Tests are carried out with a time gap of five minutes between the end and the start of each measurement.

hatched areas represent the condition with active compensation. R-Tests are carried out with a time gap of five minutes between the ending and the start of each measurement.

Figure 6.3 shows the thermally induced deviation of the C-axis in Y-direction. Throughout the whole measurement with active compensation, a slight overcompensation can be seen especially in the first three hours of the measurement. When regarding the measurement without compensation, it can be seen that in these first two hours, deviations show not a first order lag element behaviour but a more linear characteristic. This is assumed to be caused by the cooling unit of the rotary axis unit: depending on the environmental air temperature at the start of the measurement, the intervention of the cooling unit can strongly differ, because the inlet temperature in the machine tool is controlled regarding the difference between the outlet and the environmental temperature. Compared to the measured behaviour without compensation, the model predicts deviations, which shows less a linear but more a first order lag element behaviour (Figure 5.15). This difference is responsible for the slight overcompensation, which is reduced at the end of the measurement cycle. However, a significant reduction of the margin of $Y0C$ of about 55% from 29 μm to 13 μm is reached throughout the whole cycle. The arithmetic mean of $Y0C$ is reduced by 84%.

Figure 6.4 shows the thermally induced change of the Z-position of the table. The magnitudes of the residual deviation with compensation can be found after approximately 2 and 3.5 hours. They correlate with the transition from a B-axis positioning at 90° to a C-axis rotation with 400 min^{-1} at $t = 3.25$ h respectively 800 min^{-1} (Figure 5.5). The rise of the errors during this sequence can be explained by the cooling system. When the B-axis is positioned at 90°, no heat is produced by the C-axis, but the inlet of the cooling unit, which provides cooling fluid to both drives, is cooled down due to the heat produced by the B-axis drive. This leads to a significant temperature decrease in the
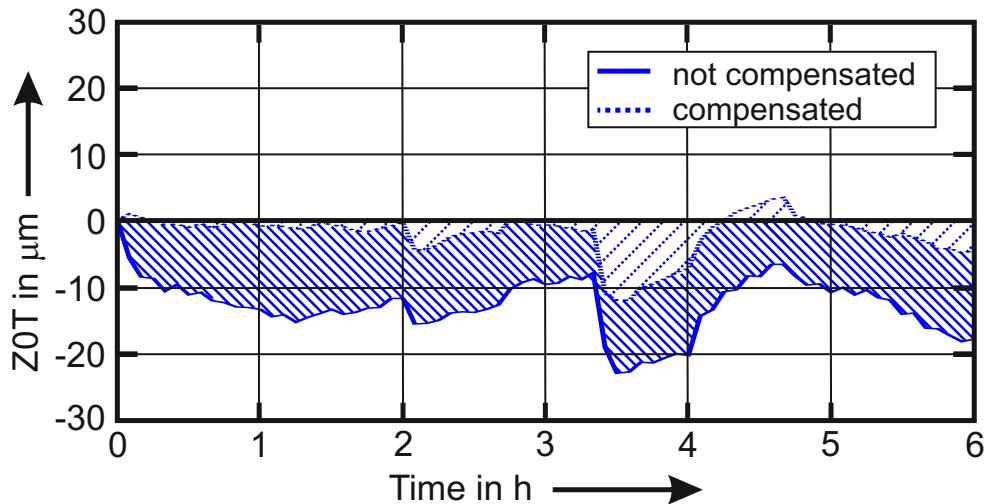
Figure 6.4: Location error $Z0T$, Z-position of table: Comparison without and with active compensation according to the load cycle presented in Figure 5.5. Both error courses are determined with R-Tests carried out with a time gap of five minutes between the end and the start of each measurement.

C-axis unit, which can be seen at the outlet temperature decrease (approx. 1.5°C) of the C-axis cooling circuit in Figure 5.7. In Figure 5.15, the computed errors and the measured errors are compared. It can be seen that the described effect is covered by the presented model, but shows a smaller magnitude. Nevertheless, the range of the axial table growth is reduced from 23 μm to 15 μm, which is approximately 35%. The arithmetic mean is reduced by 84%.

The radius error $R0T$ is illustrated in Figure 6.5. The error shows a range of 12 μm with no compensation. This can be reduced to 5 μm with compensation, which equals to approximately 58%. The compensation works satisfying throughout the whole duration: the arithmetic mean is reduced by 79%.

Regarding the squareness error A0C of the C-axis to the Y-axis as shown in Figure 6.6, only linear effects can be compensated, because the machine tool has no A-axis. According to [145], only the functional point (FP, introduced in section 2.2.2) can be compensated, not the functional orientation (FO, introduced in section 2.2.2). Therefore, the values after compensation represent the change of the Z-position due to $A0C$. The value is related to a radius of one meter. When swivelling the B-axis to 90°, the occurring errors with a magnitude of about 14 μm are not compensated by the model satisfyingly. The reason for the deviations is the cooling system, which is part of the prediction model as introduced in 5.1.1. However, because both axis are cooled within one cooling circuit, they show significant coupling effects. The cooling of the B-axis drive at the B-position 90°, when no load is applied by the C-axis, results in a contrary bimetallic effect of $A0C$. In Figure 5.15 it can be seen that the model basically covers the change of the deviation, when swivelling the B-axis to 90°, but the magnitude of the coupling effect is not covered due to the fact that the calibration procedure is only done axis by axis. Therefore, the compensated error still shows an error range of 15 μm. This equals a redution of 35% (from 23 μm to 15 μm).
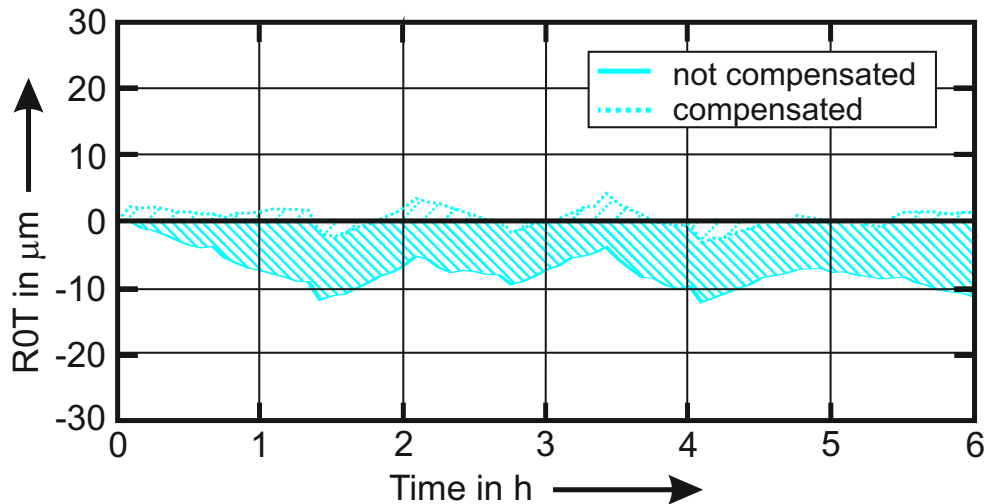
Figure 6.5: Radius Error $R0T$: Comparison without and with active compensation according to the load cycle presented in Figure 5.5. Both error courses are determined with R-Tests carried out with a time gap of five minutes between the end and the start of each measurement.

The arithmetic mean is reduced by approximately 49%.

With the presented compensation method, a significant reduction of the thermally induced errors is reached. Table 6.1 summarises values for the range and the arithmetic mean of the measured, thermally induced errors with and without compensation.

6.2 Compensation Based on Phenomenological Modelling

While the physical compensation model is implemented via the CNC, the phenomenological compensation is realised by modifying the NC-code of a planned machining process, before it is executed on a machine tool. This compensation procedure is illustrated in Figure 6.7. According to section 5.2, either the axis movement (extracted out of the NC-code) or the power demand of the axis drives (read-out of the CNC) can be used as input parameter for the prediction of thermal errors with the phenomenological model. In this section, compensation examples based on internal CNC signals (power supplied to A- and C-axis drive) of **Machine tool A/C** are presented. The first example shows the compensation of an arbitrarily chosen test cycle of the horizontal, swivelling A-axis of **Machine tool A/C**. The second example shows a compensation cycle, where both rotary axes of **Machine tool A/C**, the A-axis and the C-axis, are moved sequentially. Table 6.2 summarizes the significant deviations caused by a movement of A- and C-axis of **Machine tool A/C** found out by previous measurements. Only these deviations are considered by the phenomenological model based compensation procedure pesented here.

Figure 6.9 shows the power supplied to the A-axis drive of **Machine tool A/C** due to an arbitrarily chosen movement of the A-axis over 62 hours. Sections of movement (pendular movement between two arbitrarily chosen angular positions) are plotted in red, sections of standstill (at different arbitrarily chosen axis positions) are plotted in green. Thermally induced errors corresponding to this power supply are presented in Figures 6.10 to 6.12 without and with active compensation. Only the errors identified as
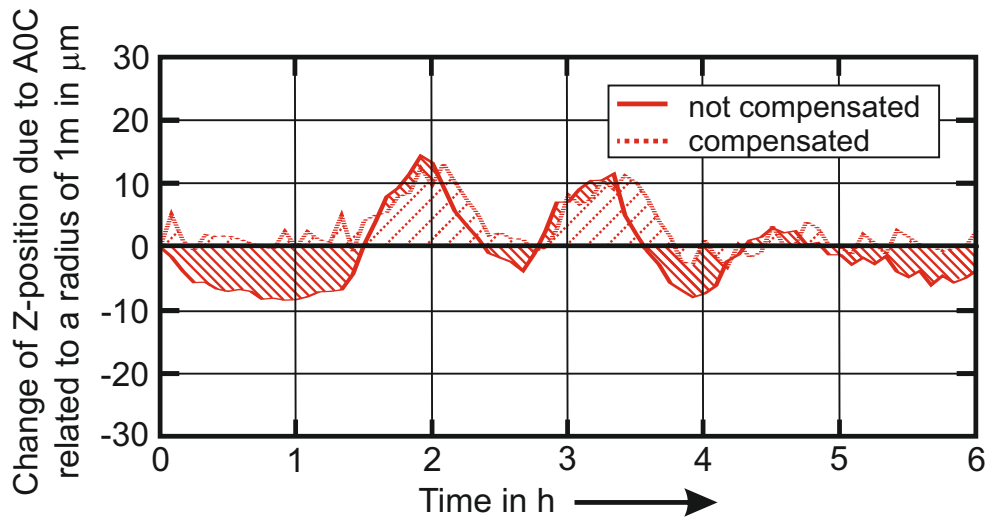
Figure 6.6: Change of Z-position due to $A0C$ related to a distance of one meter to the C-axis. Comparison of measurement without compensation and with active compensation of the functional point according to [145].

Table 6.1: Reduction of range and arithmetic mean of the measured location errors by the physical compensation model on **Machie tool B/C**.

	Range			
	$Y0C$ μm	$Z0T$ μm	$R0T$ μm	$A0C$ μm/m
Before	29	23	12	23
After	13	15	5	15
Improvement [%]	**55**	**35**	**58**	**49**
	Arithmetic mean			
	$X0C$ μm	$Z0T$ μm	$R0T$ μm	$A0C$ μm/m
Improvement [%]	**84**	**84**	**79**	**49**

Table 6.2: Significant errors of **Machine tool A/C** due to power consumption to the A- or C-axis drive, found out by R-Test measurements and considered for compensation.

A-axis movement	C-axis movement
X-deviation of functional surface table (**X0T**)	X-deviation of C-axis (**X0C**)
Z-deviation of A-axis (**Z0A**)	Z-deviation of table of C-axis (**Z0T**)
Zero position of A-axis (**A0A**)	Radius error of table (**R0T**)
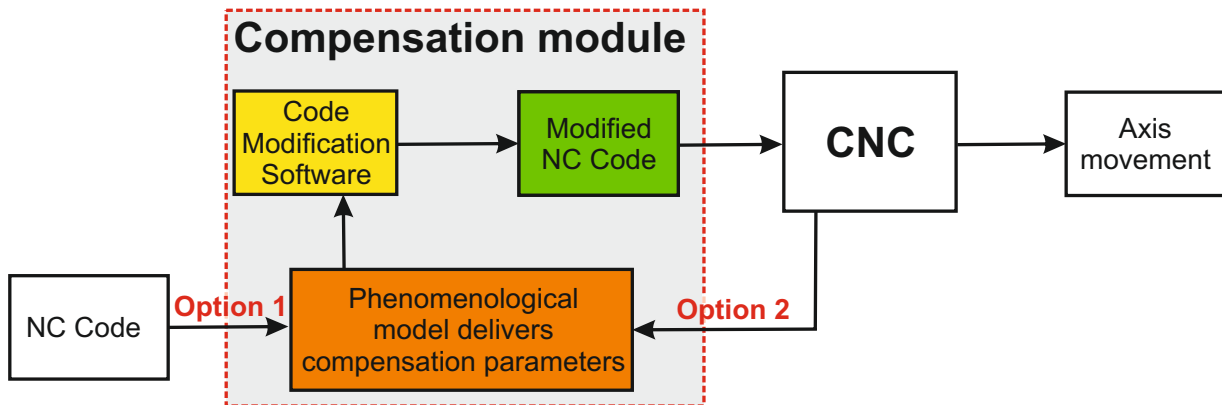
Figure 6.7: Procedure of compensation based on phenomenological model. Option 1) The Code Modification Software (CMS) reads raw NC-code and predicts thermal errors because of the axes movement described in the NC-code. Then the code is modified in order to reduce predicted errors before it is executed on the CNC. Option 2) Error prediction is carried-out based on informations about the power supplied to a certain axis drive corresponding to a certain NC-code. Then, the NC-code is modified and sent back to the CNC according to Option 1.
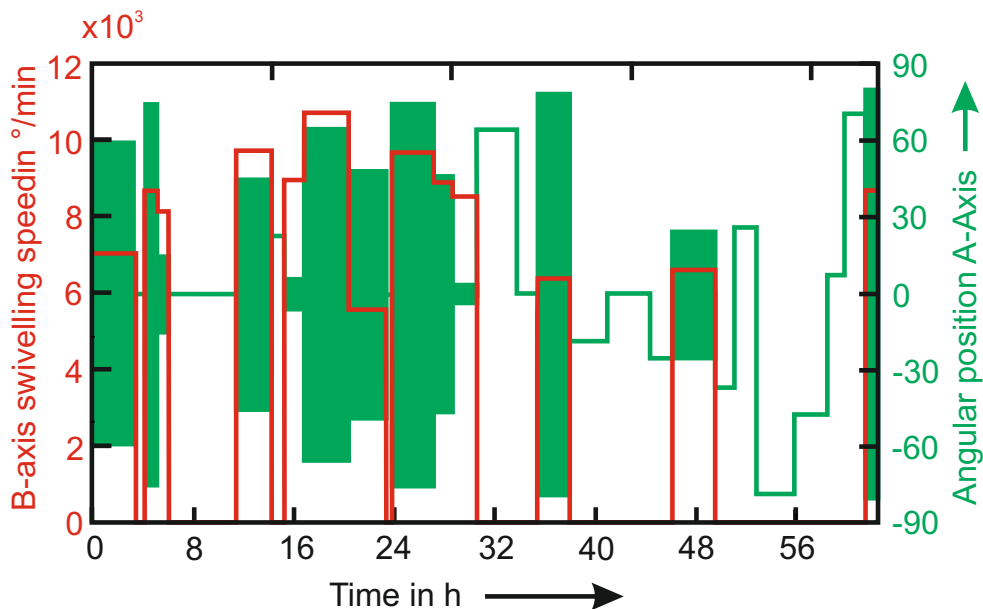
Figure 6.8: Arbitrarily chosen *A*-axis load cycle for **Machine tool A/C**. Green Areas illustrate a swivelling movement between the angular positions included by the area.
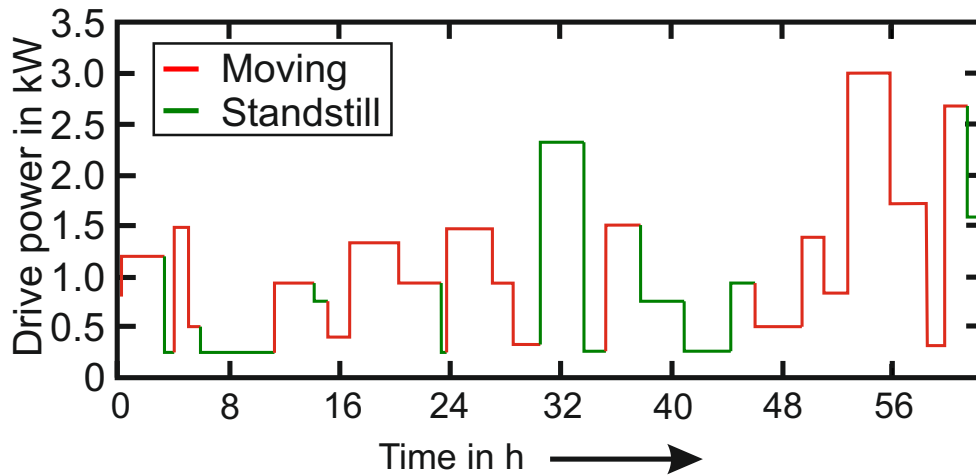
Figure 6.9: Power supplied to the A-axis drive during an arbitrarily chosen test cycle of 62 hours (Figure 6.8). Red line: axis does a pendular movement. Green line: axis stands still at different angular positions.

significant in section 4.2.2 ($Z0A$, $X0T$, $A0A$) are listed in this evaluation. The straight line / finely hatched areas represent the thermal errors without compensation, dotted lines / roughly hatched areas represent the condition with active compensation. Deviations are determined with R-Tests carried out with a time gap of five minutes between the end and the start of each measurement. $Z0A$ (Figure 6.10) shows small, load depended deviations with a range of 9.5 μm.

The error course is smoothed and the range is reduced by the compensation from 9.5 μm to 5.5 μm. A further reduction is limited due to the measurement uncertainty and the environmental influence over the long time duration of 60 hours.

With compensation, the error course is smoothed and the range is reduced to 5.5 μm, which equals a reduction of approximately 42%. A further reduction is limited due to the measurement uncertainty of the R-Test system and the environmental influence over the long time duration of 60 hours. The arithmetic mean increases by the compensation from 1.4 μm to 1.9 μm, which is neglectable small.

The results of the compensation of $X0T$ (Figure 6.11) shows an efficient reduction of the deviations throughout the complete test cycle: the range is 17 μm without compensation and is reduced to 7 μm with compensation. This is a reduction of 85%. The arithmetic mean is reduced from 7 μm to 1 μm which equals a reduction of 86%. On **Machine tool A/C**, the rotational error $A0A$ (Figure 6.12) can theoretically be fully compensated, because the machine tool has an A-axis. The measurements with correction show a slight overcompensation throughout the whole measurement cycle. Nevertheless, the range can be reduced from 34 μm/m to 15.5 μm/m, which represents a reduction of approximately 54%. The arithmetic mean is reduced from 11 μm/m to 3 μm/m (70%). Table 6.3 summarizes the presented improvements by the phenomenological model compensation.

As an additional example, the compensation of a sequentially carried-out movement of both rotary axes A and C of **Machine tool A/C** is presented. Figure 6.13 shows the

Figure 6.10: Thermally induced error $Z0T$, Z-position of table: Comparison without and with active compensation according to the power input to the A-axis drive presented in Figure 6.9. Both error courses are determined with R-Tests carried out with a time gap of five minutes between the end and the start of each measurement.

Figure 6.11: Thermally induced error $X0T$, X-position of table: Comparison without and with active compensation according to the power input to the A-axis drive presented in Figure 6.9. Both error courses are determined with R-Tests carried out with a time gap of five minutes between the end and the start of each measurement.
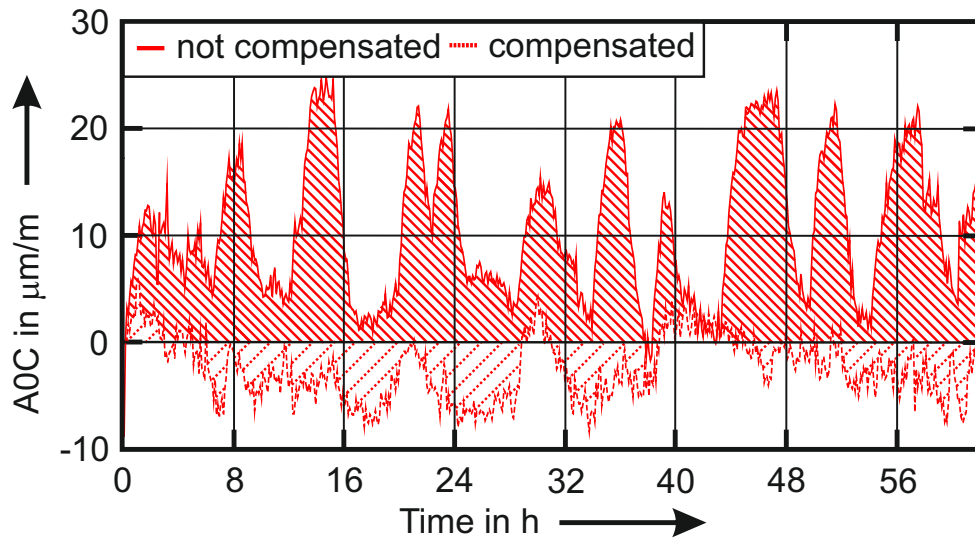
Figure 6.12: Thermally induced error $A0A$, zero position of A: Comparison without and with active compensation according to the power input to the A-axis drive presented in Figure 6.9. Both error courses are determined with R-Tests carried out with a time gap of five minutes between the end and the start of each measurement.

Table 6.3: Reduction of range and arithmetic mean of measured thermally induced errors by the phenomenological compensation model due to power supplied to the A-axis drive presented in Figure 6.9. [1] -35% equals a difference of 0.5 μm.

	Range		
	$Z0A$ μm	$X0T$ μm	$A0A$ μm/m
Before	9.5	17.0	34.0
After	5.5	7.0	15.5
Improvement [%]	**42.0**	**54.0**	**70.7**
	Arithmetic mean		
	$Z0A$ μm	$X0T$ μm	$A0A$ μm/m
Improvement [%]	**-35.0**[1]	**86.0**	**70.0**
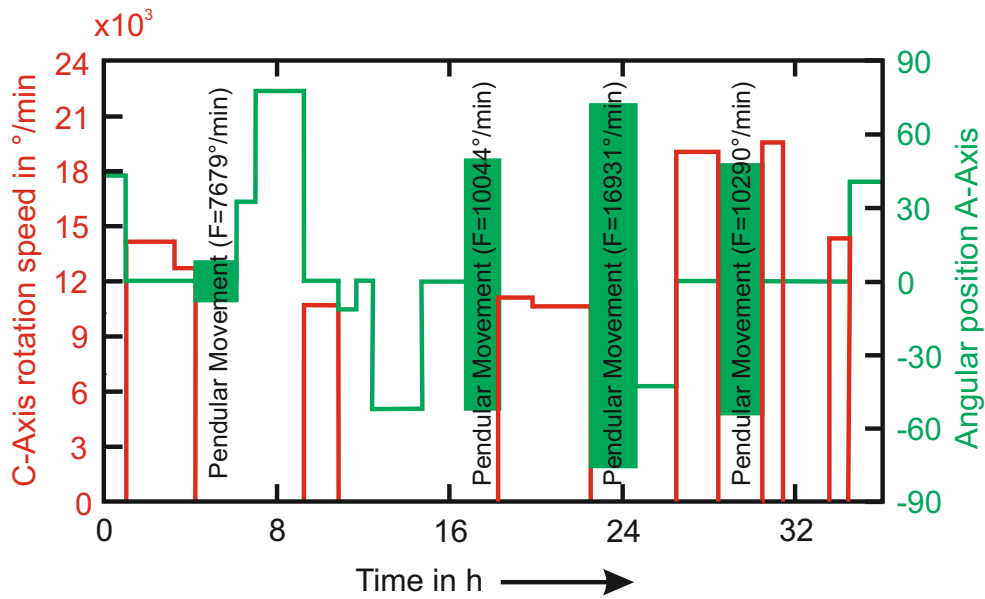
Figure 6.13: Combined load cycle of A- and C-Axis of **Machine tool A/C**. Red line: C-Axis rotation speed; Green line: Angular position A-Axis; Green areas: Pendular movement of A-Axis between the angular positions included by the area with the given feed speed;
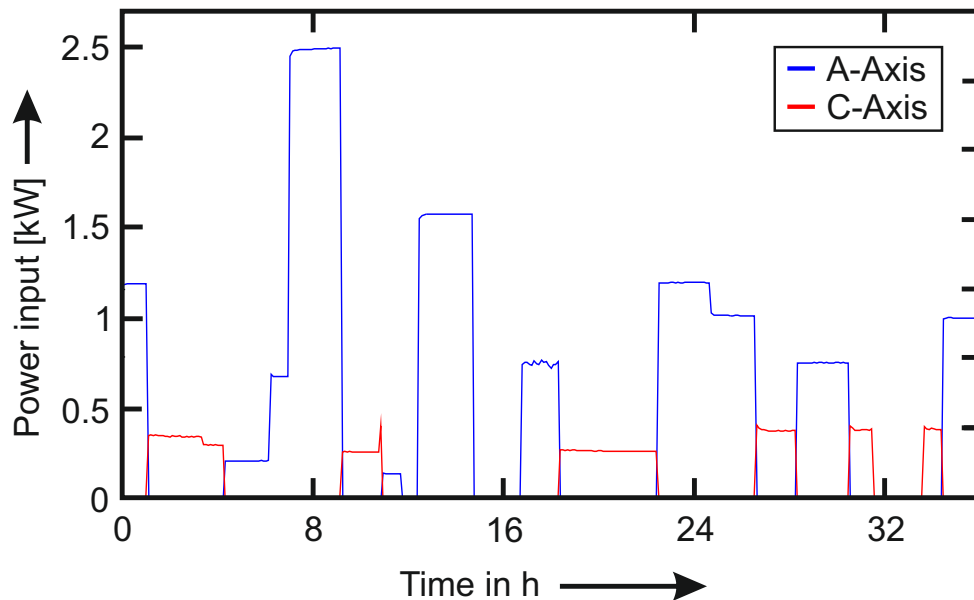
Figure 6.14: Power supply to the C-axis drive (red line) and the A-axis drive (blue line) during a combined axis movement during an arbitrarily chosen movement over 36 hours presented in 6.13.
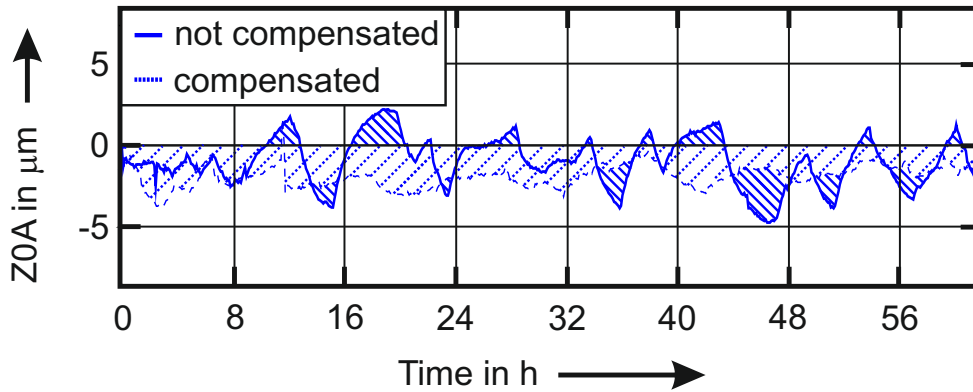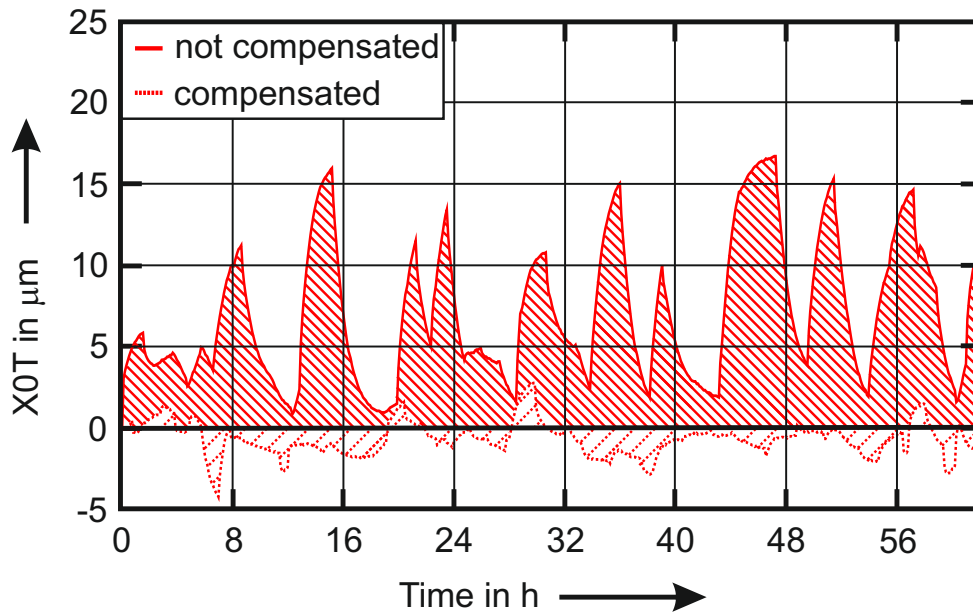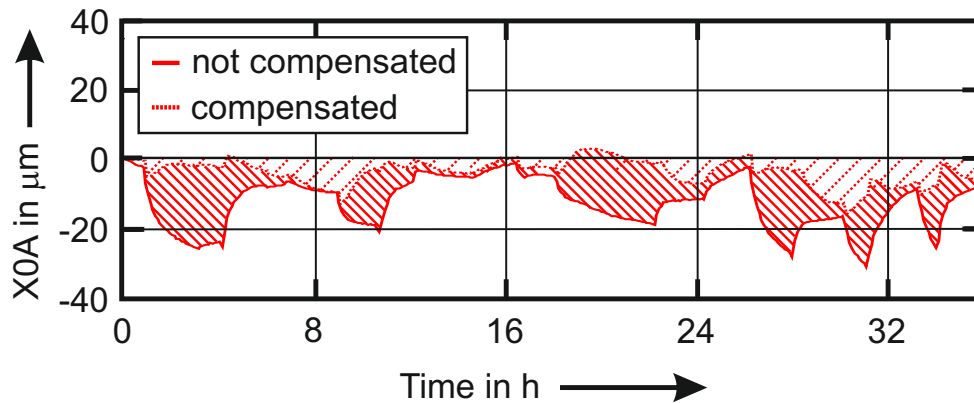
Figure 6.15: Location error $X0T$, X-position of table: Comparison without and with active compensation according to the power consumption of the drives presented in Figure 6.14. Both error courses are measured on the machine tool with R-tests [126].

axis movement of the cycle, Figure 6.14 shows the power consumption of the drives of the axes during this cycle. Significant errors (Table 6.2) are measured with the R-Test discrete.

Figure 6.15 shows the measured error $X0C$ without (straight lines, finely hatched areas) and with (dotted lines / roughly hatched areas) active compensation. Throughout the whole test cycle, a large proportion of the thermally induced errors is compensated. The range of $R0T$ is reduced from 30.5 μm to 16.0 μm, which is an improvement of 47%. The arithmetic mean is reduced by 63.5%. In Figure 6.16, the change of the Z-axis position of the machine tool table $Z0T$ is illustrated with and without active compensation. Again, a large proportion of the thermally induced errors are reduced by the phenomenological model based compensation. The range of the deviation is reduced from 90 μm to 34 μm, which equals an improvement of 62%. The arithmetic mean is improved by 68.0%. The thermally cause radius error of the machine tool table $R0T$ is illustrated in Figure 6.17 without and with active compensation. The range is reduced from 19.1 μm to 5.5 μm which is equal to 70.5%. The arithmetic mean is reduced from 7 μm to 1 μm, which equals 85.5%. Table 6.4 summarises the improvement regarding the reduction of significant errors.
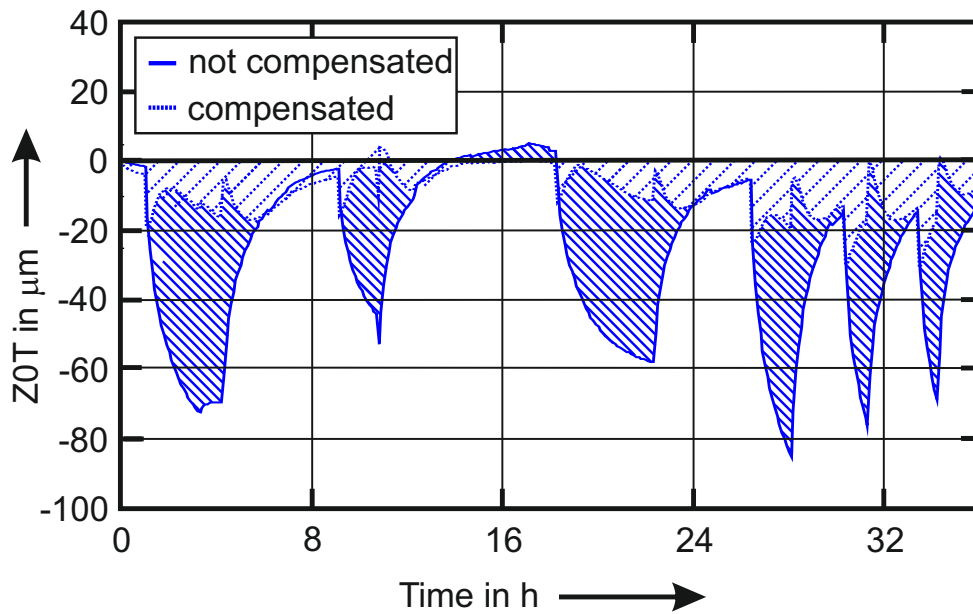
Figure 6.16: Z-position of table $Z0T$: Comparison without and with active compensation according to the power supplied to the drives presented in Figure 6.14. Both error courses are measured on the machine tool with R-tests [126].
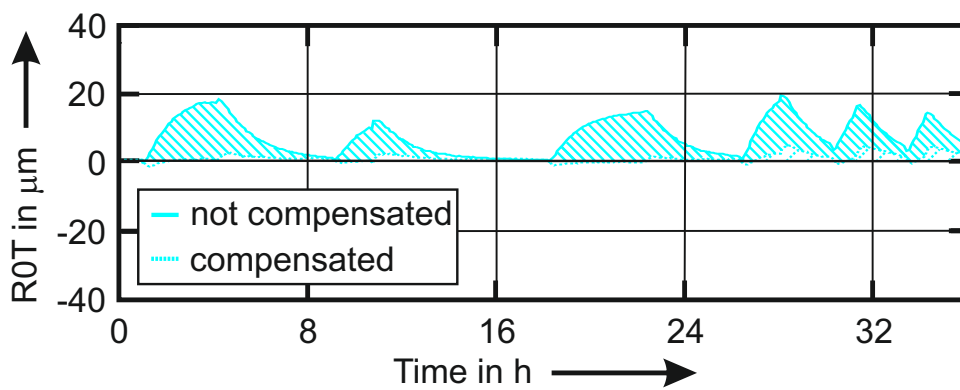
Figure 6.17: Radius error of table $R0T$: Comparison without and with active compensation according to the power supplied to the drives presented in Figure 6.14. Both error courses are measured on the machine tool with R-tests [126].

Table 6.4: Reduction of location errors due to a combined movement of the A- and C-axis of **Machine tool A/C** by the phenomenological compensation model [126].

	Range		
	$X0C$	$Z0T$	$R0T$
	μm	μm	μm
Before	30.5	90.1	19.1
After	16.0	34.3	5.6
Improvement [%]	**47.0**	**61.9**	**70.7**
	Arithmetic mean		
	$X0C$	$Z0T$	$R0T$
	μm	μm	μm
Improvement [%]	**63.5**	**68.1**	**85.5**

7 Conclusion and Outlook

In this thesis, the thermal behaviour of rotary and swivelling axes of 5-axis machine tools is characterized based on systematic temperature and displacement measurements. Temperature measurements during different operational states of the rotary axes show, that due to the power supply to the axis drives, a significant change in the temperature distribution of the machine tool structure is induced. This temporal and spatial temperature change causes significant errors between tool and workpiece of the machine tool. While international standards currently cover the thermal influences due to environmental temperature changes, the main spindle or linear axes, the influence of rotary axes is not considered yet. Results in this thesis clarify that this needs to be changed, and a proposal for the determination and evaluation of thermally induced errors of rotary and swivelling axes is given in this thesis.

Measurements of displacements on two 5-axis machine tools show, that thermally induced position and orientation errors are one order of magnitude larger than thermally induced component errors such as an axial or a radial motion error. Therefore, component errors are neglected in this thesis. Measurement cycles and procedures based on the R-Test measurement device are developed which are marvellously suited to identify thermally induced position and orientation errors of rotary axes. Thereby it is shown, that in addition to the five geometric location errors of rotary axes provided in ISO 230-1:2012, thermally induced location errors of functional surfaces, such as the axial growth (or change of Z-position) of a machine tool table, and dimensional errors, such as a radial growth of a machine tool table, have to be considered. When comparing the behaviour of machine tools during different measurements, differences in the load-cycles carried out on the machine tools have a large influence on the measurement results. Because these load cycles are strongly influenced by the measurement procedure with specific numbers of measurement cycles and cycle times, it is fundamental to specify the way measurements were carried out when thermally induced deviations of rotary axes are presented. The measurements done in this thesis are carried out according to ISO 230 under no load and cutting conditions. In addition to these investigations, some preliminary temperature and displacement measurements are carried out with cutting fluid. Also these tests show that the cutting fluid has a significant influence on the thermal behaviour of the machine tool and further studies are of essential importance.

In order to increase the accuracy of 5-axis machine tools it is necessary to minimize the thermal error induced by the rotary and swivelling axes. A lot of approaches for the reduction of thermal errors can be found in literature: besides design changes in order to avoid thermally induced errors, many different model approaches have been developed to compensate occurring errors. In this thesis, two approaches for error prediction models are presented: a physical and a phenomenological approach. Both methods use internal signals of the numeric control such as the power supplied to the axis drives or the axis

movement extracted from the NC-code for the prediction of thermal errors.

The physical model presented in this thesis consists of two elementary components: the computation of temperature changes in the machine tool structure, and the computation of thermo-elastic deformations based on these temperature changes. The idea beyond the approach is to simplify the relevant structure in single bodies assumed to be homogeneous. This enables the adaptation of the model especially regarding other machine tools with a similar kinematic setup, but it makes a calibration procedure necessary, because due to the simplification, important physical parameters are unknown and have to be estimated via measurements. In this thesis, it is shown that the method is applicable and thermally induced errors can be predicted based on internal CNC signals after calibrating the model. Due to the scientific format of this work, the calibration procedure is not implemented to run automated but the model output is fitted according to calibration measurements carried out. For an industrial application, an automated parameter identification procedure based on a standardized calibration routine is proposed as a future project.

The phenomenological model approach developed in this thesis predicts thermally induced deviations based on a pure mathematical fitting of a differential equation describing the thermal behaviour of the analysed system. Thereby, two different options can be chosen regarding the input parameters for the calculation: either the NC-code of the planned operation, which has to be compensated, is analysed by a software developed within the thesis, or the power input to the drives of the machine tool is used for error prediction. Using the axis movement extracted from the NC-code means, that the model can be used as a post processing compensation module for example within a CAM software. Using the power information of the drives means, the model can be implemented in the CNC of a machine tool. For both methods, a software is developed that allows a fully-automated identification of the fitting parameters followed by the automated modification of the TCP-path for a planned movement. Currently, this model approach is tested for rotary and swivelling axes. Due to the high automation grade regarding measurement, parameter identification and compensation, this method shows great potential for a successful, industrial transfer. In the future it could be extended in order to include other thermal influences, like the environment, the main spindle or linear axes.

Important for the user of the machine tool is the efficiency of error models during operation. Therefore, compensation measurements are carried out directly on the machine tool to verify the presented prediction methods. With both approaches, a significant reduction of the thermally induced errors up to 85% is reached, whereby thermal influences were only induced by the drives of the rotary axes and the environment. The internal cooling system of the machine tools under investigation leads to a further simplification, because thereby no mutual influences occurr.

Measurements of the cooling power during different load cycles carried out on the machine tools show that the cooling units can have a significant influence on the thermal behaviour of the rotary axes. When both rotary axes of a machine tool have the same cooling circuit, as the machine tools analysed in this thesis, this may lead to strong cross coupling effects. In order to consider these effects more detailed, the cooling system has

to be analysed. A technical way to reduce this cross-coupling influence in order to build more accurate machine tools, would be to redesign the cooling system so that every axis is equipped with a separate cooling circuit.

Both models presented in this work use internal signals for the error prediction. This leads to the major advantage that no additional sensors and monitoring systems have to be integrated in the machine tool. A disadvantage regarding the use of internal signals is, that in case of an interruption of the compensation cycle, the models have no information, which condition is present on the machine tool. Measurements of the cool-down behaviour of the analysed machine tools show short time constants due to the active cooling systems of the rotary / swivelling axis units. After at most four hours, starting conditions prevail regarding the temperature distribution. This may be too long for an industrial use. Therefore, further investigations have to be done. A promising approach e.g. is the use of 3D-probing systems, which can easily be implemented on machine tools, in combination with error prediction models. Thereby, the current condition could be estimated after an interruption or abortion of the compensation cycle, e.g. after an emergency stop. But it is necessary to analyse the significance of those testings, the places of testing and the way in which the modelling equations are updated by those measurement results.

A Appendix

In the following section the uncertainty of the R-Test measurement device is estimated according to [133]. Table A.1 summarizes the single contributors to the uncertainty as well as the extended uncertainty U(k=2) for the 3D-case on a machine tool. For all uncertainty calculations, a rectangular distribution of the deviations is assumed.

Probes (u_{Probes})

- Measuring path l_{mes}: 4 mm,

- Reference length l_{ref}: 12 mm

- Range of error (catalogue value) 2a: 0.4 μm,

$$u_{Probes} = \frac{2a \cdot l_{mes}}{\sqrt{12} \cdot l_{ref}} = \frac{1}{\sqrt{12}} \cdot \frac{0.4 \ \mu\text{m}}{12 \ \text{mm}} \cdot 4 \ \text{mm} = 0.133 \ \mu\text{m} \tag{A.1}$$

Probing tip

Regarding the probing tip, three influences are considered. The flatness error (u_{fe}), the angular error (u_{ae}) and the roughness error (u_{re}). They are considered based on following estimations:

- Measuring path l_{mes}: 4 mm,

- Range of flatness (2a): 1 μm

- Range of angular error α: 1°

- Range of influence by roughness (2a): 0.1μm

$$u_{fe} = \frac{2a}{\sqrt{12}} = \frac{1 \ \mu\text{m}}{\sqrt{12}} = 0.289 \ \mu\text{m} \tag{A.2}$$

$$
\begin{aligned}
u_{ae} &= \frac{1}{\sqrt{12}} \cdot \alpha \cdot \frac{\pi}{180°} \cdot 1000 \cdot tan(\alpha \cdot \frac{\pi}{180°}) \cdot l_{mes} \\
&= \frac{1}{\sqrt{12}} \cdot 1° \frac{\pi}{180°} \cdot 1000 \cdot tan(1° \cdot \frac{\pi}{180°}) \cdot 4 \ \text{mm} = 0.352 \ \mu\text{m}
\end{aligned}
\tag{A.3}
$$

$$u_{re} = \frac{2a}{\sqrt{12}} = \frac{0.1 \ \mu\text{m}}{\sqrt{12}} = 0.029 \ \mu\text{m} \tag{A.4}$$

Probing direction (u_{dir})

- Measuring path l_{mes}: 4 mm,

- Range of angular error β: 1°

$$
\begin{aligned}
u_{dir} &= \frac{1}{\sqrt{12}} \cdot (1 - cos(\frac{\pi}{180} \cdot \beta)) \cdot \frac{l_{mes}}{1000} \\
&= \frac{1}{\sqrt{12}} \cdot (1 - cos(\frac{\pi}{180} \cdot 1°)) \cdot \frac{4 \text{ mm}}{1000} = 0.176 \ \mu\text{m}
\end{aligned}
\tag{A.5}
$$

Roundness of sphere (u_{sph})

The roundness error of the sphere is assumed with $0.2\mu m$ ($2a$).

$$
u_{sph} = \frac{2a}{\sqrt{12}} = \frac{0.2 \ \mu\text{m}}{\sqrt{12}} = 0.058 \ \mu\text{m}
\tag{A.6}
$$

Temperature influence (u_{tem})

During a drift test over 30 minutes, a range of $0.5\mu m$ was determined.

$$
u_{tem} = \frac{0.5 \ \mu\text{m}}{\sqrt{12}} = 0.144 \ \mu\text{m}
\tag{A.7}
$$

Deformation

The deformation of the fixture of the sphere (u_{ds}) and the deformation of the probes (u_{dp}) are considered based on following assumptions:

- Measuring path l_{mes}: 4 mm,

- Fixture of sphere: $l_{fix} = 50$ mm, $d_{fix} = 10$ mm, $F = 0.5$ N

- Probes: Length: $l_{prb} = 20$ mm, Diamteter of piston: $l_{dia} = 2$ mm, Torque: $T = 1$ Nmm

- Youngs modulus E is assumed to be $210000\frac{N}{\text{mm}^2}$

$$
\begin{aligned}
u_{ds} &= \\
&= \frac{1}{\sqrt{12}} \cdot (\frac{F \cdot l_{mes}^3}{3 \cdot E(\pi \cdot (l_{mes})^4 \cdot \frac{1}{64})}) \cdot 1000 = \\
&= \frac{1}{\sqrt{12}} \cdot (\frac{0.5 \text{ N} \cdot (50 \text{ mm})^3}{3 \cdot 210000\frac{N}{\text{mm}^2}(\pi \cdot (50 \text{ mm})^4 \cdot \frac{1}{64})}) \cdot 1000 = 0.058 \ \mu\text{m}
\end{aligned}
\tag{A.8}
$$

$$
\begin{aligned}
u_{dp} &= \\
&= \frac{1}{\sqrt{12}} \cdot (\frac{T \cdot l_{prb}}{E \cdot (\pi \cdot (2 \text{ m}m)^4 \cdot \frac{1}{64})} \cdot \frac{l_{mes}}{l_{dia}} \cdot 1000 \\
&= \frac{1}{\sqrt{12}} \cdot (\frac{1 \text{ Nmm} \cdot 50 \text{ mm}}{210000 \ \frac{N}{\text{mm}^2} \cdot (\pi \cdot (2 \text{ m}m)^4 \cdot \frac{1}{64})}) \cdot \frac{4 \text{ mm}}{2} \cdot 1000 = 0.070 \ \mu\text{m}
\end{aligned}
\tag{A.9}
$$

Table A.1: Considered contributors to the uncertainty of the R-Test measurement device per axis direction under shop floor conditions. All values are related to a measuring path of $4\ \mathrm{mm}$. Correlated input quantities are underlined - uncorrelated input quantities are not underlined. The evaluation of the combined standard uncertainty u is done according to [133].

Contributor	Considered standard uncertainty
Probes	
Linear proportional error	$0.038\ \mu\mathrm{m}$
Probing surface	
Flatness error	$0.188\ \mu\mathrm{m}$
Location error	$0.352\ \mu\mathrm{m}$
Roughness error	$0.029\ \mu\mathrm{m}$
Probing direction	
Errors due to angular position	$0.176\ \mu\mathrm{m}$
Sphere	
Roundness	$0.058\ \mu\mathrm{m}$
Temperature influence	
Drifttest	$0.144\ \mu\mathrm{m}$
Deformation	
Sphere	$0.058\ \mu\mathrm{m}$
Probe	$0.070\ \mu\mathrm{m}$
Combined standard uncertainty u	$0.5\ \mu\mathrm{m}$
Extended Uncertainty $U(k=2)$	$1.0\ \mu\mathrm{m}$
Extended Uncertainty in 3D	$1.8\ \mu\mathrm{m}$

List of Publications

Conferences

- (M. Gebhardt, J. Mayr, P. Blaser, W. Knapp, K. Wegener. Physical Model Compensation for 5-Axis Machine Tools. Proceedings of the 14th euspen International Conference, Dubrovnik, June 2014. Status: *under review*)

- (M. Gebhardt, J. Mayr, N. Furrer, T. Widmer, S. Weikert, W. Knapp. High precision grey-box model for compensation of thermal errors on 5-axis machine tools. CIRP Annals - Manufacturing Technology 2014. Status: *accepted*)

- (J. Mayr, M. Gebhardt, B.B. Massow, S. Weikert, K. Wegener. Cutting fluid influence on multi axis machining. 6th CIRP International Conference on High Performance Cutting, HPC2014. Status: *accepted*)

- (M. Wiessner, M. Gebhardt, W. Knapp, K. Wegener. Test piece for visualization of thermally induced deviations on five-axis machine tools. Euspen SIG Thermal Issues Zurich, 2014. Status: *accepted*)

- (P. Blaser, M. Gebhardt, J. Mayr, W. Knapp, K. Wegener. Automatic compensation of thermally induced errors on five-axis machine tools. Euspen SIG Thermal Issues Zurich, 2014. Status: *accepted*)

- M. Gebhardt, A. Schneeberger, S. Capparelli, W. Knapp, K. Wegener. Messtechnische Charakterisierung thermisch bedingter Abweichungen von 5-Achs Werkzeugmaschinen, XXVII. Messtechnisches Symposium des Arbeitskreises der Hochschullehrer für Messtechnik e.V., 2013, Zürich, ISBN 978-3-8440-2124-0, Pages 25-36

- M. Gebhardt, A. Schneeberger, W. Knapp, K. Wegener. Measuring, modeling and compensating thermally caused location errors of rotary axes, The Proceedings of Machine Tools Technology Research Foundation 2013 Meeting, 2013, San Francisco, USA, Pages 19-24

- M. Gebhardt, S. Capparelli, M. Ess, W. Knapp, K. Wegener. Physical and phenomenological simulation models for the thermal compensation of rotary axes of machine tools, 13th International Conference of the European Society for Precision Engineering & Nanotechnology, 2013, Berlin, Germany, ISBN 978-0-9566790-2-4, Issue 1, Pages 304-309

- M. Gebhardt, W. Knapp, K. Wegener. 5-Axis Test-Piece - Influence of Machining Position, Machine Tool Technologies Research Foundation (MTTRF), 2012, Iga City, Japan, Pages 299-304

- M. Gebhardt, v. Cube, W. Knapp, K. Wegener. Measurement set ups and cycles for thermal characterization of axes of rotation, 12th International Conference of the European Society for Precision Engineering & Nanotechnology, 2012, Stockholm, Sweden, ISBN 978-0-9566790-0-0, Volume 1, Pages 486-489

- T. Liebrich, M. Gebhardt, S. Thoma, H. Nguyn, S. Weikert, W. Knapp, K. Wegener. Static and Dynamic Testing of 5-Axis Machine Tools, Proceedings of the MTTRF 2011 Annual Meeting 2010, 2010, San Francisco, USA

Journals

- (M. Gebhardt, W. Knapp, K. Wegener. Messung thermischer Einflüsse auf Werkzeugmaschinen zur steuerungsseitigen Fehlerkorrektur am Beispiel von Dreh- / Schwenkachsen. tm - Technisches Messen, 2014: *under review*)

- (M. Gebhardt, A. Schneeberger, S. Weikert, W. Knapp, K. Wegener. Thermally caused location errors of rotary axes of 5-axis machine tools, International Journal of Automation Technology: *under review*)

- M. Gebhardt, M. Ess, S. Weikert, W. Knapp, K. Wegener. Phenomenological Compensation of Thermally caused Position and Orientation Errors of Rotary Axes, Journal of Manufacturing Processes 15 (2013), Pages. 452-459 DOI information: 10.1016/j.jmapro.2013.05.007

Press articles

- M. Gebhardt, K. Wegener. Temperatureinfluss auf Werkzeugmaschinen, MB-Revue - Das Schweizer Industriemagazin. Jahreshauptausgabe 2013, Page 59-63, 2013

Talks

- M. Gebhardt. Thermische Abweichungen an Werkzeugmaschinen: Messung, Simulation und Kompensation, Fertigungstechnisches Kolloquium am Institut fr Werkzeugmaschinen und Fertigung, ETH Zürich, 2012, Zürich, Switzerland

- M. Gebhardt. Messung thermischer Einflüsse auf Drehachsen, PRODEX 2012, Internationale Fachmesse für Werkzeugmaschinen, Werkzeuge und Fertigungsmesstechnik. SWISSMEM Thementag: Mehrwert durch Präzision in der Messtechnik, 2012, Basel, Switzerland

List of Supervised Theses

The following theses (unpublished) were supervised by the author.

- T. Anliker. Prüfwerkstück für 5-Achs Bearbeitungszentrum. Bachelor thesis, 2011.

- J. Käser. Maschinenprüfung mit dem Kreisformtest. Semester thesis. 2011.

- J.P.v.Cube, Thermisches Verhalten von Dreh- / Schwenkachsen. Master thesis. 2011

- F. Heini. Messen auf Werkzeugmaschinen. Semester thesis. 2011

- J. Käser. Konstruktion und Auslegung einer alternativen Lagerung einer Rotationsachse. Master thesis. 2011

- S. Capparelli. Untersuchung thermischer Einflüsse in der Präzisionsfertigung. Bachelor thesis. 2012

- S. Müller. Konstruktion der Motoraufhängung eines Elektrofahrzeuges und Integration eines Range Extenders. Bachelor thesis. 2012

- M. Wiessner. Schwingungsanalyse und Optimierung der Motoraufhängung eines Elektrofahrzeuges. Bachelor thesis. 2012

- D. Vincent. Konzeptionierung und Konstruktion von Komponenten für Elektrofahrzeuge. Bachelor thesis. 2012

- P. Zurbrügg. Konzeptionierung und Konstruktion von Komponenten für Elektrofahrzeuge. Bachelor thesis. 2012

- I. S. Dröge. Konzeptionierung eines Brennstoffzellensystems als Range Extender für ein Elektrofahrzeug. Bachelor thesis. 2012

- S. Capparelli. Leistungsbasierte Kompensation thermisch bedingter Abweichungen auf Werkzeugmaschinen. Semester thesis. 2013

- P. Zurbrügg. Neuentwicklung von Safety Racks für Thermal/Vakuum Tests. Semester thesis. 2013

- A. Schneeberger. Identifikation und Kompensation thermisch bedingter Lageabweichungen von Rundachsen. Master thesis. 2013

- M. Wiessner. Konstruktion und Fertigung eines Prüfwerkstücks zur Visualisierung thermo-mechanischer Abweichungen. Semester thesis. 2013

- T. Widmer. Optimierung der steuerungsseitigen Kompensation thermischer Abweichungen einer Werkzeugmaschine. 2013

- P. Blaser. Optimierung einer online-Kompensation thermisch bedingter Abweichungen an Werkzeugmaschinen. Bachelor thesis. 2013

- B. B. Massow. Influence of Cooling Lubricant on the Thermal Behaviour of Rotary Axes. Master thesis. 2013

- N. Furrer. Thermo-mechanische Kompensation von 5-Achs Werkzeugmaschinen. Master thesis. 2013

- P. Blaser. Automatisierte Korrektur von Achsabweichungen auf Werkzeugmaschinen. Semester thesis. 2013

Bibliography

[1] J. Mayr, J. Jedrzejewski, E. Uhlmann, M. A. Donmez, W. Knapp, F. Haertig, K. Wendt, T. Moriwaki, P. Shore, R. Schmitt, C. Brecher, T. Wuerz, and K. Wegener. Thermal issues in machine tools. *CIRP Annals - Manufacturing Technology*, 61(2):771 – 791, 2012.

[2] J. Mayr. *Beurteilung und Kompensation des Temperaturgangs von Werkzeugmaschinen*. PhD thesis, ETH Zurich, 2009.

[3] R. Neugebauer, B. Denkena, and K. Wegener. Mechatronic systems for machine tools. *CIRP Annals - Manufacturing Technology*, 56(2):657 – 686, 2007.

[4] C. Brecher, M. Esser, and S. Witt. Interaction of manufacturing process and machine tool. *CIRP Annals - Manufacturing Technology*, 58(2):588 – 607, 2009.

[5] J. Jedrzejewski and W. Kwasny. Holistic precision error model for 5 axis HSC machining centre with rotating rolling units in direct drives. *Procedia CIRP*, 4:125 – 130, 2012.

[6] C. Brecher and A. Wiessmann. Messtechniche Untersuchung des thermo-elastischen Verhaltens von Werkzeugmaschinen. In *11. Dresdner WZM-Fachseminar - Aktuelle Ergebnisse zur steuerungsintegrierten Korrektur thermisch bedingter Fehler im Arbeitsraum*, 2006.

[7] N. Takayama, H. Ota, K. Ueda, and Y. Takeuchi. Development of table-on-table-type five-axis machining center: New structure and basic characteristics. *International Journal of Automation Technology*, 5/2:247–254, 2011.

[8] S. Weikert. When five axes have to be synchronized. *Proceedings of the 7th Lamdamap conference*, pages 87–96, 2005.

[9] B. Bringmann and W. Knapp. Model-based "chase-the-Ball" calibration of a 5-axis machining center. *CIRP*, 55/1:531, 2006.

[10] J. Bryan. Thermal effects in dimensional metrology. *ASME*, 65-PROD-13, 1965.

[11] H.P. Schossig. Thermik Forschung und die Umsetzung der Erkenntnisse in Maschinenkonzepten bei DMG. *Tagungsband 16. Dresdner Werkzeugmaschinen Fachseminar "Tradition und Gegenwart bei der Analyse des thermischen Verhaltens spanender Werkzeugmaschinen"*, 2013.

[12] A.J. White, S. R. Postlethwaite, and D. G. Ford. An identification and study of mechanisms causing thermal errors in CNC machine tools. In *Laser Metrology and Machine Performance IV*, 1999.

[13] J. Bryan. International status of thermal error research. *CIRP Annals - Manufacturing Technology*, 39(2):645 – 656, 1990.

[14] ISO 1:2002 - Geometrical Product Specifications (GPS) - Standard reference temperature for geometrical product specification and verification, Geneva, Switzerland.

[15] M. Weck, P. Mc Keown, R. Bonse, and U. Herbst. Reduction and compensation of thermal errors in machine tools. *CIRP Annals - Manufacturing Technology*, 44(2):589 – 598, 1995.

[16] M. Ess. *Simulation and Compensation of Thermal Errors of Machine Tools*. PhD thesis, ETH Zurich, 2012.

[17] J. Mayr. Nuetzen thermische Messungen auf Werkzeugmaschinen? *MB-Revue*, pages 110–117, 2007.

[18] M. Ess, J. Mayr, K. Wegener, and S. Weikert. An energy model for the calculation of losses and their effects on machining accuracy. In *European Society for Precision Engineering and Nanotechnology*, 2012.

[19] M. Ess, J. Mayr, S. Weikert, and K. Wegener. Dynamic loads and thermal errors on machine tools. Technical report, Institute of machine tools and manufacturing, ETH Zurich, 2012.

[20] K. Grossmann. Thermo-Energetische Gestaltung von Werkzeugmaschinen. *Tagungsband 16. Dresdner Werkzeugmaschinen Fachseminar "Tradition und Gegenwart bei der Analyse des thermischen Verhaltens spanender Werkzeugmaschinen"*, 2013.

[21] ISO 230-3:2007 Test code for machine tools – Part 3: Determination of thermal effects. Geneva, Switzerland., 2007.

[22] ISO DIS 10791-10:2007 Test conditions for machining centres – Part 10: Evaluation of thermal distortions, Geneva, Switzerland., 2007.

[23] ISO DIS 13041-8:2004 Test conditions for numerically controlled turning machines and turning centres - Part 8: Evaluation of thermal distortions. Geneva, Switzerland., 2004.

[24] ISO 230-1:2012 Test code for machine tools – part 1: Geometric accuracy of machines operating under no-load or quasi-static conditions, Geneva, Switzerland.

[25] ISO 230-7:2006 Test code for machine tools - Part 7: Geometric accuracy of axes of rotation, Geneva, Switzerland.

[26] M. Weck and C. Brecher. *Werkzeugmaschinen - Messtechnische Untersuchung und Beurteilung*. Number 978-3540225058. 2006.

[27] U. Heisel, G. Koscsak, and Th. Stehle. Thermografiebasierte Untersuchungen von Vorschubachsen. In *11. Dresdner Werkzeugmaschinen-Fachseminar - Aktuelle Ergebnisse zur steuerungsintegrierten Korrektur thermisch bedingter Fehler im Arbeitsraum*, 2006.

[28] J. Koscsak. *Ermittlung des instationaeren thermischen Verhaltens von Vorschubach-sen mit Kugelgewindetrieb mit Hilfe der Verarbeitung thermografischer Messdaten.* PhD thesis, Universitt Stuttgart, 2007.

[29] ISO/TC 39/SC 2 N 2062: Test conditions for metal cutting machine tools.

[30] B. Bringmann and W. Knapp. Machine tool calibration: Geometric test uncertainty depends on machine tool performance. *Precision Engineering*, 33(4):524 – 529, 2009.

[31] H. Schwenke, W. Knapp, H. Haitjema, A. Weckenmann, R. Schmitt, and F. Del-bressine. Geometric error measurement and compensation of machines - an update. *CIRP Annals - Manufacturing Technology*, 57(2):660 – 675, 2008.

[32] T. Liebrich, M. Gebhardt, S. Thoma, H. Nguyen, S. Weikert, W. Knapp, and K. We-gener. Static and dynamic testing of 5-axis machine tools. In *Proceedings of the MTTRF 2010 Annual Meeting 2010*, 2010.

[33] D. Kono, A. Matsubara, I. Yamaji, and T. Fujita. High-precision machining by measurement and compensation of motion error. *International Journal of Machine Tools and Manufacture*, 48(10):1103 – 1110, 2008.

[34] S. Parkinson, Andrew P. Longstaff, A. Crampton, S. Fletcher, G. Allen, and A. My-ers. Automation as a solution for machine tool calibration planning. In Gary Lucas, editor, *Proceedings of The Queen's Diamond Jubilee Computing and Engineering An-nual Researchers Conference 2012: CEARC 2012*, pages 57–62. University of Hud-dersfield, Huddersfield, March 2012.

[35] J.-S. Chen. A study of thermally induced machine tool errors in real cutting condi-tions. *International Journal of Machine Tools and Manufacture*, 36(12):1401 – 1411, 1996.

[36] C. Brecher and A. Wiessmann. Stressing unit for modelling of thermal behavior of a milling machine. *12th CIRP Conference on Modelling of Machining Operations*, 2:727–730, 2009.

[37] F. Klocke, K. Grossmann, M. Brockmann, and Ch. Staedel. Untersuchung des Zerspanungsprozesses hinsichtlich auftretender Waermequellenstroeme und Temper-aturen. *Tagungsband 16.Dresdner Werkzeugmaschinen Fachseminar "Tradition und Gegenwart bei der Analyse des thermischen Verhaltens spanender Werkzeugmaschi-nen"*, 2013.

[38] G.H.J. Florussen, F.L.M. Delbressine, and P.H.J. Schellekens. Assessing thermally induced errors of machine tools by 3D length measurements. *CIRP Annals - Manu-facturing Technology*, 52(1):333 – 336, 2003.

[39] N. Srinivasa, J.C. Ziegert, and C.D. Mize. Spindle thermal drift measurement using the laser ball bar. *Precision Engineering*, 18(2):118 – 128, 1996.

[40] M Franke. Measuring large 3D structures using a portable 4-am laser-interferometer. *Advances in Metrology*, pages 35–42, 2010.

[41] D. Song, L. Zeng, and C. Yin. Real-time measurement of spindle thermal deformation using interferometers. *Optical Engineering*, 39(8):2114–2118, 2000.

[42] A.J. White, S. R. Postlethwaite, and D. G. Ford. Measuring and modelling thermal distortion on CNC machine tools. In *Laser Metrology and Machine Performance V*, 2001.

[43] M. Sharif Uddin, Soichi Ibaraki, A. Matsubara, and T. Matsushita. Prediction and compensation of machining geometric errors of five-axis machining centers with kinematic errors. *Precision Engineering*, 33(2):194 – 201, 2009.

[44] S.-H. Yang, K.-H. Kim, and Y. K. Park. Measurement of spindle thermal errors in machine tool using hemispherical ball bar test. *International Journal of Machine Tools and Manufacture*, 44(2??3):333 – 340, 2004.

[45] F.L.M. Delbressine, G.H.J. Florussen, L.A. Schijvenaars, and P.H.J. Schellekens. Modelling thermomechanical behaviour of multi-axis machine tools. *Precision Engineering*, 30(1):47 – 53, 2006.

[46] K. Grossmann, M. Merx, and M. Riedel. Thermografie und Nahbereichs-Photogrammetrie zur Erfassung von Temperatur- und Verlagerungsfeldern. *Tagungsband 16.Dresdner Werkzeugmaschinen Fachseminar "Tradition und Gegenwart bei der Analyse des thermischen Verhaltens spanender Werkzeugmaschinen"*, 2013.

[47] U. Heisel, G. Koscsk, and T. Stehle. Thermography-based investigation into thermally induced positioning errors of feed drives by example of a ball screw. *CIRP Annals - Manufacturing Technology*, 55(1):423 – 426, 2006.

[48] C. Hong and S. Ibaraki. Non-contact R-test with laser displacement sensors for error calibration of five-axis machine tools. *Precision Engineering*, 37(1):159 – 171, 2013.

[49] W. Knapp and A. Wirtz. Testing rotary axes on NC machine tools. *CIRP Annals - Manufacturing Technology*, 39(1):549 – 552, 1990.

[50] S. Weikert and W. Knapp. R-test, a new device for accuracy measurements on five axis machine tools. *CIRP Annals - Manufacturing Technology*, 53(1):429 – 432, 2004.

[51] M. Ess, T. Liebrich, W. Knapp, and K. Wegener. Thermal displacements of rotary axes. *Annual Meeting MTTRF*, 2011.

[52] S. Ibaraki. Error calibration for five-axis machining centers and new proposal to ISO standards. *The 15. International Machine Tool Engineers' Conference Proceedings*, 1:72–81, 2012.

[53] C. Brecher and M. Wennemer. Eigenschaftsmodellbasierter Ansatz zur Korrektur thermo-elastischer Verlagerungen. *Tagungsband 16. Dresdner Werkzeugmaschinen Fachseminar "Tradition und Gegenwart bei der Analyse des thermischen Verhaltens spanender Werkzeugmaschinen"*, 2013.

[54] T. Stehle. *Berechnung thermischer Verformungen und Verlagerungen an Werkzeugmaschinen und Moeglichkeiten zur Kompensation.* PhD thesis, Universitaet Stuttgart, 1997.

[55] C. Jin. Wavelet neural network based on NARMAL2 model for prediction of thermal characteristics in a feed system. *Chinese Journal of Mechanical Engineering*, 23, 2010.

[56] Y. Kang, C.-W. Chang, Y. Huang, C.-L. Hsu, and I-Fu Nieh. Modification of a neural network utilizing hybrid filters for the compensation of thermal deformation in machine tools. *International Journal of Machine Tools and Manufacture*, 47(2):376 – 387, 2007.

[57] R Ramesh, M.A Mannan, and A.N Poo. Thermal error measurement and modelling in machine tools.: Part I. influence of varying operating conditions. *International Journal of Machine Tools and Manufacture*, 43(4):391 – 404, 2003.

[58] R. Ramesh, M.A. Mannan, A.N. Poo, and S.S. Keerthi. Thermal error measurement and modelling in machine tools. part II. hybrid bayesian network-support vector machine model. *International Journal of Machine Tools and Manufacture*, 43(4):405 – 419, 2003.

[59] P. Vanherck, J. Dehaes, and M. Nuttin. Compensation of thermal deformations in machine tools with neural nets. *Computers in Industry*, 33(1):119 – 125, 1997.

[60] J.-S. Chen. Neural network-based modelling and error compensation of thermally-induced spindle errors. *The International Journal of Advanced Manufacturing Technology*, 12(4):303–308, 1996.

[61] J.S. Chen and G. Chiou. Quick testing and modeling of thermally-induced errors of cnc machine tools. *International Journal of Machine Tools and Manufacture*, 35(7):1063 – 1074, 1995.

[62] G. Jungnickel. *Simulation des thermischen Verhaltens von Werkzeugmaschinen, Lehre Forschung Praxis.* G. Jungnickel, 2000.

[63] T. Holkup, H. Cao, P. Kol, Y. Altintas, and J. Zelen. Thermo-mechanical model of spindles. *CIRP Annals - Manufacturing Technology*, 59(1):365 – 368, 2010.

[64] C.H. Wu and Y.T. Kung. Thermal analysis for the feed drive system of a CNC machine center. *International Journal of Machine Tools and Manufacture*, 43(15):1521 – 1528, 2003.

[65] J. Jedrzejewski, W. Modrzycki, Z. Kowal, W. Kwany, and Z. Winiarski. Precise modelling of HSC machine tool thermal behaviour. *Journal of Achievements in Materials and Manufacturing Engineering*, 24(1):245–252, 2007.

[66] S. Strauchold J. Jedrzejewski. Directions in improving thermal behaviour of spindle bearing assemblies in FMS moduls. *Manufacturing Systems*, 23(4):317322., 1994.

[67] J. Mayr, S. Weikert, and K. Wegener. Comparing the thermo-mechanical behavior of machine tool frame design using a FDM-FEA simuiation. In *ASPE Annual Meeting*, USA, 2007.

[68] J. Mayr, M. Ess, S. Weikert, and K. Wegener. Simulation and prediction of the thermally induced deformations on machine tools caused by moving linear axis using the FDEM simulation. In *ASPE Annual Meeting*, USA, 2008.

[69] J. Mayr, M. Ess, S. Weikert, and K. Wegener. Compensation of thermal effects on machine tools using a FDEM simulation approach. In *9th International Conference and Exhibition on laser metrology, machine tool, CMM and robotic performance*, United Kingdom, 2009.

[70] K. Grossmann, A. Galant, M. Beitelschmidt, and M. Partzsch. Strukturveraenderlichkeit in FEM und Blocksimulation bei der Berechnung von Temperaturfeldern. *Tagungsband 16.Dresdner Werkzeugmaschinen Fachseminar "Tradition und Gegenwart bei der Analyse des thermischen Verhaltens spanender Werkzeugmaschinen"*, 2013.

[71] W.-G. Drossel, St. Ihlenfeldt, C. Zwingenberger, K. Grossmann, and St. Schroeder. Modellierung des Waermeaustauschs Maschine-Umgebung. *Tagungsband 16. Dresdner Werkzeugmaschinen Fachseminar "Tradition und Gegenwart bei der Analyse des thermischen Verhaltens spanender Werkzeugmaschinen"*, 2013.

[72] S. Nestmann, R. Neugebauer, and R. Lange. Thermozelle zur Untersuchung des thermischen Verhaltens von Maschinen. *Maschinenmarkt. MM, das Industriemagazin*, 104(40):34–37, 1998.

[73] R. Kneer, S. Vieler, K. Grossmann, and S. Schroeder. Messungen des Waermebergangs an Fugenkontakten von Werkzeugmaschinen. *Tagungsband 16. Dresdner Werkzeugmaschinen Fachseminar "Tradition und Gegenwart bei der Analyse des thermischen Verhaltens spanender Werkzeugmaschinen"*, 2013.

[74] J. Jedrzejewski. Zur Erwaermung von Drehmaschinen-Spindelkaesten. *WZM International*, 4:47–50, 1973.

[75] J. Jedrzejewski. Kompensation thermischer Verlagerungen einer Drehmaschine. *Werkstatt und Betrieb*, 118:85–87, 1985.

[76] E. Abele. Machine tool spindle units. *CIRP Annals - Manufacturing Technology*, 59/2:781–802, 2010.

[77] H. Li and S. C. Yung. Integrated dynamic thermo-mechanical modelling of high speed spindles part 2: Solution procedure and validation. *Journal of Manuacturing Science and Engineering*, 126:159–168, 2004.

[78] H. Li and S. C. Yung. Integrated dynamic thermo-mechanical modelling of high speed spindles part1: Model development. *Journal of Manufacturing Science and Engineering*, 126:148–158, 2004.

[79] J. Jedrzejewski, Z. Kowal, W. Kwany, and W. Modrzycki. High-speed precise machine tools spindle units improving. *Journal of Materials Processing Technology*, 162163(0):615 – 621, 2005.

[80] J.S. Chen and Wei-Yao Hsu. Characterisation and models for thermal growth of a motorized high speed spindle. *International Journal of Machine Tools and Manufacturing*, 43:1163–1170, 2003.

[81] J. Vyroubal. Compensation of machine tool thermal deformation in spindle axis direction based on decomposition method. *Precision Engineering*, 36(1):121 – 127, 2012.

[82] T. Moriwaki. Thermal deformation and its on-line compensation of hydrostatically supported precision spindle. *CIRP Annals - Manufacturing Technology*, 37(1):393 – 396, 1988.

[83] T. Moriwaki and E. Shamoto. Analysis of thermal deformation of an ultraprecision air spindle system. *CIRP Annals - Manufacturing Technology*, 47(1):315 – 319, 1998.

[84] S.C. Veldhuis and M.A. Elbestawi. A strategy for the compensation of errors in five-axis machining. *CIRP Annals - Manufacturing Technology*, 44(1):373 – 377, 1995.

[85] A. Blazejewski, W. Kwasny, J. Jedrzejewski, and T.-W. Gim. Modelling thermal deformation of tilting rotary table with direct drive system. *Journal of Machine Engineering*, 10(4), 2010.

[86] R. Guserle and M. F. Zaeh. Integrativer Einsatz von CAX-Tools auf Basis einer Multidisziplinren Simulation am Beispiel eines Produktionssystems. In *11. Dresdner Werkzeugmaschinen-Fachseminar - Aktuelle Ergebnisse zur steuerungsintegrierten Korrektur thermisch bedingter Fehler im Arbeitsraum*, 2006.

[87] C. Brecher, R. Werner, D. Haber, and S. Winkler. Verlustleistung in einer Vorschubachse und die daraus resultierende Temperaturverteilung. *Tagungsband 16. Dresdner Werkzeugmaschinen Fachseminar "Tradition und Gegenwart bei der Analyse des thermischen Verhaltens spanender Werkzeugmaschinen"*, 2013.

[88] W.S. Yun, S.K. Kim, and D.W. Cho. Thermal error analysis for a CNC lathe feed drive system. *International Journal of Machine Tools and Manufacture*, 39(7):1087 – 1101, 1999.

[89] J.-J. Kim, Y. H. Jeong, and D.-W. Cho. Thermal behavior of a machine tool equipped with linear motors. *International Journal of Machine Tools and Manufacture*, 44(7):749 – 758, 2004.

[90] R. Ramesh. Support vector machine model for classification of thermal error in machine tools. *International Journal of Advanced Manufacturing Technology*, 20:114–120, 2002.

[91] J. Mayr, M. Ess, S. Weikert, and K. Wegener. Comparing different cooling concepts for ball screw systems. In *ASPE Annual Meeting*, USA, 2010.

[92] J. Mayr and M. Ess. Thermal behaviour improvement of linear axis. In *Proceedings of the 11th euspen conference*, 2011.

[93] M. Ess, J. Mayr, S. Weikert, and K. Wegener. Thermal model of machine tool feed drive. In *American Society for Precision Engineering*, 2011.

[94] C. Brecher and A. Wissmann. Messtechnische Untersuchung des thermoelastischen Verlagerungsverhaltens von Werkzeugmaschinen. In *11. Dresdner Werkzeugmaschinen-Fachseminar - Aktuelle Ergebnisse zur steuerungsintegrierten Korrektur thermisch bedingter Fehler im Arbeitsraum*, 2006.

[95] W. Modrzyck P. Turek, J. Jedrzejewski. Methods of machine tool error compensation. *Journal of Machine Engineering*, 10(4), 2010.

[96] U. Heisel. Modelling of interaction processes in cutting. In *Proceedings of 2nd International Conference on Process Machine Interactions*, 2010.

[97] C. Brecher, P. Hirsch, and M. Weck. Compensation of thermo-elastic machine tool deformation based on control internal data. *CIRP Annals - Manufacturing Technology*, 53(1):299 – 304, 2004.

[98] J.-P. Kruth, P. Vanherck, and C. Van den Bergh. Compensation of static and transient thermal errors on CMMs. *CIRP Annals - Manufacturing Technology*, 50(1):377 – 380, 2001.

[99] C. Brecher and P. Hirsch. Kompensation thermoelastischer Verlagerungen. In *11. Dresdner Werkzeugmaschinen-Fachseminar - Aktuelle Ergebnisse zur steuerungsintegrierten Korrektur thermisch bedingter Fehler im Arbeitsraum*, 2006.

[100] J. Bryan, D. Carter, R. Clouser, and J. Hamilton. An order of magnitude improvement in thermal stability using a liquid shower on a measuring machine. *Proceedings of the SME Workshop on precision Machining*, 1982.

[101] E. Uhlmann. Kompensation thermischer Verlagerungen an Werkzeugmaschinen durch Einatz von CFK Strukturen. *Fortschrittsberichte VDI Reihe 2 - Fertigungstechnik: Hybride Techniken in der Produktion*, 675:76–77, 2010.

[102] E. Uhlmann. Application of CFRP structures for compensation of thermal strains at machine tools. *CIRP Paris January Meet STC M Paper Session*, 2010.

[103] D. Weidlich and S. Nestmann. Kompaktfuehrungen an Mineralgussgestellen. *Werkstatt und Betrieb*, 7-8:120–123, 2001.

[104] J. Jedrzejewski. Thermisches Verhalten von Werkzeugmaschinen-Gestellen. *Industrie Anzeiger*, 99(65):1243–1245, 1977.

[105] W.-G. Drossel, A. Bucht, and C. Ohsenbruegge. Materialeffekte und Funktionsmechanismen zur Waermefluss-Steuerung. *Tagungsband 16. Dresdner Werkzeugmaschinen Fachseminar "Tradition und Gegenwart bei der Analyse des thermischen Verhaltens spanender Werkzeugmaschinen"*, 2013.

[106] G. Spur, E. Hoffmann, and Z. Paluncic. Ausgleich von Axial und Winkelverlagerungen an Drehmaschinen durch Beheizen. *Industrie-Anzeiger*, 2:32–33, 1989.

[107] J. Weber, Jul. Weber, G. Schmidt, and U. Semmler. Fluidische Kuehlung von Motorspindeln und Werkzeugen. *Tagungsband 16. Dresdner Werkzeugmaschinen Fachseminar "Tradition und Gegenwart bei der Analyse des thermischen Verhaltens spanender Werkzeugmaschinen"*, 2013.

[108] A. H. Slocum. *Precision Machine Design.* Society of Mechanical Engineers, 1992.

[109] C. Brecher and A.Wiessmann. Optimierung des thermischen Verhaltens von Fraesmaschinen. *Zeitschrift fuer wissenschaftlichen Fabrikbetrieb*, 104:437–444, 2009.

[110] K. Grossmann, B. Kauschinger, and St. Rehn. Umsetzung der strukturmodellbasierten thermischen Korrektur auf der Maschinenteuerung. In *11. Dresdner Werkzeugmaschinen-Fachseminar - Aktuelle Ergebnisse zur steuerungsintegrierten Korrektur thermisch bedingter Fehler im Arbeitsraum*, 2006.

[111] M.A. Donmez, D.S. Blomquist, R.J. Hocken, C.R. Liu, and M.M. Barash. A general methodology for machine tool accuracy enhancement by error compensation. *Precision Engineering*, 8(4):187 – 196, 1986.

[112] R. Bonse. *Thermisches Last-Verformungsverhalten von Werkzeugmaschinen.* PhD thesis, RWTH Aachen, 1998.

[113] R. Bonse and M. Weck. Indirekte Kompensation thermo-elastischer Verlagerungen bei Einwirkung mehrerer Waermequellen. *VDW*, 1994.

[114] U. Herbst. Kompensation thermoelastischer Verlagerungen an Werkzeugmaschinen. *Schleiftechnisches Kolloquium*, pages 135–145, 2000.

[115] U. Herbst. *Analyse und Kompensation thermoelastischer Verlagerungen.* PhD thesis, RWTH Aachen, 2002.

[116] C. Brecher, J. Flore, M. Klatte, and C. Wenzel. In-process measurement of machine structure deformation and compensation of resulting work-piece inaccuracies. In *Laser Metrology and machine performance X*, 2013.

[117] E. Uhlmann. Adaptronic Compensation of Thermal Strain a Machine Tool Spindles using CRP-Bandages. *Proceedings of 2nd Manufacturing Engineering Society International Conference*, pages 183–186, 2007.

[118] E. Uhlmann and P. Marcks. Compensation of thermal deformations at machine tools using adaptronic CRP structures. *Proceedings of 41st CIRP Conference on Manufacturing Systems: Manufacturing Systems and Tecniques for the New Front*, pages 183–186, 2008.

[119] ISO DIS 10791-1:2013 Test conditions for machining centres – Part 1: Geometric Tests for machines with horizontal spindle (horizontal Z-axis), Geneva, Switzerland.

[120] M. Gebhardt, P. von Cube, W. Knapp, and K. Wegener. Measurement set ups and cycles for thermal characterization of axes of rotation. In *12th International Conference of the European Society for Precision Engineering & Nanotechnology.* euspen, 2012.

[121] M. Gebhardt, A. Schneeberger, W. Knapp, and K. Wegener. Measuring, modeling and compensating thermally caused location errors of rotary axes. In *Proceedings of MTTRF*, 2013.

[122] M. Gebhardt, M. Ess, S. Weikert, W. Knapp, and K. Wegener. Phenomenological compensation of thermally caused position and orientation errors of rotary axes. *Journal of Manufacturing Processes*, 15:452–459, 2013.

[123] M. Gebhardt and K. Wegener. Temperatureinfluss auf Werkzeugmaschinen. *MB Revue*, Hauptausgabe 2013:59–63, 2013.

[124] M. Gebhardt, A. Schneeberger, S. Capparelli, W. Knapp, and K. Wegener. Messtechnische charakterisierung thermisch bedingter abweichungen von 5-achs werkzeugmaschinen. *XXVII. Messtechnisches Symposium des Arbeitskreises der Hochschullehrer für Messtechnik e.V.*, pages 25–36, 2013.

[125] J. Mayr, M. Gebhardt, B. B. Massow, S. Weikert, and K. Wegener. Cutting fluid influence on thermal behavior of 5-axis machine tools. *6th CIRP International Conference on High Performance Cutting, HPC2014. Status: accepted / to appear*, 2014.

[126] M. Gebhardt, J. Mayr, N. Furrer, T. Widmer, S. Weikert, and W. Knapp. High precision grey-box model for compensation of thermal errors on 5-axis machine tools. *CIRP Annals - Manufacturing Technology 2014. Status: accepted / to appear*, 2014.

[127] M. Gebhardt, A. Schneeberger, S. Weikert, W. Knapp, and K. Wegener. Thermally caused location errors of rotary axes of 5-axis machine tools. *International Journal of Automation technology. Status: under review*, 2014.

[128] DIN EN 60529; VDE 0470-1:2000 Schutzarten durch Gehaeuse (IP-Code).

[129] T. Widmer and M. Gebhardt (Advisor). Optimierung der steuerungsseitigen Kompensation thermischer Abweichungen einer Werkzeugmaschine. Semester project, 2013, IWF ETH Zurich, unpublished.

[130] N. Furrer and M. Gebhardt. Thermo-mechanical compensation of 5-axis machine tools. Master Thesis, 2011, IWF ETH Zurich, unpublished.

[131] I. Bucher. Estimating the ratio between travelling and standing vibration waves under non-stationary conditions. *Journal of Sound and Vibration*, 270:341–359, 2004.

[132] W. Lotze. Unsicherheit des Ausgleichskreises aus Koordinatenmessungen. *Feingeraetetechnik*, 32:72–75, 1983.

[133] ISO /IEC Guide 98-3:2008: Uncertainty of measurement part 3: Guide to the expression of uncertainty in measurement. ISO, Geneva, Switzerland.

[134] B. Massow and M. Gebhardt (Advisor). Influence of cooling lubricant on the thermal behavior of rotary axes. Semester project, 2013, IWF ETH Zurich, unpublished.

[135] M. Gebhardt, S. Capparelli, M. Ess, W. Knapp, and K. Wegener. Physical and phenomenological simulation models for the thermal compensation of rotary axes of machine tools. *Proceedings of Euspen 2013 Berlin*, 1:304–309, 2013.

[136] A. Schneeberger and M. Gebhardt (Advisor). Identifikation und Kompensation thermisch bedingter Lageabweichungen von Rundachsen. Master Thesis, 2013, IWF ETH Zurich, unpublished, 2012.

[137] P. Blaser and M. Gebhardt (Advisor). Optimierung einer online-Kompensation thermisch bedingter Abweichungen an Werkzeugmaschinen. Semester project, 2013, IWF ETH Zurich, unpublished.

[138] E. Sapper, K. Langenheinecke, and P. Jany. *Thermodynamik fr Ingenieure*. Vieweg Verlag, 2004.

[139] L. Papula. *Mathematik fuer Ingenieure und Naturwissenschaftler Band 1: Ein Lehr- und Arbeitsbuch fuer das Grundstudium*. Vieweg+Teubner Verlag, 2012.

[140] VDI Gesellschaft Verfahrenstechnik und Chemieingenieurwesen. *VDI-Waermeatlas*. Springer Verlag, 2006.

[141] L. Pohlhausen K. Millsaps. Heat transfer by laminar flow from a rotating plate. *Aeronautical Science*, 1952.

[142] G. Cardone, T. Astarita, and G. M. Carlomagno. Heat transfer measurements on a rotating disk. *International Journal of Rotating Machinery*, 1997.

[143] P. Cooper. Turbulent fluid friction of rotating disks. *NASA*, 1973.

[144] W. Klingauf. Der schnelle Draht zwischen PC und CNC. *WB Werkstatt + Betrieb*, 03:58–60, 2009.

[145] N2061, ISO / DTR 16907.2: Test conitions for metal cutting machine tools - Numerical compensation of geometric errors of machine tools.